MARTIN MARIETTA ENERGY SYSTEMS LIBRARIES
3 4456 0349834 7

CENTRAL RESEARCH LIBRARY
DOCUMENT COLLECTION

AEC RESEARCH AND DEVELOPMENT REPORT

ORNL-1875
Progress

DECLASSIFIED
CLASSIFICATION CHANGED TO:
BY AUTHORITY OF: AEC 11-8-62
BY: 33 Bell 11-5-63

METALLURGY DIVISION

SEMIANNUAL PROGRESS REPORT

FOR PERIOD ENDING OCTOBER 10, 1954

CENTRAL RESEARCH LIBRARY
DOCUMENT COLLECTION
LIBRARY LOAN COPY
DO NOT TRANSFER TO ANOTHER PERSON
If you wish someone else to see this document, send in name with document and the library will arrange a loan.

OAK RIDGE NATIONAL LABORATORY
OPERATED BY
CARBIDE AND CARBON CHEMICALS COMPANY
A DIVISION OF UNION CARBIDE AND CARBON CORPORATION
UCC
POST OFFICE BOX P
OAK RIDGE, TENNESSEE

[redacted]

[redacted]

ORNL 1875

This do m t o i t f 176 p g
Copy 7 of 148 opie Series A

Contract No W 7405-eng 26

METALLURGY DIVISION

SEMIANNUAL PROGRESS REPORT

for Period Ending October 10, 1954

J H Frye Jr Director

EDITED BY

W H Bridges

DATE ISSUED

AUG 12 1955

OAK RIDGE NATIONAL LABORATORY
Operated by
CARBIDE AND CARBON CHEMICALS COMPANY
A Division of Union Carbide and C rbon Corpor tio
Post Office Bo P
Oak Ridge Tennessee

[redacted]

3 4456 0349834 7

[redacted]

INTERNAL DISTRIBUTION

1 C E Center
2 Biology Library
3 Health Physics Library
4 Metallurgy Library
5 7 Central Research Library
8 Reactor Experimental Engineering Library
9 13 Laboratory Records Department
14 Laboratory Records ORNL RC
15 C E Larson
16 L B Emlet (K 25)
17 J P Murray (Y 12)
18 A M Weinberg
19 E H Taylor
20 E J Murphy
21 E D Shipley
22 J H Frye Jr
23 F C VonderLage
24 W H Jordan
25 J A Swartout
26 S C Lind
27 F L Culler
28 A H Snell
29 A Hollaender
30 M T Kelley
31 K Z Morgan
32 T A Lincoln
33 A S Householder
34 C S Harrill
35 C E Winters
36 D S Billington
37 D W Cardwell
38 E M King
39 A J Miller
40 D D Cowen
41 P M Reyling
42 W H Bridges
43 G C Williams
44 S Cromer
45 L K Jetter
46 E J Boyle
47 W D Manly
48 C D Susano
49 W W Parkinson
50 R J Gray
51 H A Yakel
52 D C Vreeland
53 E E Stansbury
54 G P Smith
55 J E Cunningham
56 R S Crouse
57 R E Adams
58 J H Erwin
59 J O Betterton Jr
60 W O Harms
61 G M Adamson
62 E S Bomar
63 R J Beaver
64 T W Fulton
65 W J Fretague
66 R B Oliver
67 J T Howe
68 T H Blewitt
69 C R Boston
70 J H Crawford Jr
71 J C Wilson
72 H W Savage
73 E E Hoffman
74 W J Leonard
75 J A Milko
76 J M Warde
77 H G MacPherson (consultant)
78 E C Cruetz (consultant)
79 E P Wigner (consultant)
80 W W Grigorieff (consultant)
81 N J Grant (consultant)
82 T S Shevlin (consultant)
83 R W Johnson
84 J A Lane
85 ORNL Document Reference Library Y 12 Branch

[redacted]

[redacted]

[redacted]

EXTERNAL DISTRIBUTION

86-93	Argonne National Laboratory
94 101	Atomic Energy Commission Washington
102	Battelle Memorial Institute
103 106	Brookhaven National Laboratory
107	Brush Beryllium Company (N W Bass)
108 109	Knolls Atomic Power Laboratory
110 111	General Electric Company Richland
112 114	General Electric Company (ANPD)
115	Hanford Operations Office
116	Phillips Petroleum Company (NRTS)
117 120	Los Alamos Scientific Laboratory
121	Massachusetts Institute of Technology
122 123	New York Operations Office
124	Patent Branch Washington
125	duPont Company Wilmington
126-140	Technical Information Service Oak Ridge
141 144	University of California Radiation Laboratory Berkeley
145	Westinghouse Electric Corporation
146	Atomic Energy Commission Pittsburgh Area Office
147	Atomic Energy Commission Schenectady Operations Office
148	Division of Research and Medicine AEC ORO

[redacted]

[redacted]

Reports previously issued in this series are as follows

ORNL 28	Period Ending March 1 1948
ORNL 69	Period Ending May 31 1948
ORNL 407	Period Ending July 31 1949
ORNL 511	Period Ending October 31 1949
ORNL 583	Period Ending January 31, 1950
ORNL 754	Period Ending April 30 1950
ORNL 827	Period Ending July 31 1950
ORNL 910	Period Ending October 31 1950
ORNL 987	Period Ending January 31 1951
ORNL 1033	Period Ending April 30 1951
ORNL 1108	Period Ending July 31 1951
ORNL 1161	Period Ending October 31 1951
ORNL 1267	Period Ending January 31 1952
ORNL 1302	Period Ending April 30 1952
ORNL 1366	Period Ending July 31 1952
ORNL 1437	Period Ending October 31 1952
ORNL 1503	Period Ending January 31 1953
ORNL 1551	Period Ending April 10 1953
ORNL 1625	Period Ending October 10 1953
ORNL 1727	Period Ending April 10 1954

[redacted]

[redacted]

CONTENTS

SUMMARY ix

FUNDAMENTAL PHYSICAL METALLURGY 1

Preferred Orientation in Extruded Aluminum Rod 1

Representation of the Sheet Texture Type of Preferred Orientation 8

Purification of Zirconium by Zone Melting 9

PHYSICAL METALLURGY OF REACTOR MATERIALS 19

Transformation Kinetics of Zirconium Base Alloys 19

Slagging Experiments on Stainless Steel Fuel Elements 20

Reduction of UF_4 with Aluminum 21

Carburizing of Stainless Steel Fuel Elements 21

Oxidizing of Zirconium Fuel Elements 22

Metallographic Examination of Aluminum Silicon Bonded Thorium Slugs 23

CERAMICS RESEARCH 26

Development of a Ceramic Fuel Element and Associated Reactor Concepts 26

Introduction 26

Summary of Development and Testing 26

Over all Program 27

Reactor Power Plant Design Summary 27

Development and Fabrication of Fuel Plates 29

The Testing Program 37

Process for Obtaining Large Grained UO_2 43

Thorium Oxide 43

Phosphate Coating 46

Ceramic Aspects of Waste Disposal 46

Effect of Various Solutions on the Permeability of Clays 46

Permeability of Clays as Affected by W 8 Solution from the Lagoon 46

Gels Made from Hope Solution and Natural Carbonate Minerals 47

Fixation of Radioactive Isotopes in Gels 48

Retention of NO_3 Ion by Gels 49

Diffusion of Radioactive Strontium from Gels 50

Investigation of Porous Ceramics as Isotope Sorbers 51

Diamond Drilling 51

HRP METALLURGY 52

Physical Metallurgy of Titanium and of Zirconium Alloys 52

Commercial Titanium 52

Iodide-Titanium 53

Bureau of Mines Titanium 54

Zirconium Alloys 54

Welding of Stainless Steels 56

Evaluation of the Preplaced Consumable Insert Heliarc Welding Technique for Root Pass 56

[redacted]

[redacted]

Welding Development on 1 in Carbon Steel Plates Clad with Type 347 Stainless Steel 56
Type 347 Stainless Steel Welds in Which Various Type 347 Stainless Steel Filler Metals Were Used 60

Metallurgy of Corrosion in Homogeneous Reactor Environments 61
Stainless Steel Welds 61
Commercial Titanium and Zircaloy 2 Welds 65
Intergranular Corrosion of Austenitic Stainless Steels 66
Stress Corrosion Cracking in Austenitic Stainless Steels 67

PACKAGE POWER REACTOR PROGRAM 68

Fabrication of Composite Stainless Steel–Uranium Dioxide Fuel Plates 68

Component Assembly by Brazing 75

Corrosion Studies 76

MTR Irradiation Experiment 78

Control Rod Development 86

Installation of Special Equipment 86

HIGH TEMPERATURE METALLURGY 88

General Corrosion 88
Static Tests of Brazing Alloys in Fluorides and Sodium 88
Special Stellite Heats Tested in Sodium and NaF ZrF_4 UF_4 (50 46 4 mole %) 89
Hastelloy R Tested in Various Media at 816°C (1500°F) for 100 hr 90
Molybdenum Coated Inconel in NaF ZrF_4 UF_4 91
Lithium–Type 316 Stainless Steel Thermal Convection Loops 91
Carburization of Inconel by Sodium 92
Rubidium Research 94
A Special Tar Impregnated Fired Graphite 95
Corrosion Resistance of Graph i tite to Sodium and to Fluoride 44 99
Carburization of an Austenitic Stainless Steel 100
Corrosion of Al_2O_3 $MgAl_2O_4$ MgO ZrO_2 and SiC in Molten Media 101
Corrosion of Cermets by Fluoride 30 101
Beryllium Sodium Inconel Compatibility Tests 103

Welding and Brazing 104
High Temperature Brazing Alloy Development Program 104
Heat Exchanger Development 109
Examination of Intermediate Heat Exchanger 117
Fabrication 119

Mechanical Properties 123

Fabrication 125
ANP Radiator 125
Sigma Phase Alloys 126
Duplex Tubing 127
Thermal Convection Loop Fabrication 127
Nickel Molybdenum Base Alloys 128
Boron Carbide Shield for CFRE 129
Tubular Fuel Elements 129

[redacted]

[redacted]

Dynamic Fluoride Corrosion 129
UF_3 Containing Fuels 129
Temperature 131
Time 132
Additions to Fluorides 132
Uranium Concentration 133
Inconel Grain Size 134
Various Containers 134
Sodium Beryllium Inconel System 135

Physical Chemistry 136
Corrosion Testing 136
Film Formation on Metals Oxidation of Sodium 140
Flammability of Alkali Metal Solutions 142
Fused Hydroxide Chemistry 143

FABRICATION METALLURGY 160

Experimental Fabrication of Aluminum Fuel Element 160

Manufacture of Reactor Components 160
Replacement Fuel and Control Rod Units for MTR 160
New Loading of BSF Fuel Elements 160
Borax Model II Fuel Units 160
Special Fuel Assembly for LITR 160
Test Elements for Omega West Reactor 161
Control Rods for Pennsylvania State College 161
Film Boiling Experiment 161
Alclad U Al Alloy Test Plates for BNL 161
Neutron Production Slugs for Hanford and Savannah River 161
Enriched Fuel Plates for GE ANP 161

Preparation of U Al Alloy Products for Chemical Processing Studies 161
Normal Uranium MTR Fuel Components for Phillips Petroleum Co 161
Depleted U Al Alloy Slugs for DuPont 161
Miniature U Al Alloy Slugs 161
Cast and Extruded J Slugs for Phillips Petroleum Co 161
Cast and Extruded J and SRO Slugs 161

Miscellaneous Fabrication Work 161
Iodine Thorium Wire and Foil for North American Aviation Inc 161
Highly Depleted Uranium Slugs for LITR Irradiation 161
Enriched U Al Alloy Slabs for Savannah River 162
Zirconium Alloy Specific Heat Specimens 162
Enriched Uranium Disk for Lid Tank Facility 162

[redacted]

[redacted]

PUBLICATIONS

C E Curtis L M Doney and J R Johnson Some Properties of Hafnium Oxide Hafnium Silicate Calcium Hafnate and Hafnium Carbide *J Am Ceram Soc* **37** 458–465 (Oct 1954)

J R Johnson High Temperature X Ray Camera *J Am Ceram Soc* **37** 360–362 (Aug 1954)

[redacted]

[redacted]

METALLURGY DIVISION
SEMIANNUAL PROGRESS REPORT

SUMMARY

FUNDAMENTAL PHYSICAL METALLURGY

With the use of methods whereby the distribution of the fiber axis with respect to the crystallo graphic axes is obtained a study was made of the fiber texture type of preferred orientation in some extruded aluminum rod The axis distribution charts show the textures to be duplex the <111> and <001> being the preferred directions of the fiber axis For rods extruded at both slow and fast rates the ratio <111>/<001> decreases from the front to the back end of the rod and for corresponding locations is greater in the rod extruded at the faster speed

The fiber texture analysis was applied to the sheet texture type of preferred orientation by simu lating fiber axes about the rolling normal and transverse directions From the axis distribution charts the ideal texture of some cold rolled 65 35 brass was found to have the following components $\{011\}\langle\bar{1}00\rangle$, $\{011\}\langle\bar{2}11\rangle$ and $\{111\}\langle\bar{1}\bar{2}1\rangle$ The ideal texture of cold rolled 2S aluminum was found to be $\{123\}\langle\bar{4}33\rangle$

Experiments to purify zirconium by the zone melting technique have been started The technique should prove useful with this reactive material because of the high purification factor and because of the absence of contaminating crucibles

PHYSICAL METALLURGY OF REACTOR MATERIALS

Three transformation products of the decompo sition of the beta eutectoid of the Ag Zr system have been identified They are (1) a pearlitic type transformation product very similar to pearlite in steels, (2) a bainitic type transformation product very similar to bainite in steels and (3) a martensitic type transformation product formed on quenching by a diffusionless transformation The rate of transformation of the eutectoid at 750 and 800°C has been studied

The tempering of the martensitic structure of a hypoeutectoid Ag Zr alloy has been studied at 800°C The as quenched hardness decreases from 300 to 235 DPH at 15 sec and at 10 min at 800°C and to 190 DPH at 15 min and at 24 hr at 800°C The changes in the microstructure are progres sively, a precipitation of the intermetallic com pound $AgZr_2$ in the matrix the spheroidization and growth of the precipitate nucleation of new unstrained alpha grains in he matrix and the consumption of the deformed matrix by the new grains of alpha

An anodizing procedure has been developed for the identification in bright field illumination by color of the microconstituents of the Ag Zr alloys

Metallurgical treatments for the recovery of uranium from spent stainless steel fuel elements are being investigated One method involves the melting of the fuel element under a nonmetallic material such as alkaline earth fluorides with which the uranium forms a slag Another method depends on the increased reactivity of the stainless steel with the dissolver solutions when the steel has been heavily carburized

Thorium slugs sealed in aluminum cans by the Al Si bonding technique were found to be difficult to dissolve in an acid solution normally suitable for dissolving aluminum and thorium The presence of an intermetallic compound which developed between the thorium and the Al Si alloy in the canning operation was the dissolution barrier

CERAMICS RESEARCH

On the premise that a selected ceramic fuel element is useful in a practical high temperature gas cooled reactor power system a development and testing program has been undertaken

An SiC Si body chosen for its low absorption cross section suitable physical properties and raw material availability has been developed Homogeneous nonporous shapes can be produced consistently A second phase of research is under way to develop with the use of this SiC Si body a uniform fuel bearing sandwich plate

[redacted]

A testing program has been designed in order to obtain sufficient information for reactor power system studies

Some physical properties have been measured and stability under neutron bombardment has been investigated A gas loop has been made that simulates mechanical and thermal service conditions for a fuel element Fission product retention tests show that only gaseous isotopes escape from SiC Si at 1000°C and the number of these isotopes is reduced by a factor of at least 10^{-4} over unclad UO_2

Two reactor power systems have been designed by ORSORT students The first is a package reactor and the second a power breeder Both indicated considerable promise for this ceramic fuel element and for associated concepts

HRP METALLURGY

Metallurgical support to the HRP has continued Impact tests on commercial iodide and Bureau of Mines titanium have revealed that there is little if any environmental effect on the impact properties except under conditions allowing hydrogen embrittlement Several different methods of welding stainless steels were evaluated and a program was initiated to qualify the consumable insert method and set up an operator qualification standard The study of the corrosion behavior of stainless steel welds has continued and it has been found that ferrite content per se is not so significant a factor as was previously thought Corrosion testing of titanium Zircaloy 2 and stressed austenitic stainless steels has continued

PACKAGE POWER REACTOR PROGRAM

Development of a relatively cheap reliable fuel element for long time service in the Army Package Power Reactor is being vigorously pursued Recent critical mass calculations and redesign of the reactor core for 15-Mwyr service have lowered the fuel loading requirements New design specifications on the flat plate type stainless steel fuel element are presented

Results of recent brazing tests on full sized components containing normal uranium are encouraging and tend to support the selection of this method of construction Several problems encountered in the fabrication of a suitable composite fuel plate for brazing are described The compound boron carbide for instance was found not to be a suitable burnout poison for use in the preparation of uranium dioxide–stainless steel fuel plates Apparently B_4C dissociates in the presence of stainless steel under the time temperature conditions employed in the fabrication schedule and forms a low melting eutectic phase Two possible replacement compounds ZrB_2 and BN are presently undergoing rigorous time temperature compatibility studies to determine their stability in contact with stainless steel

Eighteen different brazed joints have been tested for 1000 hr in 565°F distilled water at 1200 psi in the autoclave to aid in the selection of a corrosion resistant brazing alloy Weight change and posttest metallographic data obtained are given An evaluation study was made on the six most promising brazing alloys on the basis of corrosion resistance neutron economy flow temperature availability and cost

Arrangements have been completed to construct and irradiate an experimental stainless steel fuel element in the active lattice of the MTR core The purpose of the experiment is to obtain performance data on certain engineering material combinations and design features to facilitate the construction of a highly reliable fuel component for long time service in the package reactor

HIGH TEMPERATURE METALLURGY

Brazing alloys of Ni Ge Cr and of Ni Ge Cr plus minor additions of other elements were found to be resistant to corrosion by molten fluorides and sodium

Two special Stellite compositions considered for use as hard facing alloys are resistant to attack by molten sodium but are attacked by fluorides Hastelloy R has fair corrosion resistance to fluorides sodium and lithium but is not compatible with molten NaOH or with lead

A molybdenum coating applied to Inconel specimens failed to afford protection for the Inconel against corrosion by static lithium at 1500°F

Three type 316 stainless steel thermal convection loops containing lithium were operated for 1000 hr with hot zone temperatures of 810 800 and 705°C respectively No mass transfer corrosion occurred in the 810 or 800°C loop and maximum corrosion penetration in the hot zone was 2 mils Crystals deposited by mass transfer were found in the cold zone of the 705°C loop

[redacted]

The carburization of Inconel was effected by heating the Inconel for 100 hr at 816°C in a nickel capsule containing sodium and small lumps of graphite

The rate of carburization of austenitic stainless steel in a sodium bath containing carbon was found to be greater when the carbon was present as tar impregnated graphite than when it was present as C 18 (reactor grade) graphite

Inconel has been determined to be a satisfactory container material for static rubidium at temperatures up to 900°C (1650°F) A boiling rubidium–Inconel loop has been operated for 312 hr with a maximum temperature of 825°C (1520°F) and a temperature gradient of 755°C (1360°F) with no evidence of mass transfer and a maximum corrosion penetration of 1 mil

The compounds Al_2O_3 SiC $MgAl_2O_4$ ZrO_2 and MgO were exposed for 100 hr at 816°C to sodium fluoride lithium and lead in static capsules The SiC and Al_2O_3 were found to be the most resistant to corrosion by these media Various titanium carbide cermet specimens have been screened by a dynamic corrosion test in fluoride 30

The compatibility of beryllium sodium and Inconel has been investigated in a series of nine dynamic tests in which the whirligig seesaw and thermal convection loops were used Several different temperatures as high as 1400°F were maintained for times of 270 300 and 1000 hr Four of the whirligig tests were conducted isothermally and the remainder incorporated temperature gradients Results indicate that the system is compatible at temperatures not exceeding 1200°F although a slight deposition of beryllium due to dissimilar metal transfer was detected on the Inconel tube wall The rate of attack of sodium upon beryllium appears more rapid in areas where the sodium is relatively stagnant

The oxidation resistance of several high temperature brazing alloys has been evaluated by using brazed Inconel T joints Selected compositions were slightly oxidized after 550 hr at 1700°F In another series of corrosion tests brazing alloys were held for 1000 hr in water at 250°C

Types 430 and 310 stainless steel were found to be acceptable alloys for use in clad copper radiator fins Coast Metals No 52 brazing alloy was selected for use in fabricating a radiator incorporating clad copper high conductivity fins This alloy has a lower flow temperature than does low melting Nicrobraz and is superior to the other two alloys evaluated from the standpoint of diffusion penetration into the fin and/or tube walls Oxidation resistance can be imparted to a clad copper fin by introducing aluminum onto the exposed copper surface This can be done by dipping spraying or painting followed by a diffusion anneal

One radiator assembly was fabricated by furnace brazing Inconel clad copper fins to an Inconel tube assembly with Coast Metals No 52 alloy and a sodium to air radiator was fabricated by brazing type 430 stainless steel clad copper fins to an Inconel tube assembly with the same alloy The tube to header welds for both assemblies were made by a semiautomatic Heliarc welding process

Metallographic examination of a fluoride to sodium heat exchanger which failed after 1680 hr of service under cyclic temperature conditions revealed that stress concentrations at the root of tube to header welds may initiate cracks which because of expansion and contraction of the tubes gradually grow in magnitude as stresses vary It is believed that back brazing can be used to minimize the possibility of failures of this nature

Burner nozzles for a gas fired heater have been fabricated by furnace brazing with an 82% Au–18% Ni alloy composition

Inconel pump impellers that could not be successfully cast have been fabricated by welding These impellers meet the requirements stipulated for service in the ARE system

Tube burst tests have been conducted to determine the stress rupture properties of end capped Inconel tubes and pipes stressed by internal pressure in the presence of fluorides These evaluations simulate conditions that will be encountered in the heat exchanger and pressure shell of circulating fuel reactors A decrease in rupture life with an increase in volume to surface area ratio was encountered This tends to confirm the current theory that static corrosion of Inconel occurs through the reduction of metal fluorides present as impurities

A large variation in time to rupture has been encountered for Inconel specimens of different cross sectional shapes and areas stressed at 3500 psi in argon The same phenomenon was noted when a hydrogen atmosphere was used It

[redacted]

may be concluded that engineering design data pertaining to creep rupture tests should stipulate the geometry of the material as well as the environment

The creep rupture properties of type 310 stainless steel clad copper sheet have been investigated Embrittlement of the copper core was detected in specimens stressed in excess of 1000 psi at 1500° F No embrittlement occurred in 1000 hr at 1500° F when the stress fell between 500 and 1000 psi Strains in excess of 20% were accompanied by embrittlement regardless of exposure time The thermal conductivity of 6% Al–94% Cu alloy was determined from 212 to 1562° F and that of 8% Al–92% Cu from 212 to 392° F

Tubing has been fabricated of a 48 2% Cr–51 8% Fe alloy for use in a study of sigma phase corrosion by liquid lead

An experimental investigation aimed at developing duplex seamless tubing has been initiated Various alloy combinations have been hot pressed or hot rolled into blanks The fabricability of these blanks will be determined by deep drawing

Molybdenum has been clad with Inconel by rolling at 1000°C a composite having nickel between the molybdenum and Inconel

Two stainless steel clad molybdenum thermal convection corrosion loops failed after a short period of testing as a result of the techniques used in fabricating the loops A loop has been fabricated of columbium clad with type 310 stainless steel by Heliarc welding in air Eight thermal convection loops have been fabricated of modified Inconel type alloys

An investigation of Ni Mo base alloys having compositions similar to the composition of Hastelloy B is in progress The contemplated goal is the development of an alloy having better high temperature strength and better resistance to fluoride corrosion than does Inconel and having better fabricability greater high temperature ductility and better resistance to oxidation than does Hastelloy B

The development of a high boron density shielding material by bonding B_4C with metal has been discontinued Nonmetallic bonding materials fabricated by cold pressing and sintering will be investigated The compatibility of boron and of B_4C with Inconel at 1500° F is being determined

Tubular stainless steel fuel elements containing UO_2 are being prepared for use in a study of the drawing swaging and general workability of such elements

Zirconium base fluorides containing uranium as UF_3 and as UF_3 plus UF_4 have been tested by circulation in Inconel thermal convection loops The presence of UF_3 has been found to reduce but not to eliminate corrosion A thin layer of zirconium rich material was deposited in the hot leg of the loop

Alkali metal base fluorides which are believed to have a higher solubility for UF_3 than the zirconium fluoride base mixture were found to be less corrosive when tested in thermal loops with UF_3 present The depth of subsurface voids was greatly reduced and no hot leg deposit was observed A thin layer as yet unidentified was deposited in the cold leg

Preliminary results indicate that the rate of mass transfer corrosion by fluorides increases with increasing hot leg temperature

Results of a 5000 hr fluoride thermal convection loop test confirm that second stage or mass transfer corrosion is linear Another series of loop tests conducted to obtain data on the time dependency of corrosion furnished results confirming a break in the corrosion time curve at 250 hr

The corrosion of Inconel by fluoride fuels can be reduced by zirconium hydride additions This beneficial effect is accompanied by the loss of part of the uranium in the fuel by deposition

Small additions of hydrogen fluoride gas to a fluoride fuel in an Inconel thermal loop were found to increase the initial rate of corrosive attack This is additional evidence of a negative nature – that mass transfer does not depend upon initial purity

Two additional loops containing a high purity NaF ZrF_4 UF_4 mixture with UF_4 percentage increased over the usual composition confirmed that an increased UF_4 content increases the corrosion

An attempt to determine the effect of grain size on the corrosion of Inconel by fluorides produced inconclusive results

An NaF ZrF_4 UF_4 mixture was successfully circulated in a Hastelloy B loop for 500 and 1000 hr at a maximum temperature of 1500°F Surface

[redacted]

roughening was detected in the hot zone accompanied by less than 2 mils of void penetration No appreciable mass transfer was evidenced

The substitution of molybdenum for a portion of the chromium in Inconel was found to reduce slightly the depth of fluoride corrosion The total amount of attack was considerably reduced

Sodium is being circulated in Inconel thermal convection loops which have a short beryllium cylinder inserted in the hot leg On the basis of four 500 hr tests that have been completed it is believed that Inconel beryllium and sodium in intimate contact will perform satisfactorily at 1200°F

Studies of the mass transfer by liquid lead of Ni Cr Fe and Cr Co alloys having compositions selected so that sigma phase can be produced or suppressed by heat treatment reveal that an alloy is likely to have appreciably greater resistance to mass transfer in liquid lead than its pure components will have provided that a large percentage of the alloy structure consists of the intermetallic compound

Measurements of the oxidation rate of sodium in the temperature range 25 to 47°C disclose that the oxidation of sodium does not follow a linear rate law as was expected and that it does not proceed exponentially or logarithmically with time as would be expected if any of the conventional oxidation theories applied It is suggested that more than one of the conventional mechanisms may be simultaneously or consecutively operative The presence of contaminants even in trace quantities was found to increase the oxidation rate of sodium Solutions of sodium and bismuth were found to be unreactive in dry air when the sodium mole fraction was below 0 4 In air saturated with water vapor the composition exhibiting zero reactivity was shifted toward lower sodium concentrations A decrease in air pressure from 1 to $\frac{1}{4}$ atm did not produce an appreciable change in the reactivity of sodium bismuth solution The effect of temperature and composition upon the reactivity of sodium bismuth alloys has been determined Flammability studies have been made of four alkali metal–alkali metal halide systems

Previous research on the chemistry of fused alkali hydroxides has been hindered because of the need for an adequately inert container material This fundamental requirement has been met by the discovery that vessels machined from massive single crystals of synthetic periclase (high purity magnesium oxide) have excellent resistance to corrosion by NaOH at temperatures as high as 900°C

It has been observed that the reaction between sodium and NaOH to form Na_2O and hydrogen does not proceed rapidly to equilibrium as would be expected but apparently is controlled by the diffusion rate of hydrogen in fused sodium hydroxide with the hydrogen combining with sodium to form NaH as an intermediate step

The free energies of formation of the hydroxide peroxide and superoxide of sodium have been computed as a function of temperature by the use of basic thermodynamic data taken from the literature The calculated free energy values have been used to estimate the decomposition pressures for sodium hydroxide and to show that a basic decomposition equilibrium for all the alkali metals involves the competition between the oxide ion and hydrogen for oxygen The numerical results indicate that in the absence of excess oxygen sodium hydroxide should become corrosive toward metals by virtue of peroxide formation somewhat above 600°C This result is in agreement with experimental observation

Experimental study of the dissociation of liquid sodium hydroxide has revealed that hydrogen is a significant product of the thermal dissociation of liquid sodium hydroxide

A high temperature spectrophotometer is being constructed for use in research on molten hydroxides This approach will take advantage of the marked effects of temperature blanketing atmosphere and solutes upon the color of molten hydroxides

Attempts are being made to isolate and identify the reaction products between metallic nickel and NaOH and to determine their crystal structure and chemical properties

The crystal lattice parameters of $NaNiO_2$ have been recalculated and minor corrections of the previously published values have been made

A study of $NaNiO_2$ indicates that it may undergo a displacive transformation of the martensitic type in passing from the high temperature beta structure to the low temperature alpha structure

FABRICATION METALLURGY

Fabrication studies on the preparation of thin clad MTR type fuel plates revealed the presence

[redacted]

of objectionable surface pits The pitting occurred during the flux annealing operation and was a result of zinc from the $ZnCl_2$ ingredient in the brazing flux alloying with the aluminum cladding Additional tests showed that the alloying action could be minimized either by lowering the $ZnCl_2$ content or by substituting $SnCl_2$ for $ZnCl_2$ in the brazing flux

A total of 105 replaceable fuel rod components and two control rod components were fabricated and forwarded for operation of the MTR during the period from March 1 through September 1 1954 The fuel units were the 19 plate type prepared with braze clad side material and each unit contained 200 g of U^{235}

A new loading of 68 enriched fuel elements was supplied to Argonne National Laboratory for Borax Model II experiments A hot set of fuel elements was prepared also for the Bulk Shielding Facility

Cast enriched U Al alloy billets supplied by Y 12 were extruded and drawn into rod stock for use in the production of approximately 2000 slugs for Savannah River and 5000 slugs for Hanford

Several thousand U Al alloy slugs were prepared for chemical processing studies at the Idaho Chemical Plant at Savannah River and at the Chemical Technology Division at ORNL

Experimental samples of iodine thorium wire and foil were fabricated for North American Aviation Inc Specimens of ZrAg and ZrAl alloy were prepared from solution treated arc cast melts and forwarded to Carnegie Institute of Technology for specific heat measurements

[redacted]

FUNDAMENTAL PHYSICAL METALLURGY

L K Jetter

PREFERRED ORIENTATION IN EXTRUDED ALUMINUM ROD

C J McHargue L K Jetter

With the use of methods previously described [1 2] whereby data on the distribution of the fiber axis with respect to the crystallographic axes are obtained a study was made of the fiber texture type of preferred orientation in some extruded aluminum rod

Two 0 89 in dia aluminum rods were extruded from a 3 125 in dia ingot (extrusion ratio 12 3) at a temperature of 450°F One rod was extruded at a speed of 615 fpm and the other at 0 1 fpm The rods were water quenched at the die to retain insofar as possible the as extruded structure

On 0 19 in spherical x ray diffraction specimens taken from near the front end the middle of the length and near the back end of each extrusion pole distribution data were obtained by the spectrometric method described previously [3 4]

The pole distribution charts (R vs ϕ) for the {111} {222} and the {002} {004} planes for the specimens taken from the rod extruded at the faster speed are given in Fig 1 those from the rod extruded at the slower speed are given in Fig 2 The charts were obtained by normalizing the diffraction data (I vs ϕ) It was pointed out previously that $R = I(\phi)/I_{ran}$ and that $I_{r\ n}$ can be calculated by graphical integration of the function $I \sin \phi$ from $\phi = 0$ to 90 deg for the various $\{hkl\}$ s

The axis distribution charts (T vs $\phi\ \beta$) deduced from these pole distributions are given in Figs 3 and 4 On these charts the contours indicate angular locations of equal normalized axis density (T) The pole distributions calculated from these assumed axis distributions are compared with the experimental curves in Figs 1 and 2 The calculated curves were obtained by averaging the axis density over a path through the unit triangle ϕ degrees from the pole of the plane under consideration $[R(\phi) = \overline{T}(\phi)]$

The axis distribution charts show the textures to be duplex the <111> and the <001> being the preferred directions of the fiber axis The axis density at first falls off symmetrically from the peaks at these locations but then asymmetrically to form a saddle along the <$\bar{1}$10> zone

The volume fraction of material associated with each of the <111> and <001> components was computed from the pole distribution charts of Figs 1 and 2 The results are summarized in Table 1 For both extrusions the ratio <111>/<001> decreases from the front to the back end of the rod and for corresponding locations is greater in the rod extruded at the faster speed

Associated with this increase in the volume fraction of the <100> component is an increase in the number and size of strain free grains or subgrains as shown in the photomicrographs in Figs 5 and 6 This change in structure is also evident in the increased spottiness of the Debye rings on the x ray transmission photograms reproduced in Figs 7 and 8

It appears that this decrease in the <111>/<001> in extruded aluminum rod is a result of an annealing effect The effect might be expected to be

TABLE 1 VOLUME FRACTIONS OF MATERIAL ASSOCIATED WITH THE <111> AND <001> COMPONENTS

Extrusion Speed (fpm)	Location in Extrus o	Volume Fraction <111>	Volume Fraction <001>	<111>/<001>
615	F ont	0 885	0 115	7 5
	Middle	0 840	0 160	5 2
	Back	0 490	0 510	0 95
0 1	Front	0 675	0 325	2 1
	Middle	0 475	0 525	0 9
	Back	0 310	0 690	0 45

[1] L K Jetter *Met Semiann Prog Rep Apr 10 1953* ORNL 1551 p 6

[2] L K Jetter and C J McHargue *Met Semiann Prog Rep Apr 10 1954* ORNL 1727 p 97

[3] L K Jetter *Met Quar Prog Rep Jan 31 1952* ORNL 1267 p 21

[4] L K Jetter and B S Borie Jr *Proceedings of the Spring Metallurgy Conference March 24–26 1952* vol 2 TID 5084 (June 1952) p 529

[redacted]

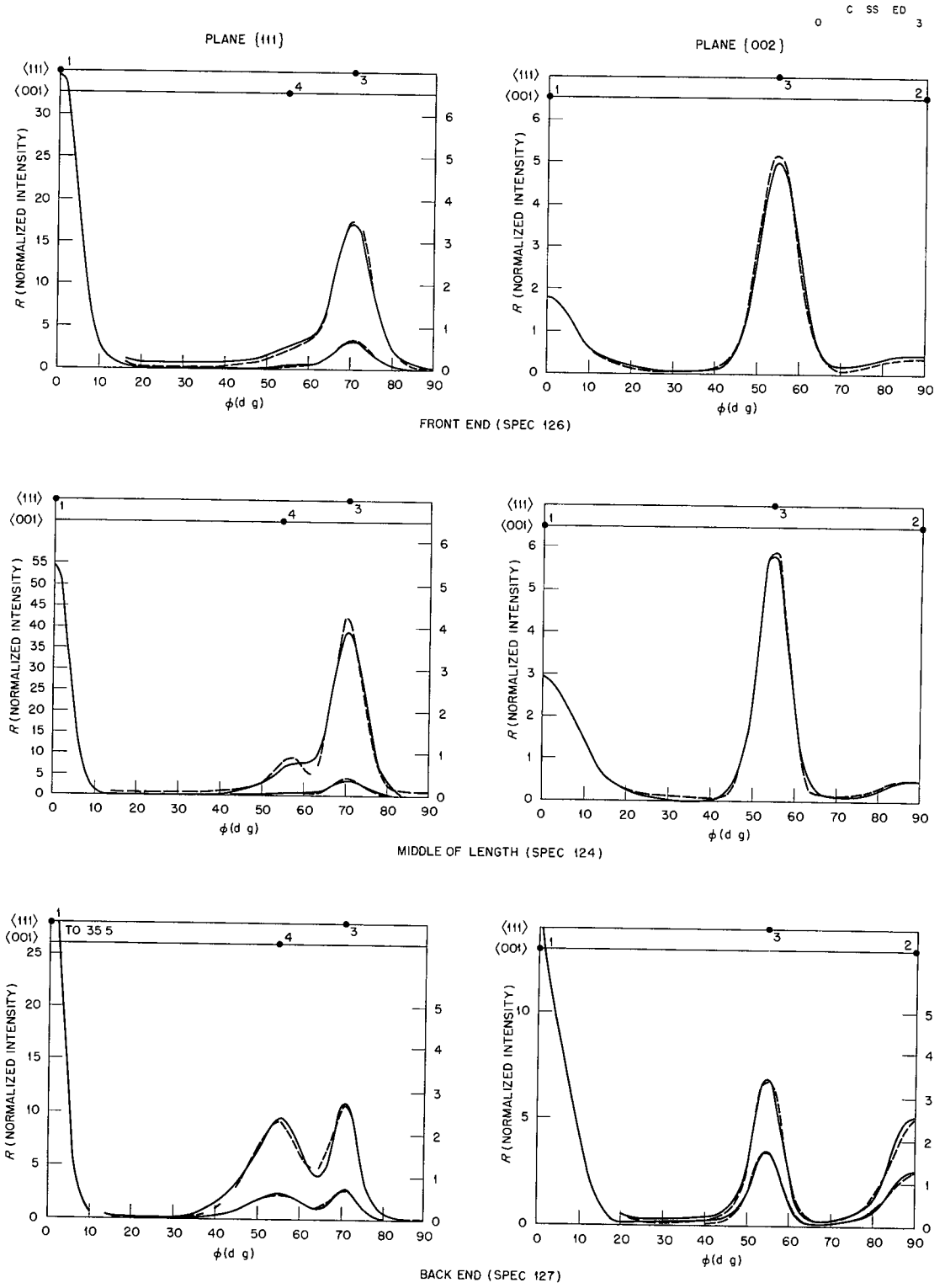

Fig 1 Pole Distribution Charts for 0 89 in dia As Extruded Aluminum Rod Extrusion temperature 450°F extrusion speed 615 fpm

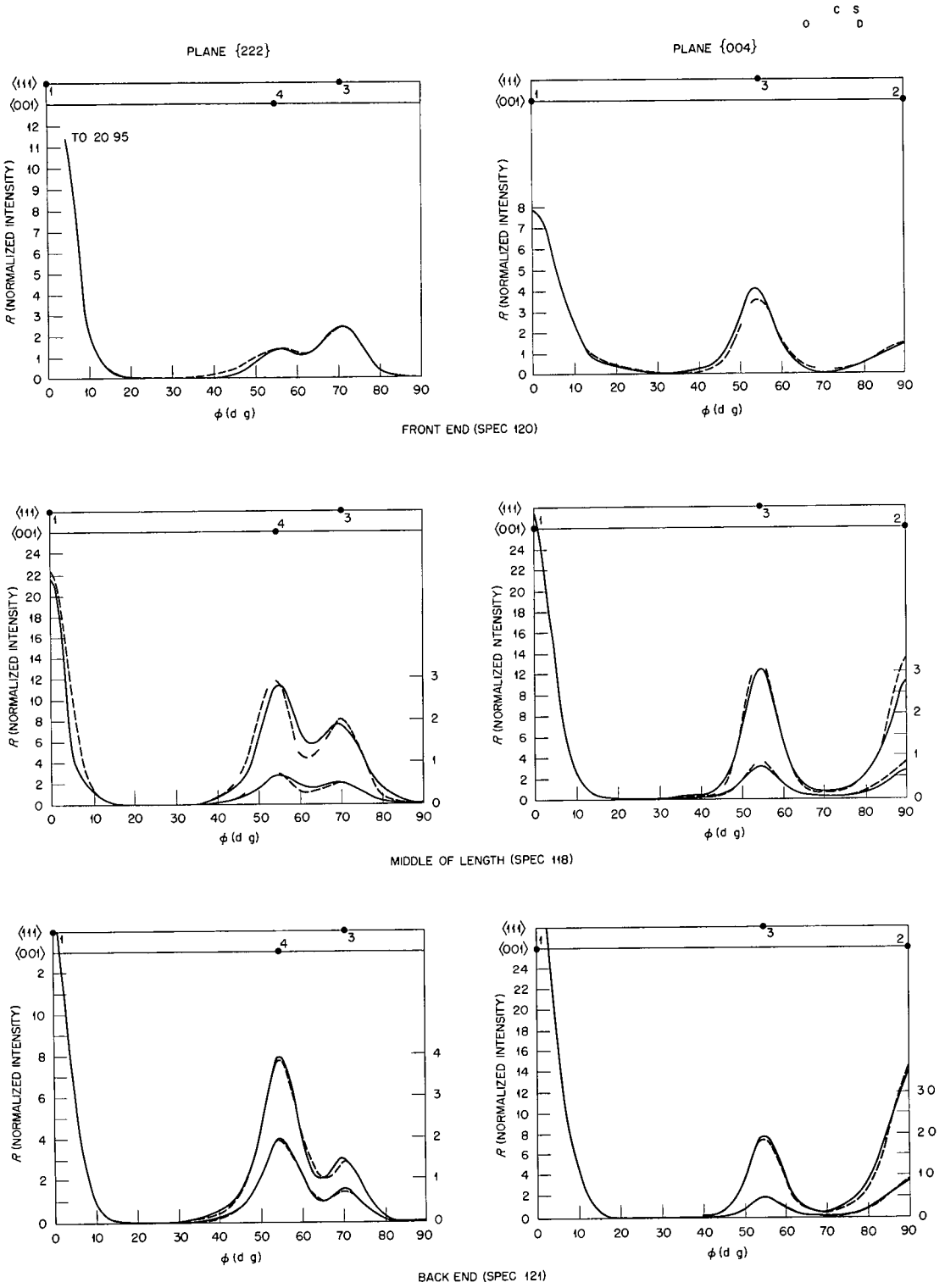

Fig 2 Pole Distribution Charts for 0 89 in dia As Extruded Aluminum Rod Extrusion temperature, 450°F extrusion speed 0 1 fpm

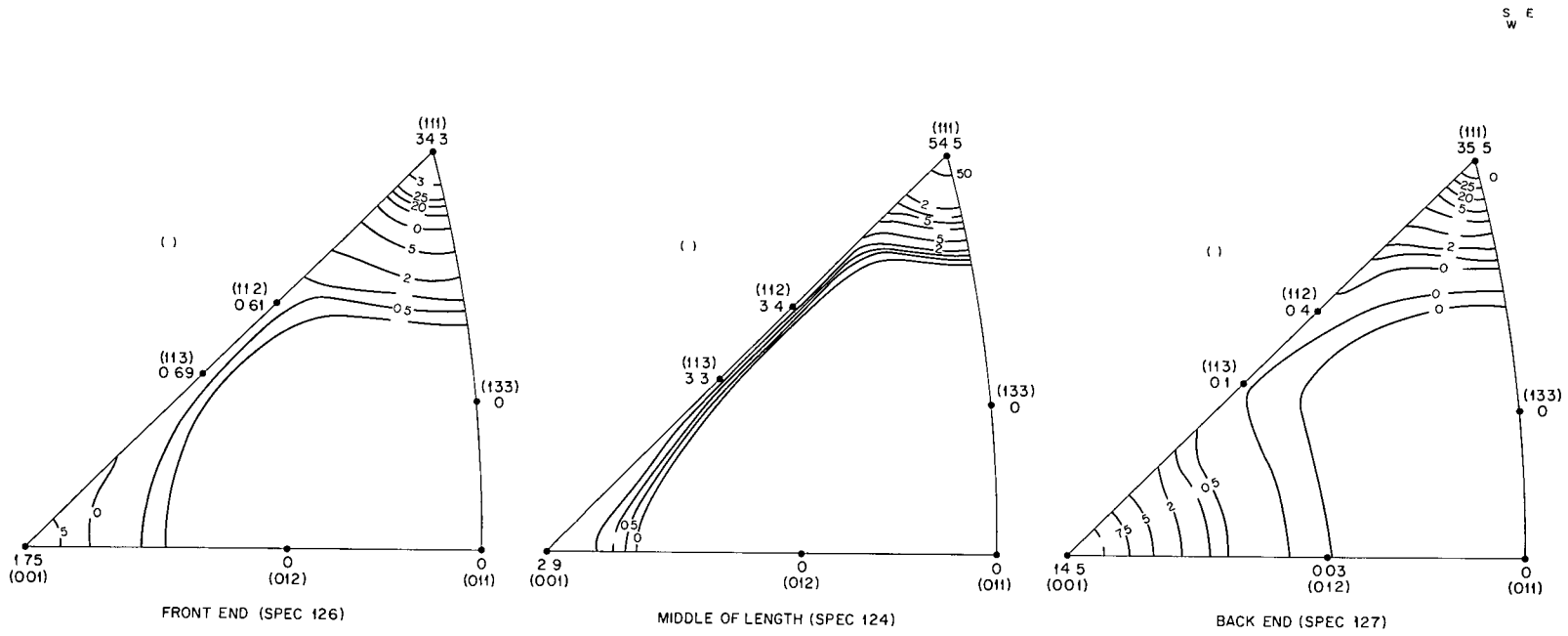

Fig 3 Fiber Axis Distribution Charts for 0 89 in dia As Extruded Aluminum Rod Extrusion temperature 450°F extrusion speed 615 fpm

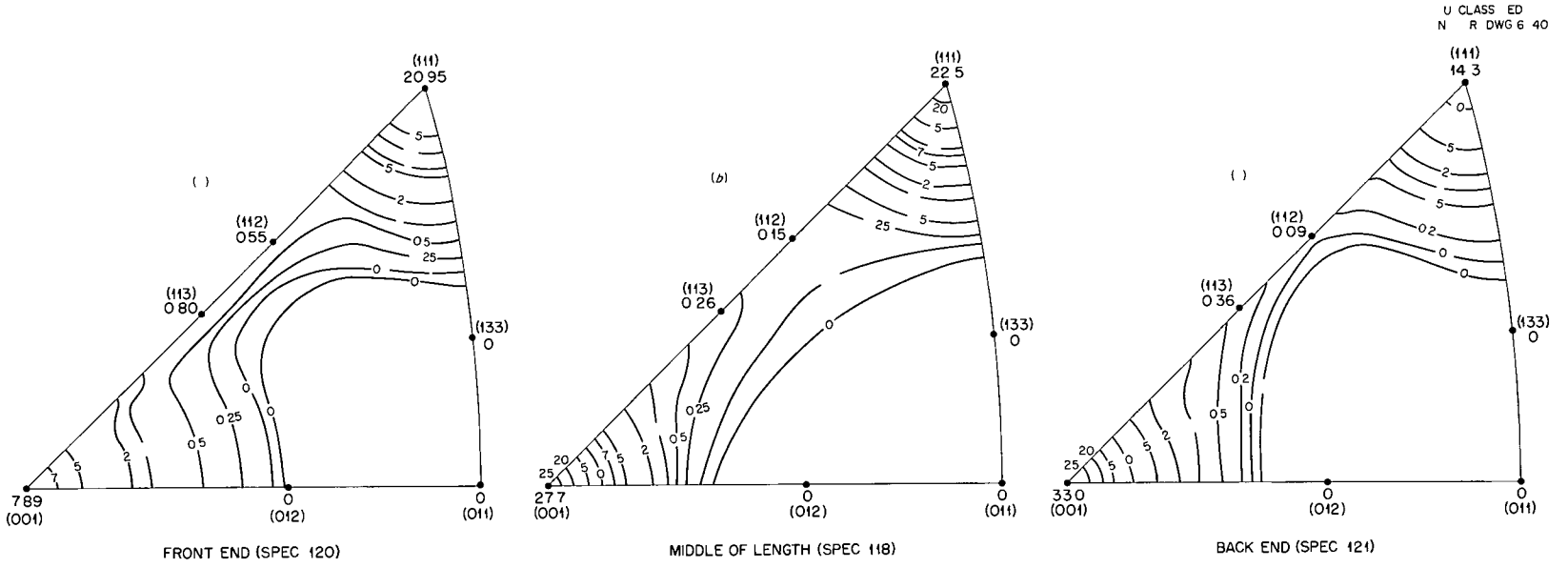

Fig 4 Fiber Axis Distribution Charts for 0.89 in dia As Extruded Aluminum Rod Extrusion temperature 450° F extrusion speed 0.1 fpm

LONGITUDINAL

TRANSVERSE

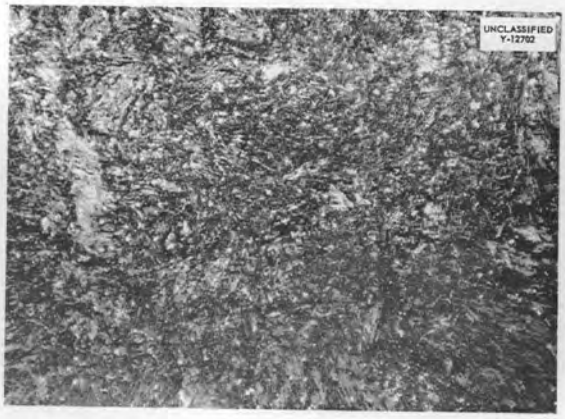

FRONT END (SPEC. 126)

MIDDLE OF LENGTH (SPEC. 124)

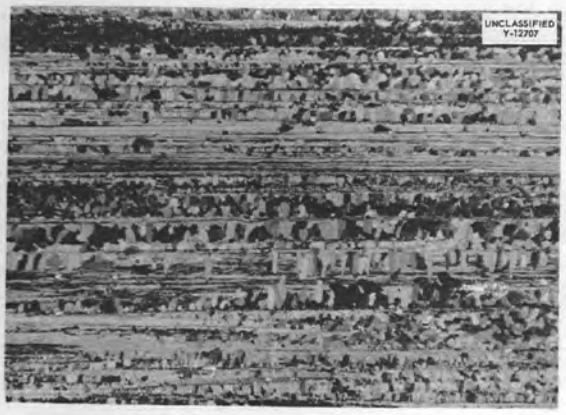

BACK END (SPEC. 127)

Fig. 5. Microstructure of 0.89-in.-dia As-Extruded Aluminum Rod. Extrusion temperature, 450°F; extrusion speed, 615 fpm.

LONGITUDINAL TRANSVERSE

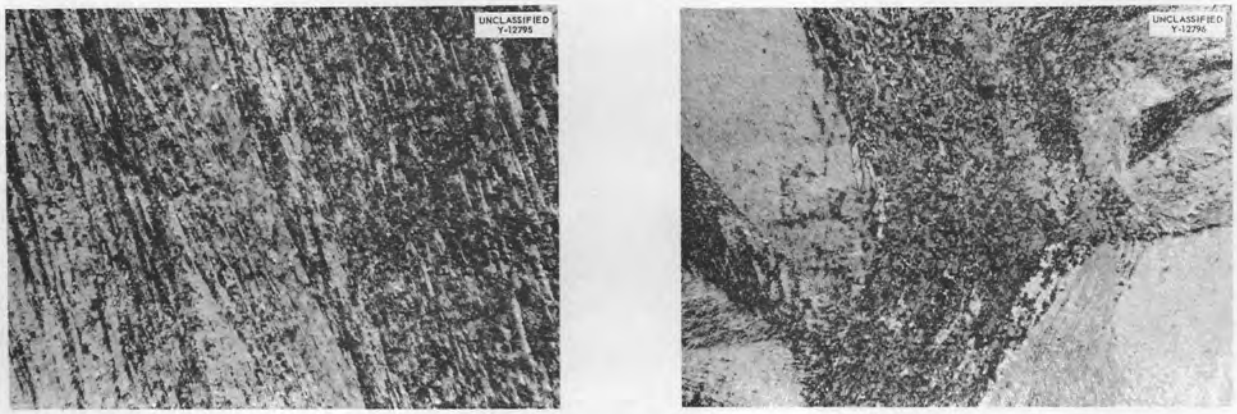

FRONT END (SPEC. 120)

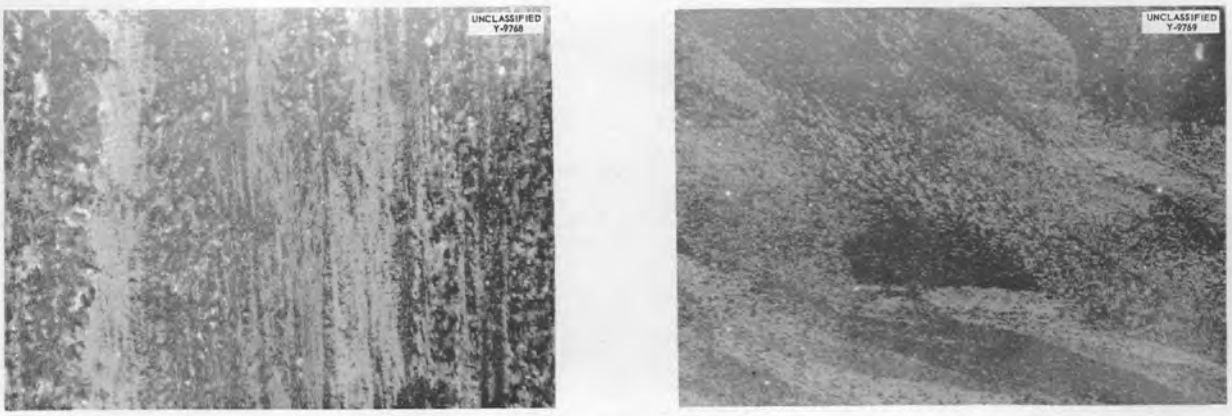

MIDDLE OF LENGTH (SPEC. 118)

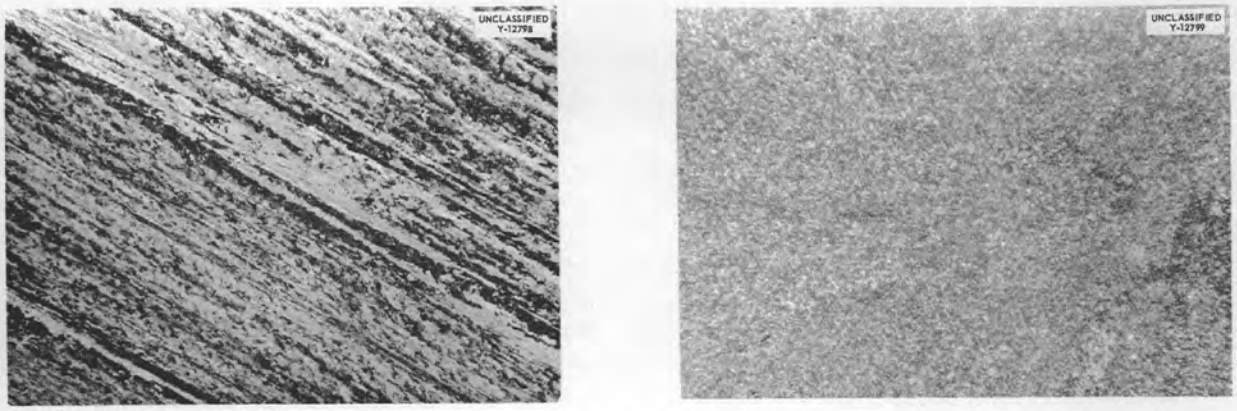

BACK END (SPEC. 121)

Fig. 6. Microstructure of 0.89-in.-dia As-Extruded Aluminum Rod. Extrusion temperature, 450°F; extrusion speed, 0.1 fpm.

FRONT END (SPEC. 126)

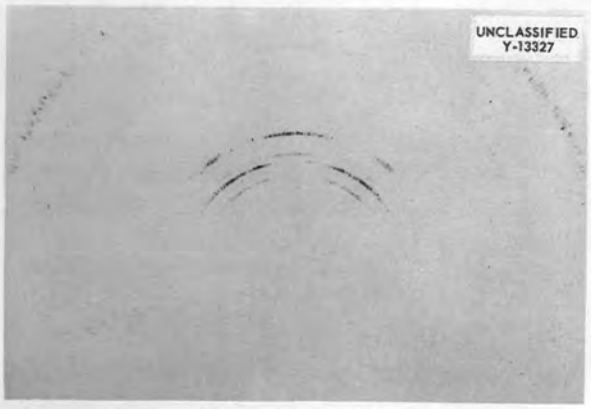

BACK END (SPEC. 127)

Fig. 7. X-Ray Transmission Photograms of 0.89-in.-dia As-Extruded Aluminum Rod. Extrusion temperature, 450°F; extrusion speed, 615 fpm.

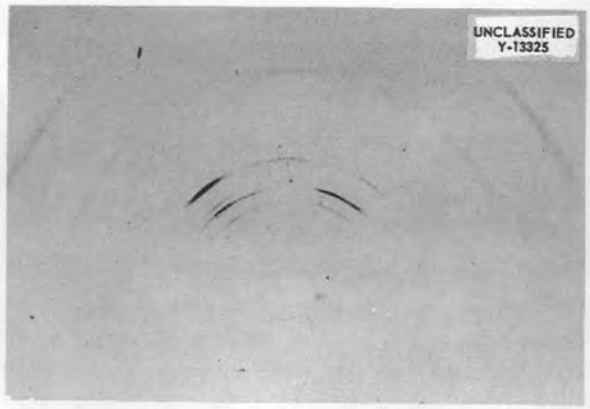

FRONT END (SPEC. 120)

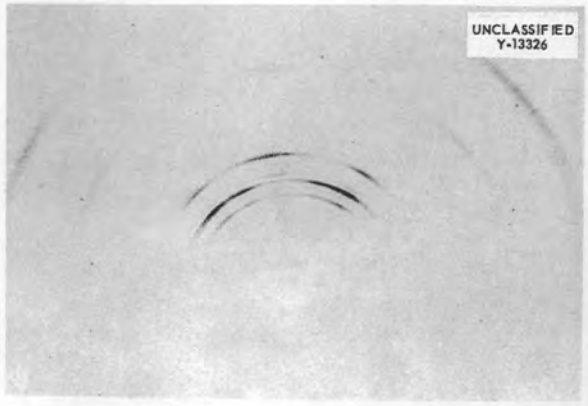

BACK END (SPEC. 121)

Fig. 8. X-Ray Transmission Photograms of 0.89-in.-dia As-Extruded Aluminum Rod. Extrusion temperature, 450°F; extrusion speed, 0.1 fpm.

greater from the front to the back end of the extruded rod, as a result of increase in temperature, and with decrease in extrusion speed, as a result of the increase in time before the extrusion enters the water spray, as is observed.

REPRESENTATION OF THE SHEET-TEXTURE TYPE OF PREFERRED ORIENTATION

C. J. McHargue L. K. Jetter

In a previous report[1] a thorough appraisal was made of methods of representing the fiber-texture type of preferred orientation. Analysis of preferred-orientation data by the conventional pole-figure method is difficult, if not uncertain, especially when the texture is complicated or not well developed. It was shown that, when the orientation distribution of the poles of the diffracting planes with respect to the fiber axis, as given by the pole figures or pole charts, is converted into orientation distribution of the fiber axis with respect to the crystallographic axes, the type and degree of preferred orientation is represented much more precisely. This new method of representation gives directly the most preferred crystallographic direction of the fiber axis for each component of the texture, the symmetry of distribution about these preferred directions, and the relative volumes of material associated with the various components.

The usual method of analysis of sheet texture data gives the same ambiguities It has been found to be instructive however to apply the fiber texture analysis to the sheet texture type of preferred orientation Some reference axis in the sheet is treated as a fiber" axis, and a fiber" texture is induced by rapidly rotating the x ray diffraction specimen about this reference axis while the specimen is scanned through ϕ, the angle between the reference axis and the dif fracting plane pole The axis distribution chart deduced from the pole distribution charts obtained in this way for each of the three reference axes of a sheet – the rolling normal and transverse directions – gives the desired data

With the use of this method some samples of cold rolled 65 35 brass sheet and of cold rolled aluminum sheet were examined Pieces of each sample were bonded with adhesive to produce laminates sufficiently thick for 0 45 in dia spherical diffraction specimens to be prepared Pole distribution data were obtained by the spec trometric method described previously [3 4]

The pole distribution charts (R vs ϕ) for the {111} and {002} planes for the brass sheet are given in Fig 9 The axis distribution charts (T vs ϕ β) deduced from these pole distributions are given in Fig 10 The pole distributions calculated from these assumed axis distributions are compared with the experimental curves in Fig 9

The more preferred crystallographic directions of the rolling direction are the <112> and the <001> The axis density falls off symmetrically and rapidly from the peak at <112> but asym metrically along the <$\bar{1}$10> zone from the peak at <001> The more preferred directions of the normal direction are the <011> and the <111> The most preferred direction of the transverse direction is the <111> although the axis density at <011> is also high These charts are con sistent with the assumption of the following ideal textures {011}<$\bar{1}$00> {011}<$\bar{2}\bar{1}$1> and {111}<1$\bar{2}$1> These are illustrated on the stereographic projection in Fig 11 The best previous determination of the texture of cold rolled brass sheet revealed only the {011}<$\bar{2}\bar{1}$1> com ponent

The pole distribution charts for the {111} and {002} planes for the aluminum sheet are given in Fig 12 and the axis distribution charts in Fig 13

The most preferred direction of the rolling direction is near <334> The axis density falls off symmetrically and rapidly from this peak The most preferred direction of the normal direction is not located at any low index direction – it is about 2 5 deg from <123> The axis density falls off asymmetrically from this peak The most preferred direction of the transverse direction is <133> The ideal texture is thus {123}<$\bar{4}\bar{3}$3> and is illustrated on the stereographic projection in Fig 14 The preferred crystallographic di rections lie 90 deg from one another as is re quired for the determination to be consistent Also illustrated in Fig 14 is the ideal texture determined by previous investigators using conventional pole figure techniques

It is quite evident that axis distribution charts provide a very satisfactory means of representing data not only of the fiber texture type but also of the sheet texture type of preferred orientation They give the desired information directly and precisely, and many features and details not readily discernible from the pole distribution charts are plainly evident

PURIFICATION OF ZIRCONIUM BY ZONE MELTING

G D Kneip J O Betterton

Isothermal heat treatment of zirconium and the establishment of the resulting phases present in equilibrium in the vicinity of the $bcp \rightarrow bcc$ tran sition temperature provide an extremely sensitive method of determining the over all impurity content of the material Studies of a number of batches of grade 1 zirconium crystal bar show a two phase region approximately 40°C wide (834–875°C) in the least pure and 20°C wide (855–875°C) in the most pure materials

For the study of the binary alloy systems of zirconium which exhibit very limited solubility of the alloying element in zirconium or which have eutectoid or peritectoid temperatures near the zirconium transition temperature a source of metal containing fewer impurities than grade 1 zirconium crystal bar is highly desirable

Because of the reactive nature of zirconium it appears that an investigation of the zone melting might be particularly fruitful because of its relatively high purification factor and because the material need not be in contact with a contami nating crucible

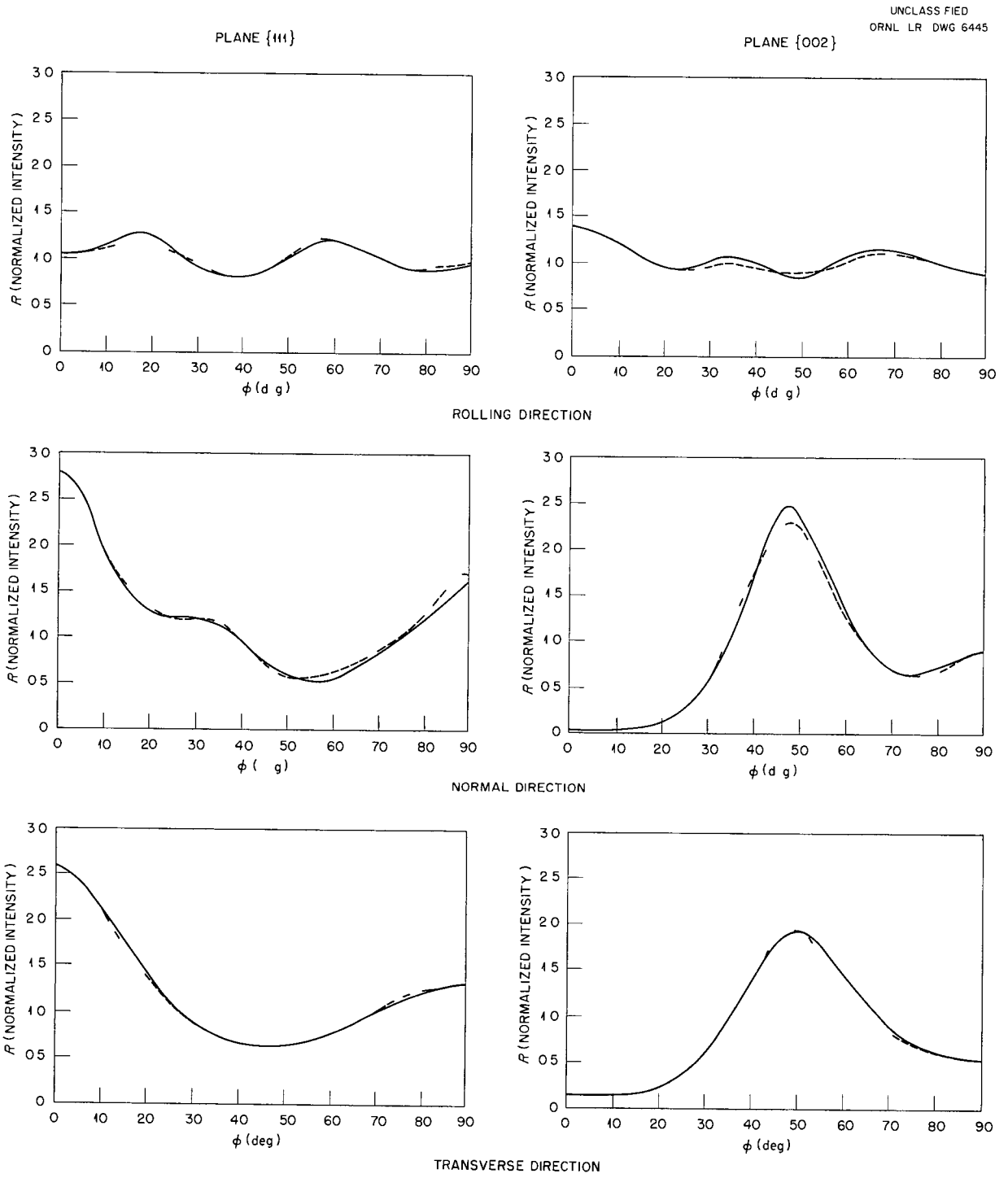

Fig 9 Pole Distribution Charts for 0 057 in Thick Cold Rolled 65 35 Brass Sheet (Specimen 110Z)

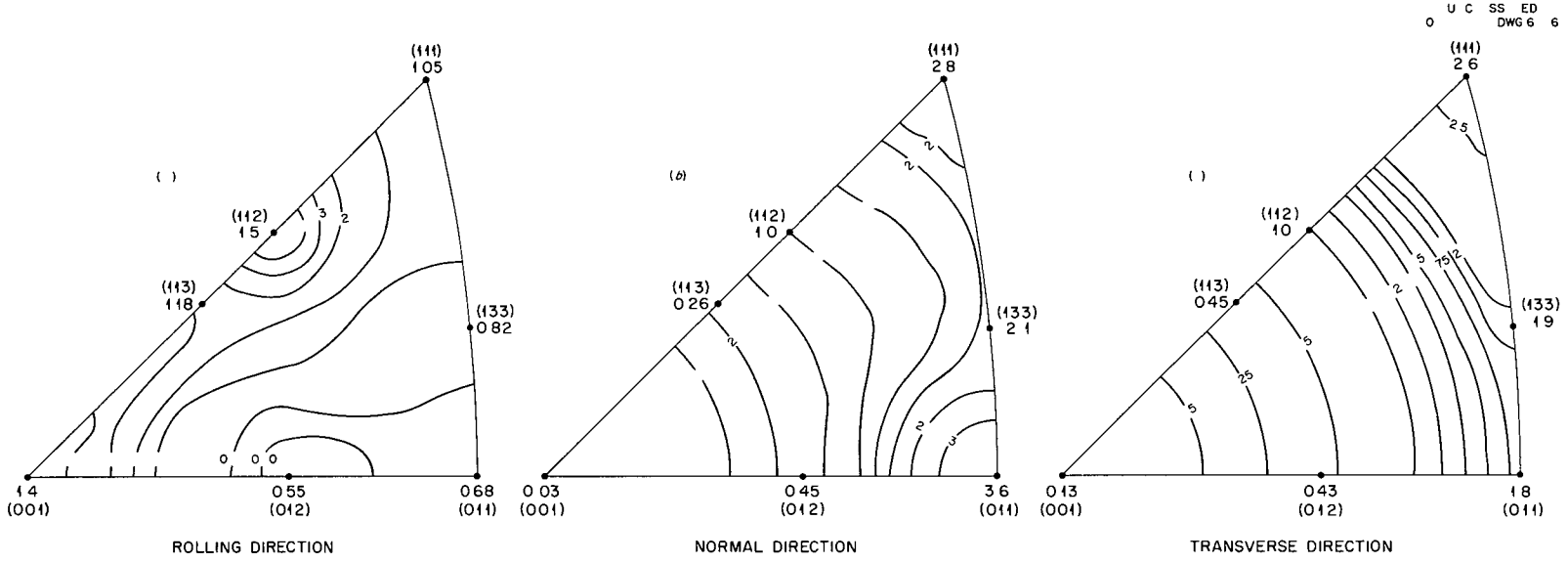

Fig 10 Axis Distribution Charts for 0 057 in Thick Cold Rolled 65 35 Brass Sheet (Specimen 110Z)

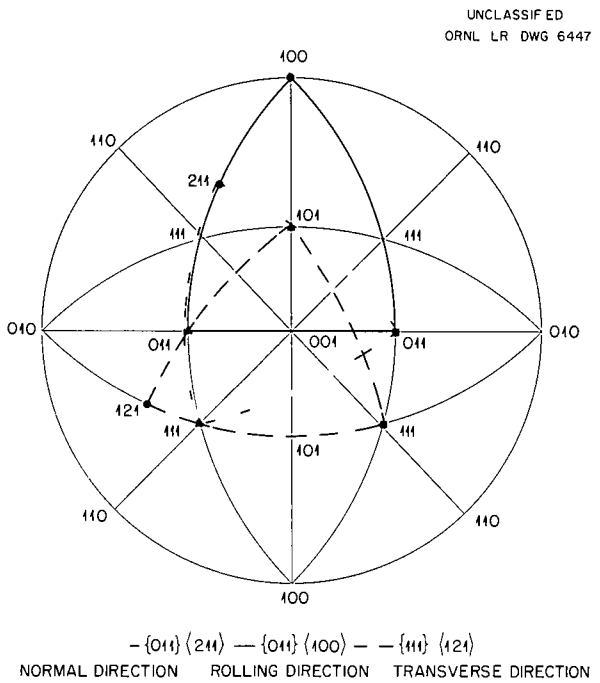

Fig 11 Ideal Textures for Cold Rolled 65 35 Brass Sheet

According to Keck Green and Polk [5] the maximum radius rod which will support a stable floating zone is given by

$$x_m = 0\ 65 \left(\frac{2\alpha}{\rho g}\right)^{1/2}$$

where α is the surface tension and ρ the density of the material Although the value of the surface tension of zirconium has not been reported in the literature it can be estimated from the shape of ingots which have been arc melted and allowed to solidify on a relatively flat surface Thus considering a mass of liquid the surface energy must equal the potential energy and assuming that the mass takes the form of an oblate spheroid as a result of the forces of surface tension and gravity then

(1) $$\alpha A = mgx$$

where

α = surface tension
A = area
m = mass of the liquid
g = gravitational constant
x = distance from the center of mass to the bottom of the spheroid

The area of the spheroid can be expressed as a function of its major and minor axes a and b, as

$$A = 2\pi a^2 + \pi \frac{b^2}{e} \ln \frac{1+e}{1-e}$$

where

$$e = \frac{\sqrt{a^2 - b^2}}{a}$$

and the mass can be expressed as a function of the density ρ and the volume of the spheroid as follows

$$m = \rho V = \rho \frac{4}{3} \pi a^2 b$$

Thus Eq 1 can be rewritten as

$$\alpha = \left(a^2 + \frac{b^2}{e} \ln \frac{1+e}{1-e}\right) = \frac{4}{3} \rho g a^2 b$$

or the surface tension α is

$$\alpha = \frac{\frac{4}{3}\rho g a^2 b}{a^2 + (b^2/e) \ln [(1+e)/(1-e)]}$$

$$= \frac{8360 a^2 b^2}{2a^2 + (b/e) \ln [(1+e)/(1-e)]}$$

where a and b are the major and minor axes respectively of the spheroid in centimeters and the density of zirconium has been taken to be 6 4 g/cm^3

With the use of this equation the value of the surface tension has been computed for a number of arc cast buttons of zirconium The values observed show some dependence on the size of the ingot as shown in Fig 15 probably because the melts were not actually spheroids and because the melts were made in a depression of hemi spherical shape in the hearth The value of the surface tension of zirconium extrapolated to zero volume to eliminate these effects is found to be 220 dynes/cm at the melting point

The maximum radius then for rods at equal radii which supports a stable floating zone of

[5] P H Keck M Green and M L Polk *J Appl Phys* 24 1479 (1953)

UNCLASSIFIED
ORNL LR DWG 6448

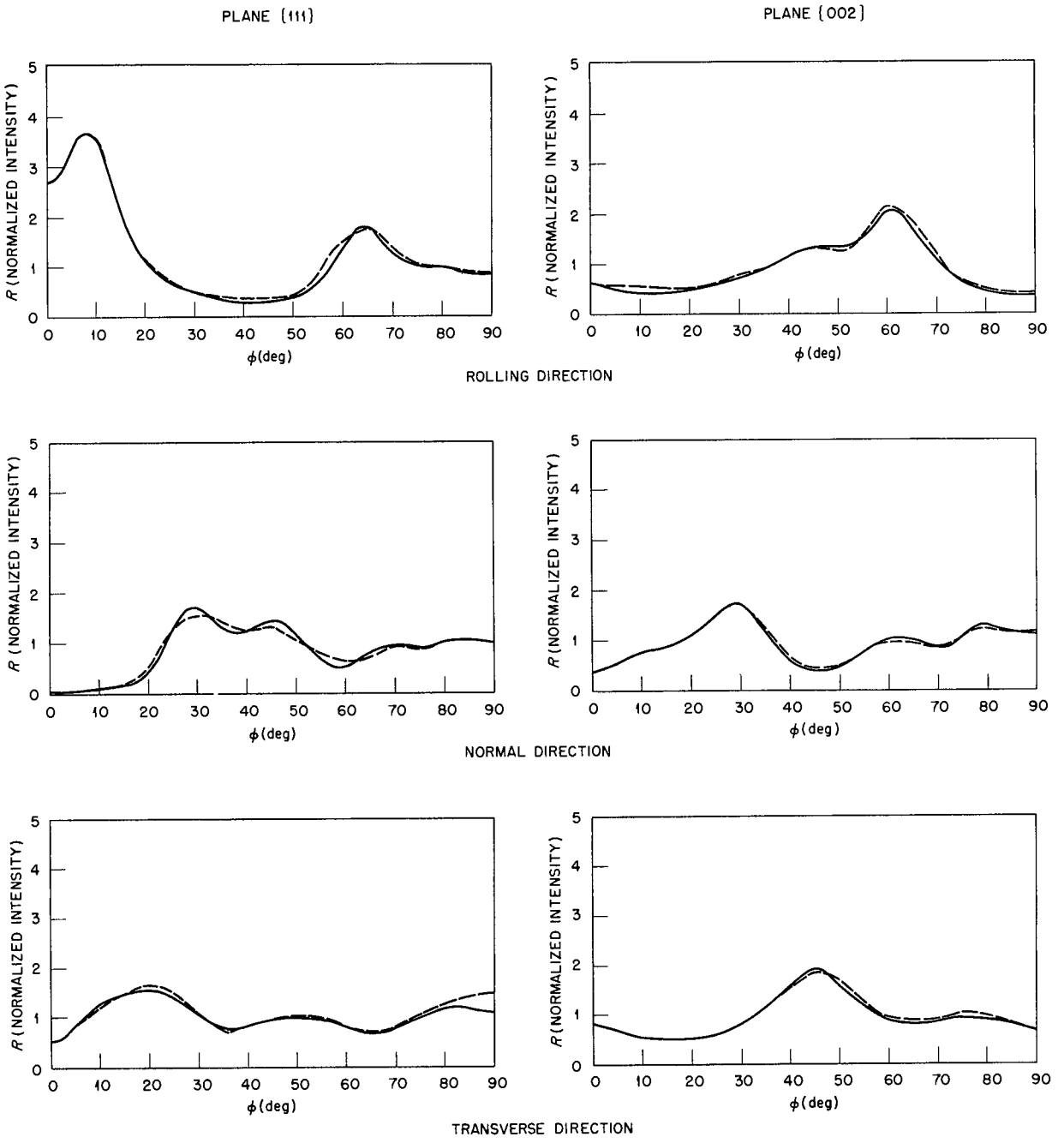

Fig 12 Pole Distribution Charts for 0 046 in Thick Cold Rolled Aluminum Sheet (Specimen 111Y)

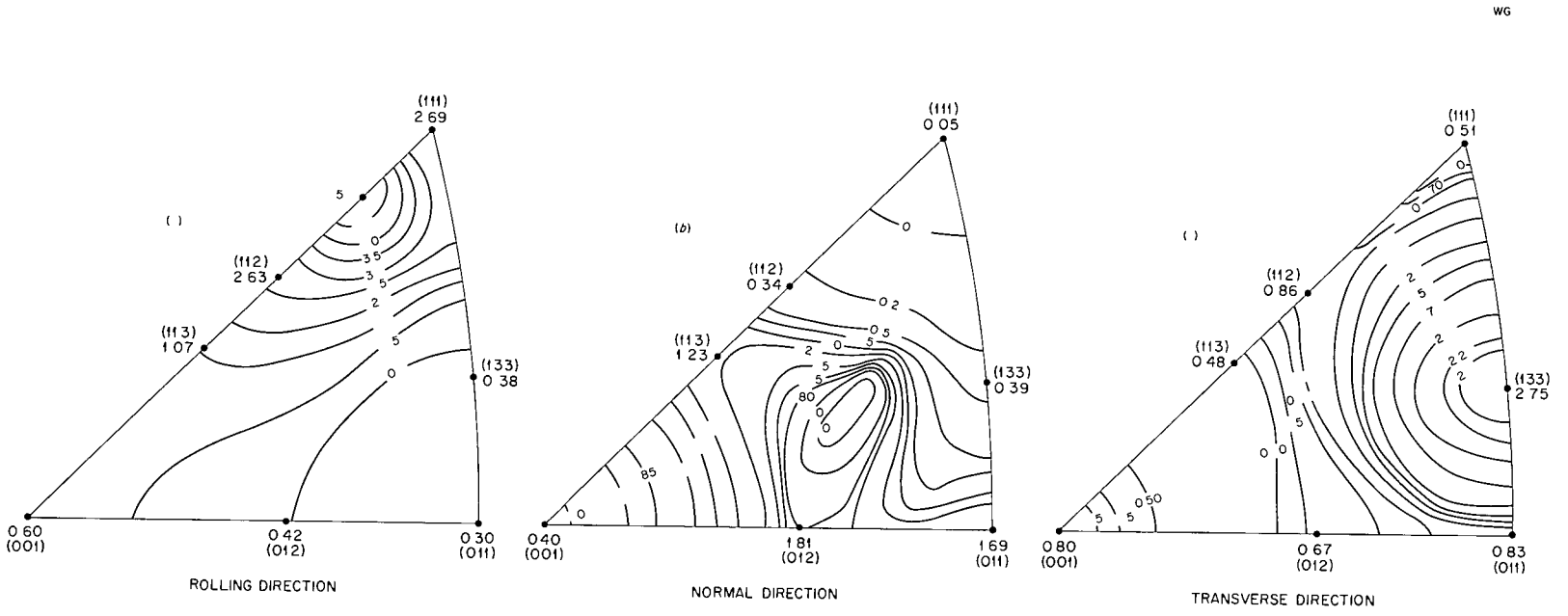

Fig 13 Axis Distribution Charts for 0 046 in Thick Cold Rolled Aluminum Sheet (Specimen 111Y)

zirconium occurs for

$$r = 0.65 \left(\frac{2\alpha}{\rho g}\right)^{1/2} = 1.7 \text{ mm}$$

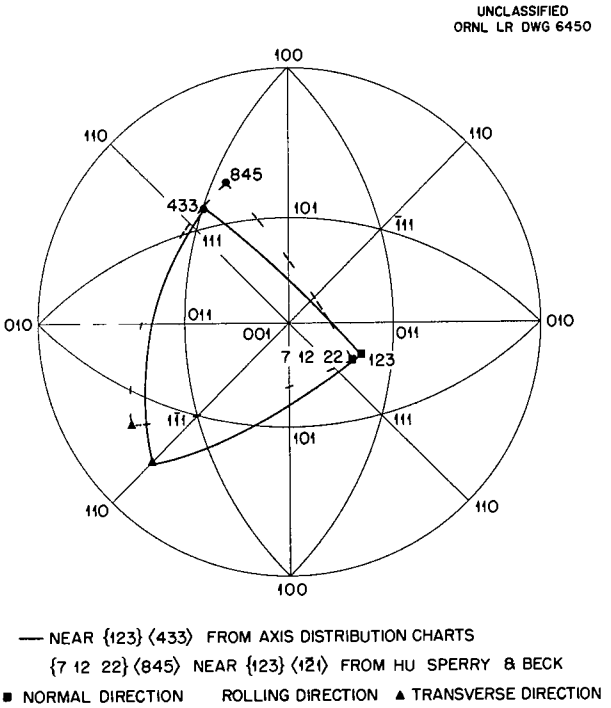

Fig 14 Ideal Textures for Cold Rolled Aluminum Sheet

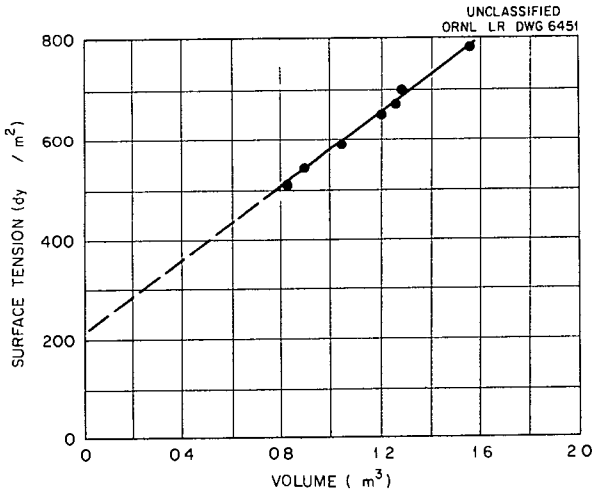

Fig 15 Surface Tension of Zirconium as Calculated from Major and Minor Axes of Arc Melted Getter Buttons vs Button Volume

Thus for zirconium the production of stable floating molten zones is possible for rods approximately 3.5 mm (1/8 in.) in diameter and smaller.

If iron is assumed to be the sole impurity affecting the zirconium $\alpha \rightarrow \beta$ transition, then from the zirconium iron diagram[6] Fig. 16 it can be seen that an iron concentration of only 50 ppm will produce a two phase region nearly 20°C wide and that the iron content must be reduced to about

[6] *The Reactor Handbook*, vol. 3, p. 567. Technical Information Service, AEC, 1953.

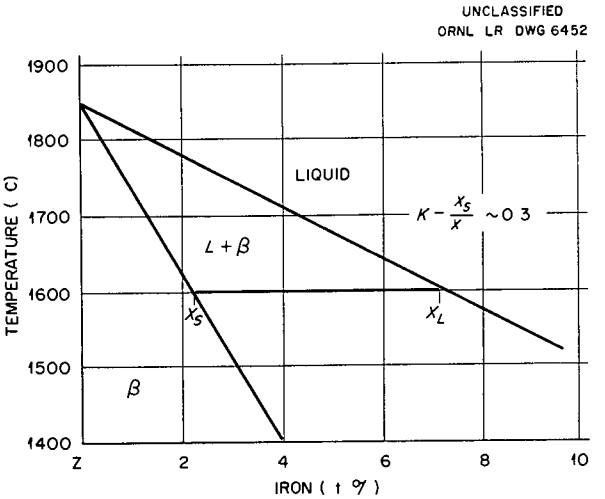

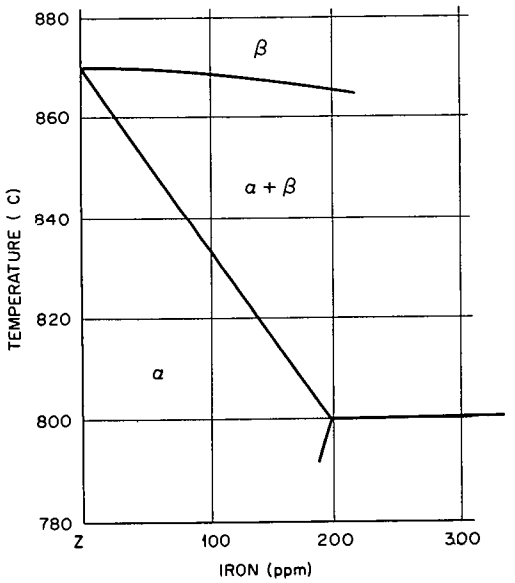

Fig 16 Portions of Zirconium Iron Phase Diagram

15 ppm to reduce the extent of the two phase region to 5°C For the case of iron in zirconium the distribution coefficient k, the ratio of the solute concentration in the solid to that in the liquid is about 0 3

According to Lord,[7] the impurity concentration after one pass $c_1(a)$ as a function of the number of zone lengths melted a is given by

$$c_1(a) = C_0[1 - (1 - k)\, e^{-ka}]$$

and after successive passes

$$c_2(a) = c_1(a) - (1 - k)C_0\, e^{-ka}\,[1 - e^{-k}\,(1 - ka)]$$

$$c_3(a) = c_2(a) - (1 - k)C_0\, e^{-ka}\left\{1 - e^{-k}\,(1 - ka) - k\, e^{-2k}\left[(1 - ka) + \frac{a}{2}(2 - ka)\right]\right\}$$

Figure 17 shows the impurity content vs distance along the bar for one pass through three passes as calculated from these equations A very few passes of the molten zone over the zirconium bar should reduce the iron content or the content of a similar impurity, at the point at which the molten zone is started to such an amount as to be undetectable as a two phase region after isothermal annealing

Movement in the opposite direction occurs for impurities such as oxygen and carbon which raise the melting point Thus in order to obtain relatively pure material it may be necessary to make quite a number of passes and then crop both ends of the ingot

A preliminary experiment conducted with an available 5 mm dia zirconium rod showed the floating zone to be on the verge of stability as

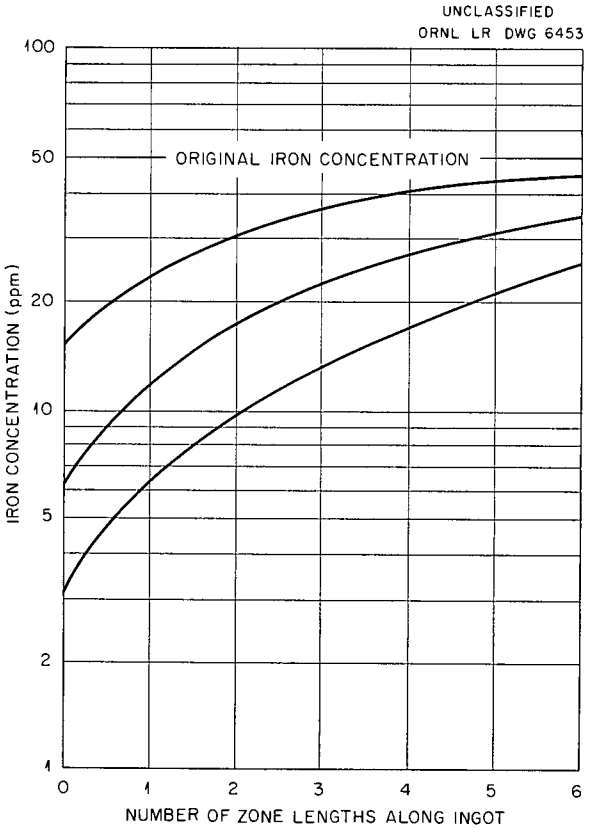

Fig 17 Impurity Concentrations After Zone Melting (k = 0 3)

had been predicted On one specimen three passes were made successfully During the fourth pass however the rod parted at about the mid position owing to the irregularities in diameter caused by the first three passes Figure 18 shows a rod after two passes of the molten zone

The experimental apparatus is illustrated in Figs 19 and 20 Three millimeter diameter zirconium rod which should support a stable zone, is being fabricated for further experiments

[7] N W Lord *J Metals* 5 1531 (1953)

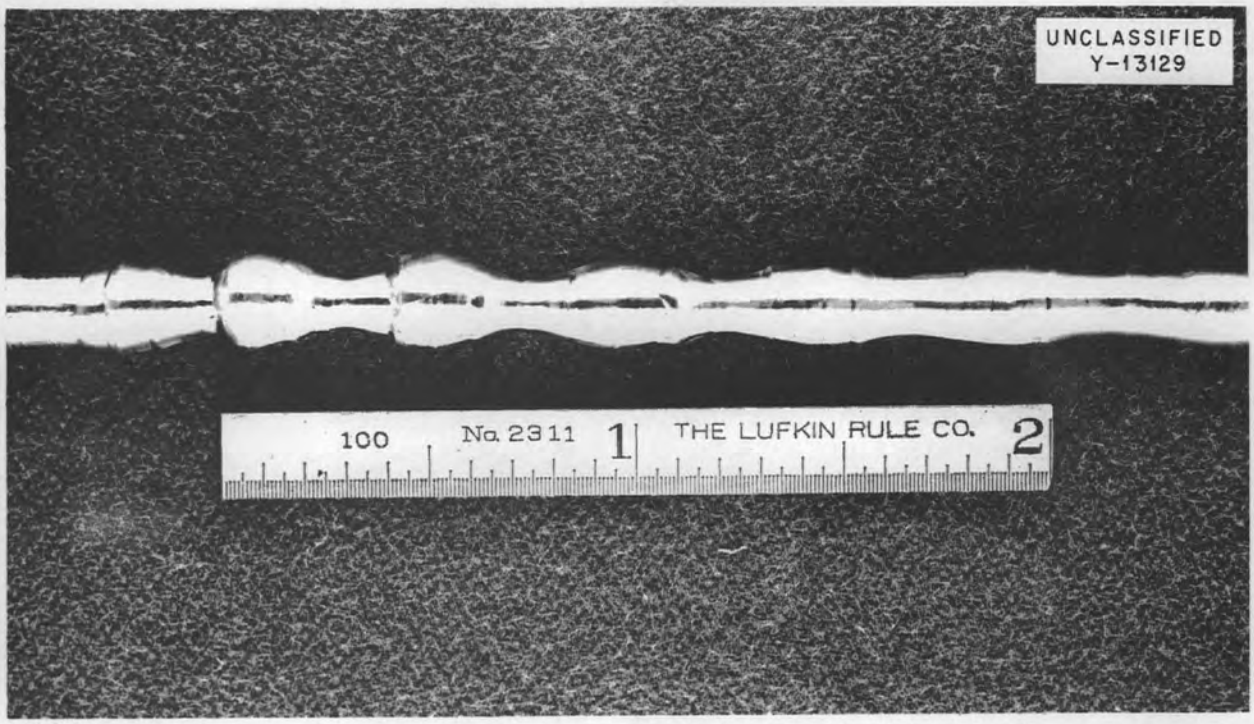

Fig. 18. Arc-Melted Zirconium Rod.

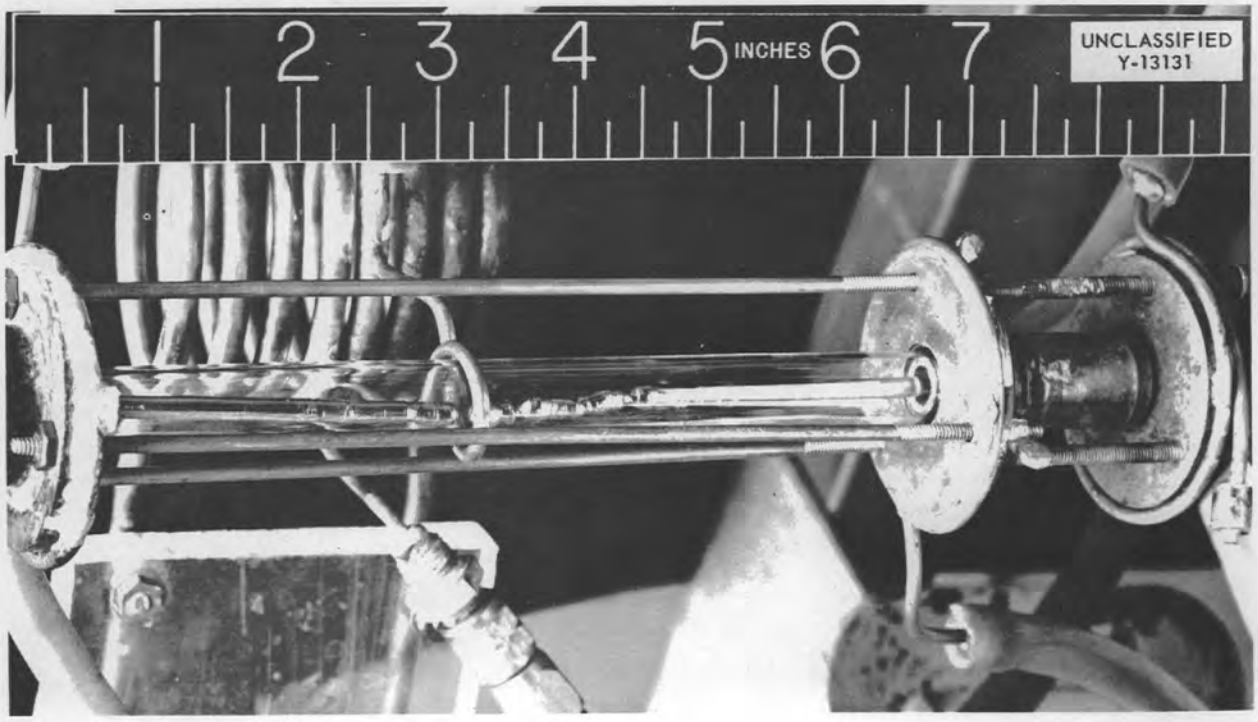

Fig. 19. Zone-Melting Furnace.

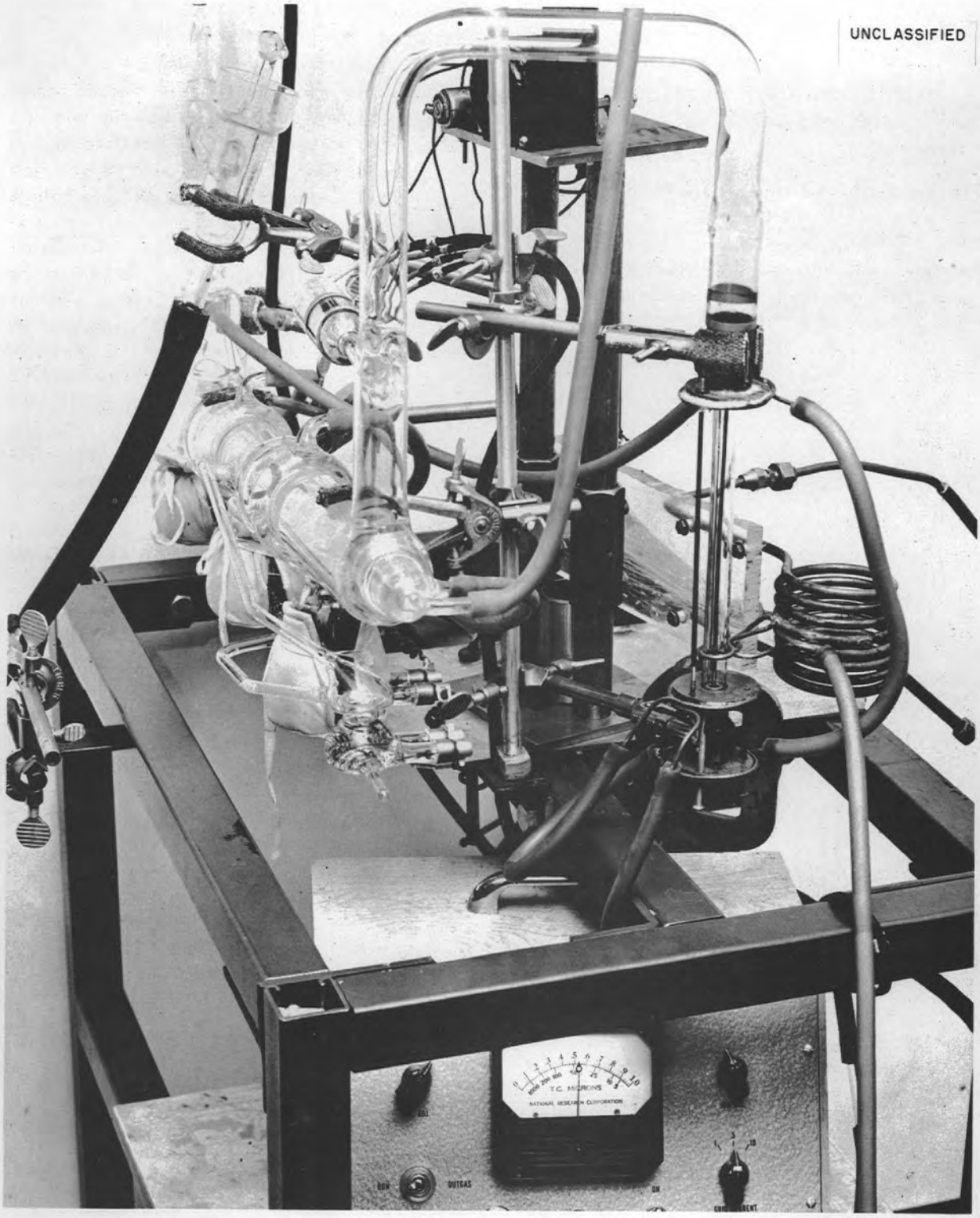

Fig. 20. Zone-Melting Equipment, Showing Traveling Work Coil.

PHYSICAL METALLURGY OF REACTOR MATERIALS

E J Boyle

TRANSFORMATION KINETICS OF ZIRCONIUM BASE ALLOYS

M L Picklesimer E E Stansbury

Phase diagram studies have shown the presence of a eutectoidal transformation in the Ag Zr system Transformation kinetics studies of these alloys have been initiated in an effort to determine whether improved mechanical properties may be derived from isothermal transformation of zirconium base alloys

Several eutectoid Ag Zr ingots of nominal 3 5 at % Ag have been arc cast in a consumable electrode arc furnace for use in studying the transformation kinetics of the Ag Zr eutectoid [1] Single melt ingots were not sufficiently homogeneous to provide enough material for the transformation studies One double melted ingot appeared to be homogeneous but it cracked when it was rolled Transformed specimens indicated that the ingot was contaminated although the contaminant has not been revealed by chemical analysis

It has been necessary to use single melt ingots to determine some of the characteristics of the transformation kinetics Three types of transformation products have been identified These are (1) a pearlitic type transformation product quite similar to pearlite in steels and having a lamellar structure which is nucleated in the grain boundaries and which grows into the grain at an approximately constant temperature (2) a bainitic type transformation product nucleated in the grain boundaries consisting of individual alpha needles surrounded generally by a precipitate presumed to be $AgZr_2$ and growing only in certain directions governed by the original beta grain and (3) a martensitic type transformation product very similar to martensite in steels consisting of fine needles and formed on the quench to room temperature by an apparently diffusionless transformation The progress of the transformation to bainite pearlite, and alpha has been studied at 750 and 800°C The partial TTT diagram is quite similar to that for a hypoeutectoid steel, with the exception that the bainitic type transformation occurs at all temperatures at which the pearlitic type occurs The progress of the transformation at 800°C may be described as follows Alpha first forms in some of the grain boundaries then bainite forms, and then pearlite All may be forming at the same time in the early stages of transformation In the alloys studied so far the alpha formation was complete at 800°C in 3 min and occupied 2% of the volume of the specimen the bainite formation was complete in 5 min and occupied 15% of the volume and the pearlite formation was complete in less than 60 min and occupied the remainder of the volume The formation of alpha and bainite reached completion before 25% of the specimen was transformed The progress of the transformation at 750°C was the same, except that it was faster Unfortunately enough homogeneous alloy was not available for the study to be continued at that time

The tempering of the martensitic structure at 800°C has been studied in another hypoeutectoid ingot of nominal 3 at % Ag Specimens were held for 30 min at 900°C and quenched in mercury in the transformation equipment [1] These specimens were reinserted individually into the center lead pot of the transformation equipment at 800°C for times varying from 15 sec to 24 hr and were again quenched in mercury The hardness of the specimens decreased from the original as quenched hardness of 300 DPH (100-g load) to 235 DPH at 15 sec, 1 min and 5 min and to 190 DPH at 15 min 2 hr and 24 hr The changes in the microstructure were (1) precipitation of the intermetallic compound in the martensite matrix (2) growth and spheroidization of the precipitate, (3) nucleation of new alpha grains in the depleted matrix and (4) growth of the new alpha grains into the depleted martensite matrix until the microstructure consisted of recrystallized large-grained alpha containing dispersed large particles of the intermetallic compound $AgZr_2$ Complete recrystallization of the depleted matrix at 800°C required at least four days Lack of sufficient material of the same composition has prevented further study at other temperatures

Considerable time and effort have been expended in developing metallographic techniques for use

[1] E E Stansbury and M L Picklesimer *Met Semiann Prog Rep April 10 1954* ORNL 1727 p 1

on these alloys Scratch free polishes have not been obtained without considerable polish relief whereas polishing with fine diamond paste leaves undesirable scratches that must be etched out Most polishing is stopped after 4 0 paper has been used and the surface is prepared for etching by chemical polishing with a solution consisting of 50 ml of H_2O 20 ml of HNO_3 5 ml of HCl and 3 ml of HF Two etching solutions have been developed that are satisfactory one working better than the other for specimens in different conditions One consists of the chemical polishing solution with HF replaced by 0 3 g of NH_4F HF and the other is the I_2 and KI etch reported previously [1]

An anodizing procedure based on the procedure and solution reported by Ence and Margolin [2] has been developed for the identification (in bright field illumination) by color of the microconstituents of the zirconium base alloys The solution consists of 20 ml of glycerine 35 ml of H_2O 60 ml of alcohol 5 ml of H_3PO_4 10 ml of lactic acid and 2 g of citric acid the composition not being very critical If the etched specimens are immersed in the solution for 1 to 4 sec (depending on the surface area) at 110 v the colors developed in bright field illumination are as follows martensite yellow pearlite red bainite dark red alpha blue to pink depending on time aged martensite brown to purple and $AgZr_2$ tan to light brown At 20 v for 2 to 10 sec the colors developed are primarily different shades of the same color However fine details of the microstructure obscured by the 110 v anodizing and not revealed by straight etching are revealed by the 20 v treatment Contrast in the microstructure under polarized light is markedly increased by the 20 v treatment The precipitate formed around the bainite needles is revealed by the 20 v treatment and is obscured by the 110 v treatment

Mounted specimens have been successfully polished electrolytically in concentrated HCl at 4 to 10 v by the following procedure Each specimen is completely immersed in the solution and the surface to be polished is situated uppermost a stainless steel wire screen cathode being placed above the specimen The polishing is difficult to control in that a gross unevenness of the surface may develop such unevenness is not too serious for cursory examination at high magnification but is unsatisfactory for low magnification The technique has been successfully used to put zirconium base alloys into solution for chemical analysis without contaminating the solution with the fluoride ion

The automatic feed mechanism for the consumable electrode arc furnace[1] has been completed and installed in the arc furnace Test melts have not as yet been made

SLAGGING EXPERIMENTS ON STAINLESS STEEL FUEL ELEMENTS

J A Milko

Work has been continued on the problem of concentrating the uranium from stainless steel fuel elements by melting the elements under a nonmetallic phase Several different types of nonmetallic phases were used as is indicated below In the work described compacts of UO_2 in a matrix of stainless steel were used to simulate fuel elements

An attempt was made to melt a compact in a graphite crucible under a cover consisting of sodium carbonate and sodium tetraborate but the cover boiled away before the compact melted

When a compact was melted under a slag consisting of 114 g of CaO 60 g of Al_2O_3 and 126 g of SiO_2 the uranium contents of the slag and metal were 11 38 and 0 001% respectively indicating that the UO_2 had been extracted by the slag almost quantitatively The cooled slag was hard and brittle and to extract the uranium from it would probably be difficult

Compacts were melted under slags consisting of CaO SiO_2 and CaF_2 in which the molecular ratio of CaO to SiO_2 was approximately 2 to 1 in an attempt to find a material that would quantitatively extract uranium from the metal phase and that would disintegrate when it was cooled None of the resulting slags disintegrated when they were cooled and the uranium was not extracted completely as is shown by the data in Table 2

A compact melted in a graphite crucible in air under a mixture consisting of 72% CaF_2 and 28% FeF_2 resulted in the extraction of substantially all the uranium into the fluoride phase the metal analyzing 0 001% uranium and the slag 8 57% uranium A test with similar materials melted in a partial vacuum was unsuccessful because too much of the fluoride volatilized In disagreement

[2] E Ence and H Margolin *J Metals* 6 346 (1954)

TABLE 2. RESULTS OF MELTING STAINLESS STEEL–UO_2 COMPACTS UNDER SILICATE SLAGS

No	Slag Composition (%)			U nium Content (%)	
	CaO	SiO_2	CaF_2	Metal	Slag
1	65	35	10	0 14	7 61
2	45	24	31	0 91	20 73
3	45	24	31	0 61	10 46

with the results of former experiments in which compacts were melted under a mixture of CaF_2 and FeF_2 a recent melt made under a mixture of 61% CaF_2 and 39% FeF_2 yielded a metallic button containing 0 93% uranium and a slag containing 17 7% uranium Further experiments are being made in an attempt to explain this discrepancy

A compact melted under a mixture of 71% NaF and 29% FeF_2 resulted in a metallic button con taining only 0 001% uranium and in a slag con taining 11 47% uranium

A test in which a compact was melted under pure CaF_2 resulted in only partial extraction of the uranium the metal contained 0 57% uranium and the slag 8 5% uranium About the same fraction of uranium was extracted when a compact was melted under a mixture of 84% CaF_2 and 16% Fe_2O_3 as is indicated by the resulting uranium content of the metal being 0 68% and that of the slag 11 14%

REDUCTION OF UF_4 WITH ALUMINUM

J A Milko

A number of years ago it was found that uranium aluminum alloys rich in aluminum could be pro duced from metallic aluminum and UF_4 by simply permitting the molten aluminum to reduce UF_4 dissolved in molten cryolite (3NaF AlF_3) When properly carried out the reduction of uranium is substantially complete Because of the possible economy of this method for making alloys for fuel elements with enriched uranium as compared with bomb reduction of UF_4 and then alloying with aluminum a study is being made of the reduction of UF_4 from molten fluorides to produce uranium aluminum alloys A large fraction of the uranium in the salt phase can be reduced and can enter the metal phase because the activity of the uranium in the metal is much smaller than unity for the alloys of interest Work has been done on the production of alloys containing 20% uranium approximately 2 8 at %

Four reductions of uranium from a fluoride phase were made the quantities of materials used are indicated in Table 3 In carrying out each re duction the fluorides were mixed added to a graphite crucible together with aluminum and then heated to a temperature of 1150°C for 10 min The quantities of aluminum and UF_4 were such that an alloy containing 20% uranium would result if all the uranium was reduced The exact amount of recovery was somewhat uncertain however because of the sampling technique used Ad ditional reductions have been made in which an improved sampling practice was used but analyses are not yet available

TABLE 3 REDUCTION OF UF_4 INTO ALUMINUM

No	We ght (g)			U ani m Content (%)	
	UF_4	Al	N F	Metal	Fluorides
1	133	416	149	17 48	1 62
2	133	416	101	18 41	5 9
3	133	416	63	18 99	1 51
4	133	416	44	19 13	1 47

CARBURIZING OF STAINLESS STEEL FUEL ELEMENTS

R E Adams

Carburization of the stainless steel fuel ele ments proposed for the Package Power Reactor is being examined as a method for facilitating ura nium recovery from the spent fuel elements Carburization of these elements causes essentially all the chromium to combine chemically with carbon This effectively removes chromium from the austenitic matrix so that the metal is not passive In this condition, stainless steel may then react with relatively weak dissolving so lutions, and the uranium can be extracted by simple chemical methods

The utility of the carburizing treatment for recovery of uranium is thus intimately related to

subsequent chemical recovery processes Uranium recovery from carburized stainless steels is being studied by J E Savolainen of the Chemical Technology Division who has established the feasibility of a possible recovery process [3]

A technical report covering both metallurgical and chemical studies on this process is being written Only a brief summary of the work will be reported here

Basic steps of a possible recovery process are listed below

1 Carburization to add carbon to the stainless steel

2 Homogenization to diffuse the carbon throughout the steel so that passivity is completely destroyed

3 Dissolution treatment with $CuSO_4$ solution which reacts with the active iron nickel matrix Iron and nickel are taken into solution and copper is plated out Uranium dioxide and chromium carbides are not affected

4 Reaction with nitric acid to dissolve the uranium dioxide and copper The chromium carbides (and some iron carbides) remain as solids which may be stored if they are sufficiently low in uranium

5 Treatment of the nitric acid solution by solvent extraction for recovery of uranium

The following test is described to illustrate techniques and as an example of the uranium recovery that has been obtained from a laboratory test

A specimen of Package Reactor fuel plate (clad with 0 005 in of type 304 stainless steel with a stainless steel core 0 020 in thick containing 34 wt % uranium dioxide) was carburized for 1 hr at 975°C The specimen then containing about 1 4% carbon was homogenized for 1½ hr at 1150°C For dissolution the specimen was treated with boiling $CuSO_4$ solution for 17½ hr The solution was analyzed for uranium The fuel element then coated with copper was treated in boiling 70% nitric acid for 2 hr and the solution was analyzed for uranium The insoluble residue was dissolved in aqua regia and analyzed for uranium

The distribution of the uranium recovered in the three solutions is shown in Table 4

[3] J E Savolainen *Recovery of Uranium from the Spent Stainless Steel Fuel Elements of the Package Reactor* ORNL CF 54 4 39

TABLE 4. DISTRIBUTION OF URANIUM RECOVERED IN THREE SOLUTIONS

Solut on	Tot l Uran um Recove ed (%)
$CuSO_4$ sol tion	0 03
HNO_3 solution	99 25
Residues in aqua reg a	0 72

These results and the techniques used are not typical of optimum procedures, but they do indicate that very high uranium recoveries may be attained

Further work is being done to optimize chemical dissolution techniques and to define the degree of carburization required Thus far, activity tests indicate that maximum dissolution rates are obtained with about 2% carbon other factors however must also be considered

Sufficient carburizing experiments have been made to show that small test specimens of type 304 stainless steel can easily be carburized to contain up to 4% carbon These experiments were made in a 2 in dia ceramic tube furnace by passing an atmosphere of about 18% methane in dry hydrogen through the furnace at about 1½ fpm Under these conditions the relation between carburizing time temperature and amount of carbon absorbed by type 304 stainless steel 0 031 in thick is shown in Fig 21

Carbon can be uniformly distributed throughout the thickness of Package Reactor fuel elements by homogenizing in an inert atmosphere for 2 hr at 1100°C This treatment is required in order to allow uniform and complete reaction between the stainless steel and the dissolving solutions The sensitizing treatment previously used to cause precipitation of the chromium carbide is not necessary since the carbides are formed directly from the austenite

From these results it seems apparent that carbon absorption and diffusion in stainless steel fuel elements will not be major problems in development of this method for recovery of uranium

OXIDIZING OF ZIRCONIUM FUEL ELEMENTS

R E Adams

Metallurgical treatments are being studied in an effort to assist in the recovery of uranium from zirconium type fuel elements

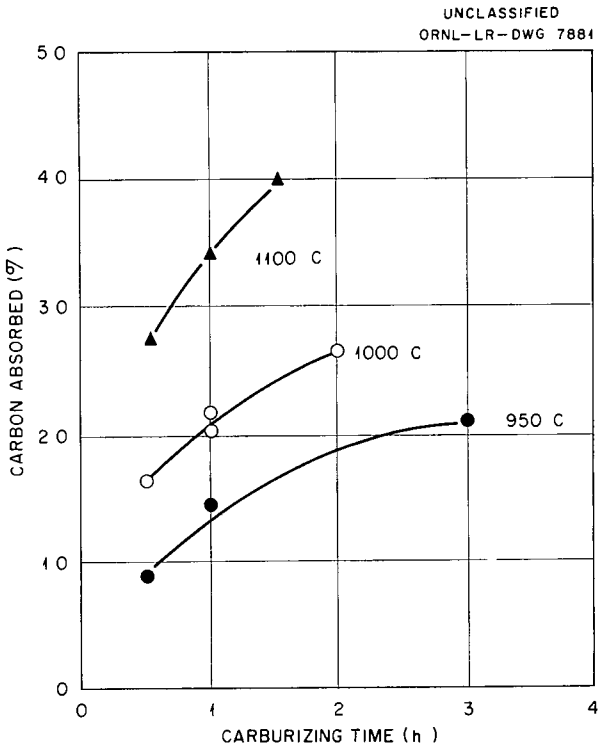

Fig 21 Effect of Time and Temperature on Amount of Carbon Absorbed in 0 031 in Thick Type 304 Stainless Steel

Preliminary work has indicated that it may be possible to oxidize zirconium type fuel elements completely and to treat the resulting oxide powder with nitric acid so that the uranium dioxide is dissolved thus leaving the zirconium dioxide as a waste solid

Oxidizing tests have indicated that specimens of dummy STR fuel plates can be reduced to an oxide powder by heating them in air for about 6 hr at 950°C Extraction with nitric acid has shown that some of the uranium is soluble The completeness of uranium recovery is not known however since uranium analysis of the zirconium dioxide residue has not yet been obtained

METALLOGRAPHIC EXAMINATION OF ALUMINUM SILICON BONDED THORIUM SLUGS

R J Gray

A thorium slug canned in aluminum by the Al Si bonding technique was examined metallographically for R P Wischow of the Chemical Technology Division of ORNL

Considerable difficulty had been encountered in dissolving the canned slug in 13 *N* HNO_3 0 038 *M* NaF and 0 0025 *M* $Hg(NO_3)_2$ Metallographic examination of the as canned slug revealed two intermetallic compounds between the Al Si alloy and the thorium as shown in Figs 22*a* and *b* These compounds were identified by R M Steele by x ray analyses as β $ThSi_2$ and $ThSi_2$ Apparently silicon diffused into the thorium and formed the two compounds It can be concluded that the diffusion was in this direction by the presence of the dark globular shaped ThO_2 within both the thorium and the compound layers A continuous fracture was also present in the intermetallic compound as shown in the photomicrographs (Fig 22) and also by the easily parted smooth bright interfaces of a semicylindrical slug section and aluminum can shown in Fig 23 This fracture would have considerable effect on the heat transfer properties from the thorium to the aluminum can if thorium slugs canned by this procedure were used in a reactor

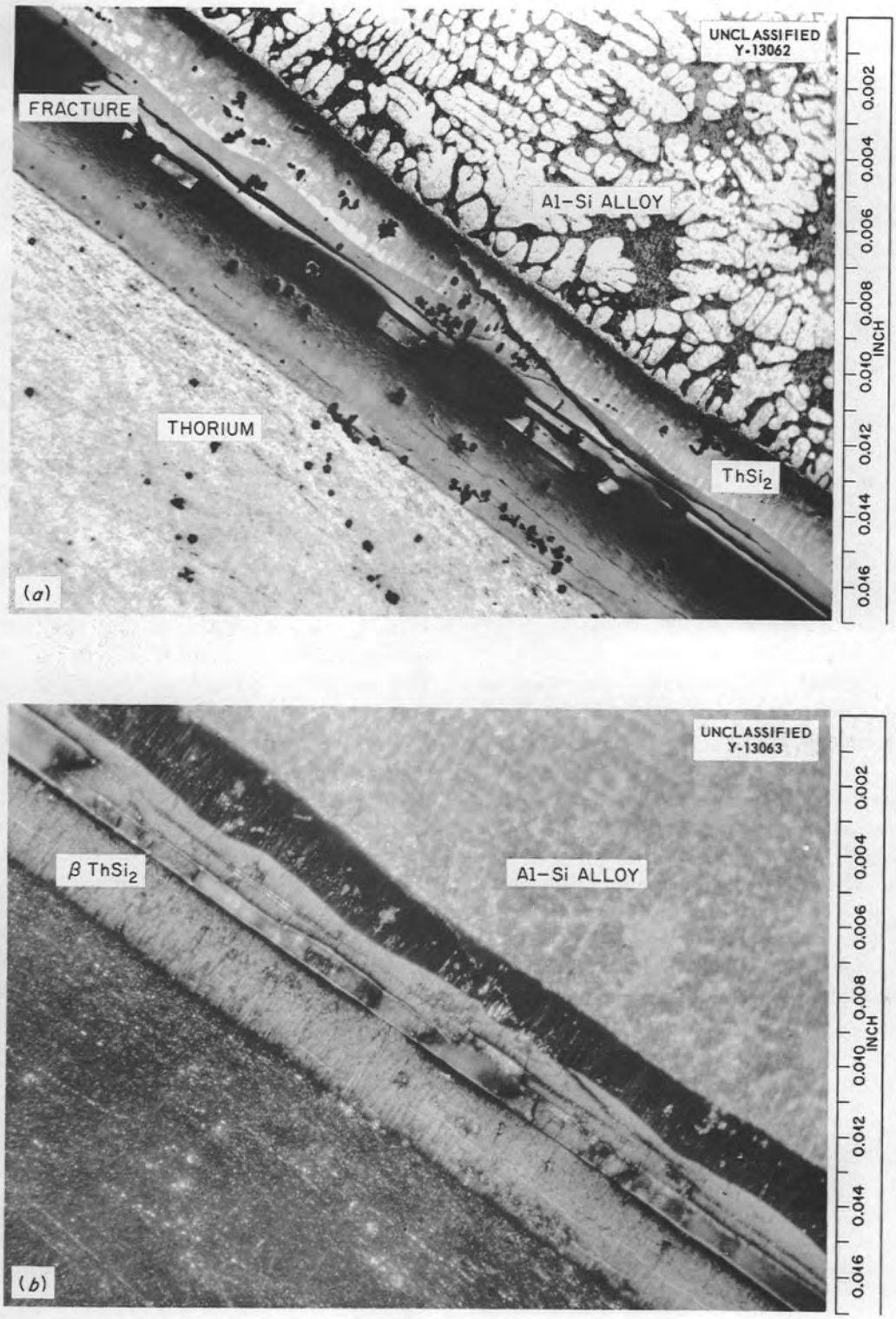

Fig. 22. Photomicrograph of Bond Between Thorium and Al-Si Alloy. (*a*) Bright field; note continuous fracture in intermetallic compounds. (*b*) Polarized light; note two compound layers.

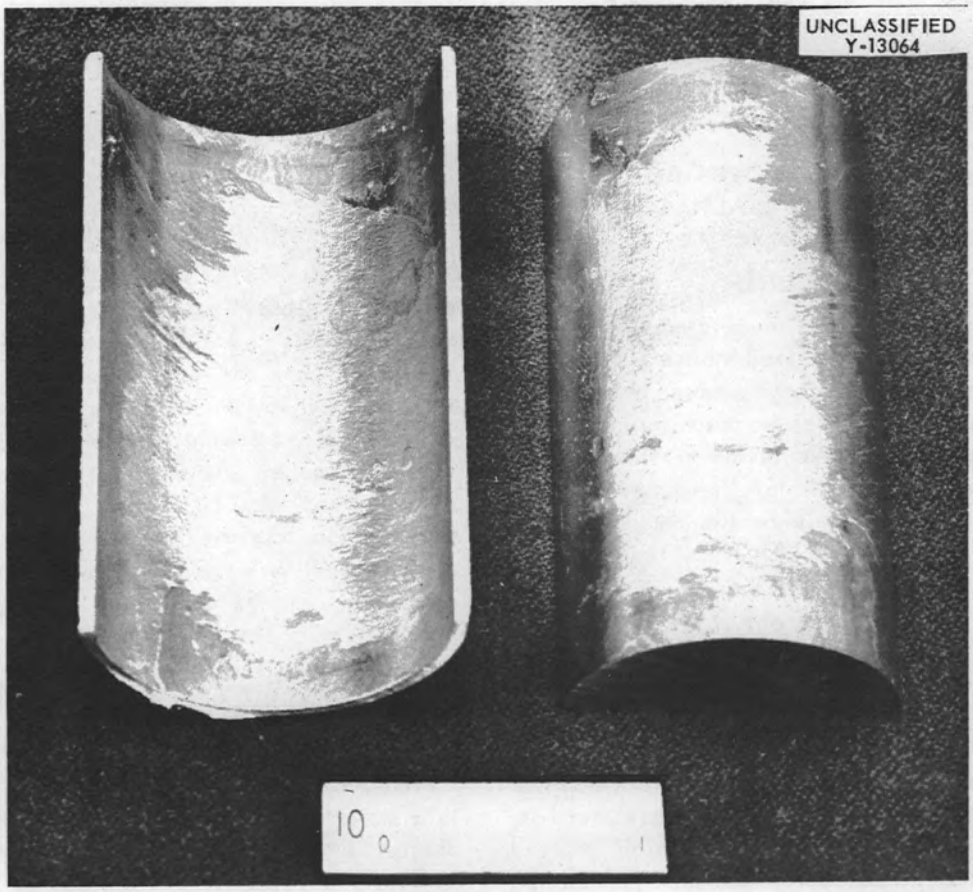

Fig. 23. Semicylindrical Section of Al-Si Bonded Thorium Slug. Note smooth bright surface of aluminum can on left and thorium on right, denoting poor bonding.

CERAMICS RESEARCH

J M Warde
J R Johnson
C E Curtis
L M Doney
S D Fulkerson
R L Hamner
A J Taylor
G D White

DEVELOPMENT OF A CERAMIC FUEL ELEMENT AND ASSOCIATED REACTOR CONCEPTS

Introduction

The advantage of high temperatures in reactor power systems can be realized by use of refractory ceramic materials Satisfactory power plants using gas coolants at high temperatures are an engineering reality Because of the brittle nature of ceramics and the fact that their corrosion resistance to high temperature liquids is not any better than that of metals in general liquid cooling of ceramics involving plumbing systems is not practical at present It was early established therefore that the most compatible and practical high temperature system would be a gas cooled reactor power plant with ceramic core materials

In the selection of materials for fuel elements and moderator three general criteria were applied

1 low thermal neutron capture cross section
2 optimum physical properties (high thermal conductivity no porosity high temperature strength low expansion high service temperature corrosion resistance to gas coolant)
3 economy (fabricability by standard methods availability of pure raw materials)

A study of known materials indicated that the oxides were generally unsatisfactory because of their pool thermal conductivities and that most carbides nitrides and silicides could not be made nonporous A silicon bonded silicon carbide was chosen for a fuel element material because it more nearly met the above requirements than any other material considered A body of this kind has been made for a number of years by The Carborundum Company under the trade mark name Durhy This product however was unsatisfactory for reactor use because of its porosity and relative inhomogeneity A program was undertaken to produce a satisfactory body containing the necessary fuel and to conduct the required tests

For economy and safety graphite was chosen over beryllium oxide as the moderator material This choice then made necessary the use of a closed cycle inert gas system Nitrogen, carbon dioxide and helium have been considered as coolants

Two reactor designs in which these principles and materials are used have been made by ORSORT summer study groups The first a package reactor indicated that a very compact and relatively simple power system could be built with the use of existing equipment The second a power breeder reactor showed that the ceramic fuel element and associated concepts had a good potential in this field also The plant design results in 60 Mw of electric power at 40% over all efficiency and a conversion ratio of 1 0 was obtained with the use of the U^{233} cycle Only equipment which is now available or considered practical was utilized in the design

Summary of Development and Testing

Producing a suitable SiC Si body for reactor use is a major development problem In attempting to obtain a nonporous homogeneous body many materials and techniques have been used The basic method for producing SiC Si invented by The Carborundum Company consists in impregnating a porous carbon body with molten silicon An exothermic reaction occurs simultaneously generating cubic SiC Previously known materials and techniques yielded unsatisfactory bodies so a special program of development was instigated

The porous carbon or graphite body may be obtained in several ways but the method most easily controlled is that of mixing powdered graphite with a material which is partially volatile so that in a subsequent baking step the graphite body formed from such a mix will be porous The additive must also serve as a binder for the formed graphite bodies so that they can be readily handled After baking it must leave a residue which tends to knit the structure together giving the baked product suitable strength This product must be strong so that it can be handled and it must hold together in the impregnation process Of a number of materials tried glucose

has been found to be the most satisfactory so far Such binders as naphthalene Carbowax etc which volatilize completely are unsatisfactory Starches sugars etc on the other hand are generally satisfactory in this respect

Another feature of the initial mix which requires careful control is the grain size Nonporous homogeneous SiC Si with a minimum of unreacted carbon can be produced only by using very fine grained (~1 to 10 μ) graphite particles and then by making certain that the graphite additive mix is also very fine grained before forming the body to the desired shape

Associated with the nature of the binder and grain size is the forming pressure The most satisfactory forming method conceived for producing fuel bearing elements of SiC Si is dry pressing of the powdered mix in a steel die The porosity and thus the impregnability of the body are sensitive to the forming pressure Many of the binders which are otherwise satisfactory are too sensitive to the forming pressure to be practical

The baking process is the simplest and most easily controlled step in the entire operation difficulties arise however from reactions of the fuel materials with water vapor and possibly other gases which are given off as the binder volatilizes Thus uranium carbide readily oxidizes and there are indications of some oxidation of the uranium silicides Also UO_2 may go to U_3O_8 These reactions involve volume changes some of which damage the body The most successful baking process when the fuel materials are either the silicides or the oxides of uranium is a 1000°C treatment in an argon atmosphere

Impregnation is best carried out by using induction heating of a graphite crucible containing the silicon The reaction forming SiC from the porous carbon body is quite rapid if the silicon is near its boiling temperature (1800–2000°C) A slower more controlled impregnation reaction occurs at about 1700°C Less warpage and less tendency to absorb excess silicon are also noted at lower temperatures

Testing of the SiC Si fuel element material should be carried out in the reactor under simulated service conditions Nevertheless, a number of useful tests can be made prior to such an experiment In addition to physical-property measurements an engineering evaluation of both the fuel element and the moderator materials is under way A device has been constructed in which nitrogen is blown over an electrically self heated specimen at high velocity This test will primarily serve to measure erosion corrosion of the graphite With the use of the same electric power source the fuel element specimens are heated in air to destruction by thermal stress to determine the maximum allowable heat flux

One of the requirements for fuel elements in a closed cycle reactor power system is that they retain fission products so as not to contaminate the power machinery An indication of fission product retention can be obtained in a simple comparative test A small button containing uranium in its core simulating a fuel element is exposed to neutrons in order to generate fission products It is then heated in a sealed silica glass tube so that volatile fission products which escape from the button are contained One end of the tube is immersed in liquid nitrogen after cooling and the fission products are condensed and frozen This end of the tube is sealed off and its activity is measured This test indicates that less than 0 01% of the xenon generated will escape at operating temperatures The activity of other products such as iodine and tellurium is too low to identify There has been some evidence of migration of neptunium to the surface of the test samples

Designs have been made for in pile gas loops for testing fuel plates containing enriched uranium The experience and data from the tests outlined above will be used to modify these designs

Over all Program

Table 5 is a proposed outline of the steps that must be taken before an actual reactor power system can be built Many of these steps (those marked with an asterisk in the table) have been under way for some time

Reactor Power Plant Design Summary

The fuel element and associated concepts are ideal for a closed cycle power system Two such systems have been designed by S T Robinson of Sanderson & Porter and are described below in the reactor power plant studies These studies were made by two independent groups of ORSORT students The Package Reactor group was headed by J Gallagher and the Breeder Reactor group was headed by J Smith

TABLE 5 CERAMIC REACTOR PROGRAM

Body Development	Test ng	Supporting Calculations	Reactor Calculations
1 Selection of bose ompos t on 2 Fuel studies 3 Improvement of body	1 Phys col p ope ty measu ements 2 Diffusion of f ssion p oducts 3 Enginee ng ev lua t on 4 Neutron d mage to S C Si 5 LITR en ched plate te t 6 In p le eng neer ng test 7 I tial eo tor ex pe ment	1 F s on p od t diffus on B ld p of volotile elements b Cool t activ ty c Adsorpt on 2 Fuel element thermol colcula tions a The m l st esses b Powe dens ty 3 Su face effe ts a Erosion co osion b Temperotu e effects	1 Effect of u an m pe entoge n element on s e 2 Effect of heot flux on s e 3 Effe t of coola t ctivity 4 C ticol ty 5 Heot emoval 6 Control 7 Initi l eocto experi ment design

Work has been prog ess for some time

Although the designs here presented are not complete or final they contain sufficient detail to indicate the usefulness of the ceramic fuel elements in two very different kinds of reactor power systems

Application of SiC Si Fuel Elements to Package Power Plants [1] – The initial application of the SiC Si fuel element to a reactor design was made in a design study of a package reactor power plant for an Arctic Air Control and Warning Station (AC and W) This power plant was to have an installed capacity of 1000 kw electrical power and 3800 kw space heating

The availability of an SiC Si fuel element to contain highly enriched uranium capable of giving gas outlet temperatures of 1300°F would make possible thermal efficiences of the order of 30 to 35% for plants with 1000 to 10 000 kw output The high temperature SiC Si element is also attractive in applications such as the AC and W stations where both power and heat are required since the gas turbine has a high outlet gas temper ature the energy available in this expanded gas can be utilized for space heating A large part of this energy in the expanded gas is normally used to preheat the compressed gas so that lower thermal efficiences (~18%) must be accepted but for a plant with a high heat to-power ratio this is of little consequence

The general cycle diagram for a closed cycle gas turbine plant to supply both heat and power is shown in Fig 24 Figure 25 shows the power plant flow sheet with temperatures and pressures at the maximum monthly output of 880 kw of electricity and 2650 kw of heat and with a reactor output of 4200 kw Under these conditions the net heat utilization is 84%

A section of the fuel element is shown in Fig 26 The initial loading of highly enriched uranium is 19 kg of which 5 15 kg is available for burnout The core of the fuel element contains 68% SiC Si 31% UO_2 and 2% B_4C The B_4C is used to control long time reactivity changes The macroscopic absorption cross section of SiC Si is only 0 0115 cm^{-1} as compared with 0 236 cm^{-1} for type 310 stainless steel The graphite core is shown in Fig 27 The entire core and reflector are con tained in a pressure shell

A top elevation of the reactor and machinery cell is shown in Fig 28 Figure 29 shows a full size model of four moderator blocks and one fuel unit assembly made of high density graphite The building is 30 × 30 × 25 ft high The control room

[1] J G Gallogher *et al* *Reactor Design and Feasibility P oblem – Gas Cooled Ceramic Package Reactor* ORNL CF 53 10 30

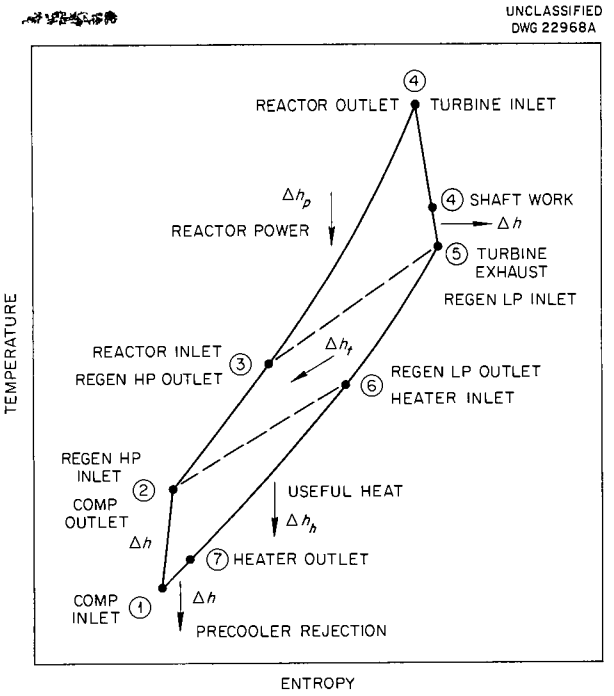

Fig 24 General Cycle Diagram for Closed Cycle Gas Turbine Plant

is located in a nearby building The shielding around the machinery compartment was necessitated by the assumption that all the volatile fission products escape into the coolant stream

A preliminary estimate of the cost is $1 000 000 including $150 000 for contingencies

Application of SiC Si Fused Elements in a Power Breeder Reactor – The use of SiC Si in fuel elements for a power breeder reactor was studied The system was designed to furnish 60 Mw of electricity and have as high a conversion ratio as possible consistent with an economically feasible system It was decided that the reactor would be cooled with helium and that the helium would be used as the working fluid in a closed cycle gas turbine Helium was chosen as the working fluid because of its superior heat transfer characteristics and its very low thermal neutron capture cross section

A flow sheet of the system chosen is shown in Fig 30 The helium at 100 psi pressure is heated to 1400°F in the reactor The heated gas is then expanded through two gas turbines the high pressure turbine driving the compressor set and the low pressure turbine driving the generator The over all station efficiency is approximately 40%

A drawing of the reactor and pressure vessel is shown in Fig 31 The reactor uses as fuel material U^{233} from thorium in an SiC Si matrix clad with SiC Si The moderator is high density graphite and the blanket is ThO_2 As can be seen in Fig 32 the fuel is arranged in flat plates five fuel plates making a fuel assembly There are 137 fuel assemblies inserted into the high density graphite moderator to form the core The blanket is ThO_2 perforated with circular coolant holes

The turbine compressor set and the turbine generator set are located above ground in the open air The remainder of the equipment is located below ground level for shielding purposes The activity of the coolant stream is kept to such a level that the turbines and compressors need not be shielded This is accomplished by bleeding off about 1% of the working fluid from the outlet of the compressor sending it through a regenerator thence through an expansion turbine and back through the regenerator to the inlet of the com pressor set The outlet temperature of the ex pansion turbine is well below –200°C – a temper ature low enough to condense any volatile fission products that may escape from the fuel element This purification system causes a very small loss (~ ¼%) in station efficiency

The reactor as designed has an initial con version ratio of approximately 1 0 It is believed that by more careful design this ratio can be increased to the point that the reactor would be a true breeder reactor with the possibility of a small over all breeding gain

A possible serious limitation of this reactor is common to all heterogeneous breeder reactors – the necessity for shutting down the system periodically to replace spent fuel elements The cycle time of the reactor as designed was 73 days but this could be increased with very little difficulty to about six months

A cost study revealed that electricity at the bus bars would cost approximately 7 9 mills/kwh This estimate was based on conservative esti mates of chemical processing and equipment costs

Development and Fabrication of Fuel Plates

General – The efforts of the Ceramics Laboratory have been directed first toward developing a

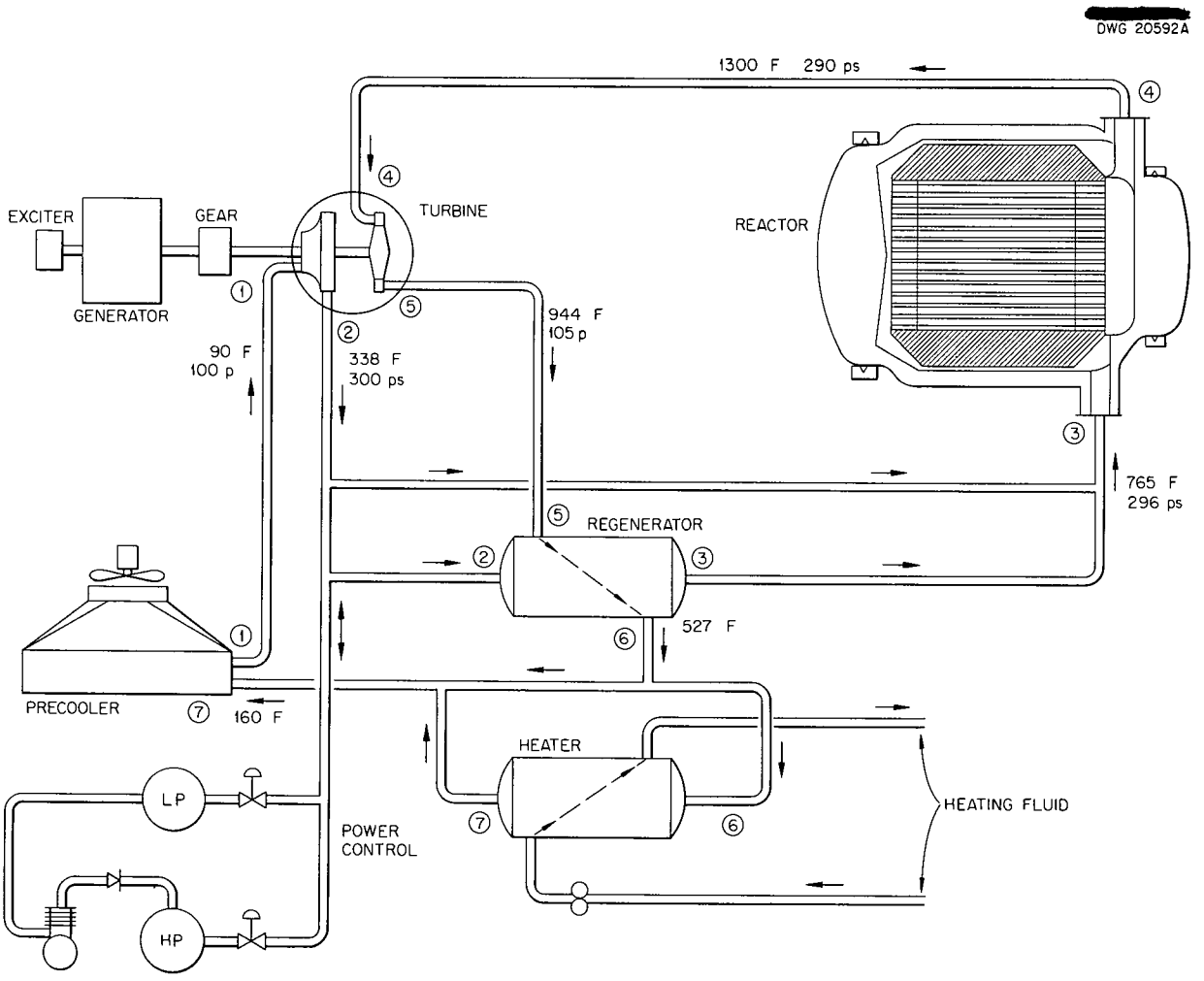

Fig 25 Power Plant Flowsheet (Temperatures and Pressures at Maximum Monthly Output)

tight and strong Si SiC body and second toward fabricating fuel elements with the Si SiC body being used as a base material

Body Development – In the search for an optimum base composition it was necessary that different grades of carbon and graphite be studied with respect to forming characteristics reactivity and structure of the finished Si-SiC product

Since there was no known technique for cold forming a porous carbon or graphite structure with sufficient strength for processing studies were made of various organic binders which could be either completely volatilized after the base structure was formed or partially volatilized leaving a carbon residue

Binder Materials – Volatile binders – naphthalene Carbowax and cetyl alcohol – were added in amounts up to 20 wt % The base structures in which these binders were used were very strong in the green state they became fragile however after the binders were volatilized and they disintegrated during the siliconizing process

The semivolatile binders included terphenyls nitrocellulose Bakelite organic flours and sugars The nitrocellulose bonded structures failed during the volatilization operation The structures exfoliated during the siliconizing process when they were bonded with terphenyls or Bakelite Wood flours proved to be poor binders in the green state Wheat flour was satisfactory as a binder when it was added in sufficient quantity (50%) however inconsistent results

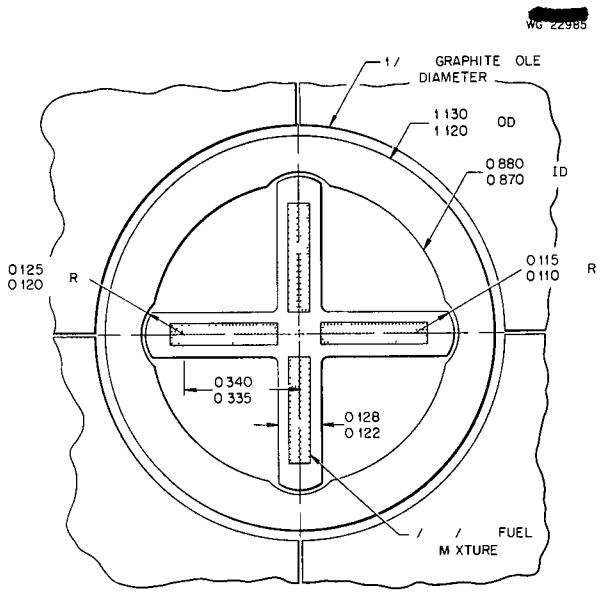

Fig 26 Section of Fuel Element for Closed Cycle Gas Turbine Plant

were obtained when the structures were siliconized

The sugars have proved to be highly satisfactory binder materials Added in the form of dextrin glucose or the commercial product Karo such additives make for a strong piece in the green state the strength increasing as the volatile materials are driven off In addition the structure of the finished Si SiC and the reproducibility of results obtained with the sugar type binders were far superior to those obtained with the other binder materials

Carbon and Graphite – Composition studies were made in which carbon and graphite available in the laboratory were used

Norblack an insulating grade of carbon was satisfactorily reactive, but due to its grainy nature was harder to form and made a rather weak green body In addition carbon particles visible to the naked eye were distributed throughout the siliconized body

The graphites were much more satisfactory with respect to formability green strength and structure of the finished piece

Selection of Base Composition – In order to determine an optimum composition for the base material an extensive experiment was conducted to select the type of graphite and the type and quantity of sugar which combined would make the best and most reproducible structure

Bodies of the Acheson and Dixon grades of graphite were prepared with the use of glucose and Karo syrup as binders in quantities varying from 18 to 48 wt % sugar content The following observations were made

1 The green strength decreased with decreasing sugar content

2 Residual carbon in the finished piece decreased with decreasing sugar content This is illustrated by *a* and *b* Fig 33

3 For a specific grade of graphite glucose produced a finer grained structure than did dextrin or Karo

4 With the use of glucose as a binder the finer grained Dixon graphite produced a finer grained structure with residual carbon than did the Acheson grade this is noted in comparing *a* and *c* Fig 33

5 For a given composition the use of a finer mix resulted in a finer grain structure and less residual carbon in the finished piece This is evidenced by *d* and *e* Fig 33

As a result of this experiment the composition T 91 A which contains 38% sugar and 62% Dixon graphite was selected for a basic material (*a* Fig 33)

Development of Fuel Body – In order that the core of meat of the sandwich type fuel plate be compatible with the shell or bread the core was composed of shell composition plus U UC_2 UO_2 U_3O_8 and USi_3

The metal and the carbide were oxidized as the volatile materials from the binder were driven off and the subsequent volume change disrupted the piece

With UO_2 U_3O_8 and USi_3 the fuel plates usually split or exploded during the siliconizing process This is understandable with the oxides because of the evolution of oxygen or carbon dioxide at impregnation temperatures which amounts to approximately 800 cc of gas per fuel plate (calculated)

The silicide has produced similar results the reason for this has not been determined although it is possible that impurities such as sulfur introduced during the process of materials preparation may be at fault

The present approach to this problem is either to introduce the uranium as a more pure silicide or to introduce the uranium as the oxide and carburize

[redacted]
DWG 22980A

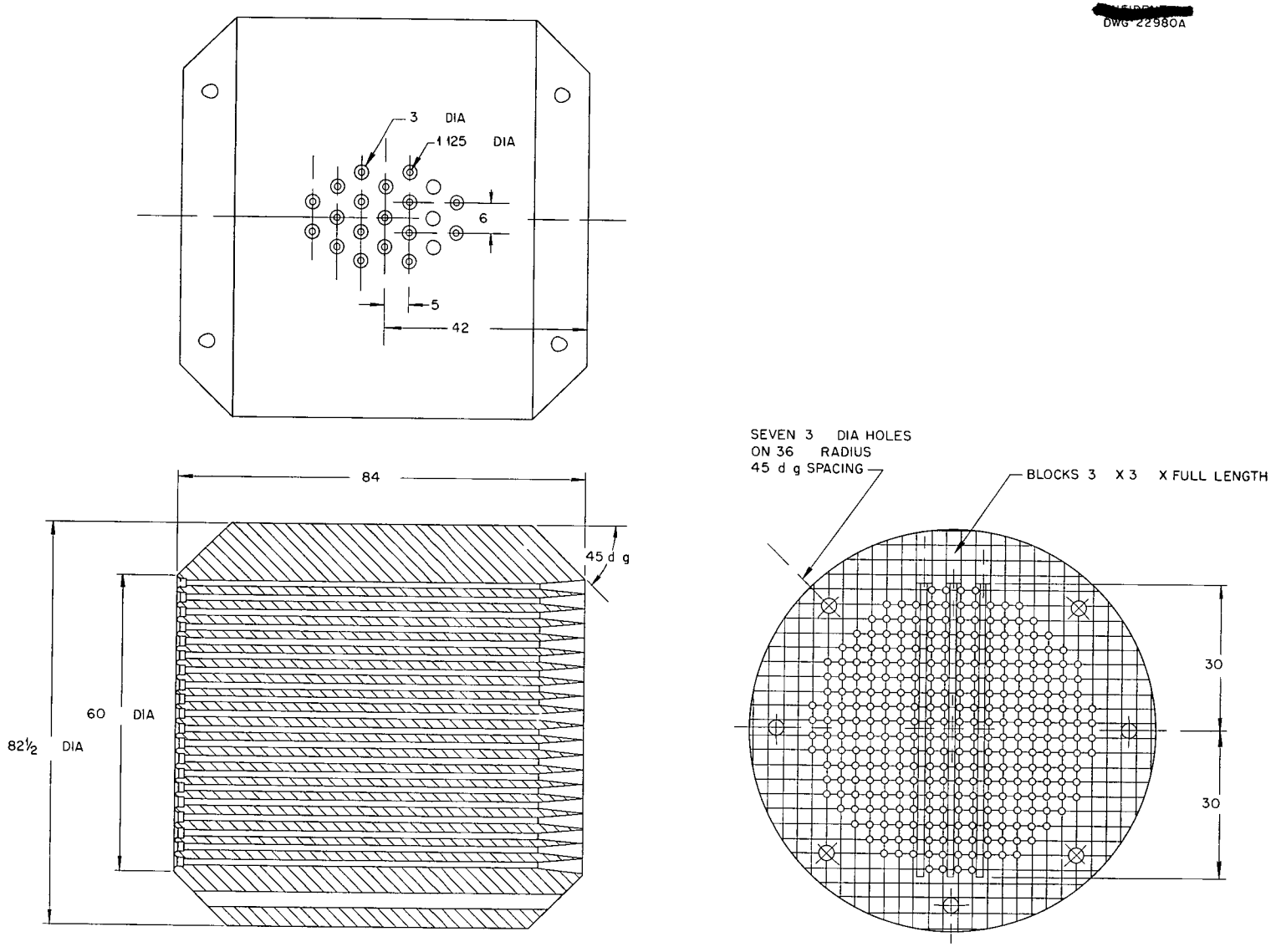

Fig 27 Graphite Core for Closed Cycle Gas Turbine Plant

[redacted] [redacted]
DWG 23008A

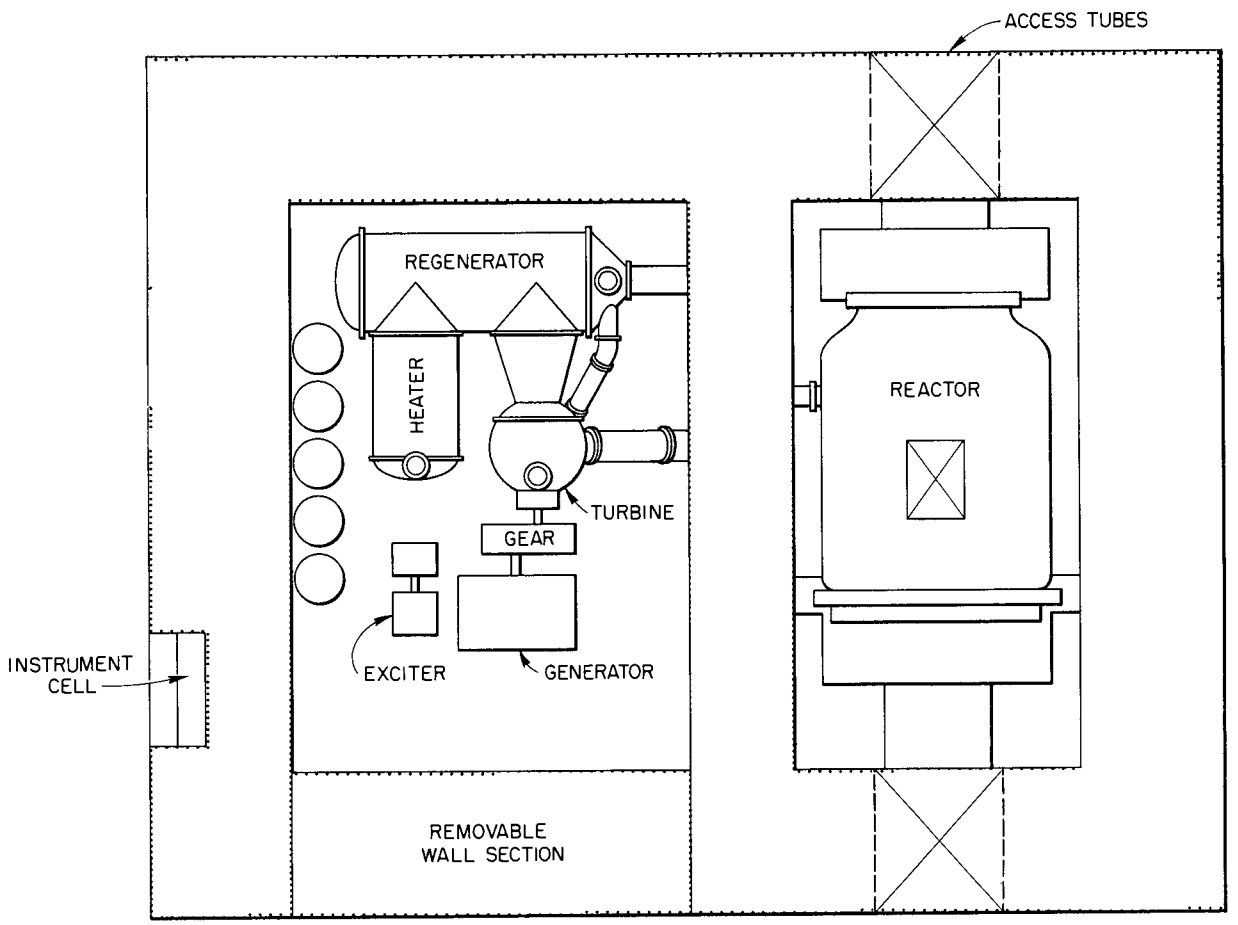

Fig 28 Top Elevation of Reactor and Machinery Cell

it in place before impregnation In addition efforts are being made to ensure against disruption due to differential shrinkages between the core and the shell which could break the bonds between the two or prevent their bonding as the volatile materials are driven off

Fabrication – *Preparation of Raw Materials* – The preparation of raw materials was accomplished as follows

1 The raw materials graphite plus glucose are wet mixed to form a stiff dough

2 The dough is dried in an oven at 140°C leaving a hard mass of graphite and sugar

3 The hard dough is ground in a hammer mill and screened through a 325 mesh sieve Most of the particles fall in the range of 5 to 10 μ

The fuel material is prepared in the same manner the fuel being wet mixed with the base composition

Forming of Plates – The forming of the initial structure is illustrated in Fig 34

Processing of Green Plates – After the body is formed the volatile materials are driven off by baking the specimen in an argon atmosphere at 1000°C This leaves a strong wood like structure of graphite particles bonded by the coke from the sugar this structure can be readily handled without being damaged

Siliconizing – The plate is placed on a graphite ladle and lowered into a graphite crucible containing molten silicon at approximately 1800°C An exothermic reaction is evidenced by an increase in specimen temperature to approximately 2300°C

Fig. 29. Full-Size Model of Four Moderator Blocks and One Fuel-Unit Assembly Made of High-Density Graphite.

When it is evident that the reaction has subsided, the specimen is withdrawn from the crucible and cooled in air.

Finishing. – Since the piece is coated with some excess silicon and silica as it emerges from the crucible into the air, the rough surface must be ground so that the finished plate will be within the prescribed tolerances.

Inspection. – The plate is x-rayed standing on edge and resting on the flat side. The radiograph indicates unreacted portions, placement of the uranium, cracks, or any leakages of the uranium phase that might have occurred during the siliconizing operation.

Principal Problems Encountered in Fabrication. – (1) Effect of pressure. – The pressure used in the cold-forming operation has been observed to be one of the major variables throughout the process. Both the initial and finished pieces are markedly affected by pressures in the relatively short range from 50 to 300 psi. At the lower pressures the green strength is decreased; shrinkage during the bakeout is decreased; the reaction rate with the silicon increases; the number and size of silicon pockets are increased. As the pressure is increased in the cold-forming operation, the reaction rate is slowed; the amount of residual carbon increases until a point is reached at which only a skin reaction takes place, leaving a porous carbon core. The effect of increasing the pressure is illustrated by *b* and *d*, Fig. 33.

Since the compressibility of any body composition

[redacted]

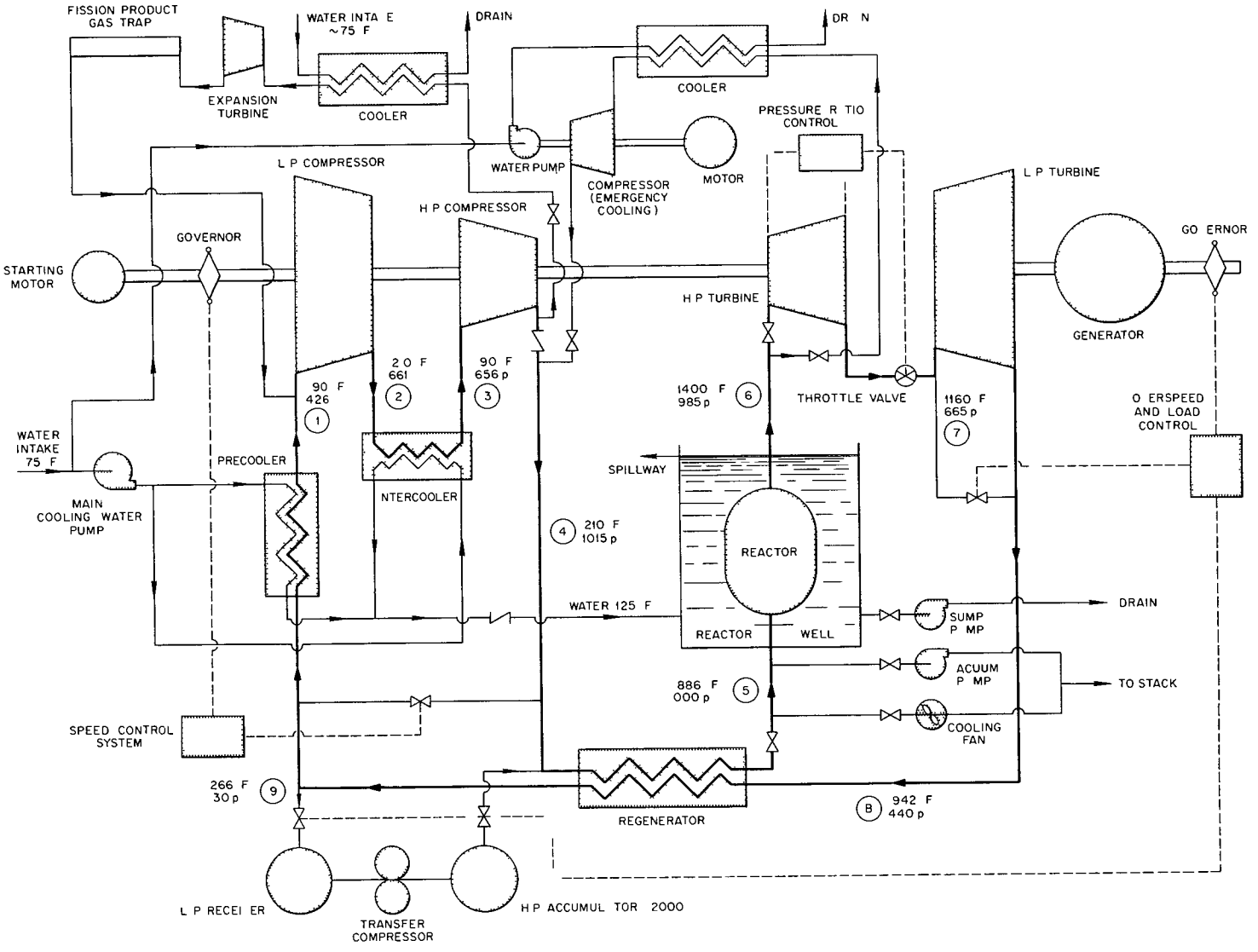

Fig 30 Flowsheet of Power Breeder Reactor System

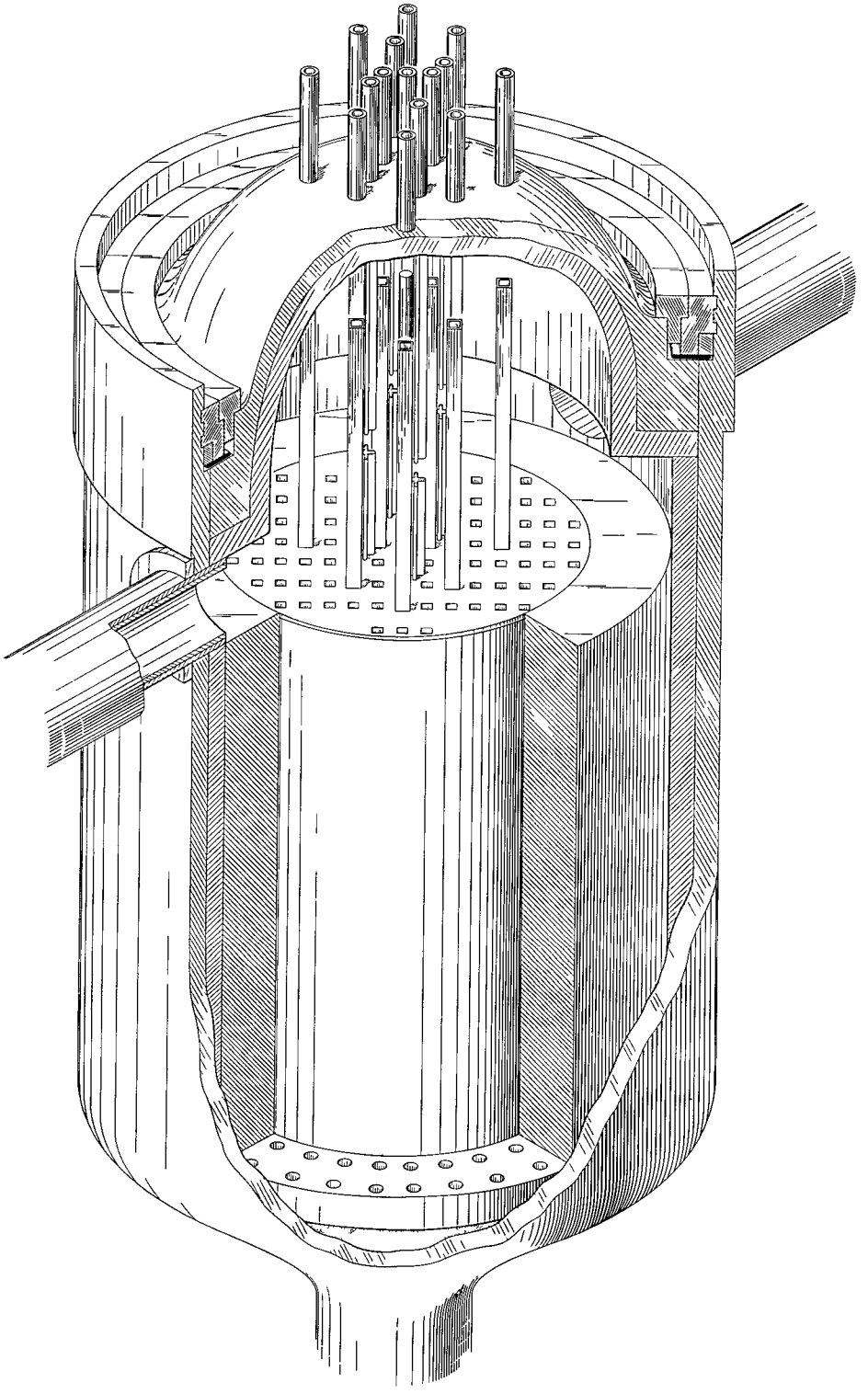

Fig 31 Power Breeder Reactor and Pressure Vessel

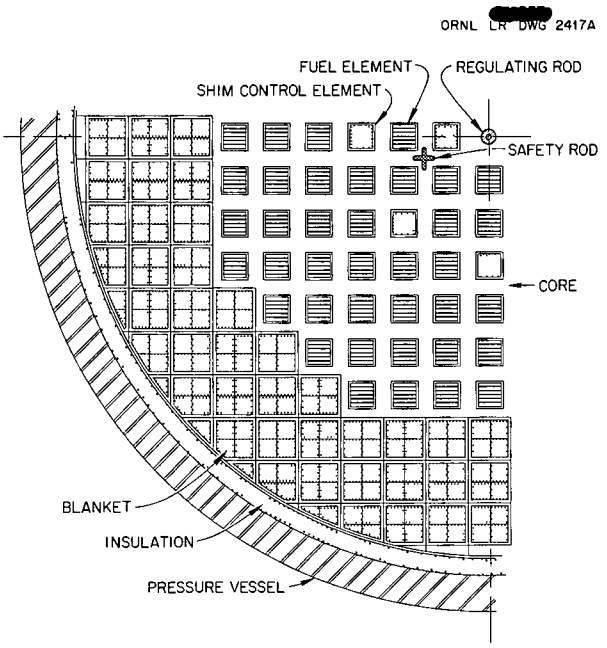

Fig 32 Cross Section of Power Breeder Reactor

is different from that of any other it was necessary to determine an optimum pressure for every body composition investigated The upper limit for most compositions was approximately 100 psi

The bodies in which sugar was used as a binder have proved to be less sensitive to pressure than any other compositions These bodies were impregnated at forming pressures up to 300 psi and reproducible results were obtained the upper limit for pressure has not yet been determined

(2) Effect of temperature – Although the silicon becomes molten at approximately 1420°C reaction with the carbon structure has not been observed to take place below 1700°C At this temperature the surface tension of the silicon appears to remain very high and the reaction is slow to start As the temperature is increased the rate of reaction increases but the specimen is more prone to warp during impregnation The degree of warpage, however, is not attributed entirely to increasing temperatures Because of the relatively small size of the present setup for impregnation plates can only be immersed endwise which enhances the chance for warpage A larger setup is being designed which will allow a plate to be immersed in any position For the composition selected temperatures in the range 1700 to 1800°C have been the most satisfactory

(3) Sweating – Excess silicon is taken into the structure during the impregnation operation and sweats out as the specimen cools Attempts are being made to improve the impregnation technique so that only the amount of silicon required for complete reaction enters the structure thus preventing or minimizing the sweating problem

Status of Fuel Element Fabrication – The first phase of the fuel element program is considered to be satisfactorily complete that is a strong tight fine grained Si SiC body has been developed which should serve as a very good base material for the proposed fuel element

There still remains considerable work to be done in completing the second phase that of reproducibly fabricating fuel plates This is believed to be partly a matter of improving tech nique but it is expected that a major effort will be involved in developing a satisfactory fuel mix

The Testing Program

Physical Properties – Some physical property measurements have been made on the Si SiC bodies and are given below in cgs units except as noted (Thermal conductivity was calculated from a comparative thermal diffusivity test with alumi num a direct measurement 100 to 1000°C is under way The T 91 A body was described in the preceding section Selection of Base Composition)

Dens ty	3 0	T 91 A body
Specif c heat (see Fig 35)	0 293 (400–1000°C)	T 91 A body
Thermal conductivity	0 4 (100°C)	T 91 A body
Te sile st ength ps	~10 000	Whe t flo r body
Expansion per °C	$4\ 2 \times 10^{-6}$ (0–1000°C)	T 91 A body

In addition oxidation resistance was noted to be excellent A microscopic film of silicon dioxide forms on the surface and acts as a barrier to further oxidation This test was conducted at 1000°C for two weeks The weight gain of a 15 g sample with a 4 in ^{2} surface was 0 08%

Bench Loop Test – A circulating gas loop with provision for electric self heating of the fuel elements or graphite plates has been made Figure 36 shows this test apparatus A plate type test specimen is on the table in the foreground

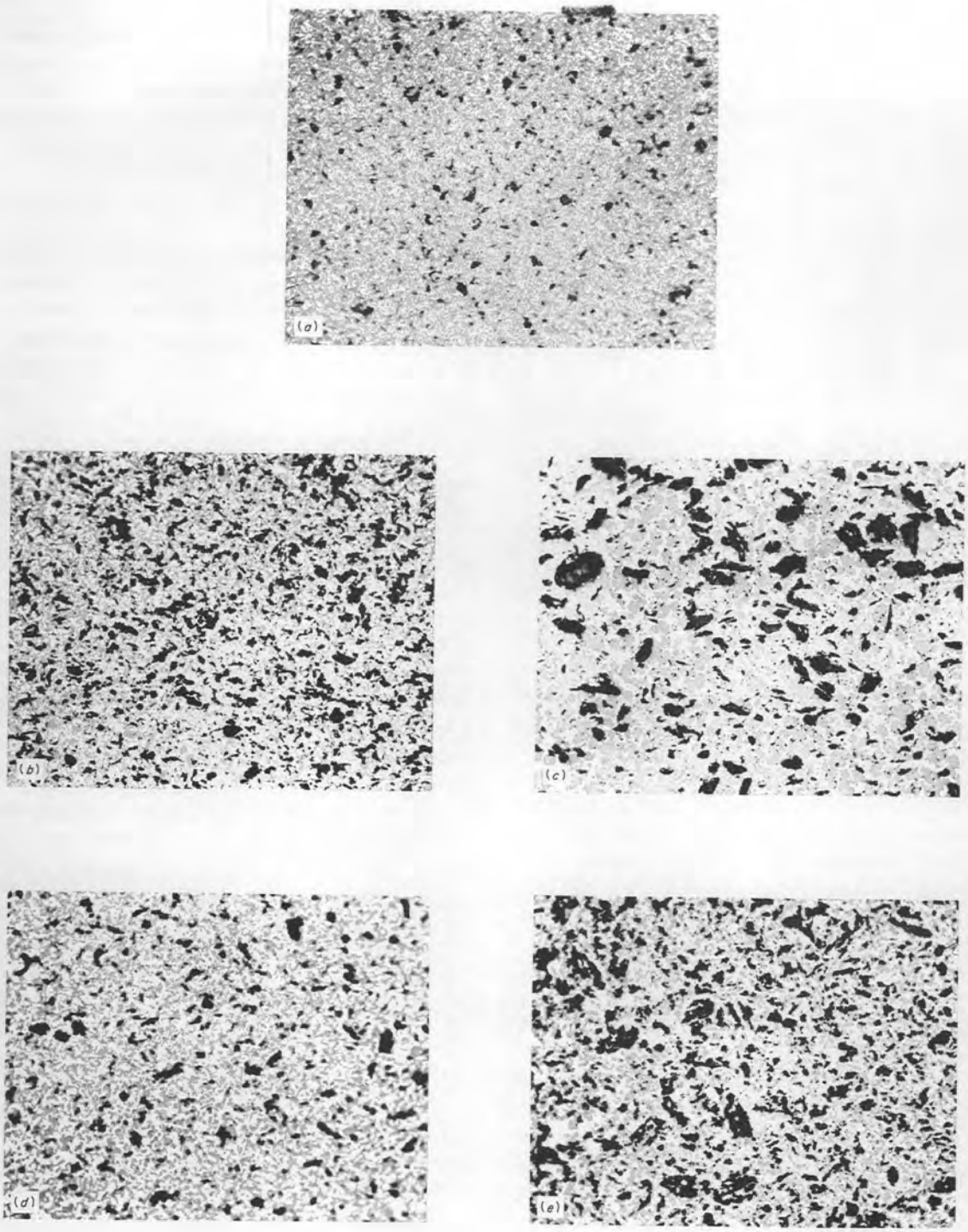

Fig. 33. Si-SiC Bodies; Black Phase, Graphite; Gray Phase, Cubic SiC; White Phase, Silicon. (*a*) 62% Dixon graphite–38% sugar; 300 psi; (*b*) 52% Dixon graphite–48% sugar; 300 psi; (*c*) 62% Acheson graphite–38% sugar; 300 psi; (*d*) 52% Dixon graphite–48% sugar; 70 psi; fineness of grind, over 50% less than 20 μ; (*e*) 52% Dixon graphite–48% sugar; 70 psi; fineness of grind, over 50% between 20 and 44 μ. 250X. Reduced 31.5%.

UNCLASSIFIED
ORNL LR DWG 6454

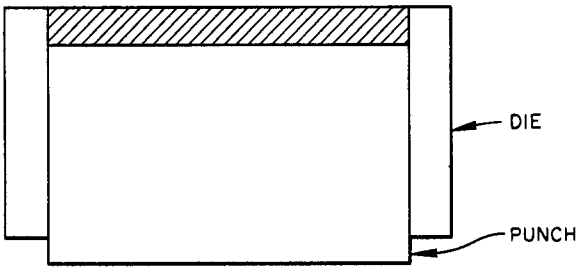

1 PUNCH IS LOWERED TO PREDETERMINED DEPTH AND DIE CAVITY FILLED WITH BASE-MATERIAL MIX

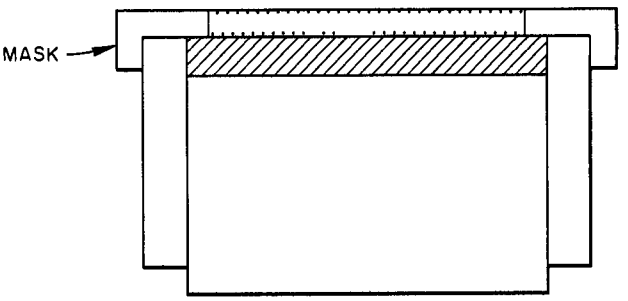

2 MASK IS PLACED OVER DIE AND MASK CAVITY FILLED WITH FUEL MIX

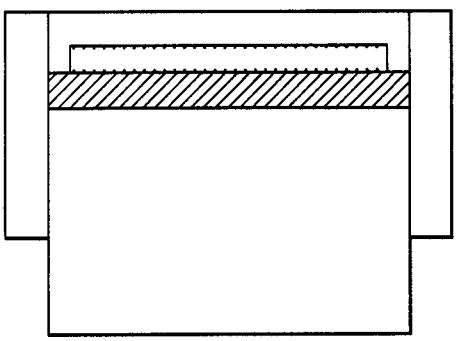

3 MASK IS REMOVED AND PUNCH LOWERED FOR RECEIVING MORE BASE-MATERIAL MIX

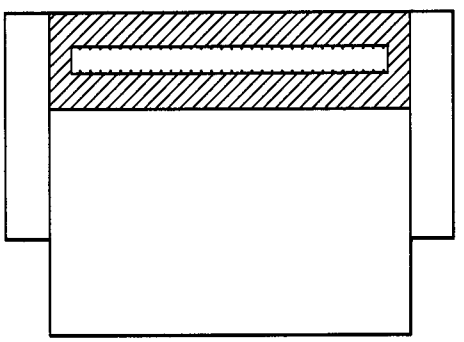

4 CAVITY IS FILLED WITH BASE-MATERIAL MIX TO FORM TOP ENDS AND SIDES OF SANDWICH

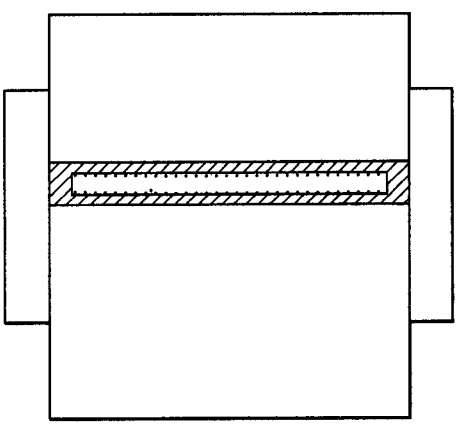

5 TOP PUNCH INSERTED AND PRESSURE APPLIED TO FORM INITIAL FUEL-PLATE STRUCTURE

Fig 34 Cross Section Illustrating the Cold Forming of Initial Fuel Plate Structure

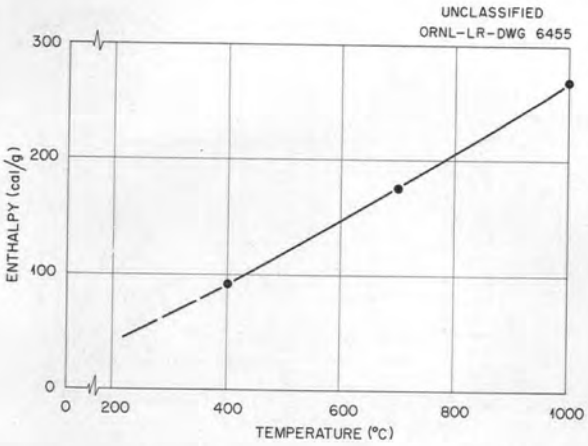

Fig. 35. Heat Content, SiC-Si; Specific Heat, 0.293 (400 to 1000°C).

Only preliminary studies have been made. Gas velocities of 200 fps can be attained. A 12-kw low-voltage power source is available to the equipment. Two SiC-Si plates, $3 \times 1 \times \frac{1}{8}$ in., have been heated in static air, with 700 and 1200 w/in.^{2} being driven from them at failure. The 700-w plate had an obvious defect. The 1200-w plate was representative of the better specimens. Failure occurred only after repeated heating and cooling at this load.

A 1000-hr erosion-corrosion test with high-density graphite plates as samples is the next experiment.

Neutron-Damage Test. – A neutron-radiation experiment carried out by M. Wittels, of the Solid

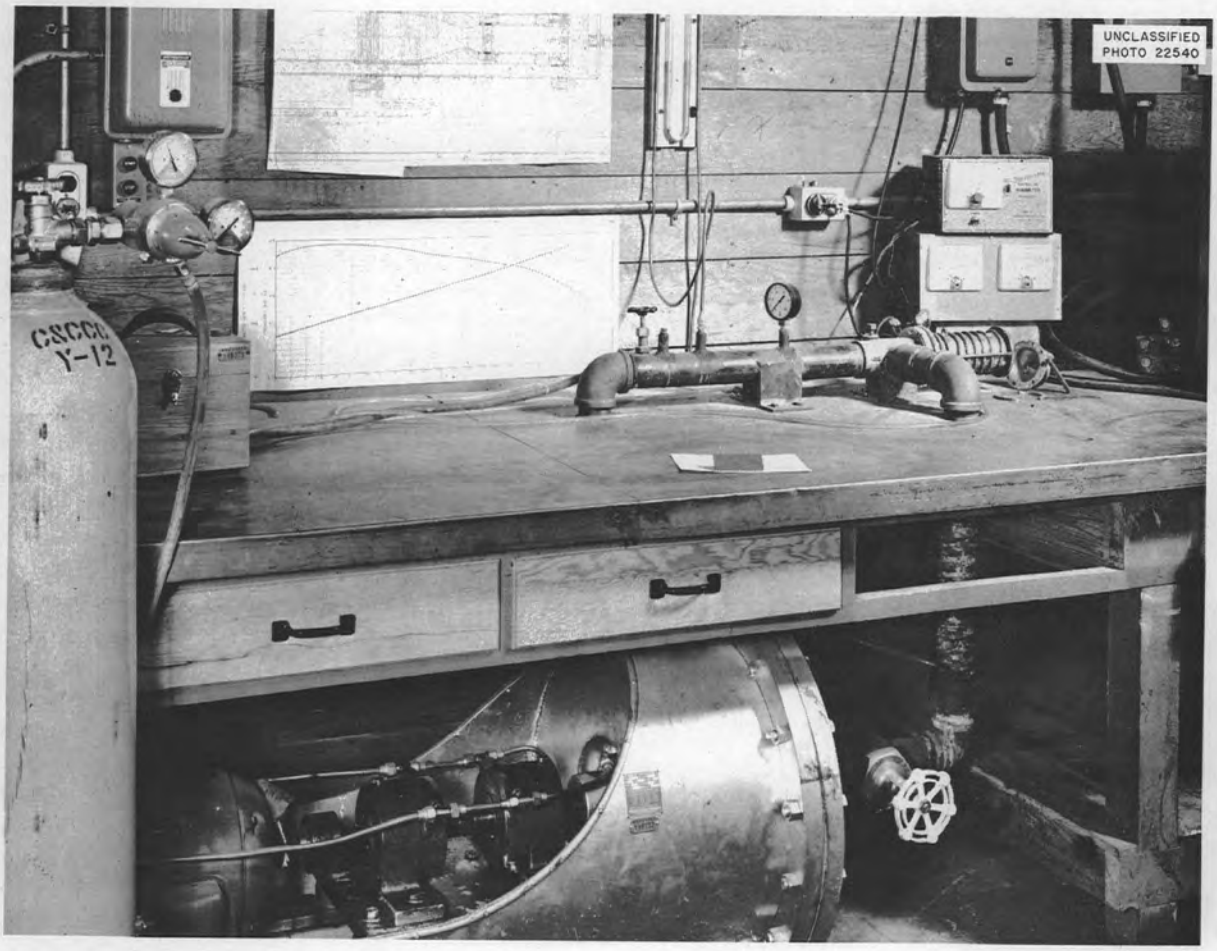

Fig. 36. Circulating-Gas Loop Test.

State Division revealed the following

Exposure f st neutrons	1 09 × 10^{20}
X ray latt ce	S no ch nge
Measurements	β SiC a_0 expanded 0 76 ±0 10%
Temperature of expos re °C	~100

Wittels believes that the lattice expansion will approach a maximum at less than 1 25% Since most ceramics self heal or anneal out such damage when heated to temperatures in the range 600 to 1000°C it is not expected that radiation damage will be a problem inasmuch as the operating temperatures for the SiC Si fuel element will be in this range The irradiated sample above has been recharged into the LITR for further bom bardment when it is removed it will be examined to determine the annealing temperature range

Fission Product Diffusion Test – The relative ability of materials to retain fission products is being measured with the use of a simple heating collecting system It is recognized that these results are not necessarily indicative of retention ability in a fuel bearing material which has under gone considerable burnup however they serve to screen materials and indicate their probable usefulness as fuel element materials In addition to the SiC Si specimens several other cermets have been examined Stainless steel and some oxide compacts will be tested in the future

A schematic view of the test is shown in Fig 37 The specimen is irradiated for seven days in a flux of 5 × 10^{11} neutrons/cm^2/sec It is then sealed in a silica glass container (Fig 38) and heated for 24 hr at a selected temperature On removal from the furnace the stem end of the container is immersed in liquid nitrogen for 5 hr after which the stem is sealed off from the con tainer and removed for radiochemical analysis The equipment for this process is shown in Fig 39 Activities are measured and isotopes are identified with the use of an ionization chamber a scintillation counter and a gamma spectrometer

The activities of the specimens are compared with the activities of standard samples which contain the same amount of UO_2 enclosed only in an aluminum silicate glass wool so that gaseous or volatile fission products can escape with little or no hinderance during furnace heating It is evident from Table 6 that the volatile fission

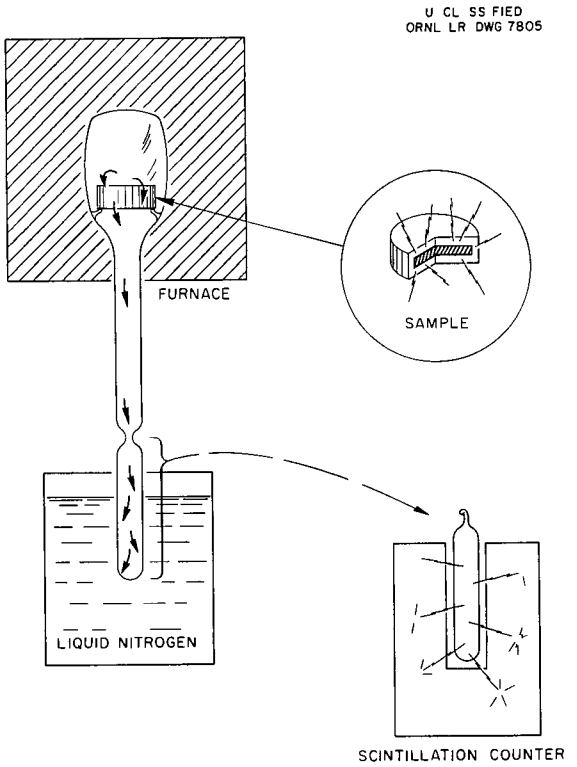

Fig 37 Fission Product Diffusion Test

products are retained in the UO_2 grains at irradiation temperatures The standard for the SiC Si specimens (G-224 1) contains 22 4 mg of UO_2 and the standard for the other cermets con tains 3 3 mg of UO_2

The isotopes which are pure beta emitters and those having very short half lives would not be detected in this experiment Xe^{133} $I^{133\ 132\ 131}$ Te^{132} and Mo^{99} were found Small amounts of other activities were found when the container tube of a standard sample was washed It was also discovered that neptunium apparently migrated to the surface of the specimens Some was also found in the glass wool surrounding the speci mens The neptunium was found to be on the surface of the specimens immediately after irradiation before heating It must be pointed out that the specimens were probably self heated (100–300°C) during reactor exposure Neptunium was not found in the sealed off tubes Tables 6 7 and 8 show the results of a number of tests

The data presented in Tables 6 7 and 8 indicate that in all probability only gaseous or volatile fission products will be of concern The

TABLE 6 TABULATED RESULTS FOR STANDARD COMPACTS

Compact Specimen No	Isotope	Measured Activ ty (photons/m n)	Act v ty Corrected (d/min)	Number of Atoms Diffused Through at Time of Removal from Fu nace ($N_1 \times 10^{10}$)	Theo etical Total Numbe of Atom at T me of Removal from Furnace[a] ($N_0 \times 10^{10}$)	Eff ciency of Collect ng System (%)	Estimated Accu acy (±%)
G33 3[b]	Xe^{133}	3×10^6	9×10^6	11 00	17 72	62	30
	I^{133}	2×10^6	$2\ 2 \times 10^6$	1 15	1 72	68	30
	Te^{132}	3×10^6	3×10^6	2 68	8 85[c]	30	30
	I^{132}	7×10^6	7×10^6	2 62	2 20	118	30
	I^{131}	3×10^6	$3\ 75 \times 10^6$	7 02	15 2	46	30
	Mo^{99}	3×10^6	$3\ 3 \times 10^6$	2 68			
			Activity Rat o to G33 3[d]	UO_2 Ratio	Efficiency Rat o Change		
G224 1[e]	Xe^{133}	3×10^7	10	6 8	1 47	91	50
	I^{133}[f]	2.5×10^7	11 5	6 8	1 69	115	50
	Te^{132}[g]	$1\ 7 \times 10^7$	5 7	6 8	0 838	25	50
	I^{132}	3×10^7	4 3	6 8	0 633	75	50
	I^{131}	2×10^7	6 7	6 8	0 985	45	50
	Mo^{99}	$1\ 5 \times 10^7$	5 0	6 8	0 736		

[a]Calculated by use of data from LRL 153 *Theoretical Study of Fission Product Gaseous Activity from a Homogeneous Reactor* by J R Donaldson (June 1954)

[b]Detailed rad ochemical analysis of 87% of the activity dissolved from tube in dilute nitric ac d g ven in Table 7

[c]Calculated from data and not from LRL 153

[d]$\frac{\text{Act vity atio to G33 3}}{UO_2 \text{ at o}} \times \%$ efficiency of G33 3 = effic ency of G224-1

[e]Rough cal bration absolute error probably les than 50%

[f]Some Ru^{103} may contribute

[g]Some $Xe^{133m\ 135}$ may contribute gammas

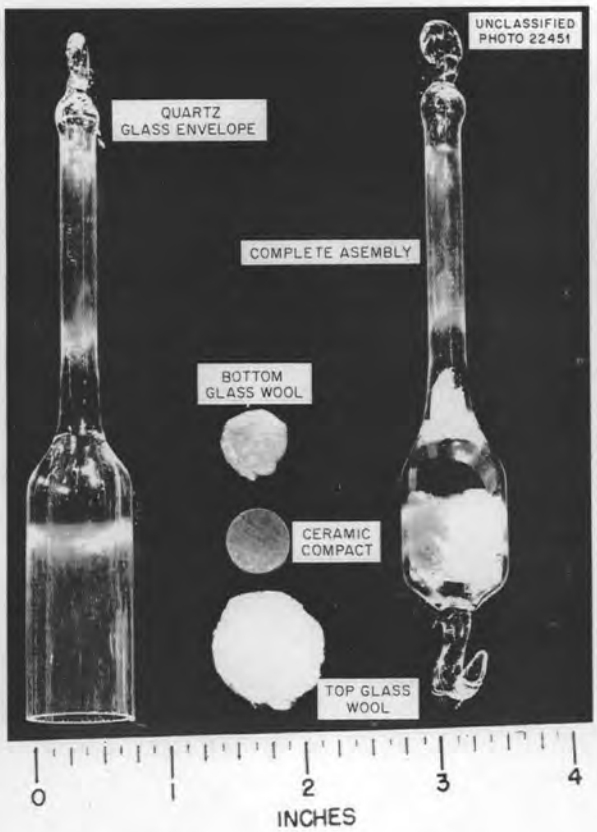

Fig. 38. Glass-Envelope Assembly.

TABLE 7. RADIOCHEMICAL ANALYSIS OF G33-3 NITRIC ACID WASH FROM TUBE*

Component	Counts/min/ml	Percentage of Gross
Gross gamma	7.7×10^4	
Tellurium gamma	2.9×10^4	38
Iodine gamma	2.0×10^4	26
Molybdenum gamma	6.3×10^3	8
Rare-earth gamma	810	1
Barium gamma	186	0.2
Zirconium gamma	100	0.1
Gross beta	7130	
Rare-earth beta	113	1.6
Strontium beta	45	0.6

*Determination made after approximately one week of decay from time of removal from furnace or ten days from time of removal from irradiation.

observed reduction of these fission products is sufficient to make some of the cermets interesting for fuel-element applications. In a reactor, further reduction can probably be obtained by continuously bleeding-off a portion of the coolant gas and passing it through an expansion turbine, where it is cooled to about −115°C. The cooled gas, going next through a coil immersed in liquid nitrogen, will lose its volatile fission products by condensation and freezing.

More detailed studies are in progress. A continuation of the neptunium study is intended.

PROCESS FOR OBTAINING LARGE-GRAINED UO_2

For a number of applications, particularly for fabrication of stainless steel fuel elements, UO_2 in grain sizes from 50 to 120 μ is required. Fusion and sintering are not acceptable methods for producing large-grained UO_2; fusion is wasteful of material, and sintering tends to produce agglomerates which are not so strong as desired.

A process has been developed which yields large-grained UO_2 and has no complicated or wasteful features. Large-grained anhydrous UO_3 was heated in a hydrogen atmosphere to about 1500°C. Large crystals of UO_2, the stable high-temperature oxide, developed from the UO_3. The UO_3 can be made in large crystals by autoclaving at 250°C fine-grained material which contains a trace of nitrate. In all probability 1200°C heating will be adequate. A detailed investigation is under way.

THORIUM OXIDE

Two thorium oxide rods clad with aluminum were irradiated in the LITR ($\sim 2 \times 10^{20}$ nvt) for 120 days. One of the rods was ½ in. in diameter by 4.5 in. long and consisted of pure ThO_2 (86% of theoretical density); the other was 1.1 in. in diameter by 4.5 in. long and consisted of ThO_2 plus ½ wt % CaO (96% of theoretical density). After the exposure the ends of the aluminum cladding were removed, and it was seen that the color of the ThO_2 had changed to a dark chocolate brown. No cracks were observed in the rods, and they appear to be mechanically sound. The aluminum cladding showed no significant dimensional changes, which indicates that the ThO_2 is dimensionally stable under the above exposure conditions.

TABLE 8 TABULATED RESULTS FOR CERMET COMPACTS

Compact Specimen No	Tempe atu e of 24-hr Heat ng (°C)	Type of Activ ty Detected as P oducts of Diffus on	Rat o of Diffused Act vity to Act vity of G33 3 Standard Fiss on Product Retention Facto	Compact Composition	U n um Compound n Compa t	Rem rks
A33 5	1000	W^{187} in all A samples (forming impurity) and const tuted majority of activity Xe and I present	$2\ 4 \times 10^{-1}$	28% Al_2O_3–72% C	UO_2 3 3 mg	W^{187} contaminat on n all A spec mens due to gr nding med a contam nat on in spec men p epa ation
7	1000		$1\ 5 \times 10^{-3}$	28% Al_2O_3–72% C	UO_2 3 3 mg	
3	900		2×10^{-4}	28% Al_2O_3–72% Cr	UO_2 3 3 mg	
4	900		4×10^{-4}	28% Al_2O_3–72% C	UO_2 3 3 mg	
1	800	Not identif ed	4×10^{-5}	28% Al_2O_3–72% Cr	UO_2 3 3 mg	
2	800	Not identified	8×10^{-5}	28% Al_2O_3–72% C	UO_2 3 3 mg	
B33 2	1000	Xe Te I	$3\ 3 \times 10^{-2}$	80% Z C–20% Fe	UO_2 3 3 mg	UO_2 d st buted throughout spec mens
5	1000	Xe Te I	$1\ 5 \times 10^{-2}$	80% ZrC–20% Fe	UO_2 3 3 mg	
C33 3	1000	Xe Te I	1×10^{-1}	80% T C–20% Ni	UO_2 3 3 mg	UO_2 distr buted thro ghout spec mens
6	1000	Xe Te I	6×10^{-2}	80% TiC–20% N	UO_2 3 3 mg	
D33 7	1000	Xe Te I	2×10^{-3}	80% MgO–20% N	UO_2 3 3 mg	
9	1000	Xe Te I	3×10^{-3}	80% MgO–20% Ni	UO_2 3 3 mg	
1	900	Not identified	4×10^{-5}	80% MgO–20% N	UO_2 3 3 mg	
2	900	Not dentified	9×10^{-5}	80% MgO–20% Ni	UO_2 3 3 mg	
3	800	Broken specimen		80% MgO–20% N	UO_2 3 3 mg	
4	800	Not ident f ed	2×10^{-5}	80% MgO–20% N	UO_2 3 3 mg	
E224 1	900	Xe Te I t ace Au^{198}	7×10^{-4}	S C S	US_3 26 5 mg	Str nger af US_3 to su face of spe imens the efo e u face of spec mens contam nated with uran um
2	900	Xe Te I	9×10^{-4}	SiC S	USi_3 26 5 mg	
3	900	No elements could be dentif ed	2×10^{-4}	S C Si	UO_2 22 4 mg	

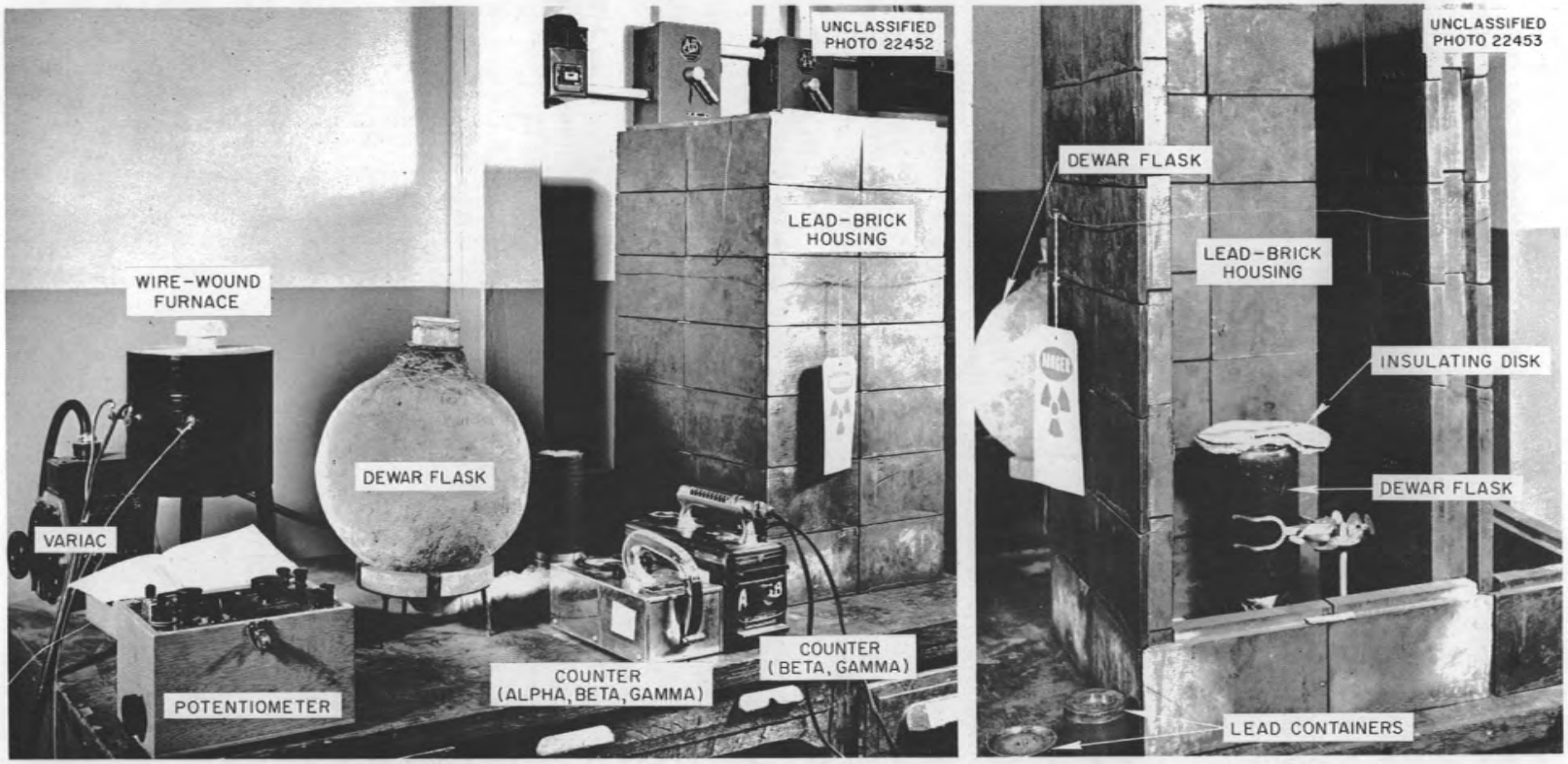

Fig. 39. Apparatus and Equipment for Fission-Product Diffusion Test.

PHOSPHATE COATING

Further work progressed on a fluoride resistant phosphate coating for mild steel Phosphate coated mild steel will ultimately be substituted for nickel coated steel vessels now in use in the gaseous diffusion process

Preliminary tests of two coatings P 6 and P 8 (Table 9) applied to mild steel have been per formed in UF_6 at 250°C Coating P 6 was resistant to the fluoride however P 8 was badly attacked The thermal expansion of coating P 6 was too low for good adherence to the metal to be obtained In order to increase the thermal expansion of the coating modifications of P 6 were made Compo sition P 19 is the best coating thus far produced It has not yet been tested for fluoride resistance

CERAMIC ASPECTS OF WASTE DISPOSAL

The safe disposal of high level radioactive wastes is of basic importance to future reactor operations and studies by the Ceramics Group include examination of the possibility of under ground fixation of dangerous isotopes in ceramic masses utilizing the heat present in the radio active wastes to effect partial fusion and the evaluation of natural impermeable barriers to the passage of waste solutions

Effect of Various Solutions on the Permeability of Clays

A series of experiments was performed in order to obtain preliminary data concerning the effect of various solutions on the permeability of various clays and combinations of clays

Ordinary 500 ml graduates were used (ten divisions on the graduate are equivalent to 1⅛ in in length or 50 ml in volume) and all measurements will be reported in divisions of the graduate

Tap Water – Clay was tamped into the bottom of the graduate and was then covered with three divisions of –200 mesh bentonite At the end of six days the clay underneath the bentonite was damp This experiment was repeated with ten divisions of granular bentonite (No 90 American Colloid Co) The bentonite swelled and separated but the bottom clay has remained dry over a period of several weeks This is not unusual since bentonite sandwiches have been used for sealing lagoons containing fresh water

Simulated W 8 Solution – Ten divisions of dry clay followed by four divisions of bentonite followed in turn by three divisions of dry clay were placed in the column Simulated W 8 so lution which is strongly basic rapidly permeated the bentonite layer and went into the clay under neath This solution destroys to a considerable extent the coherence of the bentonite gel With such solutions bentonite would not be a satis factory sealing material

Hope Solution – For the test with Hope solution the column was packed as follows nine divisions of dry clay six divisions of bentonite and a layer of clay placed on top The graduate was then filled with the solution The bentonite swelled to about 15 divisions It moved up the tube as a small amount of the solution went through the bentonite and reacted with the calcite which is in the clay forming CO_2

Summary – Bentonite sandwiches would not be suitable for sealing pits containing either W 8 or the acid Hope solution

Permeability of Clays as Affected by W 8 Solution from the Lagoon

In these experiments 1000-ml graduates were used They were fitted with a stopcock and a tube at the bottom as shown in Fig 40 and were packed with various clays and combinations of clays They were filled with radioactive waste from the lagoon the stopcock was opened and the solution was allowed to flow into beakers All measurements were made in terms of divisions on

TABLE 9 COATING COMPOSITIONS IN WEIGHT PERCENTAGES OF OXIDES

Coating	P_2O_5	Al_2O_3	BaO	BeO	SrO	ZnO	Sb_2O_3	Li_2O	Na_2O
P 6	70	15				10	5	2	
P 8	57 9	7 9	26 3			2 6	3 6		1 7
P 19	73	10		6	2	5	2	2	

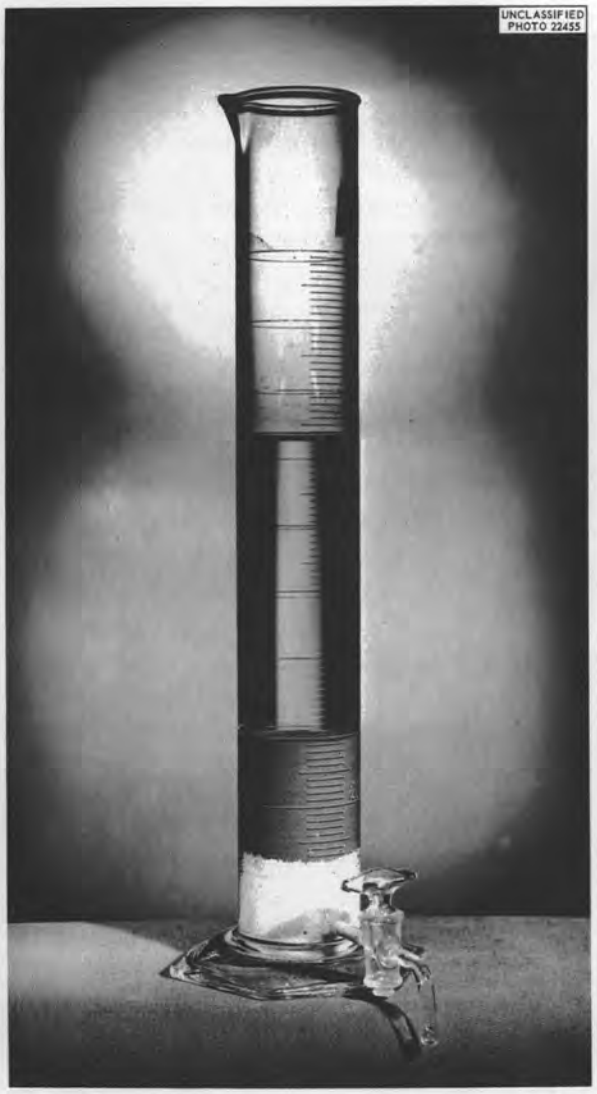

Fig. 40. Graduate (1000 ml) Used in Testing Permeability of Clays.

the graduates (ten divisions equal 1½ in. or 100 ml); –8 +50 mesh crushed insulating brick was used in the bottom of the graduates. The results of the tests are as follows:

1. Thirteen divisions of insulating brick and 16 divisions of finely ground Conasauga top soil packed damp were used. Tap water rapidly permeated the clay.

2. The column was packed the same as for test 1. W-8 solution (from the lagoon) rapidly permeated the clay.

3. Thirteen divisions of insulating brick, five divisions of Conasauga clay, six divisions of No. 90 coarse bentonite, and five divisions of Conasauga clay were used. The solution penetrated the bentonite within one day.

4. Thirteen divisions of insulating brick, six divisions of Conasauga clay, and ten divisions of mixed 75% Conasauga clay and 25% bentonite started to leak at the end of 48 hr. This mixture was better than the bentonite alone but was not satisfactory.

5. Thirteen divisions of insulating brick, six divisions of Conasauga clay, ten divisions of air-floated Gleason ball clay (H. C. Spinks Clay Co., Inc., Paris, Tennessee) did not leak even after ten days and evidently makes a good seal. This clay costs $17.50 per ton, f.o.b. Paris, Tennessee; consequently, this experiment will be repeated, and the shredded Gleason clay, which costs $7.50 per ton, will be used.

6. Thirteen divisions of insulating brick, six divisions of Cordova, Alabama, fire clay (16 mesh) was examined three days after the W-8 solution had been poured in, and the solution had permeated the clay.

7. Thirteen divisions of insulating brick, six divisions of Conasauga clay, ten divisions of mixed 50% Gleason clay and 50% Conasauga clay had leaked within three days but not so rapidly as had No. 6.

Conclusions. – To date, the only clay found to be impermeable to the waste solution is the air-floated Gleason ball clay.

Gels Made from Hope Solution and Natural Carbonate Minerals

At the start of this investigation, gels were formed by adding either finely ground Knox dolomite or Chickamauga limestone to Hope solution and by stirring the mixture frequently. The gel is evidently aluminum hydrate. Ordinary 500-ml graduates were used. The graduate was packed with ten divisions of dry Conasauga clay, seven divisions of bentonite, and four divisions of dry clay. The gel was formed by frequent stirring of 142 g of Knox dolomite and 500 ml of Hope solution. The gel was strongly acid but contained unreacted dolomite. The gel was poured into the graduate and did not wet the top clay. Two inches of the gel was removed from the top of the graduate, and the graduate was filled with water. The bentonite swelled and separated,

leaving a gap and the clay underneath remained dry A similar column was arranged by using finely ground Chickamauga limestone and it behaved in the same manner as the graduate containing the Knox dolomite gel

Conclusions – The above tests indicate that the gel will be inactive when it is poured into a pit which has a dry clay bottom Consequently a more thorough study of the jelling characteristics of carbonates and Hope solution was indicated

Gel Formation – Agricultural limestone (dolomite) was obtained from Mascot Tennessee As received practically all of it would pass –20 mesh The following proportions were used

No	Mascot-20 Mesh Dolomite (g)	Hope Solution (ml)
1	65	250
2	70	250
3	75	250

These were mixed with frequent stirring by hand and none of them formed a gel readily The sample was then passed through a hammer mill which reduced it to about –50 mesh The mixtures were stirred by hand as before and the following results were obtained No 1 gel formed in 6 hr No 2 soft gel was formed in 6 hr No 3 gel was not formed in 6 hr These results showed that the speed of gel formation is increased by grinding the dolomite

A further series of experiments was made in which a Hamilton Beach mixer was used for stirring With 60 g of the –20 mesh Mascot dolomite and 250 ml of Hope solution a gel was formed in 80 min The same dolomite after being passed through a hammer mill which reduced it to about –50 mesh formed a gel in 50 min Another series of experiments gave the following results

Mascot-20 Mesh Dolomite (g)	Hope Solution (ml)	Time of Gel Formation
50	250	No gel 3 hr
55	250	Gel 2 h
60	250	Gel 50 min
65	250	Gel 50 min

It was then considered that 60 g of Mascot –20 mesh dolomite with 250 ml of Hope solution would make a satisfactory gel This is equivalent to 2 lb of dolomite per gallon of Hope solution

The test was repeated and –20 mesh Chickamauga limestone screenings from the quarry near X 10 were used Limestone screenings too fine for use in construction are available in large quantities and it would be inexpensive to screen this material through –20 mesh

The results of the test were as follows

Chickamauga-20 Mesh Limestone (g)	Hope Solution (ml)	Time of Gel Formation
50	250	No gel 60 min
55	250	Soft gel 60 min
60	250	Soft gel 50 min

Other results indicate that the limestone forms a gel more readily than the dolomite However with 250 ml of Hope solution and either 60 g of the –20 mesh Mascot dolomite or 60 g of the –20 mesh Chickamauga limestone a satisfactory gel can be formed in about 1 hr providing that there is rapid thorough mixing This proportion is equivalent to 2 lb of either of the carbonate minerals to 1 gal of Hope solution Calculations show that to form a satisfactory gel it is not necessary to add enough of the carbonate to react with all the aluminum nitrate

Fixation of Radioactive Isotopes in Gels

It was thought that it should be possible to form a ceramic body by (1) making a gel with limestone and Hope solution with the simultaneous addition of local clays or silica (2) dehydrating the gel and (3) sintering the resulting mixture Chemical analyses were made of the Chickamauga limestone and the Conasauga surface clay with the following results

Chickamauga Limestone

Component	Per Cent
Acid insoluble largely SiO_2)	8 21
R_2O_3	1 23
CaO	46 10
MgO	3 03
Ignition loss	39 40
	97 97

Conasauga Clay
(Composite sample from 12 ft of drill hole)

Component	Per Cent
SiO_2	65 1
Al_2O_3	14 6

Component	Per Cent
Fe_2O_3	5 69
CaO	2 50
MgO	1 23
Na_2O	0 23
K_2O	3 50
Ignition loss	6 63
	99 48

The following compositions were made

No	Chickamauga −20 Mesh Limestone (g)	Hope Solution (ml)	Conasauga Clay (g)	Silica (Potter s Flint 99+% SiO_2) (g)
1	60	250	50	
2	60	250	100	
3	60	250	50	50

In all cases the gels were formed in less than 1 hr The calculated chemical analyses of these mixtures (ignited) are as follows

No	SiO_2 (%)	R_2O_3 (%)	CaO + MgO (%)	Alkalies (%)
1	36 7	30 6	30 9	1 8
2	47 1	27 9	22 5	2.5
3	57 6	20 5	20 7	1 2

The proportions of materials used for each gallon of Hope solution are given below

No	Chickamauga Limestone (lb)	Conasauga Clay (lb)	Silica (lb)
1	2	1 67	
2	2	3 33	
3	2	1 67	1 67

The mixtures were partially dehydrated in a dryer but dehydration was not complete – gummy masses remained These were placed on a hot plate and copious fumes of NO_2 were evolved They were then fired at 1700°F for about 3 hr and additional NO_2 was given off Pieces of the fired bodies were placed in water the water surrounding No 1 was highly basic that sur rounding No 3 was moderately basic and that surrounding No 2 was only slightly basic These basicities resulted because the lime had not completely reacted with the other materials present The most complete reaction was obtained with No 2 All the bodies will be fired at a series of higher temperatures

It should be noted that the gels melted as soon as they were heated which indicates that if such gels are placed in a pit and they become warm a liner may be needed

After the conditions for making a satisfactory ceramic body from the gels with various additions have been determined radioactive Hope solution will be used and leaching tests will be carried out to determine whether the radioactive isotopes can be fixed in such a composition

Retention of NO_3 Ion by Gels

With the knowledge that NO_3 ion has been found in the vicinity of some of the present pits the following experiments have been carried out to determine whether the gels retain NO_3^- Five hundred milliliter graduates with openings at the bottom and at the 50 100 and 150 ml graduations (Fig 41) were used in these experiments

Experiment 1 – Conasauga clay was packed in the bottom of the cylinder to just above the 150 ml graduation A gel was made with 60 g of the −20 mesh Chickamauga limestone and 250 ml of the Hope solution and the gel was poured into the cylinder Water was admitted through the bottom opening to thoroughly saturate the clay

At the end of five days the following qualitative results of tests for NO_3^- were obtained with the use of diphenylamine indicator

Opening	Indication of NO_3^-
150 ml	St ong
100 ml	Moderate
50 ml	Weak
Bottom	Trace

These results indicate that there was little migration of NO_3^- under static conditions The cork from the bottom opening was removed and water was poured into the graduate After nine days the following observations were made

Opening	Indication of NO_3^-
150 ml	Strong
100 ml	St ong
50 ml	Weak
Bottom	Trace

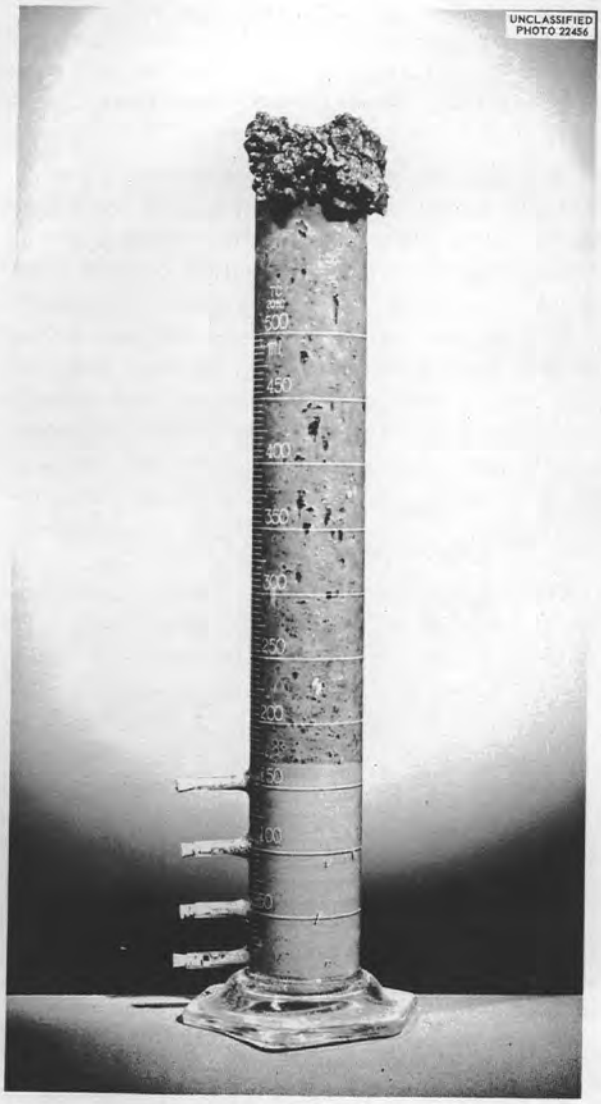

Fig. 41. Graduate (500 ml) Used in Testing Retention of NO_3 Ion by Gels.

Some migration of NO_3^- had occurred, but it was not marked.

Experiment 2. – Another graduate was used, and eight divisions of bentonite No. 90 were placed between the Conasauga clay and the gel. The bottom clay was saturated, as before, and after five days the following observations were made:

Opening	Indication of NO_3^-
150 ml	Trace
100 ml	Barren
50 ml	Barren
Bottom	Barren

Water was added to the graduate, as in experiment 1, and after nine days the following observations were made:

Opening	Indication of NO_3^-
150 ml	Moderate
100 ml	Weak
50 ml	Trace
Bottom	Barren

Conclusion. – A bentonite layer is fairly effective in reducing migration of NO_3^-.

Diffusion of Radioactive Strontium from Gels

Experiment 1. – Radioactive strontium was added to the Hope solution in sufficient quantity to give 15,000 counts/min/ml. This solution was used to make the gel, which contained 154 g of Chickamauga limestone to 500 ml of Hope solution. The graduate was packed to the top of the 150-ml opening with Conasauga clay; ½ in. of bentonite was placed on the clay and was, in turn, covered with a thin layer of the clay. The gel was poured into the graduate, and water was admitted through the bottom opening to saturate the clay. Small quantities of the clay were removed through the openings, and counts were made. This method is not precise because of the difference in the size of the samples. The results, however, are comparative.

Opening	Counts per Minute		
	After 9 Days	After 13 Days	After 18 Days
150 ml	42	319	1050
100 ml	27	55	624
50 ml	24	12	745
Bottom	8	12	270

The nine-day counting was done under static conditions. Water was poured on top of the gel at the end of nine days, and the bottom cork was removed. The gel had about 13,000 counts/min, and the water surrounding the gel 80 counts/min for a volume equal to that of the samples removed through the bottom openings. It is quite evident that fission products pass through the bentonite sandwich.

Experiment 2. – A graduate was packed in a manner similar to that used in experiment 1, except that the bentonite layer was omitted. The results

were as follows

Opening	Counts per Minute	
	After 5 Days	After 9 Days
150 ml	647	1250
100 ml	41	1028
50 ml	20	552
Bottom	Backg ound	76

The five day counting was done under static conditions Water was poured on top of the gel at the end of five days and the bottom was left open

The bentonite layer is of some assistance in retarding the passage of radioactive strontium

Experiment 3 – A graduate similar to the two used previously was packed After five days the bottom clay was damp but was not impregnated with water Water was then allowed to flow into the bottom of the cylinder for one day and the stoppers were replaced The following results were obtained

Opening	Counts per Minute		
	After 5 Days	After 6 Days	After 41 Days
150 ml	66	682	1446
100 ml	Background	Background	704
50 ml	Background	Background	313
Bottom	24	6	290

Results – The results of these experiments show that the radioactive strontium will diffuse from the gel into wet clay underneath This indicates that if gel were placed in a pit below ground water the radioactive isotopes would diffuse into the wet clay

Investigation of Porous Ceramics as Isotope Sorbers

An investigation was carried out with porous fired clay slugs which are capable of removing through absorption and selective absorption a considerable amount of radioactive particles and ions from waste liquors A preliminary investi gation suggests that the effect of cataphoresis in attracting radioactive ions into the clay slugs is somewhat erratic and does not change the order of removal from that accomplished by mere soaking under the conditions investigated Acid liquors do not give up the radioactivity to the slugs nearly so efficiently as do basic liquors The removal of radioactive isotopes from basic waste liquors is selective in that the concentration of such radio isotopes in the enveloping liquid is materially reduced The clay slugs are capable of being glazed and rendered virtually unleachable Porosity of the slug is more important than the type of clay Almost any type of clay is effective

Diamond Drilling

Four cored holes have been drilled 200 ft deep in an area 400 × 400 ft lying between Haw Ridge and Copper Ridge this area is under consideration as a test pit site From drill records it appears that the weathered zone extends to 14 ft from the surface below this zone is a fractured zone to 65 ft from the surface At greater depth the core strata appear to be relatively impervious

HRP METALLURGY

E C Miller

PHYSICAL METALLURGY OF TITANIUM AND OF ZIRCONIUM ALLOYS

W J Fretague

Commercial Titanium

Impact tests have been completed on specimens machined from an unalloyed titanium corrosion specimen holder (RC 70 heat 3102 REED item 11) Table 10 presents the loop history of the specimen holder

In addition to the tabulated exposures the holder was cathodically defilmed frequently in inhibited 5% sulfuric acid at room temperature

Sufficient material of similar analysis (RC 70 heat 3102 REED item 11) in the as received condition was available for 12 multiple break impact specimens

The impact data plotted in Fig 42 indicate that the combination of loop exposure and cathodic defilming has drastically embrittled the material raising the transition temperature from approximately 100 to above 200°C This result is contrary to previous experience attempts to embrittle unalloyed titanium both by cathodic treatment[1] in H_2SO_4 and by loop exposure to simulated HRP environments[2] have in the past been unsuccessful The cathodic defilming procedure may have introduced hydrogen into the metal and thus produced the observed embrittlement

Additional impact tests have been performed on unalloyed titanium 75A heat L782 REED item 24 These specimens were exposed to the loop environment described in Table 11 in the as swaged and machined condition in an effort to study the effect of cold working on the rate of hydrogen adsorption

[1] W J Fretague A R Olsen R G Berggren and J J Woodhouse *Met Semiann Prog Rep Oct 10 1953* ORNL 1625 p 9–10 and Fig 5

[2] W J Fretague *Met Qua Prog Rep Oct 31 1952* ORNL 1437 p 41

TABLE 10 HISTORY OF UNALLOYED TITANIUM CORROSION SPECIMEN HOLDER

HRP Loop Run No	Solution: Uranium Concentration as UO_2SO_4 (g of U per liter)	Solution: Additions	Temperature (°C)	Time (hr)
I 3	40	0 042 *M* H_2SO_4 200 psi O_2	250	1036
F 20	300	200 psi O_2	250	117
D 1	300	50 ppm Tc 200 psi O_2	250	101
D 2	300	200 psi O_2	250	100
H 15		1 0 *M* HCl 1 4 *M* H_2SO_4 0 2 *M* H_2O_2 Alkyl pyridine inhibitor 200 psi He	85	4
H 16	25	200 psi O_2	250	200
H 17	25	200 psi O_2	250	400
				1958

Decontamination run

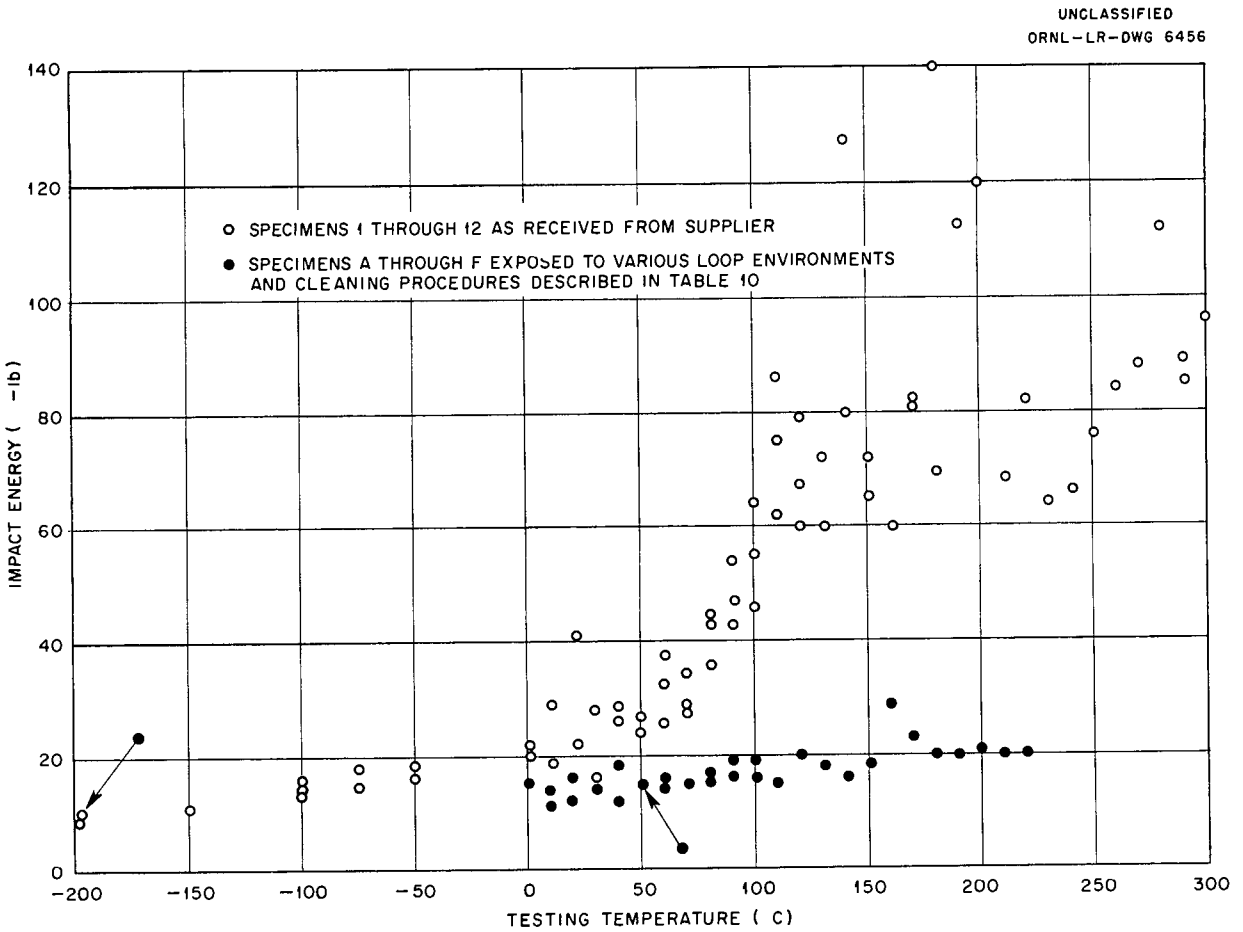

Fig 42 Impact Energy vs Testing Temperature for Titanium (RC 70) Reed Item 11 Heat 3102

by titanium as measured by the impact behavior The impact data obtained from these specimens are plotted in Fig 43 A comparison of these results with those obtained for as swaged[1] and for swaged and vacuum annealed unalloyed titanium[3] does not reveal any effect on the impact properties that could be attributed to the treatment given to the specimens (prior to exposure) or to the corrosive environment in which they were exposed

Four multiple break impact specimens of unalloyed titanium (Ti 75A heat L782 REED item 24) in the vacuum-annealed condition were impact tested after exposure to the loop environment described in Table 12 The impact data obtained are plotted in Fig 44 No significant difference in the impact behavior of these specimens as compared with that of similar specimens exposed under similar conditions,[3] was observed

Samples from the pressurizer section of an all titanium loop that failed in service were analyzed for hydrogen by the vacuum fusion method at Battelle Memorial Institute and at ORNL The results are presented in Table 13 with a notation as to the location from which the sample was obtained

Iodide Titanium

Impact tests have been completed on a series of four iodide titanium specimens that were exposed to simulated HRP environments in a dynamic corrosion loop under the conditions outlined in Table 14 The impact data obtained are presented in Fig 45 together with data previously obtained

[3] W J Fretague A R Olsen and R G Berggren *Met Semiann Prog Rep April 10 1953* ORNL 1551 p 13–15 and Fig 12

TABLE 11 LOOP HISTORY OF AS SWAGED AND MACHINED UNALLOYED TITANIUM IMPACT SPECIMENS

HRP Loop Run No	Solution: Uranium Concentration as UO_2SO_4 (g of U per liter)	Solution: Additions	Temperature (°C)	Time (hr)
A 67	15	0 006 *M* H_2SO_4	310–320	977

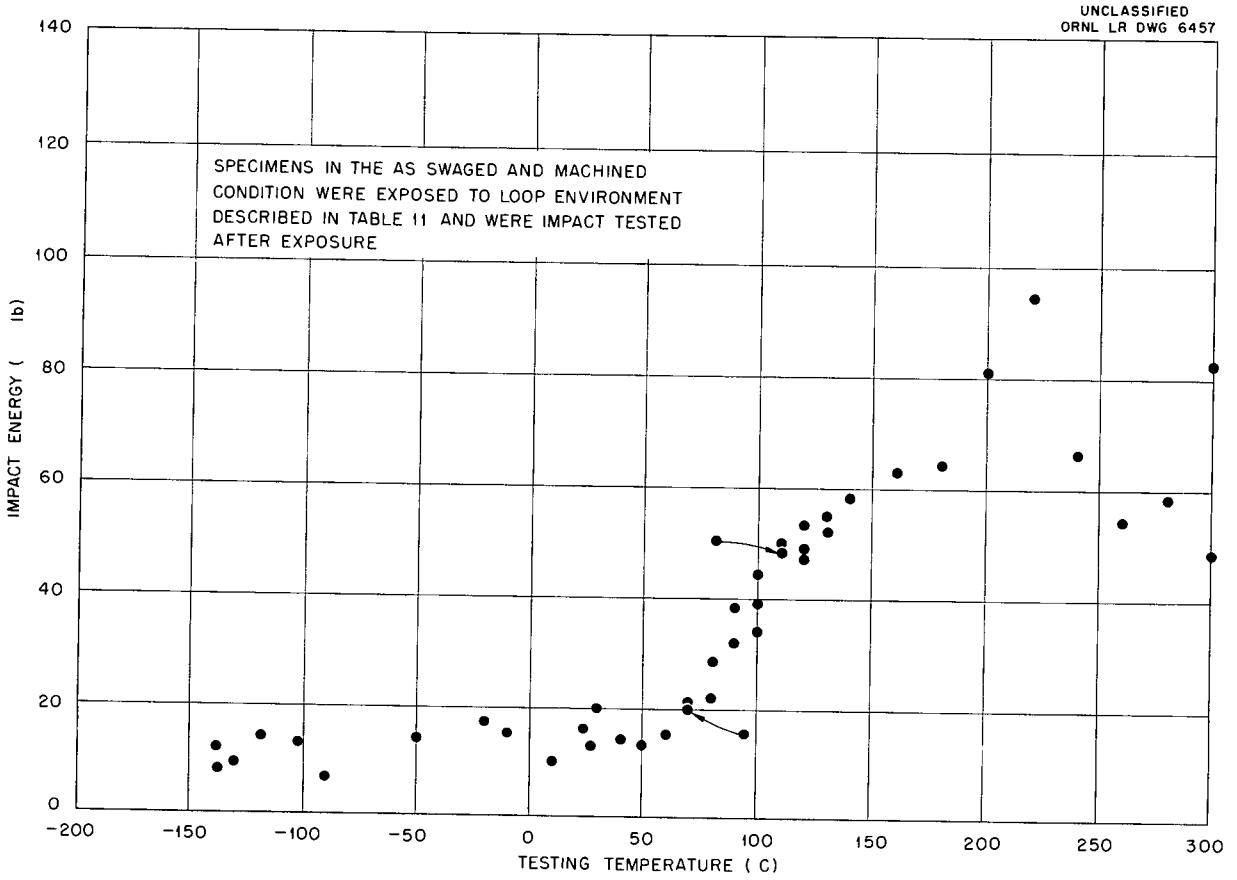

Fig 43 Impact Energy vs Testing Temperature for Ti 75A Reed Item 24 Heat L782

for vacuum annealed iodide titanium Exposure to the corrosive environment under the test conditions outlined had little or no effect on the impact behavior of the material tested

Bureau of Mines Titanium

Impact specimens exposed to the HRP loop environment described in Table 15 were impact tested The resultant data are presented in Table 16 A comparison of these data with impact data on unexposed vacuum-annealed Bureau of Mines titanium[4] does not reveal any effect of the corrosive environment on the impact properties of the exposed samples under the test conditions

Zirconium Alloys

Zircaloy 2 rod (3/8 in in diameter) was cold swaged to 0 217 in in diameter sandblasted

[4] W J Fretague and J O Betterton *HRP Quar Prog Rep July 31 1953* ORNL 1605 p 121

TABLE 12 LOOP HISTORY OF VACUUM ANNEALED UNALLOYED TITANIUM IMPACT SPECIMENS

HRP Loop Run No	Solut on: Uranium Concentr tion s UO_2SO_4 (g of U per liter)	Solut on: Additions	Temperature (°C)	Time (hr)
G 11	300 (1 34 *M*)	0 3 *M* H_2SO_4 1000 ppm O_2	300	150

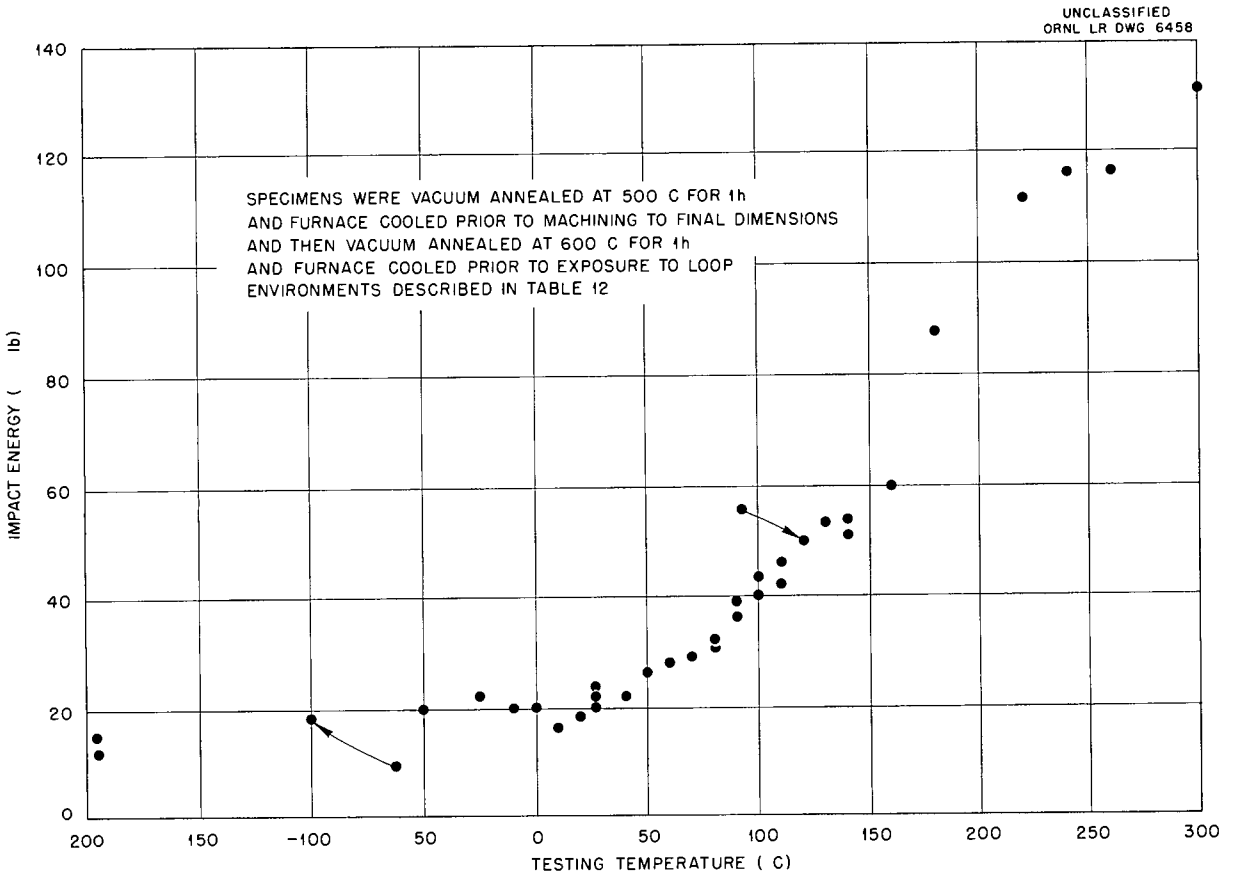

Fig 44 Impact Energy vs Testing Temperature for Ti 75A Reed Item 24 Heat L782

pickled and vacuum annealed at 750°C for 2 hr and furnace cooled Impact specimens were machined from this annealed rod and tested over the temperature range from −197°C (liquid nitrogen) to +300°C The impact data obtained are presented in Fig 46 These data serve as a base line for comparison with similar specimens exposed to HRP loop environments prior to impact testing

Tensile tests have been performed at room temperature and at 600°F on specimens cut from 5/16 in thick welded Zircaloy 2 plate fabricated by Newport News Shipbuilding & Drydock Co The results of these tests are listed in Table 17

TABLE 13 HYDROGEN IN UNALLOYED TITANIUM FROM RUPTURED PRESSURIZER TUBE

Laboratory Performing Analysis					
Bottelle Memorial Institute			Oak Ridge National Laboratory		
Sample code	Location	Hydrogen content (wt %)	Sample code	Location	Hydrogen content (wt %)
N 1633	As-rece ved material	0 0109 0 0113	N 1640	As received material	0 011
N 1635	Ruptured section of pipe	0 0083 0 0089	N 1639	Ruptured section of pipe	0 0086
N 1636	Section adjacent to fracture	0 0061 0 0061	N 1638	Section djacent to fracture	0 0048
			N 1641	Section way from fracture	0 0064

*This sample was sm ller in si e (0 7 g) than the other samples (1 2 to 1 9 g) nd this probably acco nts for the difference between results obtained by the two laboratories

WELDING OF STAINLESS STEELS

W J Leonard

Evaluation of the Preplaced Consumable Insert Heliarc Welding Technique for Root Pass

Weld penetration and soundness requirements stipulated by the HRE and HRP Welding Specifi cations when the manual inert gas shielded non consumable electrode welding process is used re quire a great deal of operator training and qualifi cation time Even after having received such training a qualified welder has difficulty in con sistently meeting the quality requirements for the root pass Therefore the process used by Electric Boat Div [5] was evaluated for use in pipe welding Type 347 stainless steel preplaced root wire machined to the proper dimensions was obtained Type 347 stainless steel piping sizes 3 to 8 in in diameter and with wall thicknesses of schedules 20 and 40 was machined to proper weld groove dimensions and assembled for welding

The chemical compositions of the two heats of root wire were balanced so as to give 6 and 8% ferrite respectively The base metal was fully austenitic Wall thicknesses varied from 0 200 to 0 322 in Root passes made by this method were satisfactory and well within the HRP specification requirements They required less operator skill than do existing welding methods and there was no apparent difference in welding time Improved weld quality resulted but was obtained at a some what higher cost because of the added expense of preplaced wire and initial machining

A program is now under way to qualify this com plete procedure and to set up an operator qualifica tion standard

Welding Development on 1 in Carbon Steel Plates Clad with Type 347 Stainless Steel

The pressure vessel in the HRT design is to be a spherical outer container of 4 in carbon steel plate clad with type 347 stainless steel on the interior with an internal diameter of approximately 5 ft The design is such that the final girth weld must be made from the outside only rather than by the more common back chipping method which allows welding from both sides Where the welding must be done from the carbon steel side only one suggested procedure is to fill the root and groove with stainless steel weld metal to a point above the interface between the carbon steel and stain less steel follow this with an intermediate layer of a few passes of a material such as ingot iron, low carbon steel type 308L stainless steel or

[5] T A Risch and A E Dohna *Welding J (NY)* 33 670 (1954)

TABLE 14 LOOP HISTORY OF IODIDE TITANIUM IMPACT SPECIMENS

HRP Loop Run No	Solution: Uranium Concentration as UO_2SO_4 (g of U per liter)	Solution: Additions	Temperature (°C)	Time (hr)
A 67	15	0 006 M H_2SO_4	310–320	977

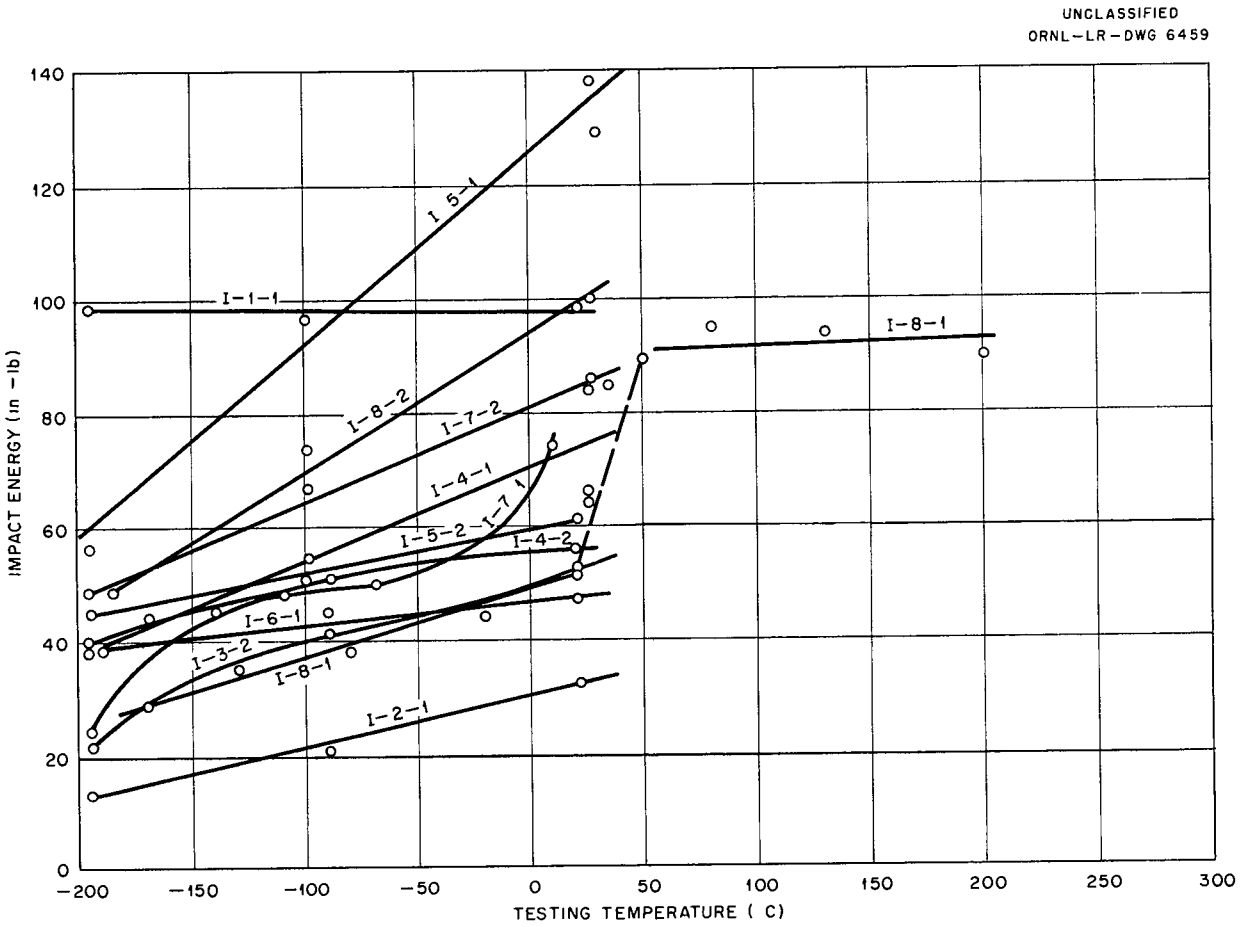

Fig 45 Impact Energy vs Testing Temperature for Arc Melted Swaged and Vacuum Annealed Iodide-Titanium Specimens I 4 1 I 5 1 I 7 2 and I 8 2 were exposed prior to impact testing under the conditions listed in Table 14 All other specimens were tested in the vacuum annealed and machined condition

TABLE 15 LOOP HISTORY OF BUREAU OF MINES IMPACT SPECIMENS

HRP Loop Run No	Solution		Temperature (°C)	Time (hr)
	Uranium Concentration as UO_2SO_4 (g of U per liter)	Additions		
G 9	300	50 psi O_2 at room temperature	300	427

TABLE 16 IMPACT ENERGY vs TESTING TEMPERATURE DATA FOR BUREAU OF MINES TITANIUM SPECIMENS EXPOSED IN HRP LOOP RUN G-9

(Scale used 0–200 in lb)

Specimen No	Break No	Temperature (°C)	Impact Energy (in lb)	Remarks
B2 1	1	27	125	Threaded end
	2	27	148	Did not break
	3	–197	182	50% fracture
B2 2	1	27	100	Threaded end
	2	27	144	50% fracture
	3	–197	178	50% fract re
B3 1	1	27	100	Threaded end
	2	27	133	60% fracture
	3	–197	142	75% fracture
B3 2	1	27		Broken by hand
	2	27	128	60% fracture
	3	–197	156	60% fr cture

The ends of the specimens were threaded to e able them to be held n the spe men f xt re the loop the thread extended below the point of mpact of the strik ng hammer of the mp ct te ter and the defo mat on of the threads on mpa t give r se to some error in the re ding

Specimen was too short to be broken by the impact tester

TABLE 17 RESULTS OF TENSILE TESTS ON ZIRCALOY 2 WELDED PLATE

Specimen No	Testing Temperature	Yield Strength 0 2% Offset (psi)	Tensile Strength (psi)	Elongation (%)	Reduction in Area (%)
ZW 33 1	Room temperature	55 000	55 000	0	0
ZW 33 2	600°F	28 000	37 000	20	63 4

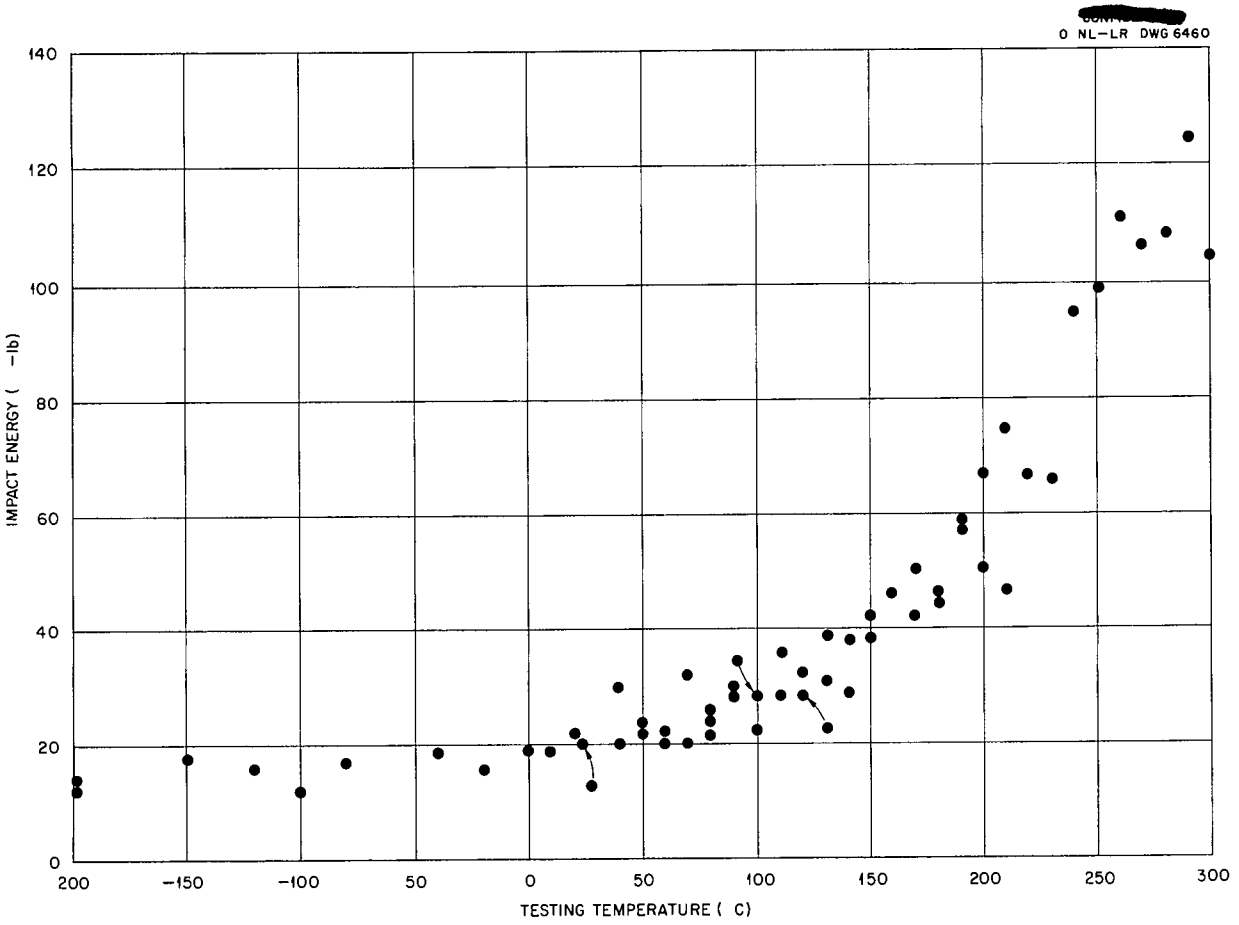

Fig 46 Impact Testing Behavior of Zircaloy 2 ($\frac{3}{8}$ in Rod Swaged to 0 217 in dia Rod Sand Blasted Pickled Vacuum Annealed at 750°C for 2 hr and Furnace Cooled)

type 310 stainless steel and complete the weld with low hydrogen mineral coated carbon steel electrodes

To evaluate several variations of this proposed welding sequence a 1 in thick plate of ASTM A201 grade A carbon steel with a 20% cladding of type 347 stainless steel was obtained The root face and groove were prepared by machining test specimens to accommodate the preplaced wire used in the Electric Boat Heliarc welding method Previous work and qualification on this method of Heliarc welding indicated the desirability of using this method rather than manual Heliarc welding in conformance with HRP welding specifications to obtain closer control of root penetration and weld soundness

Six welds of this type were made in these specimens (Fig 47) by using the Heliarc welding method described with type 347 preplaced wire Amperage was varied from 140 maximum to 90 minimum for different weld metal passes travel speed of the electrode was varied from 1 to 4½ in /min These manipulations allowed control of the heat input per pass thus regulating the resulting penetration and dilution At each amperage level used a heat input over a certain critical value resulted in cracking of the root pass At a 140-amp welding current a minimum welding speed of 4 in /min must be maintained to secure a sound root pass At 90 amp a speed of 1 in /min or greater resulted in sound welds At lower amperages travel speed is less critical because of greater dissipation percentagewise of the total heat by the base plate All passes that cracked were ground out and rewelded so that eventually all plates had sound root passes

These welds were completed up to the carbon steel and stainless steel interface by filling with coated electrode type 347 stainless steel Some

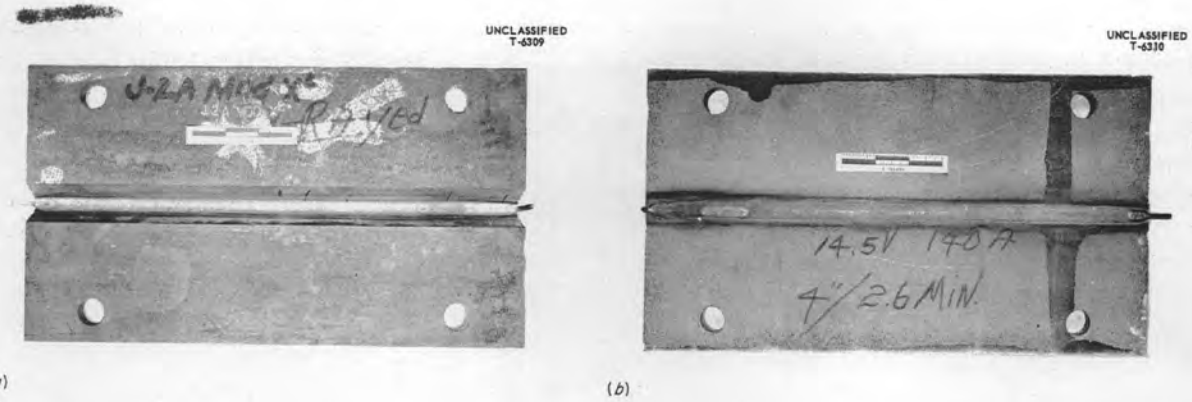

Fig. 47. Carbon Steel–Type 347 Stainless Steel Clad Plate with Heliarc Root Pass (Electric Boat Welding Technique). Cracking which occurred during welding shown from (*a*) face and (*b*) root side of weld.

were then given a cover pass or two of type 310 or 308L stainless steel coated electrode in accordance with the schedule set up for the program. One was finished by using carbon-steel electrodes of low-hydrogen mineral-coated types E6016 and E7016. The balance are to be completed by various special techniques.

The one completed weld indicates that this technique produces a sound weld, based on radiographic and liquid-penetrant inspections. However, until the specimens are sectioned for micrographic examination for microfissuring and are mechanically tested, no definite conclusions can be made as to the acceptability of this method of producing pressure-vessel welds.

Type 347 Stainless Steel Welds in Which Various Type 347 Stainless Steel Filler Metals Were Used

W. J. Leonard T. M. Kegley, Jr.

A grooved fillet weld was made to the inner wall of a type 347 stainless steel pipe ($\frac{1}{4}$-in. wall thickness) by using a $\frac{5}{8}$-in. plate (Fig. 48). A J-groove design was used, and the starting point of each successive pass was moved a short distance along the periphery so that sectioning of the weld would allow the weld cross section to be viewed at any stage of completion.

Figure 48 shows a section after the first pass, while Fig. 49 shows a section approximately half completed and a completed weld.

Figure 50 shows a cross section of this weld (*A*) and a similar weld (*B*). A further description of the passes, identified in Fig. 50, is given in Table 18.

Weldment *A* was made by using Heliarc welding for the first three passes. Cracks developed in the second and third passes. This area, which was almost fully austenitic, as a result of dilution of the base metal, is thought to be most susceptible to cracking under conditions of restraint. Figures 51 through 55 illustrate the microstructure at the indicated positions. It will be noted that cracking occurs in the filler metal of low ferrite content such as at positions *A*1 and *A*3.

Weldment *B* was made by Heliarc welding (inert-gas-shielded arc, tungsten electrode). The root

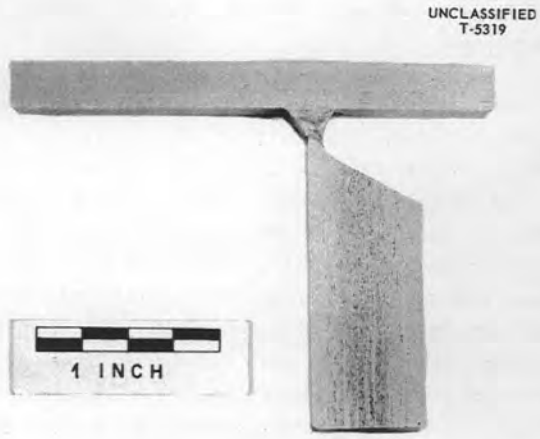

Fig. 48. Weld Cross Section with Root Pass, Illustrating Groove Design Used.

passes were made with low-ferrite filler metal and completed with high-ferrite filler wire. Some small cracks were observed in the root, where considerable dilution of the weld metal and base metal occurred. Figures 56 and 57 are photomicrographs of these areas. Cracking can be noted in the root of this weld (Fig. 50), whose microstructure is represented by Fig. 56.

[6]W. O. Harms and W. J. Leonard, *Met. Semiann. Prog. Rep. April 10, 1954*, ORNL-1727, p 19.

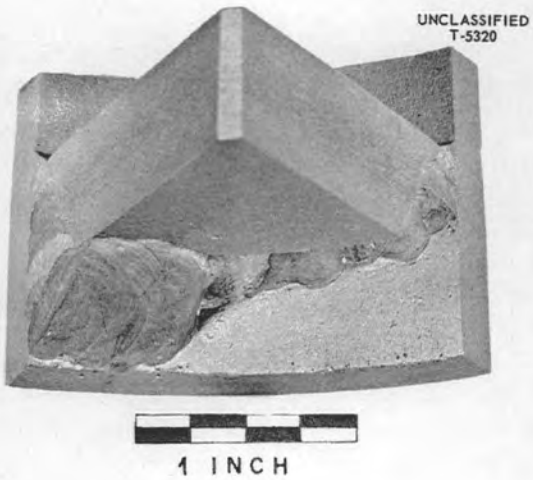

Fig. 49. Section of the Pipe Weld, Illustrating Welding Sequence.

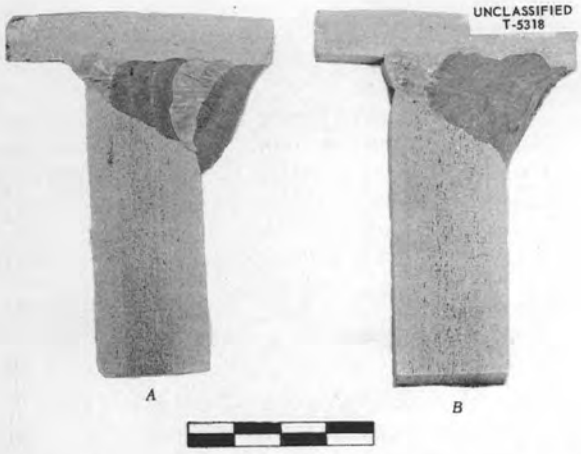

Fig. 50. Weld Cross Section with All Welding Passes Completed. (*A*) Heliarc root pass with the balance coated electrode. (*B*) Heliarc weld.

METALLURGY OF CORROSION IN HOMOGENEOUS REACTOR ENVIRONMENTS

W. O. Harms W. J. Leonard

Stainless Steel Welds

The special flat-plate-type corrosion specimens described previously[6] were tested in oxygenated

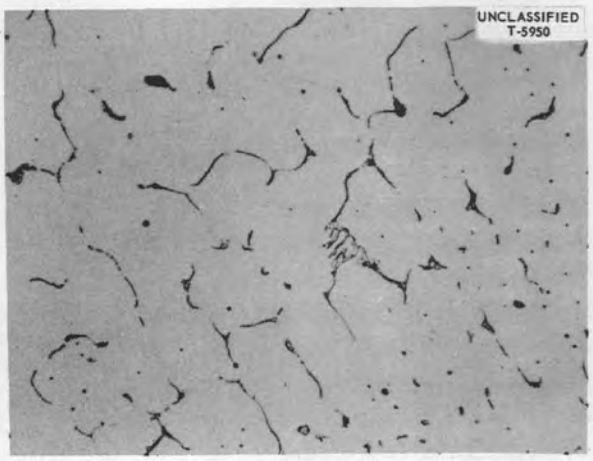

Fig. 51. Photomicrograph of Low-Ferrite Heliarc Root Pass at Position *A*1. Etchant: glyceria regia. 750X. Reduced 32%.

TABLE 18. DESCRIPTION OF WELDING PASSES SHOWN IN FIG. 50

Weld Position	Type	Welding Wire	Ferrite in Weld (%)
*A*1	Heliarc	Low ferrite	½
2	Metallic arc	Commercial coated electrode	5½, 6, 7
3	Metallic arc	Commercial coated electrode	1½
4	Metallic arc	Commercial coated electrode	6
5	Metallic arc	Commercial coated electrode used in 4; diluted 3 and base metal	
*B*6	Heliarc	Low ferrite	1
7	Heliarc	High ferrite	10

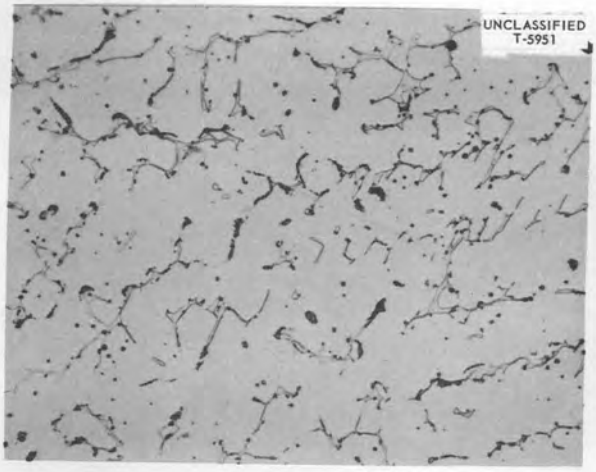

Fig. 52. Photomicrograph of Coated-Electrode Pass at Position *A*2, Having Ferrite and Carbides. Etchant: glyceria regia. 750X. Reduced 32%.

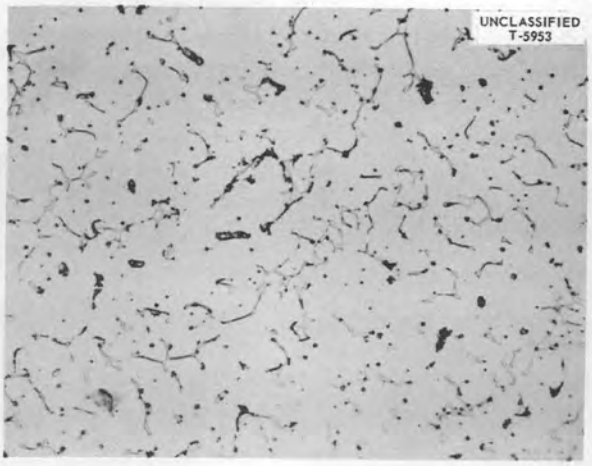

Fig. 54. Photomicrograph of Coated-Electrode Filler Pass at Position *A*4, Having Ferrite and Carbides. Etchant: aqua regia. 750X. Reduced 32.5%.

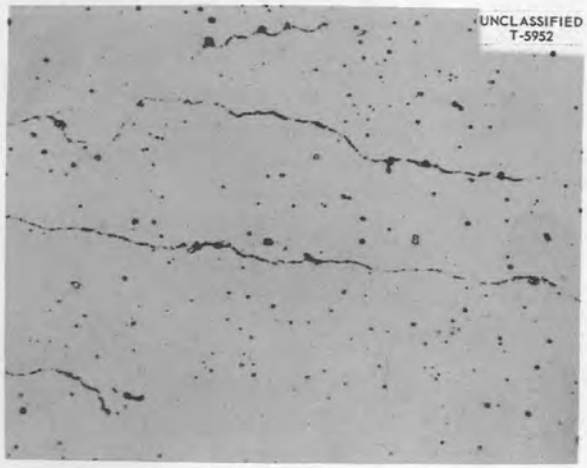

Fig. 53. Photomicrograph of Coated-Electrode Pass at Position *A*3, Having a Trace of Ferrite and Grain-Boundary Carbides. Etchant: glyceria regia. 750X. Reduced 31%.

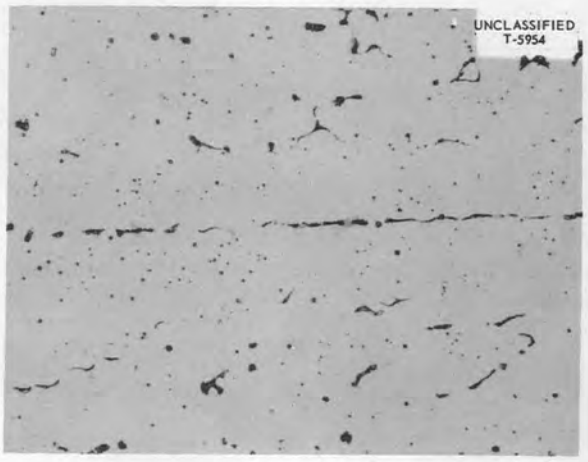

Fig. 55. Photomicrograph of Diluted Area at Position *A*5, Having Slightly Higher Ferrite Content Than Position *A*3. Etchant: glyceria regia. 750X. Reduced 32%.

0.17 *m* uranyl sulfate at 250°C and at a velocity of 20 fps for 400 hr. The results of this test, along with those of the previous 200-hr run made under otherwise similar conditions, are given in Table 19.

Specimens containing weld deposits of Composition H (experimental columbium-stabilized 18% Cr–13% Ni–5% Mn steel) exhibited superior corrosion resistance in holder B, but in holder A only small differences in weight losses were observed among the type 347, type 308L, and Composition H welds, and, in general, corrosion damage was substantially lower in holder A. This difference in behavior is difficult to understand, since the Reynolds modulus for flow through holder A was higher than for that through holder B, in which the specimens were 20% thicker.

Figure 58 shows the peculiar effect observed on Composition H welds in holder B. The zones near

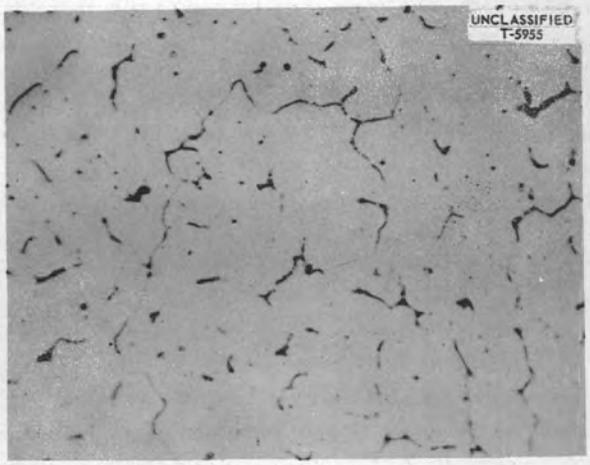

Fig. 56. Photomicrograph of a Low-Ferrite Heliarc Root Bead in Weld *B* (Position *B*6). Etchant: glyceria regia. 750X. Reduced 32%.

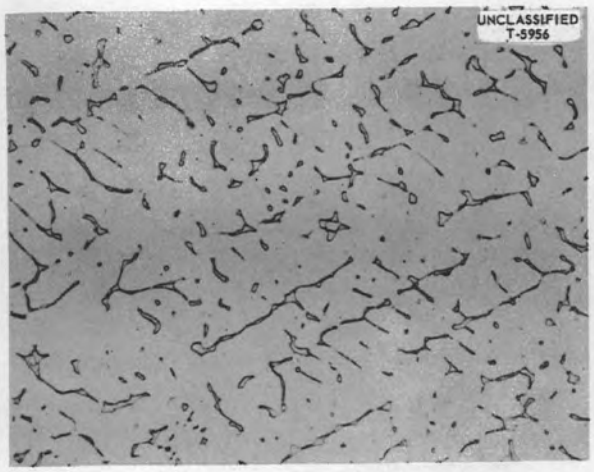

Fig. 57. Photomicrograph of a High-Ferrite Heliarc Filler Pass in Weld *B* (Position *B*7). Etchant: glyceria regia. 750X. Reduced 32%.

TABLE 19. RESULTS OF DYNAMIC-CORROSION TESTS ON SPECIAL FLAT-PLATE-TYPE WELDED AND BASE-METAL AUSTENITIC STAINLESS STEEL SPECIMENS*

	Base Metal	Weld Metal	Ferrite in Weld (%)	Defilmed Weight Loss (mg)	
				200 hr	400 hr
Holder A	347	None		83.0	115.4
	310	None		179.4	209.8
	347	347	8.0–8.5	73.9	111.7
	309SCb	None		81.9	196.1
	347	Composition H	0	96.1	186.7
	304L	None		53.6	114.1
	347	308L	9.0–11.0	98.0	174.9
	304	None		55.7	190.9
	347	Composition H	0	90.9	199.8
	347	None		84.9	199.3
Holder B	347	None		67.8	307.2
	347–304L	Composition H	0	51.8	396.6
	304L	Composition H	0	40.1	438.4
	304L	Composition H	0	**	473.4
	304L	None		39.2	504.5
	304L	308L	9.0–11.0	56.8	921.2
	304L–347	308L	9.0–11.0	68.3	893.1
	304L–347	347	8.0–8.5	78.2	560.0
	304L	347	8.0–8.5	57.6	712.3
	347	None		83.0	339.7

*Specimens were tested in 0.17 *m* uranyl sulfate, 250°C, 20 fps. Thicknesses of specimens in holder B were 20% greater than those in holder A. Welded specimens were tested in the as-welded condition, and wrought specimens were tested in the solution-annealed condition.

**Weighing error.

Fig. 58. Special Flat-Plate Welded Corrosion Specimen of Type 304L Stainless Steel Joined by Composition "H".

the top of each weld pass maintained protective oxide films, while bare-metal corrosion occurred on the remaining portions. A small amount of this type of behavior was observed on type 347 welds, but type 308L showed practically none. Metallographic examination revealed that the portions supporting stable films contained many randomly dispersed carbide particles, while the remainder exhibited the more typical quasi network due to interdendritic segregation. The thermal cycle corresponding to that undergone by the top portion of each pass has been calculated so that an all-weld-metal or a cast specimen can be heat-treated similarly and corrosion-tested at a later date.

Two additional sets of special flat-plate-type dynamic-corrosion specimens were machined from ¼-in. type 347 plates containing type 347 welds made by the Heliarc process with the use of a low-ferrite wire (2–4%) for one set and a high-ferrite wire (7–9%) for the other. Weld reinforcements were left on in the majority of cases so that the flow over coupons would approximate actual service conditions in butt-welded pipes. Differences in height of the face and the root reinforcements on these coupons caused variations in solution velocity, and the velocity effects were probably more severe than would normally be experienced at a butt-welded pipe joint. The specimens were tested in oxygenated 1.34 *m* uranyl sulfate solution at 250°C for 100 hr. The average velocity was 10 fps and the maximum was 16 fps. While averaged defilmed-weight-loss data hardly justified a distinction between the corrosion resistance of the high- and low-ferrite welds, it was observed that the films on samples containing 2 to 4% ferrite were somewhat more tenacious.

In order to get more information on the effect of ferrite content on the dynamic-corrosion resistance of austenitic stainless steel welds, all-weld-metal specimens ranging in ferrite content from 0 to 12% were tested in 0.17 *m* uranyl sulfate at 250°C under oxygen pressure and at velocities of 15 and 30 fps for 200 hr. These specimens were machined from the top half of ½-in.-thick weld pads deposited on type 347–buttered carbon-steel plate by using the argon-shielded tungsten-arc process under the following conditions: 200 to 220 amp, 12 to 16 v, and average travel speed of 4 in./min.

The results of runs M-23 and M-24 are shown in Table 20. Included in the main line in run M-23 was a chromized tube bundle consisting of seven tubes, ⅜-in. OD and 0.049-in. wall thickness, which underwent severe corrosion attack causing abnormally high concentration of hexavalent chromium ion in the solution. Since this is known to inhibit attack in uranyl sulfate, it was believed that the results of run M-23 required confirmation. Run M-24 was undertaken for this purpose, and it was observed that, although relative behavior was similar in both runs, differences were much more pronounced in the check run. These results indicate that, since alloy No. 4 (containing only a small amount of ferrite) showed by far the highest weight losses, the ferrite content per se is not so significant a factor in corrosion behavior as was suggested in previous runs. Previous data, however, indicate that ferrite has a deleterious effect on corrosion at higher uranium concentrations.

The several test results reported here indicate that factors other than ferrite content are operating to render these welds more or less corrosion resistant, at least at concentrations up to 0.17 *m* UO_2SO_4. To solve this problem will require considerable work in the identification of the various microconstituents and in the separation of these constituents so that independent chemical-composition and crystal-structure studies can be undertaken.

TABLE 20 DYNAMIC CORROSION OF AUSTENITIC STAINLESS STEEL WELD METAL CONTAINING VARYING AMOUNTS OF FERRITE

Alloy[a]	Ferrite in Weld[b] (%)	Weight Loss (mg/cm^2)			
		Run No M 23[c]		Run No M 24[c]	
		14 0 fps	28 4 fps	15 5 fps	30 5 fps
F	None	2 8	4 2	2 7	9 3
		1 5	1 6	3 6	8 0
H	None	2 5	13 8	3 5	51 5
		2 5	3 8	3 5	18 2
4	3 5–4 5	1 5	11 8	4 1	134 8
		1 2	11 6	4 2	154 9
P	6 0–6 5	1 7	3 1	2 3	10 2
		1 9	2 5	2 8	8 8
1	6 5–7 5	2 1	3 2	2 9	24 7
		1 2	2 9	2 4	15 2
3	7 5–8 5	1 1	2 4	1 3	6 2
		1 2	2 2	1 9	5 9
2	11 5–12 5	5 9	2 8	2 0	8 0
		5 9	2 7	2 0	6 7
Wrought annealed type 347		1 3	12 7	5 7	4 6
		2 6	2 5	2 0	8 8
		1 4	11 8	5 8	5 8
		0 9	1 3	2 0	5 5
Wrought annealed type 17 4 PH		0 7	1 3	1 4	8 2
		0 7	1 0	1 3	2 7

[a]Alloys 1 2 3 and 4 are type 347 stainless steel weld wires
Alloy H is 19 13 5 Cr Ni Mn columbium stabilized alloy
Alloy F is 19 10 5 Cr Ni Mn not stablized
Alloy P is 19 10 2 5 max Cr Ni Mn partially ferritic alloy
Alloy 17 4 PH is 17 4 4 precipitat on harden ng Cr Ni C alloy n unhardened cond t on
[b]Ferrite content determined by Magne gage measurements
[c]Conditions of runs M 23 and M 24 0 17 *m* uranyl sulfate 250°C 200 hr Rapid corrosion of a chromized tube bundle in the main line of run M 23 caused abnormally high concentration of Cr^{6+} in solution and correspondingly lower corrosion losses on specimens

Commercial Titanium and Zircaloy 2 Welds

Welds were made in ¼ in plates of Ti 75A and Zircaloy 2 with wire of the same compositions in a dry box under a helium atmosphere Special flat plate-type corrosion specimens were machined from these plates without affecting the weld re inforcements Four specimens of each type were tested in oxygenated 1 34 *m* uranyl sulfate at 250°C for 200 hr and at solution velocities ranging from 50 to 92 fps Tenacious bulk scales of iron and chromium oxides were deposited on these speci mens but a thin light green substrate film on the titanium and a thin gold colored substrate film on the Zircaloy 2 protected the materials so that corro sion was negligible The as removed and scrubbed weight gains were comparable to those for samples of base material which were included in the run for comparison

Intergranular Corrosion of Austenitic Stainless Steels

W. O. Harms

Tubing from H Loop Pressurizer Mixing Line. – Three failures occurred in the ¼-in. tubing of 0.035-in. wall thickness in the pressurizer mixing line of dynamic loop H during exposure to 1.34 *m* uranyl sulfate at 225°C and at an estimated velocity of 25 fps. A type 347 seamless tube failed after 492 hr, a type 316 welded tube after 22 hr, and a type 347 welded tube after 188 hr. The seamless-tube failure was not so clearly intergranular as were the failures in the welded tubes. Figure 59 illustrates the welded-tube failures.

Letdown Valve in HRE Mockup. – The components of a letdown valve in the HRE mockup, which was removed because of excessive leakage, consisted of type 347 stainless steel with a Stellite 6 overlay in the seat and on the guide stem and of a solid Stellite 6 plug. The weld deposit in both the seat and the stem exhibited porosity, and chemical analysis showed that cobalt and probably tungsten had been selectively leached from this alloy. Severe intergranular penetration in the type 347 material near the fusion zone was observed. This penetration was apparently due to the diffusion of carbon from the stellite, followed by precipitation of chromium carbides on slow cooling through the sensitizing temperature range.

Pin-Type Corrosion Specimens. – Metallographic examination of pin-type specimens of stainless steel types 316L, 316, 304L, 309SCb, 347, and 304 sensitized, which had been tested in oxygenated 1.34 *m* uranyl sulfate at 225°C and at flow rates of 17–18 and 65 fps, revealed the following:

1. Only the type 304L specimen escaped intergranular attack in high-velocity runs, in which types 316L, 316, and 309SCb showed poorest resistance to this type of attack.

2. At the low flow rates, types 316L, 304 sensitized, and 316 were intergranularly attacked. A typical microstructure of the type 304 specimen is shown in Fig. 60.

Huey Tests on Tubing and Plate Stock. – In cooperation with the HRP Static Corrosion Group, an investigation was initiated to determine whether HRP stainless steel stock passed laboratory-type corrosion tests. Seven samples of types 304L and 347 tubing and plate were subjected to the boiling 65% nitric acid test (Huey test) to determine their susceptibility to intergranular corrosion. This test, which consists of up to five 48-hr exposures to the boiling acid, requires that acceptable material show corrosion rates of less than 2.0 mils per month for each 48-hr period. Results of this study, the details of which have been reported elsewhere,[7] were as follows:

[7] J. L. English, *HRP Quar. Prog. Rep. April 30, 1954*, ORNL-1753, p 106.

Fig. 59. Microstructure at Penetration in Type 316 Stainless Steel Welded Tubing from Pressurizer Mixing Line of H Loop. Etchant: aqua regia. 250X. Reduced 32%.

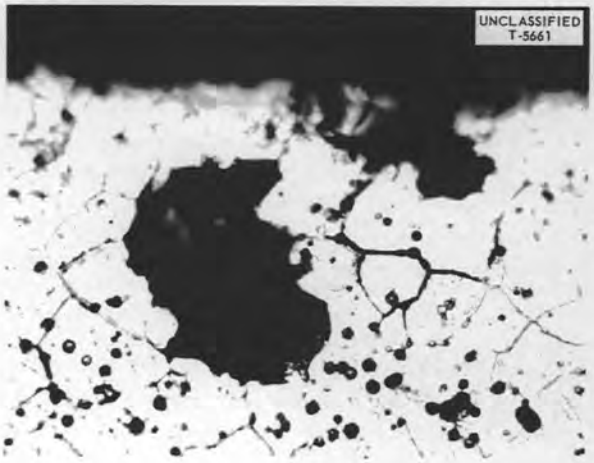

Fig. 60. Microstructure of Sensitized Type 304 Stainless Steel After Corrosion Testing in 1.34 *m* Uranyl Sulfate at 225°C. Etchant: aqua regia. 1000X. Reduced 32%.

1 Welded type 304L tubing from one supplier showed corrosion rates as high as 58 5 mils per month after a sensitizing treatment Chemical analysis later revealed that this material contained 0 075% carbon and was either a straight type 304 stainless steel or had picked up a substantial amount of carbon during processing

2 Seamless type 347 stainless steel tubing from another supplier failed the Huey test after a sensitizing treatment Chemical analysis then showed this material to be deficient in columbium the Cb/C ratio being 0 3 instead of 10

3 Even though catastrophic corrosion due to the dropping out of grains did not occur within the five test periods some type 304L and 347 materials maintained corrosion rates from 1 to 3 mils per month greater than the rates allowable in existing specifications

Stress Corrosion Cracking in Austenitic Stainless Steels

Tubing Failures in Dynamic Loop C – Two transgranular failures on the inside of 90- and 180 deg bends of ⅜ and ½ in schedule-40 type 347 stainless steel are believed to have occurred as the result of the combined effects of stress and corrosion Details of an investigation of these failures and photomicrographs have been published elsewhere[8] It was interesting to note that these parts, which had not been stress relieved after bending were in service for almost 7800 hr before failing The failures occurred shortly after a 1000-hr run at 100°C, in which Oak Ridge tap water was sprayed on the pipe for temperature control The scale that formed on the first failure was of the boiler type containing large amounts of calcium and magnesium The second failure had received considerable protection from the magnesia base lagging material but still had been wet by the tap water The presence of 7 to 10 ppm of chloride ion in the water may have figured in the transgranular stress corrosion observed The boiling 42% magnesium chloride test showed that specimens from the bent portion of the tube were considerably more susceptible to transgranular cracking than was a specimen from a straight pipe section

Failure of Type 347 Capillary Tubing in In Pile Mockup Loop – Leaks in the 0 060 in capillary tubing of both the hydrogen and the oxygen lines of in pile mockup loop BB 2 resulted when transgranular cracking occurred The presence of caked uranyl sulfate in the oxygen line suggested that cracking was due to stress corrosion Since the time of this failure two of the small pressurizer assemblies have been given partial stress relief heat treatments at 950°F for 6 hr in hydrogen

Laboratory Tests – Two simulated HRT tube to tube sheet assemblies in which ⅜ in OD 0 049 in wall type 347 stainless steel tubes had been expanded in a rolling operation by 0 006 and 0 0015 in were tested in boiling 42% magnesium chloride solutions In addition as received tubes were tested for comparison Cracks were observed after 5 hr in the expanded end of the 0 006 in rolled specimen, near the surface of the tube sheet After 10 and 15 hr tubes in this assembly showed many cracks in those areas where the rollers machined into the tubing On the other hand the 0 0015 in rolled material showed only a few minor superficial cracks even after 15 hr of exposure No cracks were observed in the as received tubing This indicates that the use of the lighter expansion renders much less probable a stress corrosion failure in the HRT heat exchanger

The addition of new personnel has made possible a continuation of the research program outlined in the previous report[9] One hundred and sixty constant stress specimens have been formed in the special jig These include two compositions of type 304L and one each of types 347 309SCb and 316L covering a large range of martensite forming susceptibilities

[8] E C Miller W O Harms and T W Fulton *HRP Quar Prog Rep April 30 1954* ORNL 1753 p 117–119

[9] W O Harms and E C Miller *Met Semiann Prog Rep April 10 1954* ORNL 1727 p 20

PACKAGE POWER REACTOR PROGRAM

J E Cunningham

Work is continuing on the development of a relatively cheap reliable stainless steel fuel element for service in the proposed Army Package Power Reactor Results of recent brazing tests on full scale components containing normal uranium dioxide are encouraging and tend to support the selection of this method of construction

Careful inspection and metallographic examination of composite fuel plates reveal that boron carbide is not a suitable burnout poison for use in the preparation of stainless steel–uranium dioxide fuel plates Apparently B_4C dissociates or is reduced in contact with stainless steel under the time temperature conditions employed in the fabrication schedule and forms a low melting eutectic phase Two possible replacement compounds ZrB_2 and BN are presently undergoing rigorous time temperature studies to determine their stability in the presence of stainless steel for the proposed application

The Package Reactor core has recently been redesigned for a service life of 15 rather than 30 megawatt years (Mwy) Also results of new critical mass calculations have further lowered the fuel loading requirements These design changes have altered several features of the stainless steel flat plate type fuel element New specifications on the modified fuel element for 15 Mwy operation in the Package Reactor are given below

Number of f el plates	18
Side plate th ckness mils	50
Clad core clad thickness mils	5 20-5
Core composition wt %	17 92 UO_2 0 75 ZrB_2 81 33 SS
Water gap spacing mils	134 ± 13
U^{235} content g	398 34
Natural boron content g	3 9
Metal to water volume ratio	0 26
U^{235} concentration g/cm^2	0 062
Total absorpt on cross section cm^2	1001
Total fission cross section cm^2	587
Average burnup of U^{235} atoms %	42
Average burnup of total atoms in core mixture %	1 5

The metal to water volume ratio was calculated on the basis of assigning one half the water gap spacing between adjacent fuel assemblies to a single fuel unit The total absorption value given does not take into account the water surrounding the unit If the water is included this value must be increased to 1053 cm^2

Effort by the Metallurgy Division on the Package Power Reactor program during the past six months was primarily concerned with fabrication of composite stainless steel–uranium dioxide fuel plates component assembly by brazing corrosion studies MTR irradiation experiments and equip ment design for the manufacture of enriched stainless steel fuel elements Experimental results and progress on each phase of work are reported in detail below

FABRICATION OF COMPOSITE STAINLESS STEEL–URANIUM DIOXIDE FUEL PLATES

R J Beaver

One hundred and fifty plates of UO_2 in a stainless steel matrix clad with type 304L stainless steel have now been fabricated The majority of the plates contained 34% UO_2 and 0 5% B_4C but several plates have recently been fabricated with 25 9 and 17 9% UO_2 This composition change apparently has little effect on the fabricating characteristics of the plates At present the billet is being prepared by blanking the stainless steel frame inserting the cermet core and edge-welding the cover plates to the frame The billet corners are left unwelded to permit expulsion of entrapped air during the first rolling pass

A double shear angle type punch and die set has been successfully designed and constructed to blank 0 250 to 0 300 in thick stainless steel picture frames The new tool has already simpli fied the experimental plate fabrication schedule and should be valuable in future production work

Protection of the plate surfaces during preheating and during reannealing between passes has been

satisfactorily accomplished with a hydrogen muffle furnace. Results obtained from rolling the plates out of a three-compartment muffle revealed that the technique could result in a continuous rolling operation. The approximate maximum number of plates that can be rolled in this manner in a day is 60, with an estimated hydrogen consumption of 1200 ft^3.

In the course of the fabrication and subsequent heat treatment of the stainless-steel-clad UO_2 cermets, several problems have arisen. Two effects have been encountered which result in considerable deviation in the length of the fabricated core. The first is a "fishtailing" effect observed at the ends of the core after fabrication. To illustrate this defect, a longitudinal section of the end of a core is shown in Fig. 61. Whenever the plate is rolled in the same direction – that is, so that the same end enters the mill during the reduction sequence – the fishtail is confined to the leading end of the core, while the trailing end acquires a taper. In some cases, the fishtail has been observed to string-out to a length of 0.750 in. This situation causes concern, since it increases the probability of exposing the core during the subsequent shearing and machining operations. The upper section of Fig. 62, a view of the surface of the Package Reactor fuel plate, shows the core in outline and shows the additional increase in core length caused by the tapered ends of the core. This effect is quite common in the plates and is assumed to be the result of hand-rolling. As an example of this condition, in a recent fabrication of 22 fuel plates, the as-rolled cores with square ends measured 20.500 in. in length, whereas plates with tapered ends had core lengths as long as 21.375 in. – a difference of 0.625 in. The rainbow in this particular plate is also evident. This condition is not common and is related to hand-rolling.

The bottom view of Fig. 62 is an excellent example of a plate that was blistered by entrapment of air within the billet. This condition has been eliminated by allowing the corners of the billet to remain unwelded, which permits the entrapped air to be expulsed during the first mill pass.

The influence of cold reduction on stringering and fracturing of the uranium oxide particles is illustrated in Figs. 63 to 68. Results of the study indicate that the amount of cold reduction during finishing should be less than 30% in thickness.

The grain size in the stainless steel cladding of the composite plate, after (1) fabrication at 1220°C, (2) a 2½ cold reduction, and (3) a 20% cold reduction followed by an anneal at 1180°C, is illustrated in Figs. 69 to 71. As can be seen, the grain size is quite large, approximately 1½ grains per cladding thickness (0.005 in.). The amount of cold-finishing in the range investigated had very little effect on the final grain size in the composite fuel plates.

Recent fabrication and heat-treatment tests have indicated that B_4C may not be usable in Package Reactor fuel plates. The first observation indicating the possibility of difficulty with this compound occurred during metallographic examination of a section from a plate which had been heat-treated for 1½ hr at 1180°C following fabrication. As can be seen in Fig. 72, an unidentified phase exists at the intersection of three grains in the stainless steel cladding. It is suspected that this is an iron-rich boron phase, caused by diffusion of boron into the cladding. Later, in attempting a high-temperature annealing treatment, a number of

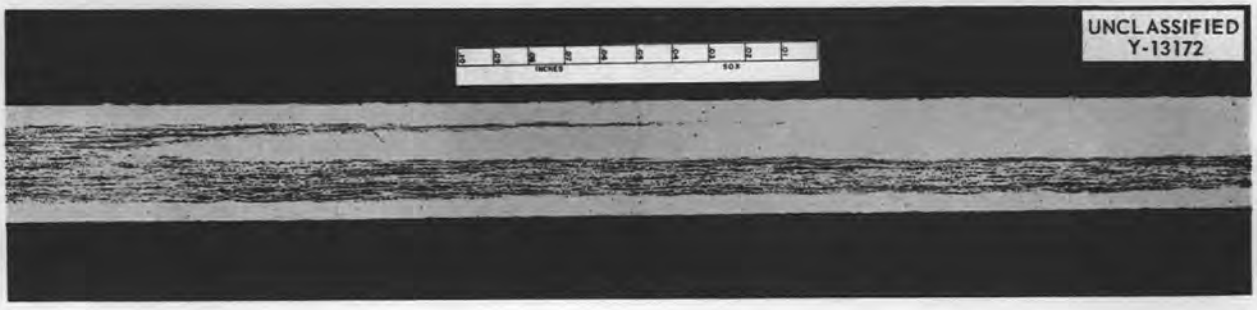

Fig. 61. Longitudinal Section at the Leading End of Plate, Showing Fishtailing of the UO_2–Stainless Steel Core.

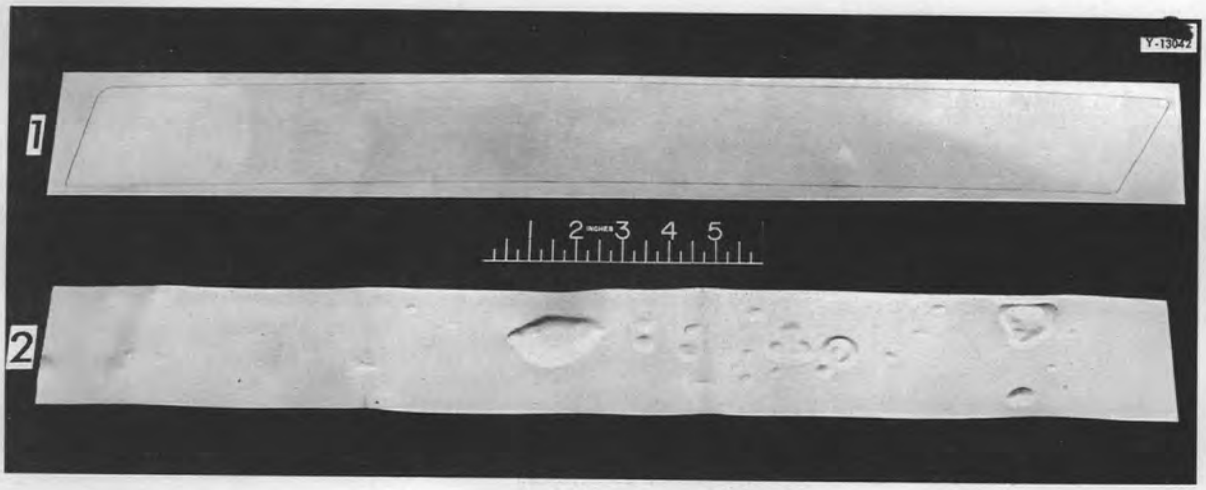

Fig. 62. Surface of Stainless-Steel-Clad UO_2 Cermet Plate, Showing (1) Tapers at the Core Ends and Rainbowing of the Core and (2) Blisters Formed During Fabrication.

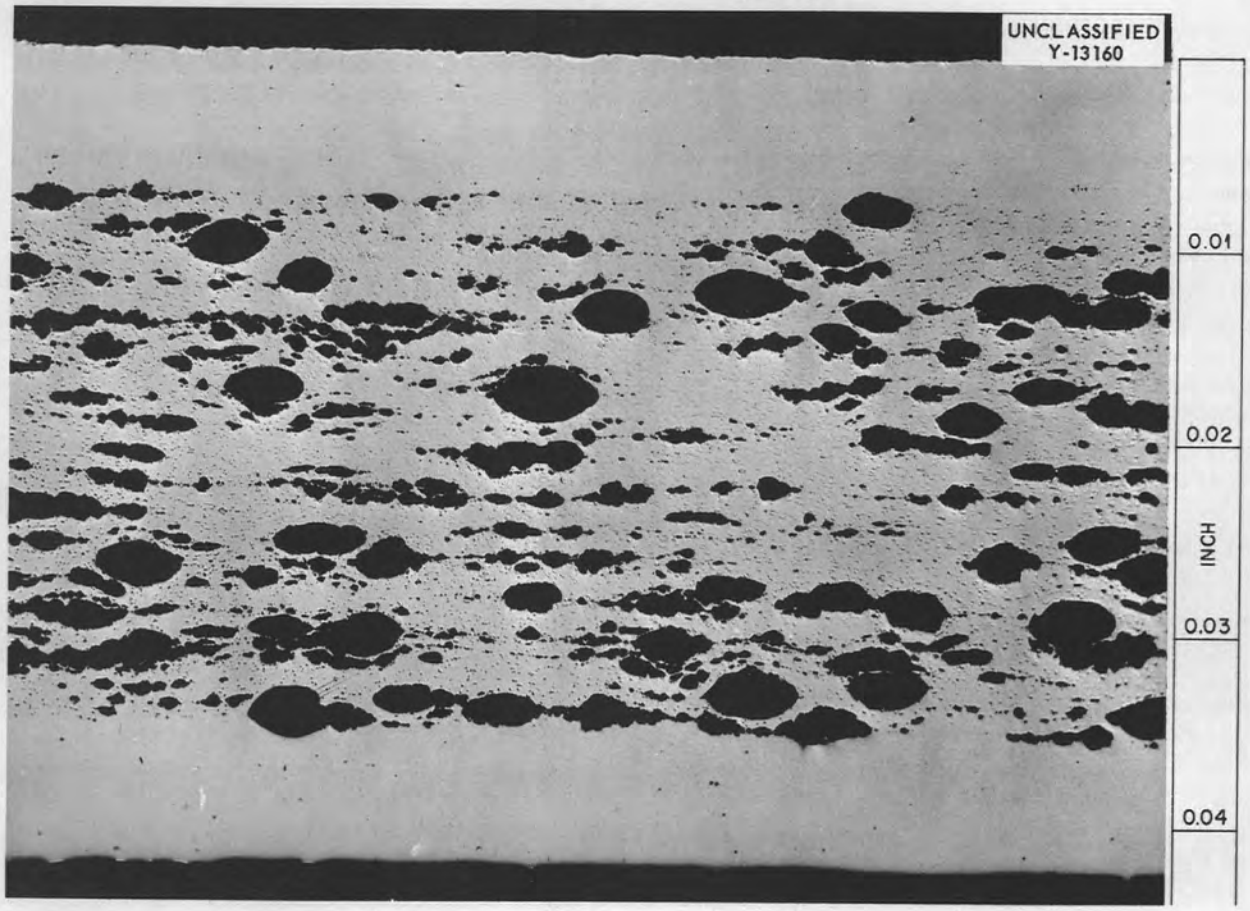

Fig. 63. Longitudinal View of Uranium Oxide After Hot Rolling. Core composition: 34 wt % UO_2, 0.5 wt % B_4C, 65.5 wt % stainless steel.

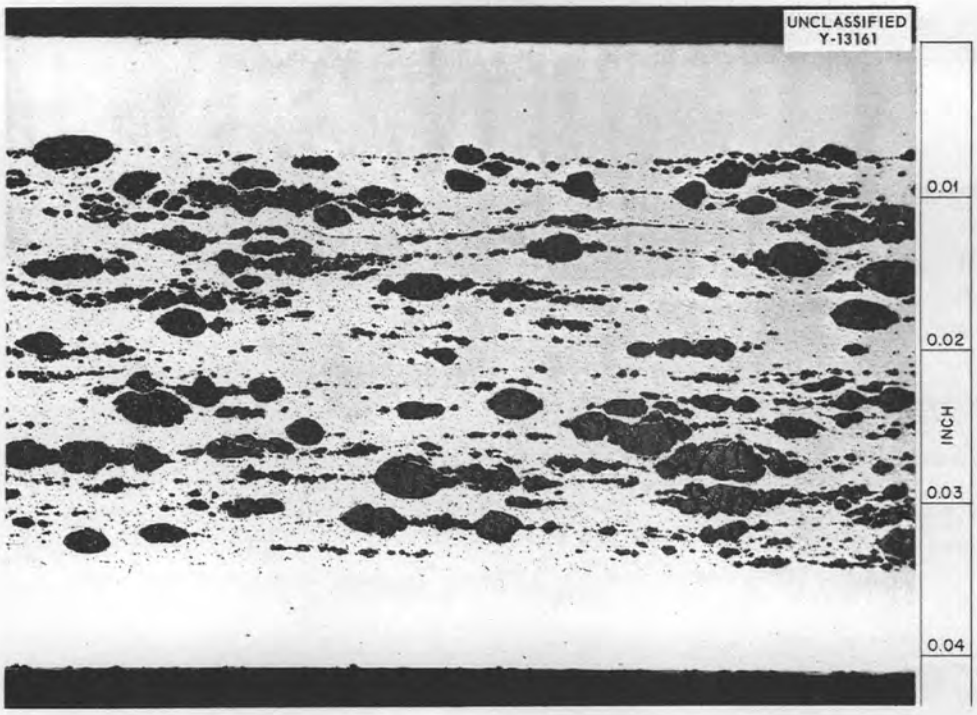

Fig. 64. Longitudinal View of Uranium Oxide (Fig. 63) After 2 ½% Cold Reduction, Showing the Effect of Cold Reduction upon Stringering and Fracturing.

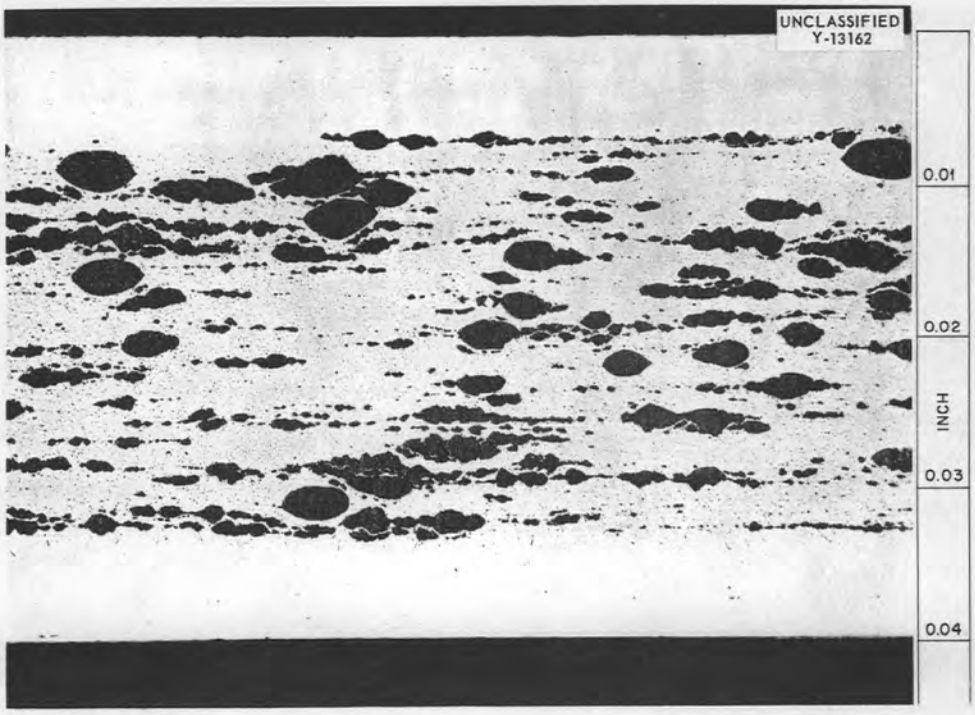

Fig. 65. Longitudinal View of Uranium Oxide (Fig. 63) After 5% Cold Reduction, Showing the Effect of Cold Reduction upon Stringering and Fracturing.

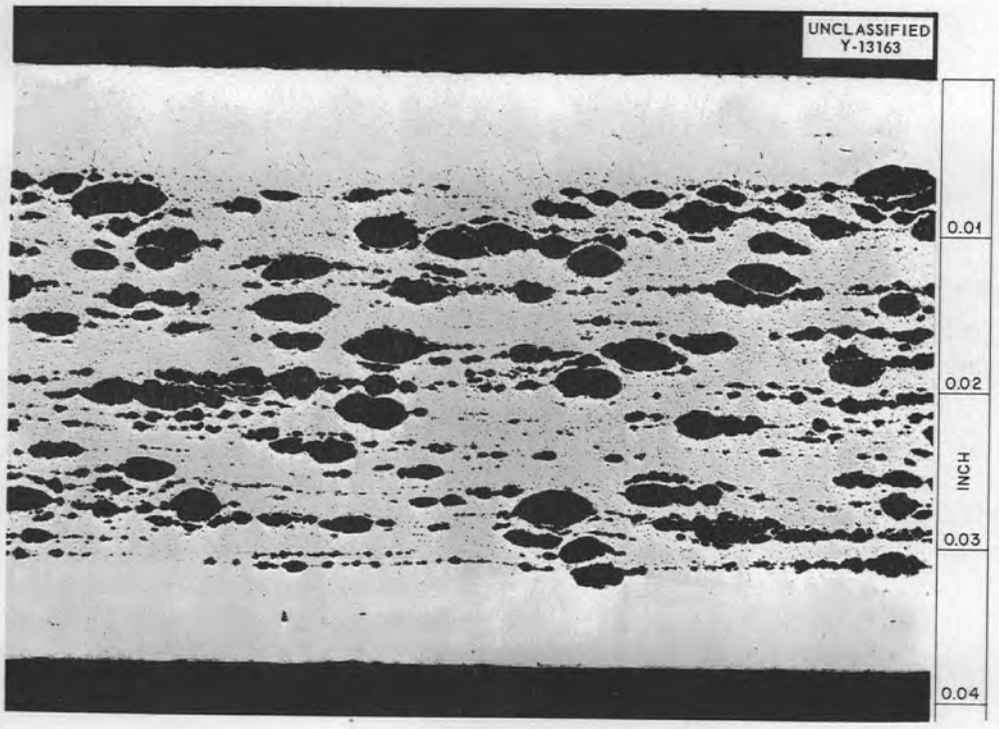

Fig. 66. Longitudinal View of Uranium Oxide (Fig. 63) After 10% Cold Reduction, Showing the Effect of Cold Reduction upon Stringering and Fracturing.

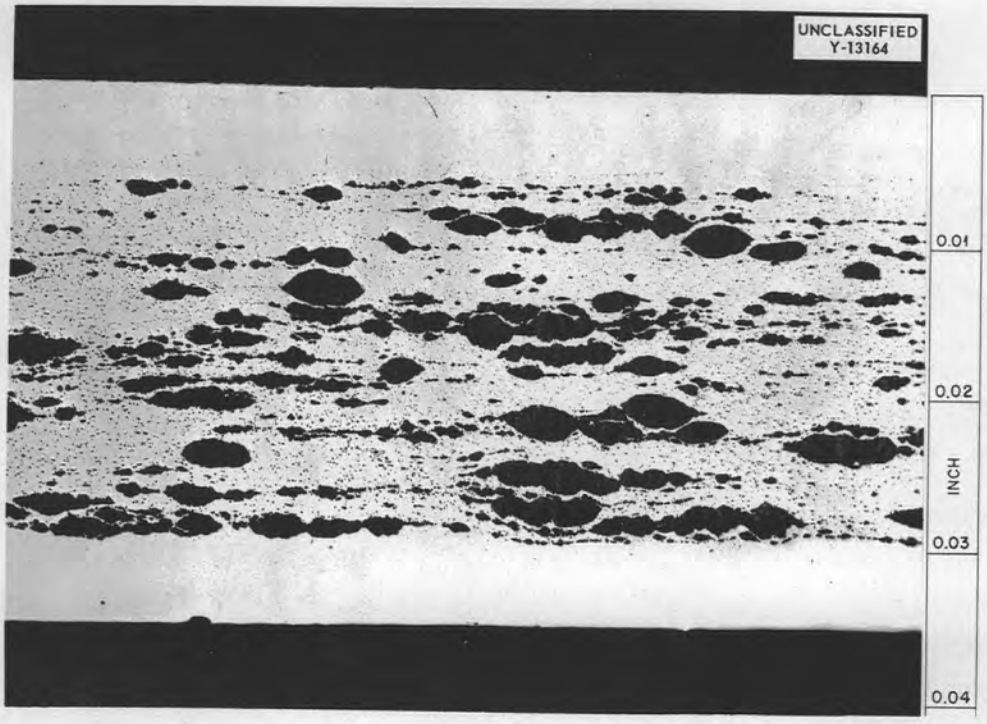

Fig. 67. Longitudinal View of Uranium Oxide (Fig. 63) After 20% Cold Reduction, Showing the Effect of Cold Reduction upon Stringering and Fracturing.

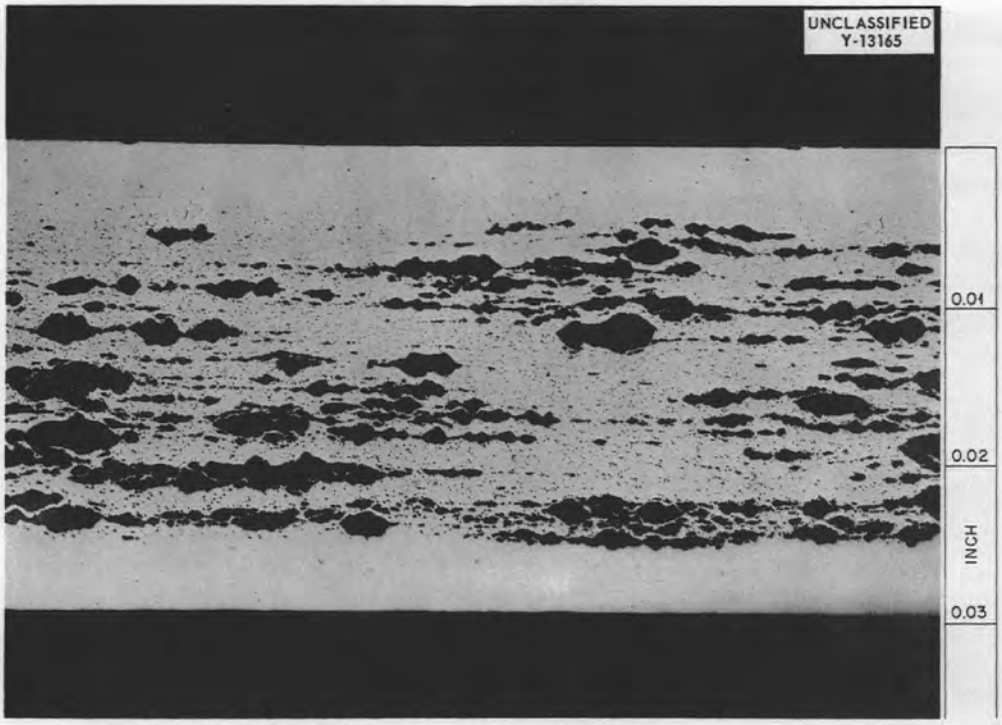

Fig. 68. Longitudinal View of Uranium Oxide (Fig. 63) After 30% Cold Reduction, Showing the Effect of Cold Reduction upon Stringering and Fracturing.

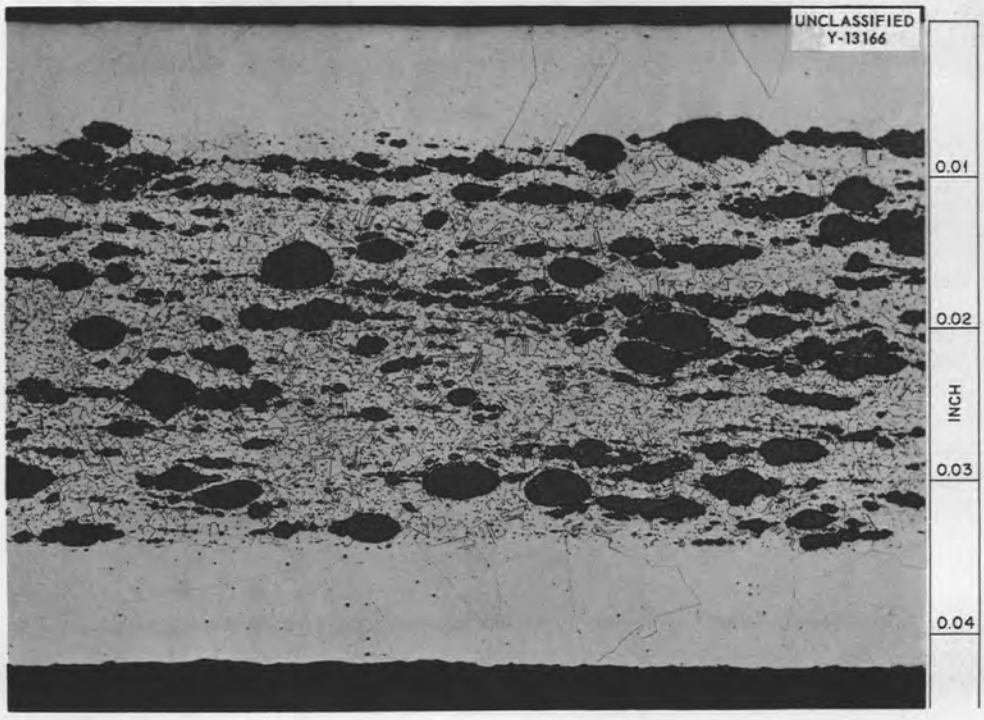

Fig. 69. Grain Size in Stainless Steel Cladding of Plate After Hot Rolling at 1220°C.

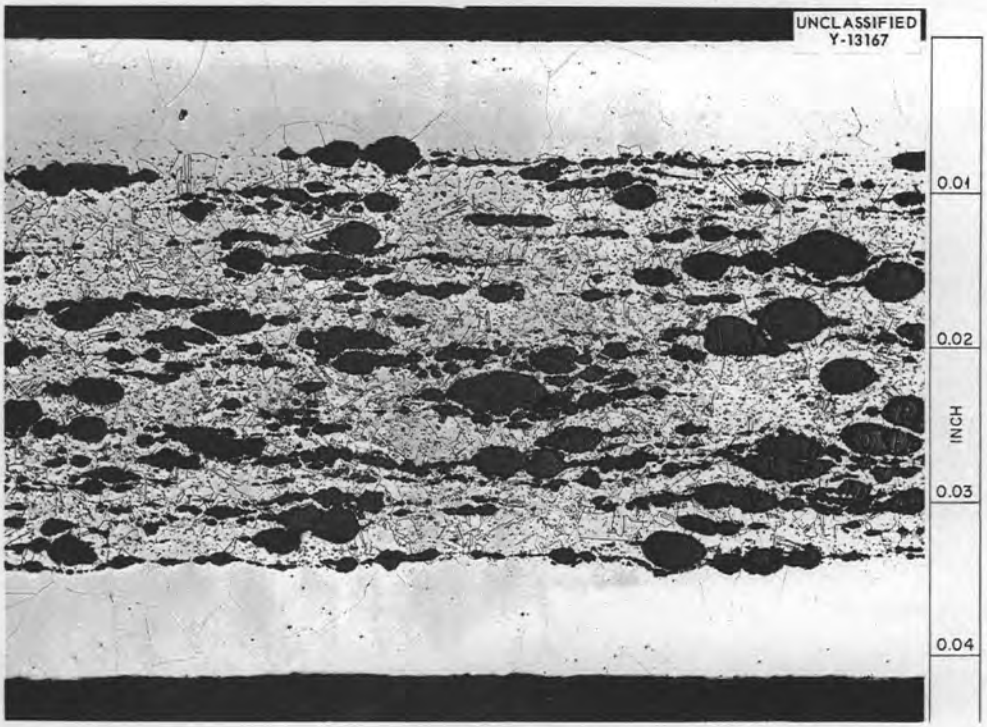

Fig. 70. Grain Size in Stainless Steel Cladding of Plate After 2½% Cold Reduction, Followed by a 1½-hr Anneal at 1180°C.

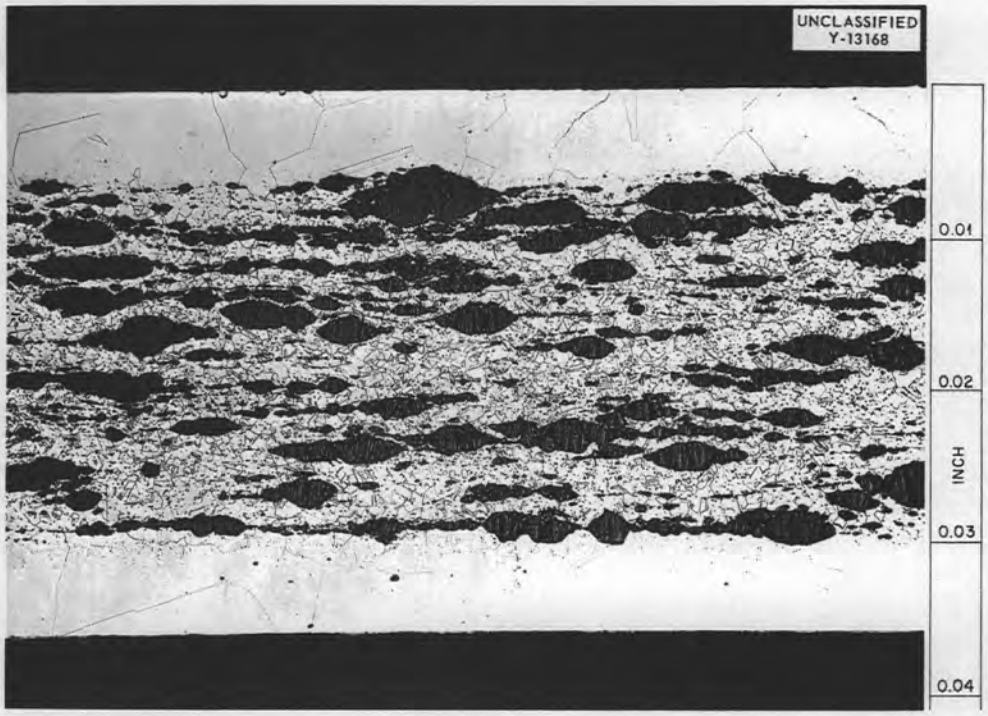

Fig. 71. Grain Size in Stainless Steel Cladding of Plate After 20% Cold Reduction, Followed by a 1½-hr Anneal at 1180°C.

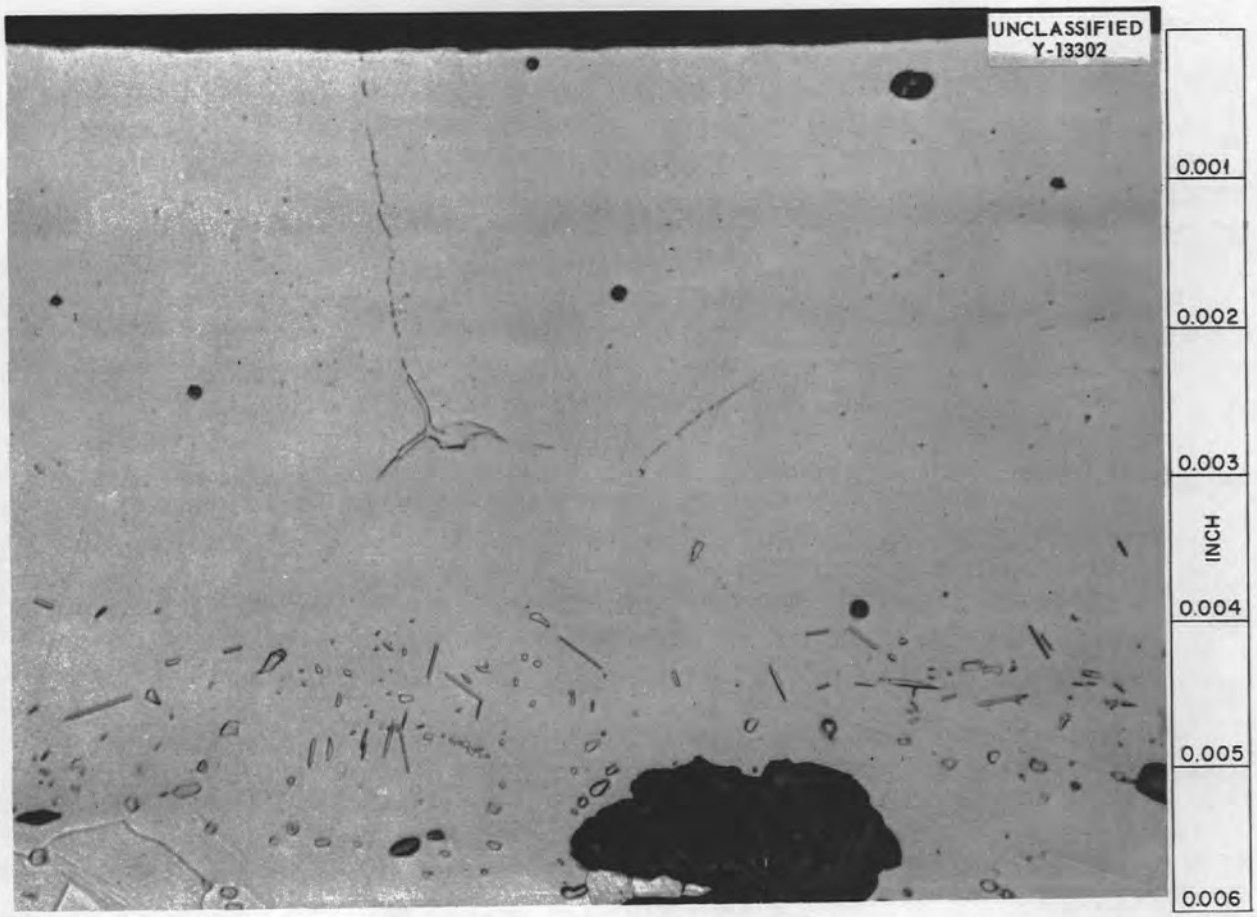

Fig. 72. Unidentified Phase, Believed to Be Iron-Rich Boron, at the Intersection of Stainless Steel Grains, Half the Distance into the Cladding of a Stainless-Steel-Clad UO_2-B_4C Cermet Composite Plate, Heat Treated for $1\frac{1}{2}$ hr at 1180°C Following Hot Fabrication at 1225°C. Core composition: 34 wt % UO_2, 0.5 wt % B_4C, 65.5 wt % stainless steel.

clad plates, painted with aluminum to prevent self-welding, were annealed at 1225°C without any apparent damage, but, after an additional 3 hr at 1250°C, the plates appeared to be welded together. As shown in Fig. 73, the weld was a phase, believed to be an iron-rich boron, which segregated and melted at the grain boundaries of the stainless steel. Another alarming incident attributed to boron diffusion occurred when a hole was punched in a clad plate while attempts were being made to remove the plate from the furnace after the 2-min anneal at 1225°C, which follows hot fabrication. Inspection of the section adjacent to the failure revealed that melting had occurred. The resulting structure is shown in Fig. 74.

In view of these results, an investigation is presently being conducted to determine the stability of zirconium diboride and boron nitride, with the intention of replacing the boron carbide with one of these two compounds.

COMPONENT ASSEMBLY BY BRAZING

R. J. Beaver

The first phase of the brazing investigation, which comprised brazing of solid stainless steel plates to form an assembly of the same dimensions as the Package Reactor fuel unit, has been successfully completed. Approximately six assemblies have been brazed within the required dimensional tolerances. Assembly 9 is shown in Fig. 75, with the measured dimensions listed in Table 21. It will be observed in Table 21 that plate spacing 1-2 is on the upper side of the 0.134-in. nominal

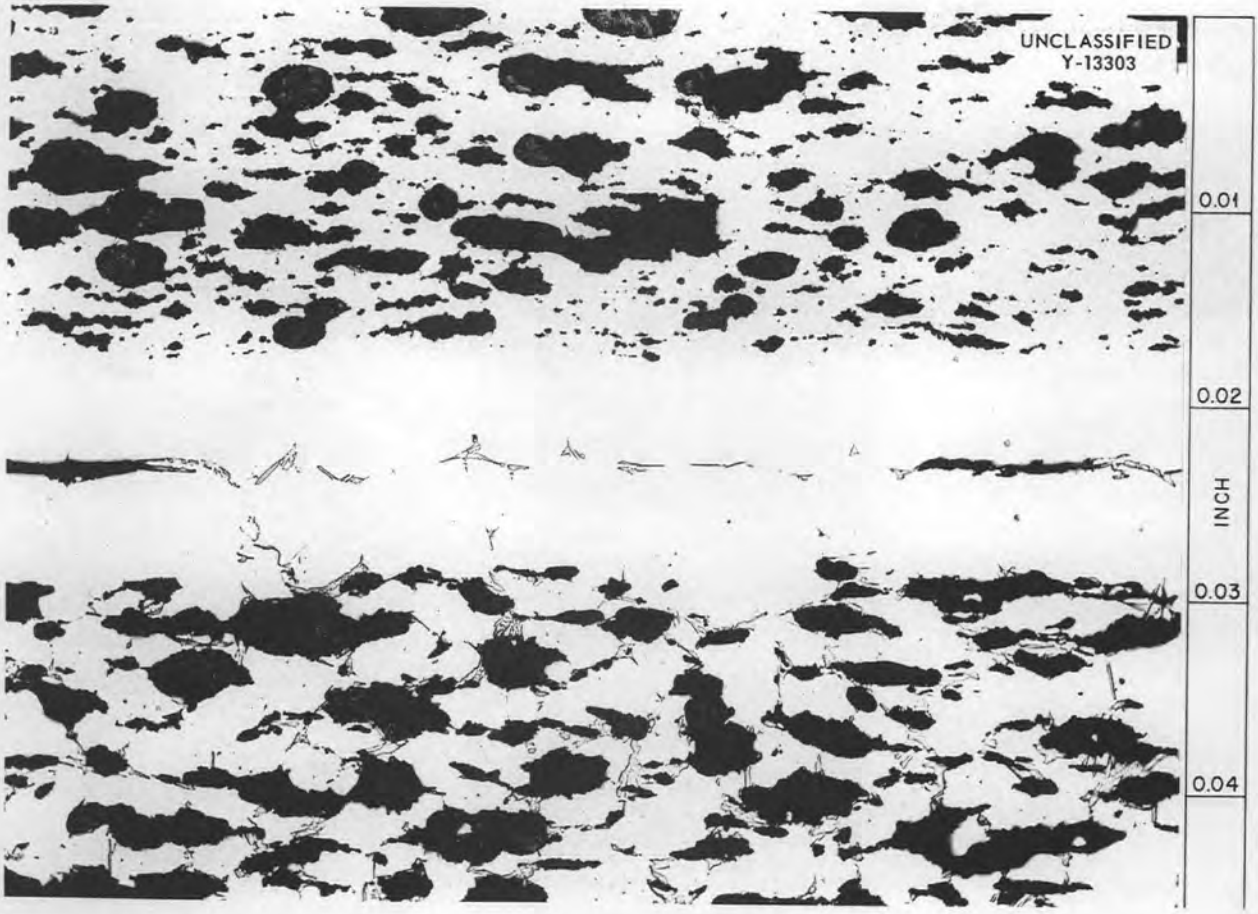

Fig. 73. Evidence of Phase, Believed to Be Iron-Rich Boron, at the Junction Between Two Stainless-Steel-Clad UO_2-B_4C Cermet Composite Plates, Apparently Caused by Diffusion of Boron in the Stainless Steel Cladding After 2 hr at 1225°C and an Additional 3 hr at 1250°C. Core composition: 34 wt % UO_2, 0.5 wt % B_4C, 65.5 wt % stainless steel.

plate spacing but well within the 10% tolerance tentatively specified. It is characteristic of these assemblies for spacings 1-2 and 17-18 to be slightly larger than the average spacing.

Assemblies have been brazed with the following alloys:

70% Ni–15% Cr–5% Fe–5% Si–5% B (Nicrobraz)
66% Ni–19% Cr–10% Si–4% Fe–1% Mn (GE 81)
50% Ni–30% Fe–12% Si–4% P–4% Mo (Coast Metals NP)

After brazing with the GE 81 alloy, numerous cracks were observed in the brazed joints, whereas the joints in assemblies brazed with Nicrobraz and Coast Metals NP were free of cracks. These results indicate that the GE 81 alloy is not sufficiently strong to withstand the thermal stresses encountered in the present brazing process. Typical assembly joints brazed with GE 81, Nicrobraz, and Coast Metals NP are shown in Figs. 76, 77, and 78, respectively.

The first experiment in brazing an assembly of Package Reactor fuel plates containing normal uranium was unsuccessful. Serious warpage of the plates occurred, with the result that the majority of the plate spacings were considerably out-of-tolerance. Further investigation is being conducted to determine the cause of the unexpected warpage of the fuel plates and to find a method for circumventing this situation.

CORROSION STUDIES

R. J. Beaver

In considering the corrosion resistance of the Package Reactor fuel unit in pressurized water at

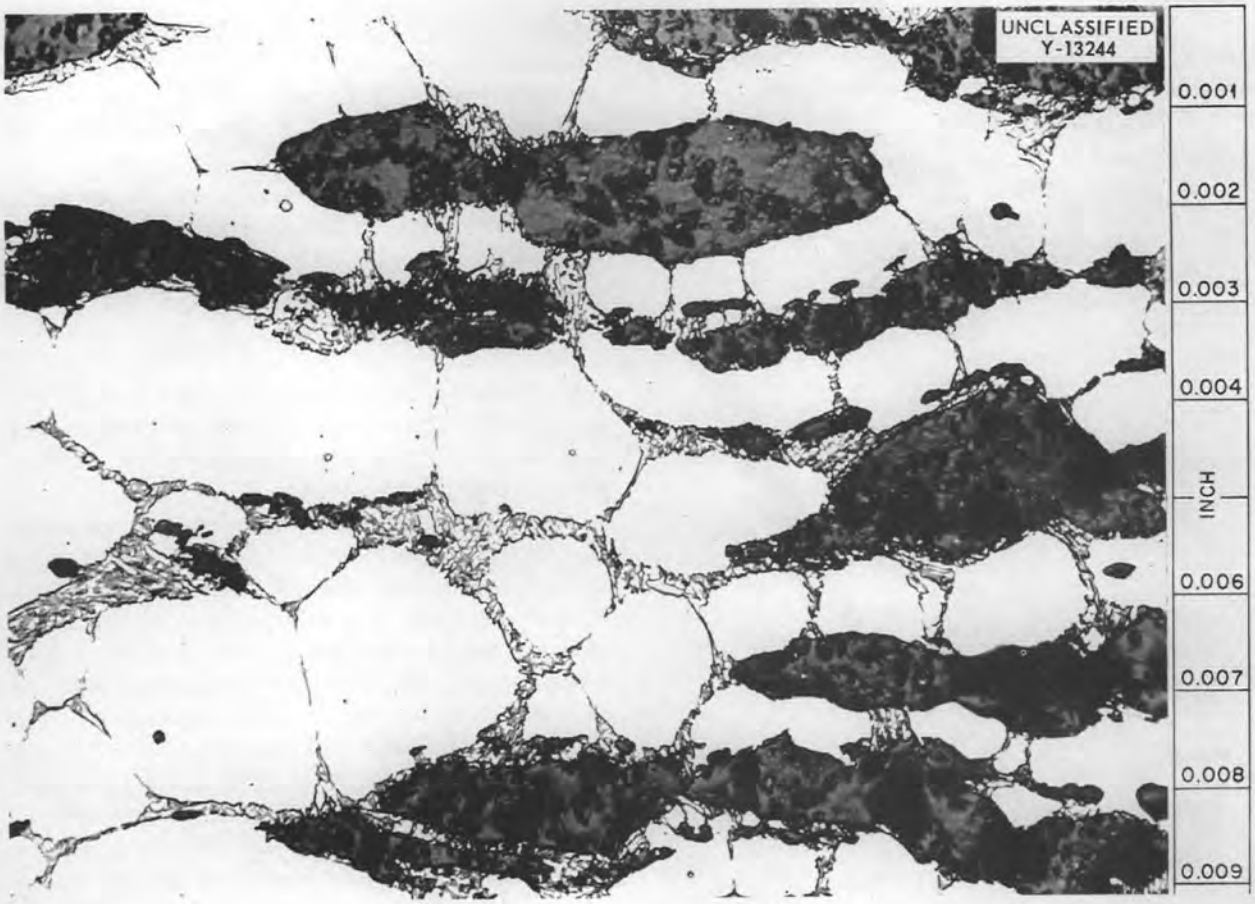

Fig. 74. Structure Adjacent to Failure in Stainless-Steel-Clad UO_2-B_4C Cermet Composite Plate Observed When Plate Was Being Removed from Furnace After a 2-min Anneal at 1225°C Following Fabrication. Core composition: 34 wt % UO_2, 0.5 wt % B_4C, 65.5 wt % stainless steel.

232°C, relatively little is known about the ability of the brazed joints to withstand the environment for long periods of time. The corrosion resistance of the brazed joint is, therefore, of prime consideration in the selection of a brazing alloy. Data, obtained from a preliminary screening test of brazed joints of 18 brazing alloys, are listed in Table 22. The data indicate that 10, or possibly 12, of the alloys might have satisfactory corrosion resistance. From this listing, alloys 2, 3, 6, and 7 were selected for extensive testing. Brazed joints of these alloys, after a 1000-hr test, are shown in Figs. 79 to 84.

In addition, the following two alloys were added to the intensive testing program: 57% Ni–13% Cr–30% Ge and 80% Cu–20% Ni.

Testings of these alloys will be conducted in an environment as similar to the Package Reactor environment as possible.

The advantages and disadvantages of the six selected alloys can be reviewed on the basis of the data listed in Table 23. At the present time, Coast Metals NP shows considerable promise. It is inexpensive, has shown only very slight attack, has a neutron-absorption cross section comparable to that of stainless steel, and flows at a reasonable temperature. Low-melting Nicrobraz, with B^{11} replacing B^{10}, falls in the same category. The GE 81 alloy can be classified with the other two, with the exception that numerous cracks have been observed in joints brazed with this alloy. The GE 75 and Pd-Ni-Si alloys appear to have excellent corrosion resistance, but they are expensive and flow at a relatively high temperature. In addition, the Pd-Ni-Si has a rather high neutron-absorption cross section. The 80% Cu–20% Ni alloy is being considered because it is the only alloy of the

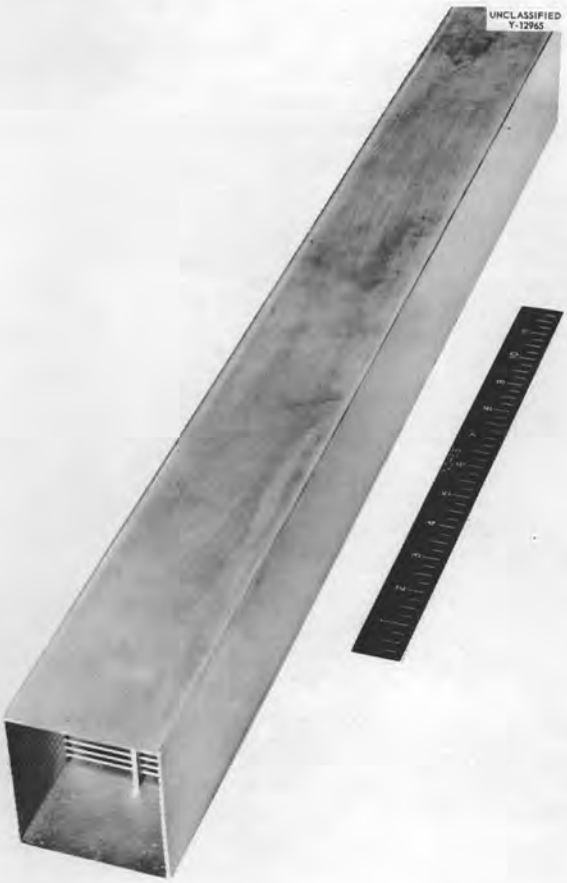

Fig. 75. Dummy Package Reactor Unit No. 9, Consisting of Solid Stainless Steel Plates Brazed with Nicrobraz.

group that has reasonable ductility. Its corrosion resistance, however, is questionable, and its flow temperature is high.

MTR IRRADIATION EXPERIMENT

J. E. Cunningham

It is planned to construct and irradiate an experimental stainless steel fuel element in the active lattice of the MTR core. The purpose of the experiment is to obtain performance data on certain engineering-material combinations and design features in order to facilitate the construction of a a highly reliable fuel component for long-time service in the Package Reactor. In addition, an attempt will be made to obtain a plot of fission-fragment damage to the sintered stainless steel powdered-core matrix as a function of UO_2 particle size in the range of 7 to 105 μ.

Unfortunately, the stainless steel fuel element cannot be exposed in its design form in the active lattice of the MTR. The main obstacles which prevent direct use are the flat-plate type of construction and the high uranium investment.

To permit irradiation, it was necessary to modify the stainless steel element somewhat to conform with the curved-plate configuration and heat-transfer limitations encountered in the MTR core. The test component was designed on the following basis:

1. Wherever possible, employ only the engineering materials and methods of construction developed and adapted for use in manufacturing the Package Power Reactor fuel elements.

2. House the stainless steel element in an aluminum transition box to adapt the flat-plate unit to the curved-plate configuration, and space the water gap between adjacent stainless steel fuel plates at 119 mils so that the pressure-drop and water-flow conditions through the inside of the boxed element are essentially the same as those that exist in the present 19-plate MTR fuel assembly.

3. Use standard MTR end-box castings of type 356 aluminum alloy in the T-7 heat-treatable condition for end fittings. This will permit the outside dimensions of the boxed element to be identical in all respects to a regular MTR fuel unit; this ensures that dimensional specifications for direct insertion into the MTR core will be met.

4. Limit the U^{235} fuel distribution in the stainless steel fuel plates to less than 0.032 g/cm^2, which is slightly larger than the design figure of 0.030 g/cm^2 on the present 200-g MTR assembly. Although the composite stainless steel fuel plates are designed for a much higher temperature, this measure is taken primarily to prevent film boiling at the water-plate interface.

5. Maintain the fuel concentration in the core, or fuel-bearing section, in accordance with PPR design specifications for 15- and 30-Mwy service. The lower value required for U^{235} fuel distribution (see above) must be obtained by regulating the thickness of the fuel-bearing section, rather than by altering the UO_2 concentration in the UO_2-ZrB_2-SS core-material combination.

6. The minimum permissible cladding thickness on the fuel plates is 5 mils.

The test component for irradiation, therefore, consists of two parts, namely, the aluminum transition box fitted with standard MTR end-box adaptors

TABLE 21 FABRICATION RECORD FOR PACKAGE REACTOR FUEL UNIT NO 9

(Nicrobrazed Solid Type 304 Stainless Steel)

Space No	Plate Spacing (mils)				Location	Critical Dimensions (in)			
	Location (in)					A	B	C	VCH
	2½	12	16	24½					
Nominal	134	134	134	134	Nominal	2 860	2 860	2 860	2 820
1 2	138	138	140	144	2½	2 858	2 858	2 856	2 823
2 3	130	133	135	131	7	2 859	2 858	2 856	2 825
3 4	131	131	133	133	12	2 856	2 855	2 852	2 827
4 5	131	139	133	133	16	2 857	2 856	2 852	2 827
5 6	132	134	138	131	21	2 852	2 853	2 852	2 828
6 7	134	138	135	132					
7 8	133	136	136	134					
8 9	137	134	135	134					
9 10	133	140	138	130					
10-11	131	131	131	132					
11 12	133	137	139	132					
12 13	133	134	136	135					
13 14	132	135	133	134					
14 15	132	131	138	134					
15 16	131	134	136	132					
16 17	132	138	136	131					
17 18	139	135	135	140					

and the modified stainless steel fuel elements which are encased with proper clearance in the aluminum box A cross sectional view of the test component is shown in Fig 85 Additional details are given in ORNL engineering drawings C 20375, D 20376, C 20377 C 20378 C 20379 and C 20380

The modified stainless steel element is composed of 19 fuel plates spaced 119 mils apart and brazed into two 50 mil thick stainless steel side plates to form a single unit or assembly The fuel plates consist of highly enriched UO_2 particles uniformly dispersed and embedded in a matrix of sintered stainless steel powder which is clad on all sides with wrought type 304L stainless steel A small quantity of burnout poison in the form of ZrB_2 is deliberately added to the fuel bearing section to facilitate control of the Package Power Reactor

Additional information on the proposed irradiation experiment is presented on the design and exposure data sheet in Table 24 The test component contains approximately 3425 g of stainless steel 1593 g of aluminum 245 g of uranium dioxide and 12 g of zirconium diboride calculated on the basis of a 22 in (55 88 cm) effective length The total absorption cross section for these materials for thermal neutrons is 609 and 557 cm^2 with and without the water respectively These values correspond to similar absorption values of 416 and 367 cm^2 respectively for the present 19 plate 200 g MTR fuel assembly

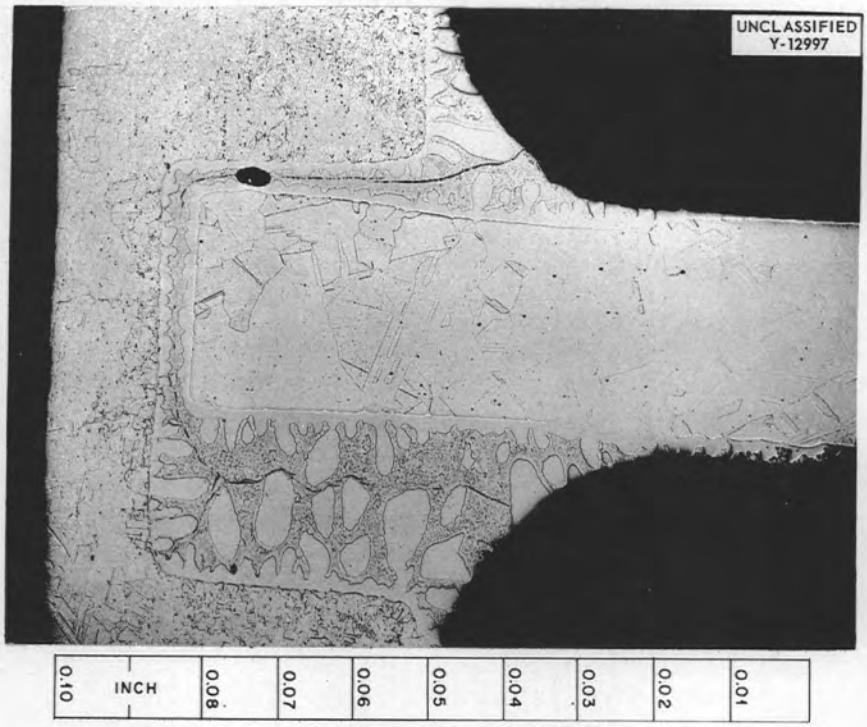

Fig. 76. Typical G-E 81 Brazed Joint, Brazed at 1180°C; Section from Assembly 14, Showing Cracking in Fuel Plate–Side Plate Joint. Etchant: glyceria regia.

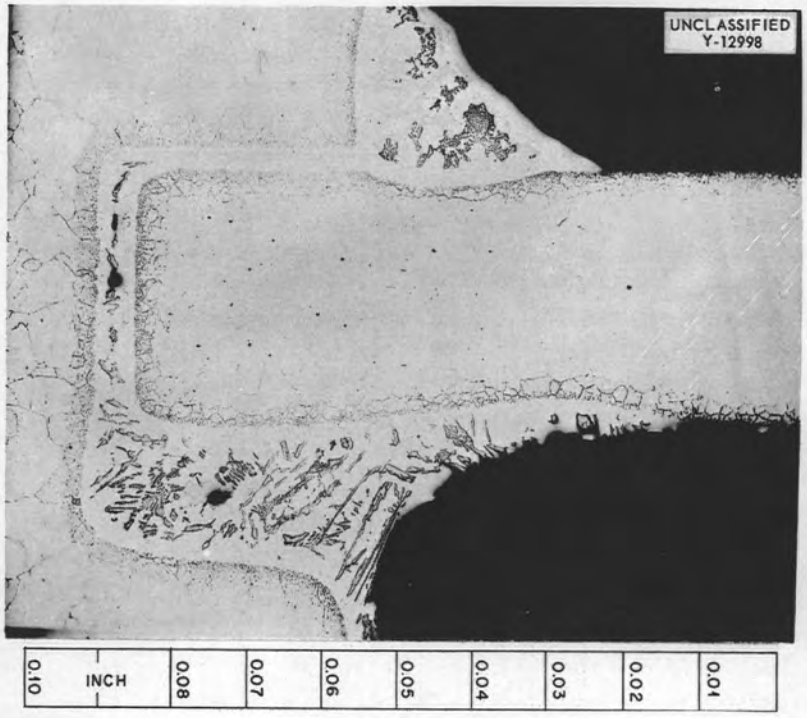

Fig. 77. Typical Nicrobrazed Joint, Brazed at 1180°C; Section from Assembly 6, Showing Fuel Plate–Side Plate Joint. Etchant: glyceria regia.

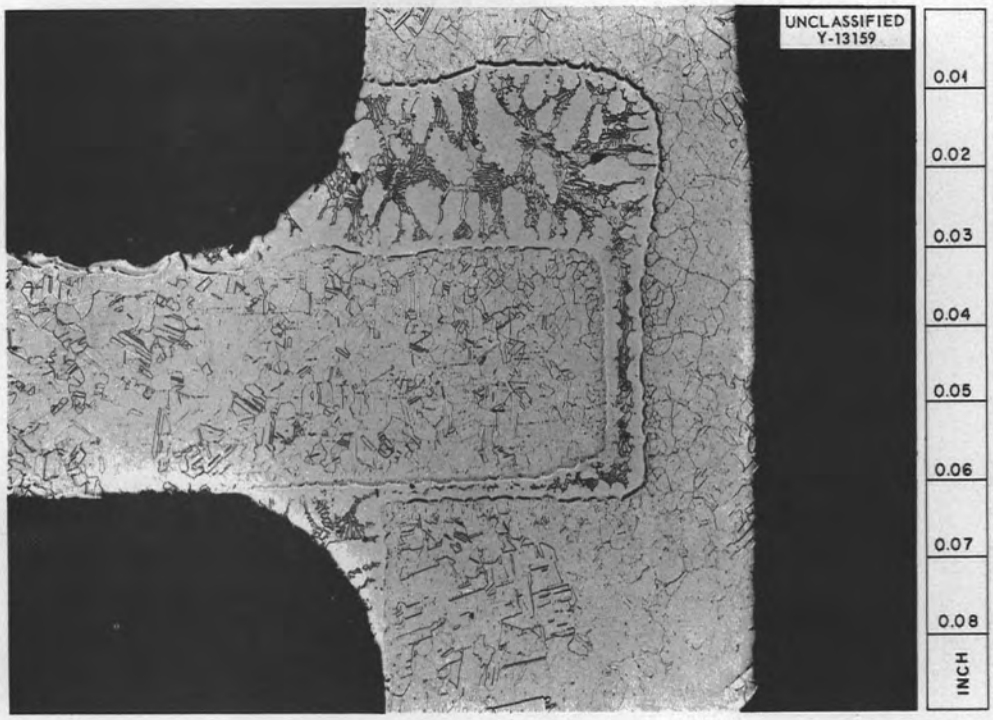

Fig. 78. Typical Coast Metals NP Brazed Joint, Brazed at 1180°C; Section from Assembly 18, Showing Fuel Plate–Side Plate Joint. Etchant: glyceria regia.

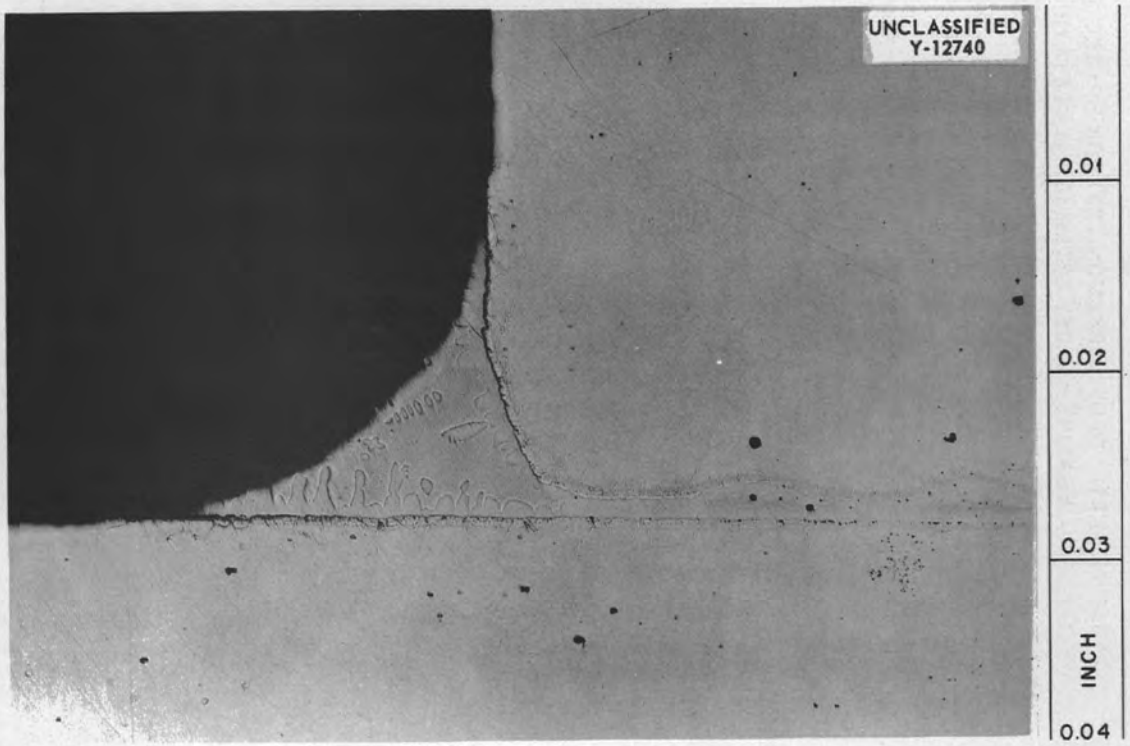

Fig. 79. Brazed Joint of Low-Melting Nicrobraz, 80% Ni–5% Cr–5% Fe–5% Si–5% B, After 1000 hr in 295°C Water at 1200 psi. 100X.

TABLE 22 RESULTS OF CORROSION TESTS ON BRAZED T JOINTS OF TYPE 304L STAINLESS STEEL AND VARIOUS BRAZING ALLOYS AFTER 1000 hr IN STATIC DISTILLED WATER AT 1200 psi AND 565°F

Testing conditions: Water changed after 48 160 325 490 655 a d 815 hr
Init al pH of water 5 45
Initial resistivity of water 0 21 megohm cm at room temperature

Rating	Chemical Composition (wt %)	Weight Change (mg/cm^2)	Type of Attack	Depth of Attack (in)
		Group I		
1	82 Au–18 Ni	–0 01	General	0 001
2	80 Ni–5 Cr–5 Fe–5 Si–5 B	–0 01	Localized	0 0005
3	60 Pd–37 Ni–3 Si	–0 02	Localized	0 002
4	60 Pd–40 Ni	+0 03	General	0 0005
5	80 Ni–10 Cr–10 P	+0 03	Local ed subsurface voids	0 004
6	50 Ni–30 Fe–12 Si–4 P–4 Mo	–0 04	General	0 0015
7	66 Ni–19 Cr–10 Si–4 Fe–1 Mn	–0 05	General	0 0015
8	91 Ni–5 Si–3 B–1 Fe	–0 05	Localized	0 002
9	93 Ni–4 Si–3 B	–0 07	General	0 0015
10	70 Ni–15 Cr–5 Fe–5 Si–5 B	–0 08	Intergranular	0 004
		Group II		
11	75 Ni–25 Ge	–0 10	General	0 0015
12	90 Ni–10 P	–0 12	Local zed	0 0005
13	68 Ni–32 Sn	–0 17	General	0 002
14	100 Cu	–0 21	General	0 0015
		Group III		
15	60 Mn–40 Ni	–0 21	Complete destruction of fillet	
16	72 Ag–28 Cu	–0 50	Complete destruction of fillet	
17	92 Cu–8 Si	–0 79	Severe intergranular	
18	89 Ni–5 Si–4 B–2 Fe	–1 04	Severe intergranular	

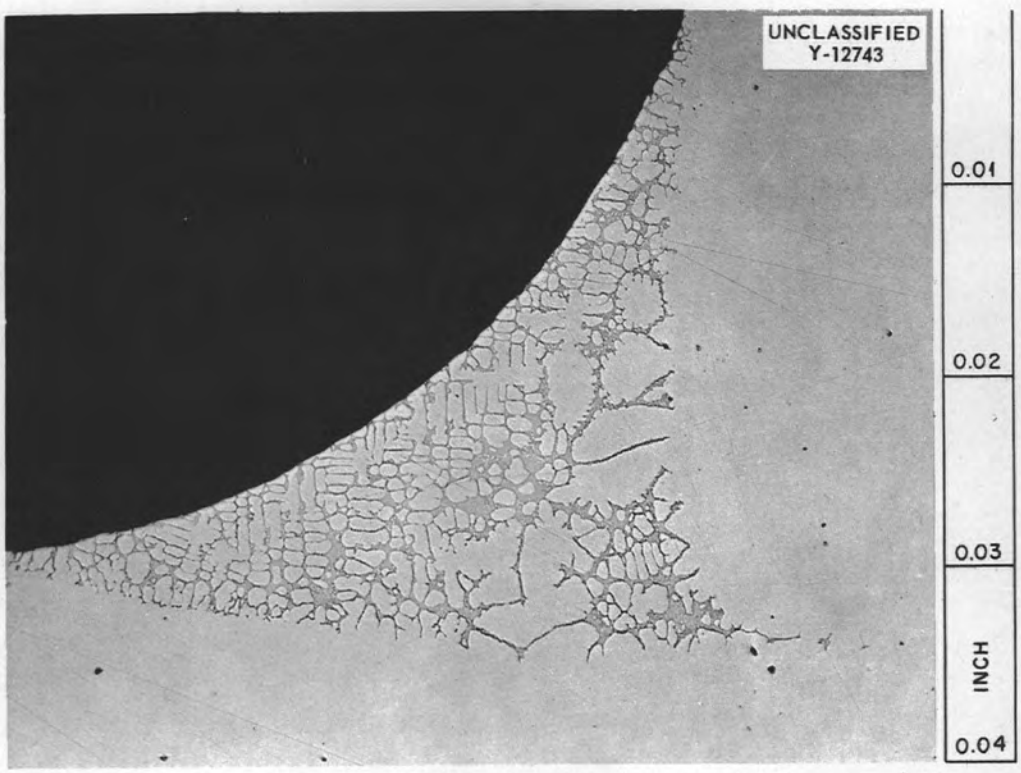

Fig. 80. Brazed Joint of 60% Pd–37% Ni–3% Si, After 1000 hr in 295°C Water at 1200 psi. 100X.

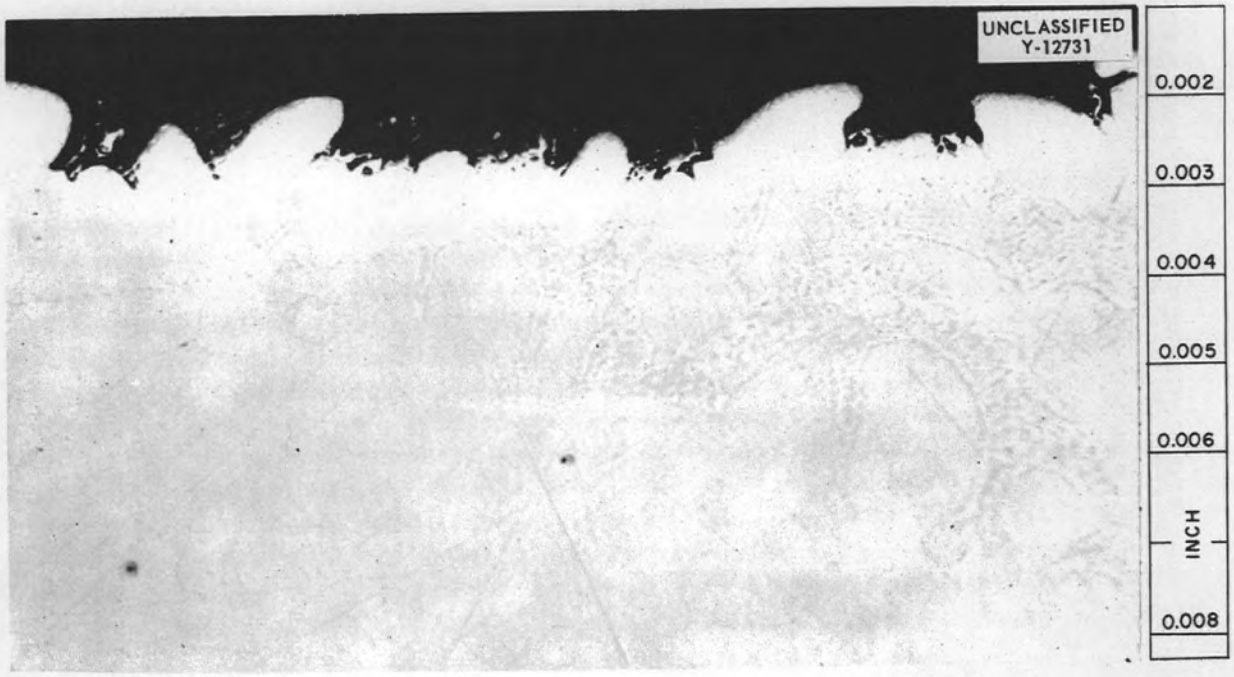

Fig. 81. Brazed Joint of G-E 81 Alloy, 69% Ni–20% Cr–11% Si, After 1000 hr in 295°C Water at 1200 psi. 100X. Reduced 5%.

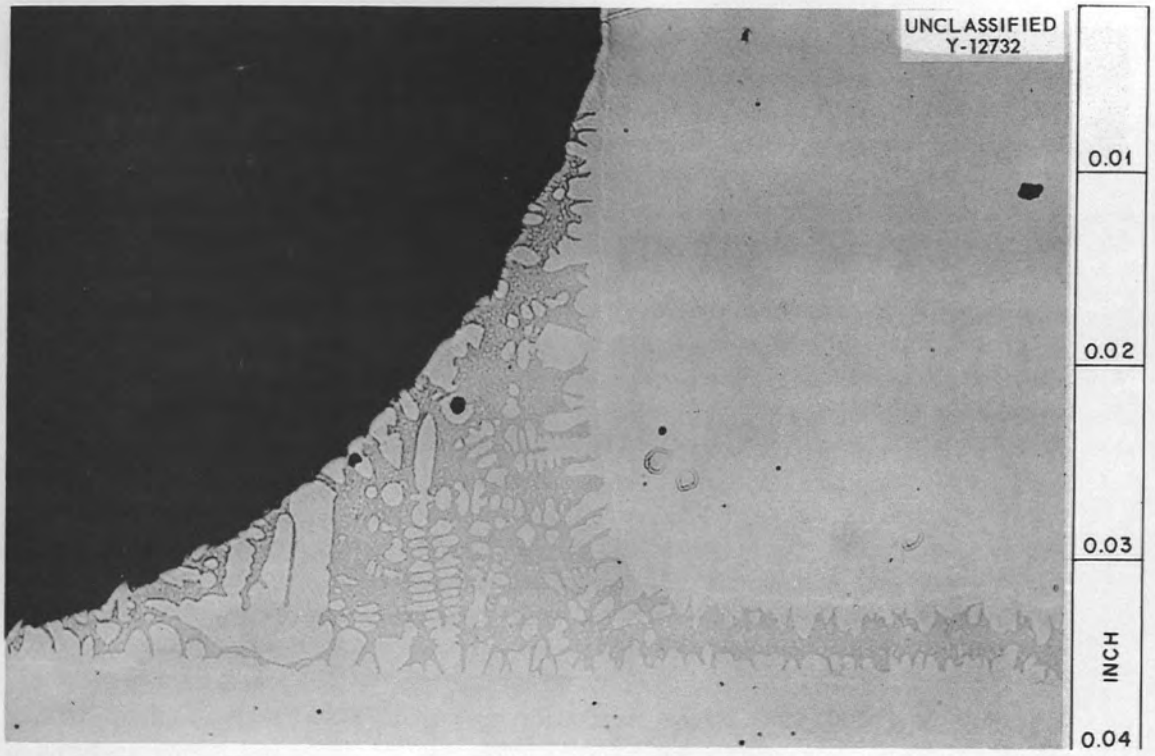

Fig. 82. High-Magnification View of Surface of Joint Shown in Fig. 81. 500X.

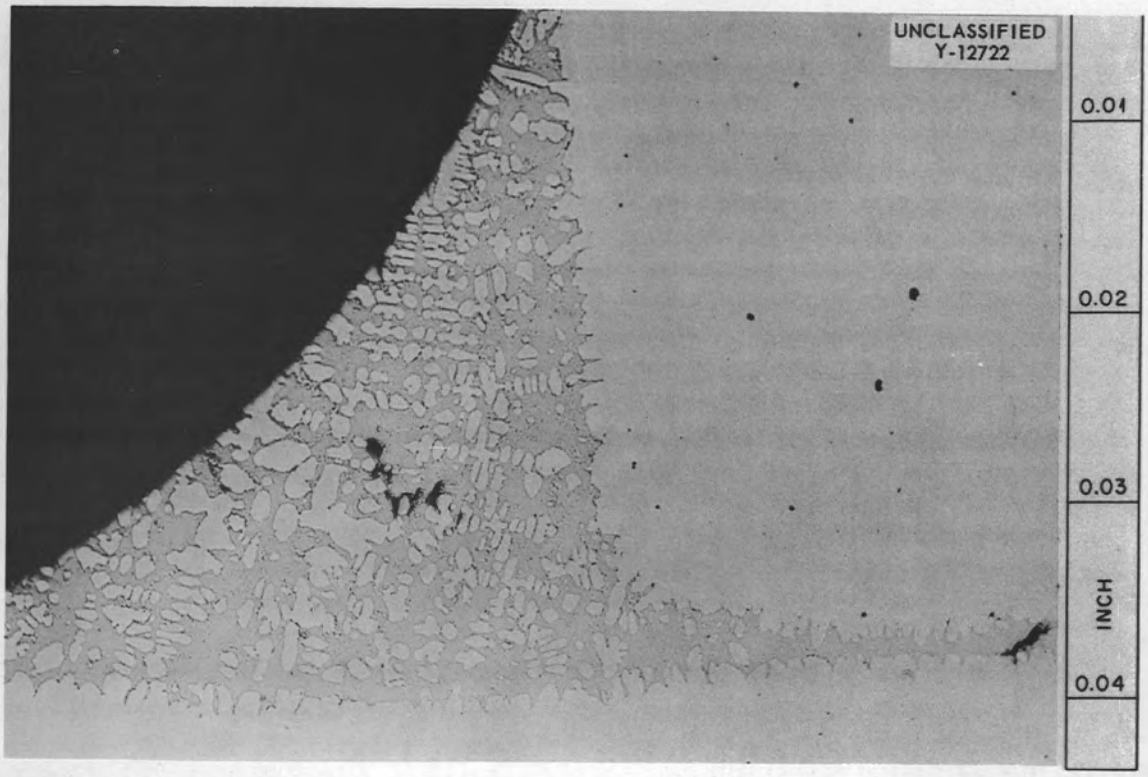

Fig. 83. Brazed Joint of Coast Metals NP, 50% Ni–30% Fe–11.5% Si–4.5% P–4% Mo, After 1000 hr in 295°C Water at 1200 psi. 100X.

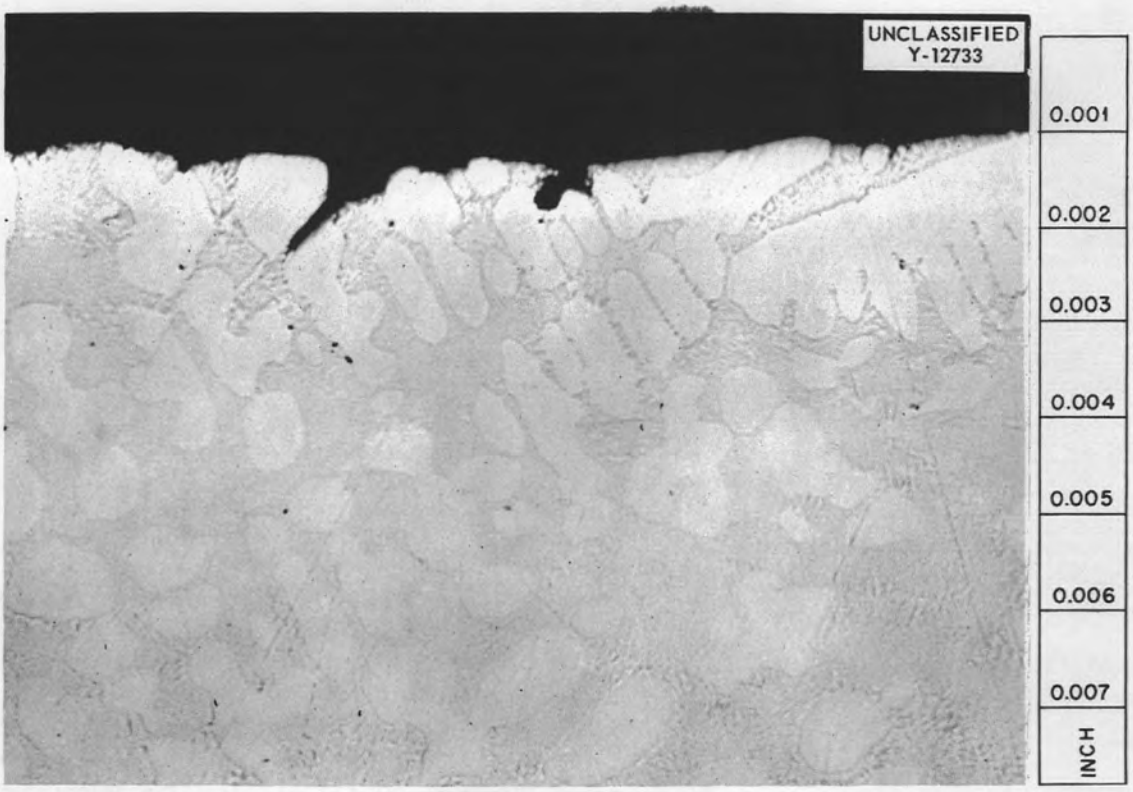

Fig. 84. High-Magnification View of Surface of Joint Shown in Fig. 83. 500X.

TABLE 23. ALLOYS WHICH APPEAR MOST PROMISING FOR BRAZING PACKAGE REACTOR FUEL ASSEMBLIES

Rating	Designation	Chemical Composition (wt %)	Flow Temperature (°C)	Neutron-Absorption Cross Section (barns)	Estimated Cost per Pound	Corrosion Resistance
1	Coast Metals NP	50 Ni–30 Fe–12 Si–4 P–4 Mo	1150	2.67	$ 15.00	Slight general attack*
2	Low-mélting Nicrobraz	80 Ni–5 Cr–5 Fe–5 Si–5 B[11]	1050	3.14	15.00	Negligible attack*
3	GE 81	66 Ni–19 Cr–10 Si–4 Fe–1 Mn	1150	3.30	10.00	Slight general attack*
4	GE 75	57 Ni–13 Cr–30 Ge	1180	3.69	100.00	Unattacked**
5	Pd–Ni–Si	60 Pd–37 Ni–3 Si	1180	5.22	250.00	Negligible attack*
6	Copper-nickel	80 Cu–20 Ni	1200	3.77	5.00	Intergranular attack**

*After 1000 hr in water at 295°C.

**After 725 hr in supercritical water at 1300°F.

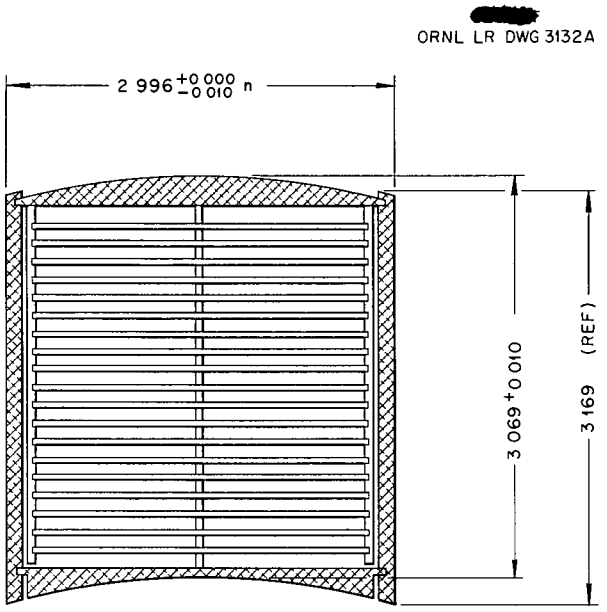

Fig 85 Cross Sectional View of MTR Irradiation Experiment Test Component

The amount of burnup of U^{235} atoms desired is 58% It was assumed that the average thermal neutron flux in the MTR core would be approximately 2×10^{14} neutrons/cm^2/sec The time of of exposure required to achieve this desired fuel burnup was calculated to be approximately 90 days which corresponds roughly to four three week cycles in the MTR core

CONTROL ROD DEVELOPMENT

J H Coobs

Two composite plates containing a sintered core of 16% B_4C–84% Cu were successfully clad with stainless steel by rolling at 1000°C the total reduction in thickness being 50% in seven passes The cladding and frame of these composites were welded with a series of spot welds as well as heavy edge welds with an inert gas shielded arc to prevent rupture during hot rolling by excessive spreading of the frames Two plates rolled previously failed in this manner one on the second pass and the other on the third pass The 5 mil layer of copper placed between the core and cladding was apparently successful in promoting bonding by reducing surface contamination of the stainless cladding from impurities in the B_4C

These initial results are encouraging but no attempt has been made as yet to mock up a full size absorber section for use in the Package Reactor control rod

INSTALLATION OF SPECIAL EQUIPMENT

E S Bomar

The fabrication of equipment necessary for the handling of enriched fuel mixtures is nearly complete Provisions are being made so that weighing blending and pressing of the fuel core mixtures can be done in isolation hoods which meet health physics standards for such uses

Weighing and blending of the component powders of stainless steel zirconium diboride and uranium dioxide will be done in a hood provided with a triple beam balance a small jar mill and suitable containers The working area is approximately 2 ft in depth by 3 ft in length Materials will be introduced into the hood through a chamber equipped with an inner and an outer door The operator has access to the hood through two glove ports Negative pressure will be maintained on the hood by a duct connected to the building exhaust system A filter cartridge will be incorporated in this exhaust line to prevent the loss of any enriched material as the result of air sweeping through the box during loading or unloading

The powder prepared in the above hood will be transferred to a second hood mounted in the $1\frac{1}{2} \times 3$ ft working area of a 150 ton press The necessary equipment for consolidating the loose powders is contained in this unit This equipment includes a hardened steel die punches pushout blocks and die holder The upper platten of the die holder is mounted on springs this arrangement permits a double acting effect during pressing and also permits ejection of the pressed part by pushing the die down with the lower punch in pressing position Pressure is applied to the top punch with an extension mounted on the press head A seal between the extension and Plexiglas cover of the hood is obtained with rubber O rings Access for performing the necessary manual operations is provided by two pairs of glove ports one pair on each side of the press Material is introduced or removed through a set of pass doors as in the other hood Negative pressure inside the hood is again assured by an arrangement identical to that for the blending hood

TABLE 24 DESIGN AND EXPOSURE DATA ON IRRADIATION TEST ELEMENT

Composite Stainless Steel Fuel Plate Data		
	Type I (15 Mwy)	Type II (30 Mwy)
Number required	4	15
Clad core clad thickness mils	5 10 5	6 5 7 6 5
Core mixture composition wt %	17 92 UO_2–0 75 ZrB_2–81 33 SS	25 81 UO_2–1 40 ZrB_2–72 79 SS
U^{235} enrichment %	93 5	93 5
U^{235} content per plate g	10 36	10 72
U^{235} fuel distribution g/cm^2	0 031	0 032

Aluminum Boxed Stainless Steel Test Element	
Water gap spacing mils	119 ± 12
U^{235} content g	202 ± 1
Natural boron content g	2 3
Metal to water volume ratio	0 43
Total absorption cross section cm^2	
With aluminum box and water	609
With no water	557
Total fission cross section cm^2	298

Burnup and Exposure Data	
Desired burnup of U^{235} atoms %	58
Estimated average thermal neutron flux neutrons/cm^2/sec	2×10^{14}
Exposure time days	90
Integrated flux nvt	$1\ 2 \times 10^{21}$
Burnup of total atoms in core mixture %	
Type I fuel plates	2 2
Type II fuel plates	3 2

HIGH TEMPERATURE METALLURGY

W D Manly

GENERAL CORROSION

E E Hoffman

W H Cook C F Leitten

Static Tests of Brazing Alloys in Fluorides and Sodium

The brazing alloys listed below were submitted by the Welding and Brazing Group for corrosion testing in NaF ZrF_4 UF_4 (53 5-40 6 5 mole %) and sodium

(A) 67% Ni–13% Ge–11% Cr–6% Si–2% Fe–1% Mn
(B) 65% Ni–25% Ge–10% Cr
(C) 72% Ni–18% Ge–7% Cr–3% P

The specimens used in the corrosion tests were cut from 5 in T joints of Inconel which had been brazed in a dry hydrogen atmosphere The purpose of these tests is to attempt to find a brazing alloy which has good corrosion resistance both to fused salts and to sodium If a suitable brazing alloy can be found it could be used to back up tube to header welds The brazing alloy would be exposed to the fused salt and resistance to attack by sodium would be required in the event of fractures in the tube to header welds

These brazed Inconel specimens were static tested for 100 hr at 816°C (1500°F) in ½ in OD 0 035 in wall Inconel container tubes The brazed specimens were carefully cleaned before the test Following the test the specimens were carefully cleaned so as to remove only the adhering corrosion media in order to obtain weight change data The specimens were nickel plated following the test in order to prevent rounding over of the specimen edge during metallographic polishing

It may be seen in Table 25 that alloys A and B had very good resistance to attack by the fluoride salt (see Figs 86 and 87) Alloy A is shown in Figs 88 and 89 at low magnification in the as brazed and as tested condition Alloy C was attacked slightly by the fluoride salt All the alloys

TABLE 25 RESULTS OF STATIC TESTING OF BRAZING ALLOYS IN NaF ZrF_4 UF_4 (53 5 40 6 5 mole %) AND SODIUM AT 1500°F FOR 100 hr

Bra ng Alloy	Bath	Weight Change (g/ n ^{2})	Metallographic Notes
(A) 67% N –13% Ge–11% Cr–6% Si–2% Fe–1% Mn on Inconel (br ed at 1120°C for 10 m)	Fluor de	+0 0003 (+0 024%)	Very little attack slight amount of surf ce roughening to depth of ¼ mil
	Sod m	–0 0003 (–0 017%)	Attacked n the form of sub s rfoce voids to a maximum depth of 3 to 4 mils
(B) 65% N –25% Ge–10% Cr on I conel (brazed at 1140°C far 10 mi)	Fluor de	–0 0010 (–0 077%)	No attack a sl ght mou t of niform solution would ccount for weight loss
	Sod um	–0 0013 (0 116%)	Braze fillet attacked to a max mum depth of 8 mils
(C) 72% Ni–18% Ge–7% Cr–3% P on Inco el	Fluoride	–0 0005 (0 041%)	Surface of the braze fillet at tacked to a depth of 2 to 3 mils in the form of subsurface voids
	Sod um	–0 0008 (–0 058%)	Braze fillet attacked to a depth of 3 to 6 mils in the form of subsurface voids

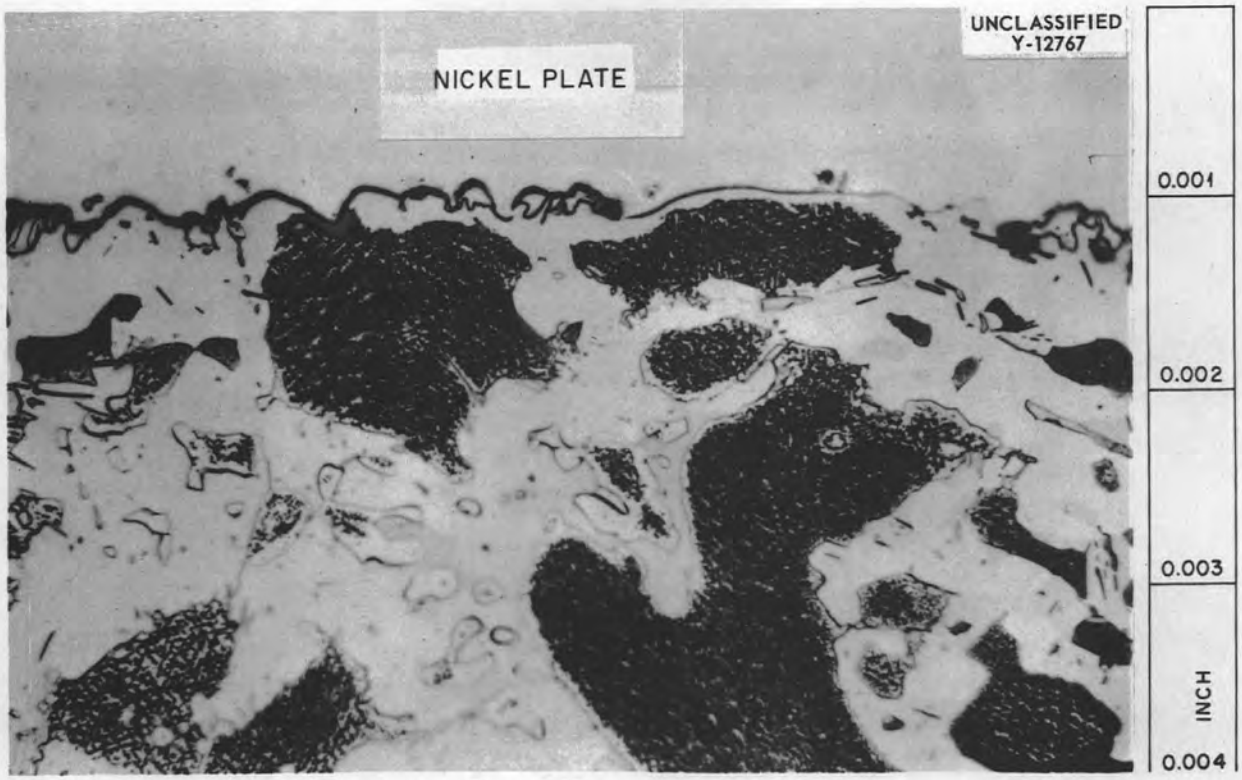

Fig. 86. Alloy A, Ni-Ge-Cr-Si-Fe-Mn, Brazing Alloy Fillet Surface After Exposure for 100 hr at 1500°F in $NaF-ZrF_4-UF_4$ (53.5-40-6.5 mole %). Specimen was nickel-plated following test in order to preserve the edge during polishing. Etchant: oxalic acid. 1000X.

were attacked slightly by sodium, but alloy A was attacked to a maximum depth of only 3 to 4 mils, which is not serious, since sodium would be in contact with this alloy only in the event of a tube-to-header weld fracture. It may be concluded from the results of these tests that further study is warranted on alloys A and B, since both had good resistance to attack by the fluoride salt; special emphasis should be given to alloy A, since it exhibited superior resistance to attack by sodium.

Special Stellite Heats Tested in Sodium and $NaF-ZrF_4-UF_4$ (50-46-4 mole %)

Two special heats of Stellite, heats B and C, were submitted by the Union Carbide and Carbon Metals Research Laboratories for corrosion-testing purposes. These specimens were sand-cast and have Rockwell C hardnesses as follows: heat B, 39 to 42; heat C, 42 to 43. The as-received specimen microstructure consisted of Cr_7C_3 particles in a cobalt-rich matrix.

The approximate compositions of these heats are as follows:

	Heat B (%)	Heat C (%)
Carbon	1	0.30
Chromium	35.0	28.0
Tungsten	5.0	
Molybdenum		12.0
Manganese	0.50	0.50
Silicon	0.50	0.50
Nickel		3.0
Cobalt	Balance	Balance

The specimens were tested statically for 100 hr at 816°C (1500°F). Inconel container tubes were used, and duplicate tests were run. The results are presented in Table 26.

Both of the Stellite compositions (heats B and C) were heavily attacked along the carbide network

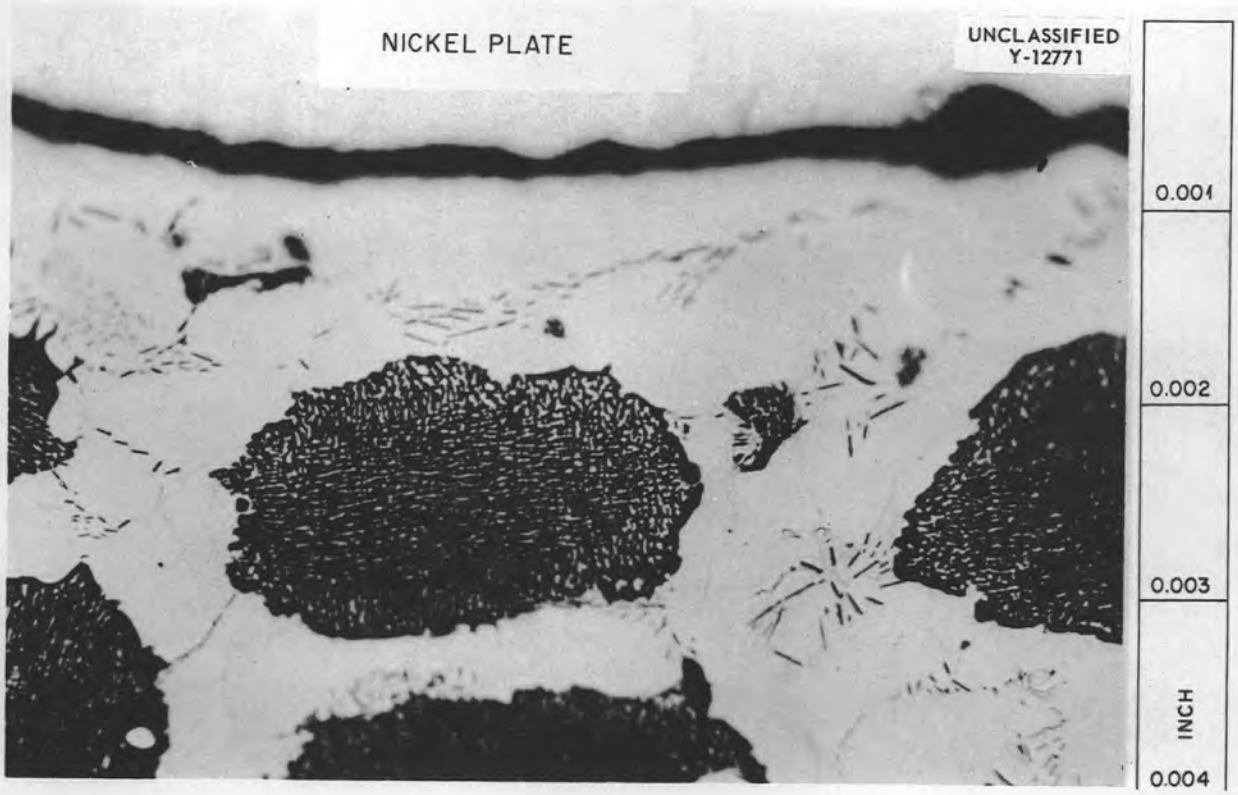

Fig. 87. Alloy B, Ni-Ge-Cr, Brazing Alloy Fillet Surface After Exposure for 100 hr at 1500°F in $NaF-ZrF_4-UF_4$ (53.5-40-6.5 mole %). Specimen was nickel-plated following test in order to preserve the edge during polishing. Etchant: oxalic acid. 1000X.

in fluoride 30 (see Figs. 90 and 91). The attack varied from a minimum of 7 mils to a maximum of 20 mils. The depth of attack varied with the orientation of the carbide network with relation to the specimen surface; the attack was deepest when the network was perpendicular to the surface.

None of the specimens were attacked in sodium; however, in heat B there were no large equiaxed carbide particles in a 1- to 2-mil area adjacent to the surface. The carbide particles in this area appeared to have been transformed into a very fine structure. There was also a large amount of fine precipitate in the cobalt-rich matrix near the surface.

Heat C had slightly better resistance to attack by sodium than did heat B, and both heats had very poor resistance to attack by the fluoride salt. Several of the specimens had shrinkage voids near the surface, one 7 mils in diameter, and the attack was deeper in these areas.

Hastelloy R Tested in Various Media at 816°C (1500°F) for 100 hr

Centerless, ground and annealed rods of Hastelloy R were received from the Haynes Stellite Company. These rods were ¾ in. in diameter and 8 in. in length. A specimen (¼ × ¼ × ¾ in.), container, and plug were machined from each rod. The specimen and bath were loaded into the container, and the plug was welded in place in a purified-helium-atmosphere dry box. The nominal composition of this alloy is 65% Ni–14% Cr–10% Fe–6% Mo–3% Ti–2% Al.

These specimens were tested in the various media for 100 hr at 816°C (1500°F), and the results are presented in Table 27.

This alloy had good resistance to attack by fluoride 30 (see Fig. 92) and lithium. The fact that this alloy had better resistance to attack by

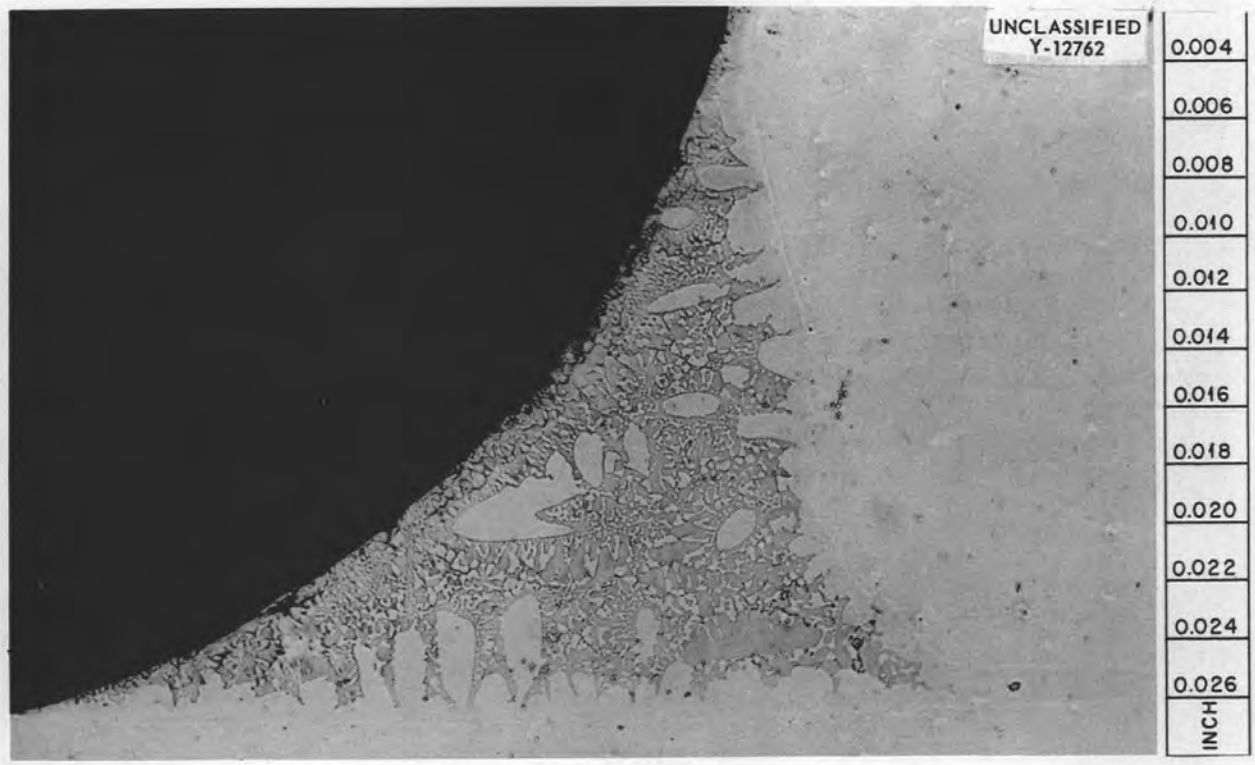

Fig. 88. Alloy A, Ni-Ge-Cr-Si-Fe-Mn, Brazing Alloy on Inconel T-Joint in As-Brazed Condition. Etchant: oxalic acid. 150X.

lithium than it had to attack by sodium is surprising in view of the heavy attack which usually occurs on high-nickel alloys – Inconel, for example, when placed in contact with lithium at 1500°F (816°C).

The sample tested in sodium was attacked to a slight degree, while the specimen tested in lead was heavily attacked. The specimen tested in sodium hydroxide was attacked throughout its entire thickness.

Molybdenum-Coated Inconel in $NaF-ZrF_4-UF_4$

Inconel specimens, which were coated with molybdenum by the Crawford Fitting Co., were tested in static lithium at 1500°F for 100 hr. Lithium was chosen as the corroding media in order to determine whether the molybdenum coating was continuous, because molybdenum is resistant to attack by molten lithium at this temperature and Inconel is heavily attacked. Examination of the as-received sample revealed a ½- to ¾-mil molybdenum-rich surface layer. The molybdenum-rich phase penetrated the grain boundaries to a depth of 1½ mils beneath the surface layer. Examination of the tested specimen showed very heavy intergranular attack to a depth of 35 mils; the molybdenum surface layer was, therefore, either not corrosion resistant or not continuous.

Lithium–Type 316 Stainless Steel Thermal-Convection Loops

Tests have recently been completed on three lithium–type 316 stainless steel thermal-convection loops. These loops were constructed of type 316 stainless steel pipe which had a 0.840-in. OD and a 0.147-in. wall thickness. The loops had hot and cold legs 15 in. in length, with 15-in. connecting legs inclined at an angle of 20 deg. The entire loading and welding operations on the loops were performed in a purified-helium dry box.[1] The loops operated for 1000 hr, and at no time during the tests was there any indication of plug formation. After the tests the loops were sectioned

[1] E. E. Hoffman and W. H. Cook, *Met. Semiann. Prog. Rep. April 10, 1954*, ORNL-1727, p 37.

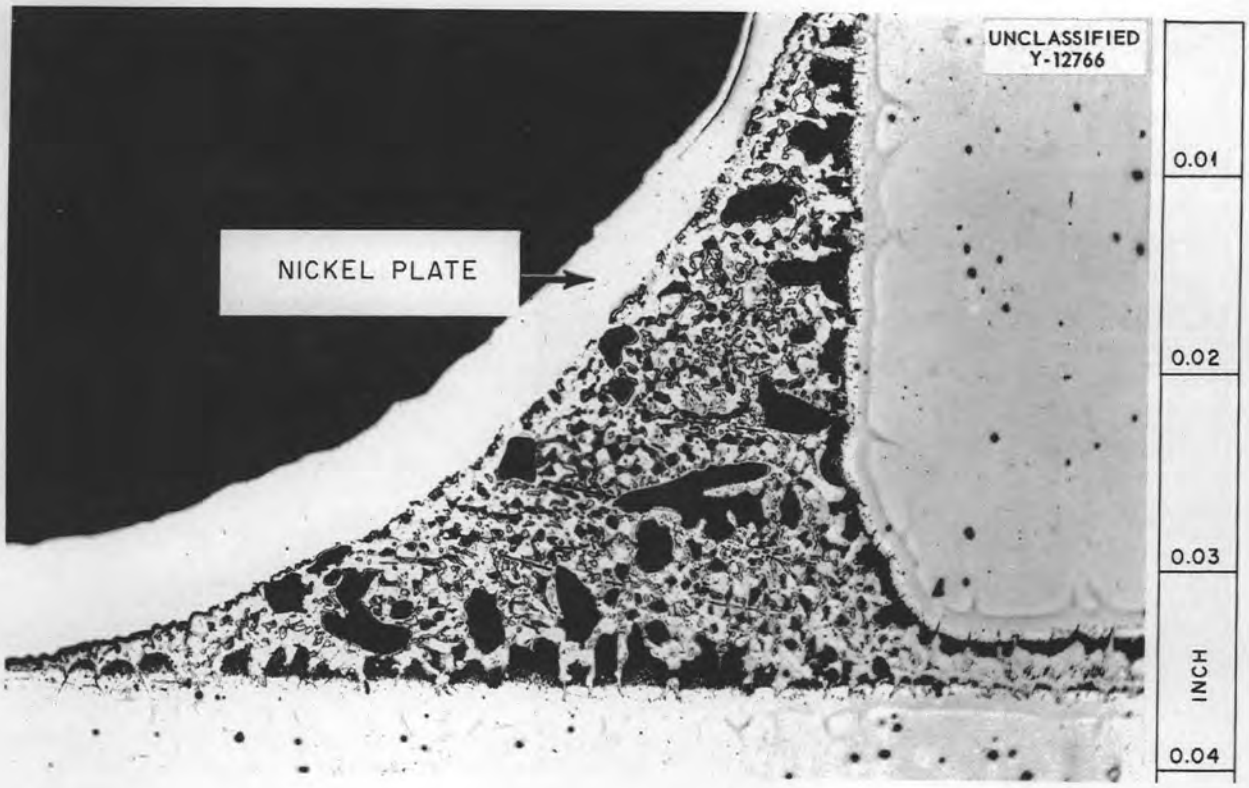

Fig. 89. Alloy A, Ni-Ge-Cr-Si-Fe-Mn, Brazing Alloy on Inconel T-Joint After Exposure for 100 hr at 1500°F in NaF-ZrF_4-UF_4 (53.5-40-6.5 mole %). Braze fillet surface may be seen in Fig. 86 at higher magnification. Dark areas are not areas of attack. Specimen was nickel-plated following test in order to preserve the edge during polishing. Etchant: oxalic acid. 100X.

and macroscopically examined; there was no apparent difference between the hot- and cold-zone surfaces in tests 1 and 2 (see Fig. 93). The conditions under which the loops were operated are listed in Table 28.

Only loop 1 has been examined completely. Loops 2 and 3 have been sectioned and macroscopically examined. Loop 2 was very similar in appearance to loop 1; no crystal deposition had occurred. Loop 3, however, when sectioned, revealed mass-transfer crystals attached to the cold-zone walls. These crystals did not plug the loop or noticeably affect the circulation. The crystal deposition was much heavier on the major radius of the exposed loop-bend wall in the cold zone. This loop has not yet been examined metallographically.

Loop 1, which was operated at the highest temperature and with the highest temperature differential (see Fig. 93) of the three loops, had no mass-transfer crystals in the cold zone, and the maximum attack in the hot zone was 1 to 2 mils (see Fig. 94). Table 29 gives the results of chemical analysis of the lithium and the amount of crystals recovered from the lithium.

At present, it is not understood why so little mass transfer occurred in loops 1 and 2, since in all three loops the same procedure, bath, and testing technique were used. Some as-yet-undiscovered factor seems to have a profound effect on the rate of mass transfer.

Carburization of Inconel by Sodium

It is well known that sodium can decarburize metals and that, in some cases, it can carburize them if the carbon concentration in the sodium is high enough. Carbon contamination of sodium may possibly be due to contact with hydrocarbons or to the carbonate impurity which forms on exposure of sodium to air. The purpose of this investigation was to determine whether it is possible to make small additions of carbon to sodium that will

prevent the decarburization of Inconel specimens during long time creep tests of this material in contact with sodium at elevated temperatures In these static tests A nickel containers were used so that the ratio of Inconel surface area to sodium volume would be small The maximum solubility of carbon in nickel at 816°C (1500°F) is approximately 0 1% and therefore the carburization of the nickel container in these tests is considered to have been very slight since the A nickel container analyzed 0 05% carbon prior to the test The ratio of Inconel surface to sodium volume in these tests was 0 76/in

The Inconel specimens used in these tests were of 0 049 in sheet which was reduced to 0 015 in by cold rolling and then annealed for 2 hr at

TABLE 26 RESULTS OF STATIC TESTING OF SPECIAL STELLITE HEATS IN SODIUM AND NaF ZrF_4 UF_4 (50 46 4 mole %) AT 1500°F FOR 100 hr

Material	Bath	Weight Change (g/ n ^{2})	Metallographic Notes
Heat B as received			Structure cons sted of large fairly equiaxed particles of complex carbide (Cr_7C_3) sur ou ded by a eutectic structure in a cobalt rich matrix
Heat B	Sodium	+0 008	No attack however there were no globular particles of the carbide phase in a 1 to 2 mil area adjacent to the surface carbide particles in this area were completely transformed to a very fine precipitate quite a bit of precipitation also occurred in the matrix especially near the exposed surface
	Sodium	+0 016	Same as above
	Fluoride 30	−0 052	Attack on carbide phase varied from 8 to 19 mils the mi im m attack 8 mils occurred on the specimen where the dendrites of cobalt-rich solid solution sur rounded by the carbide particles were oriented parallel to the specime surface the maximum att ck 19 mils o cur ed where these dendrites were oriented perpen d cular to the specimen surface a large amount of fine prec p tat on occurred in the matrix during the test due to aging
	Fluor de 30	−0 060	Same as bove
Heat C as rece ved			The ca bide part cles n th s specimen wh ch u rounded the de drites of the ob lt ch sol d sol t on had a very fine structure only a few of the equiaxed carbide particles seen throughout heat B could be found
Heat C	Sodium	+0 002	No attack ve y little difference in as received and tested structures
	Sodium	+0 003	Same as above
	Fluoride 30	−0 045	Carbide network attacked to a depth of from 7 to 20 mils depending on the orientation of the network
	Fluoride 30	−0 057	Same as above

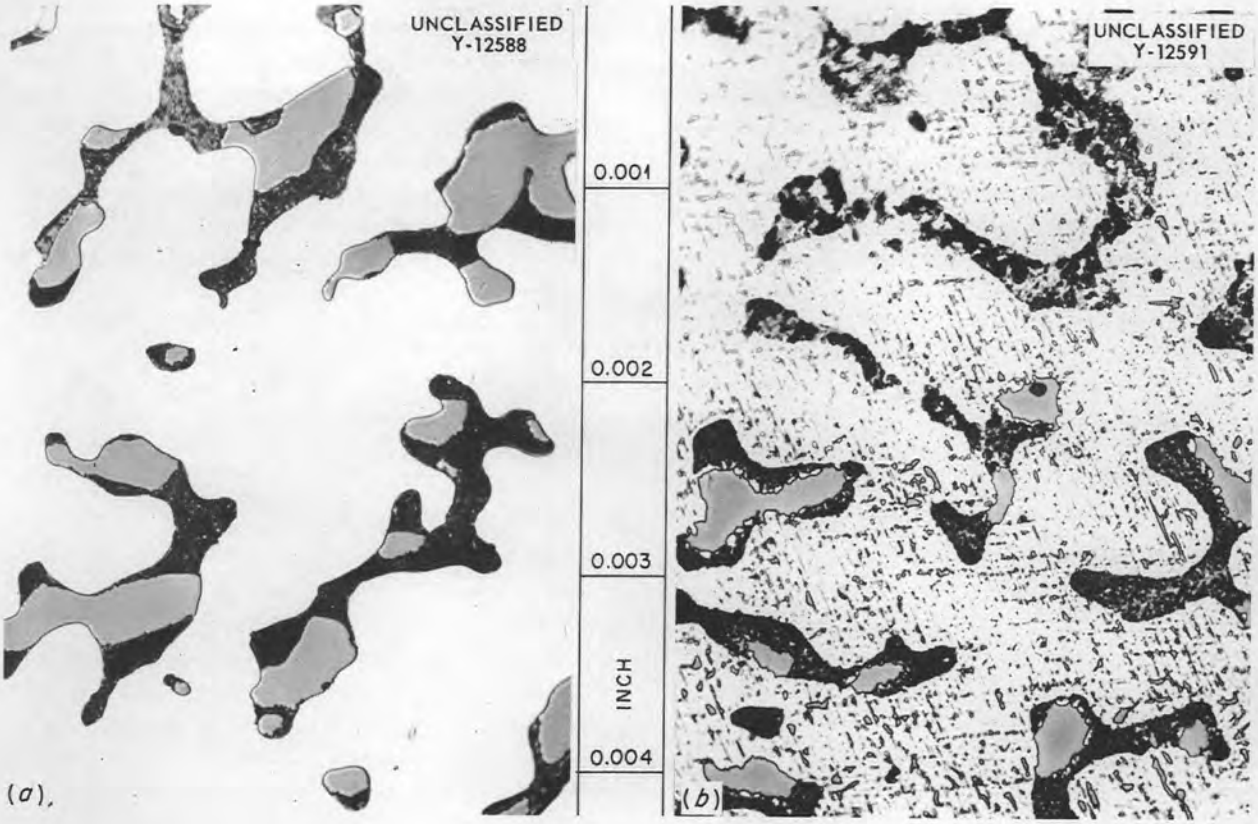

Fig. 90. Special Stellite Composition (Heat B) Before (Left) and After (Right) Static Test in NaF-ZrF_4-UF_4 (53.5-40-6.5 mole %) for 100 hr at 816°C (1500°F). Photomicrograph on right shows area where attack terminated on carbide phase (Cr_7C_3). Etchant: KOH-$K_3Fe(CN)_6$. 1000X.

1650°F. The carbon additions (1, 5, and 10 wt %) were made in the form of small lumps of reactor-grade graphite.

The test containers were loaded with graphite and sodium in a purified-helium-atmosphere dry box and sealed under vacuum. The tests were conducted at 816°C (1500°F) for 100 hr. The results of these tests may be seen in Table 30. All specimens in this series were very heavily carburized (see Fig. 95) and extremely brittle following the tests. The specimens were found to be partially covered with a green surface film, which was identified by x-ray analysis as Cr_2O_3. The oxygen source was first attributed to graphite, which was not given a degassing treatment prior to testing; however, further tests since this time with degassed graphite and standard tests with no graphite addition also exhibited a Cr_2O_3 film. Preparations are under way to construct a sodium-distillation rig in order to obtain oxygen-free sodium.

Rubidium Research

Recent tests have been conducted on rubidium metal in cooperation with an ORSORT summer project group. Rubidium having a low melting point (39.0°C) and boiling point (688°C) is being considered as a moderator coolant for reactors of the CFRE type, heat being extracted from the moderator by the boiling rubidium. The rubidium metal used in the experiments to date was prepared by calcium reduction of the rubidium fluoride salt by the Stable Isotope Research and Production Division.

An initial attempt to determine the relation between vapor pressure and temperature up to 898°C (1650°F) was unsuccessful. The test equipment has been redesigned, however, and another attempt

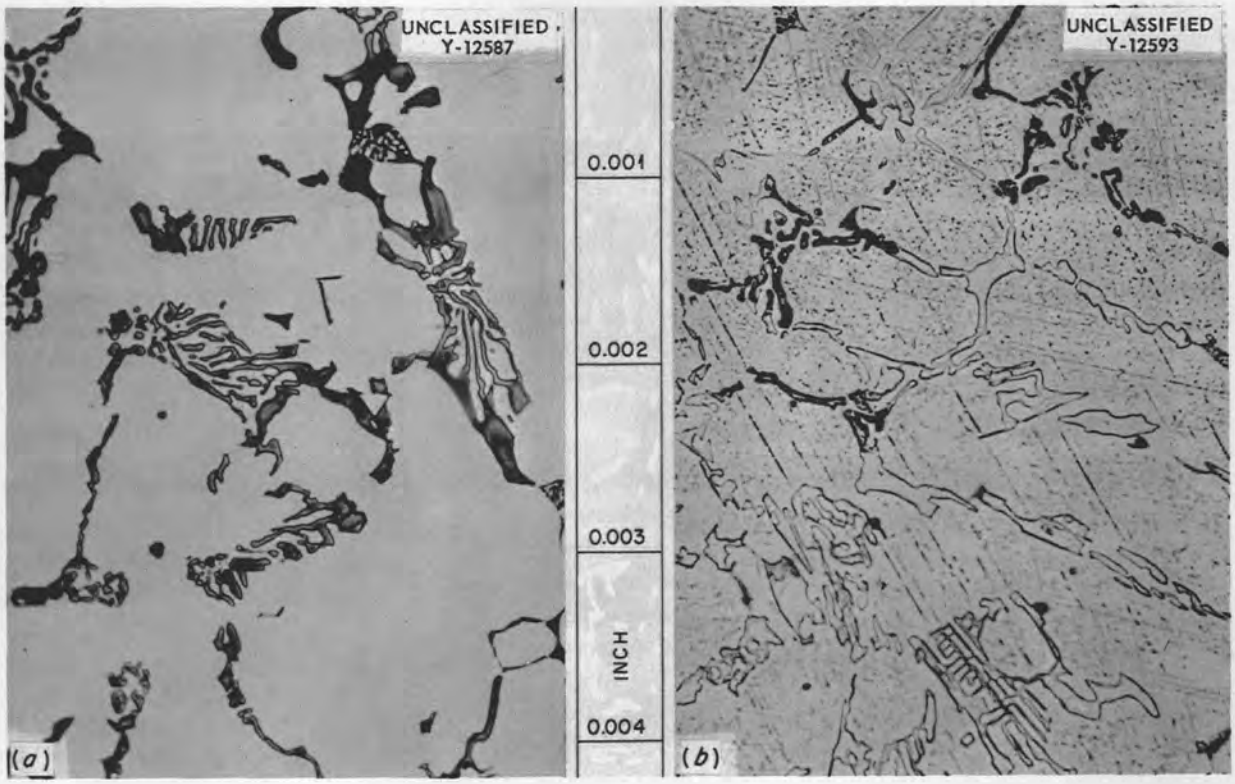

Fig. 91. Special Stellite Composition (Heat C) Before (Left) and After (Right) Static Test in NaF-ZrF_4-UF_4 (53.5-40-6.5 mole %) for 100 hr at 816°C (1500°F). Photomicrograph on right shows area where attack terminated on carbide phase (Cr_7C_3) Etchant: KOH-$K_3Fe(CN)_6$. 1000X. Reduced 2%.

will be made in the near future. Inconel has been tested in contact with static rubidium for 100 hr at 1650°F. The attack varied from 0.5 mil in the vapor zone to a maximum of 1.5 mils at the liquid-gas interface (see Fig. 96). The rubidium used in this test was not distilled prior to testing and is known to have contained several per cent sodium and some oxygen contamination. Further tests are now under way with triple-distilled rubidium.

A boiling-rubidium–Inconel loop (see Fig. 97) has been tested for 312 hr at a hot-zone temperature of 1520°F. The boiler and superheated vapor-line sections of this loop were constructed of ½-in.-OD, 0.049-in.-wall Inconel tubing. The condenser and the aftercooler section were of ¼-in.-OD, 0.035-in.-wall Inconel. The loop operated satisfactorily at the indicated temperatures and showed no evidence of mass transfer. The condenser and the aftercooler section were uninsulated, and a sharp temperature gradient was maintained between the vapor and liquid regions by the condensing rubidium vapor. Specimens from the various sections of the loop were examined metallographically, and the heaviest attack (1 mil) was observed in the hottest portion of the boiler section (see Fig. 98). Here the attack was intergranular in nature, and one grain appeared to be ready to fall out of the tube wall. The weld zone just below the liquid level in the boiler section showed a very small amount of intergranular attack (see Fig. 99).

A Special Tar-Impregnated Fired Graphite

A special tar-impregnated fired graphite, Graph-i-tite, has been tested in order to determine its corrosion resistance to sodium and fluoride 44. The carburization of an austenitic stainless steel capsule containing sodium and a Graph-i-tite specimen vs that of a capsule containing sodium and a C-18 graphite (reactor grade) specimen was studied.

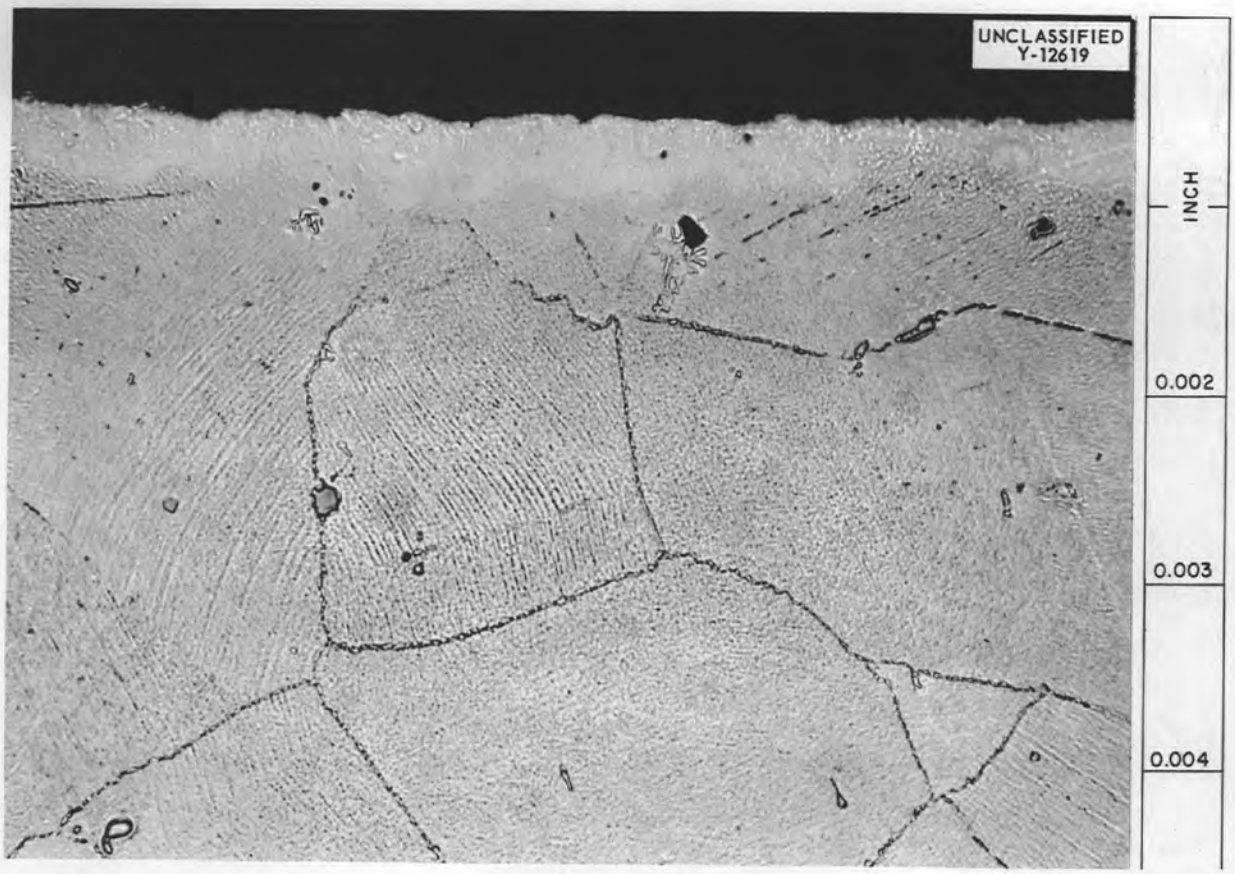

Fig. 92. Hastelloy R Exposed to Fluoride 30 in Static Test for 100 hr at 816°C (1500°F). Etchant: aqua regia. 1000X. Reduced 3%.

TABLE 27. RESULTS OF STATIC TESTING OF HASTELLOY R IN VARIOUS MEDIA AT 1500°F FOR 100 hr

Bath	Weight Change ($g/in.^2$)	Metallographic Notes
Fluoride 30	−0.0037 (−0.05%)	Specimen unattacked except in one small area, where voids extended to a depth of 1 mil; no attack on vapor zone of tube
NaOH	+0.6088 (+7.9%)	Specimen $\frac{1}{4}$ in. square attacked throughout entire thickness
Sodium	−0.0021 (−0.06%)	Specimen and bath zone were attacked to a depth of $\frac{1}{4}$ to $\frac{1}{2}$ mil in the form of voids; the exposed surface of bath zone of the container was partially decarburized to a depth of 1 mil
Lithium	−0.0047 (−0.07%)	Small voids to a depth of $\frac{1}{4}$ mil in specimen and bath zone of tube; surface partially decarburized by lithium
Lead		Specimen heavily attacked to a depth of 3 mils maximum (average 2 mils); bath zone attacked to a depth of $1\frac{1}{2}$ mils uniformly; phase change appears to have occurred in attacked areas; vapor zone unattacked

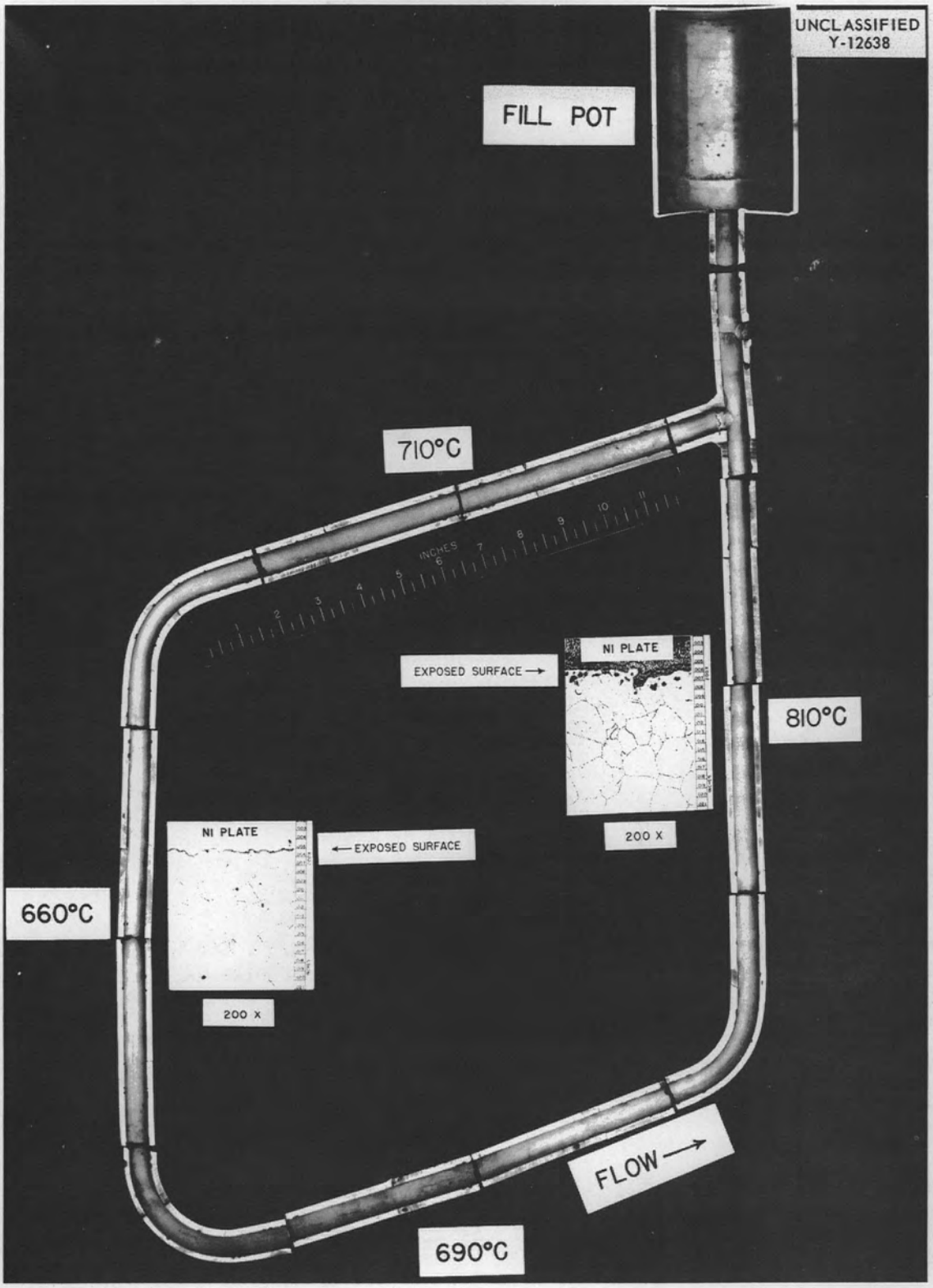

Fig. 93. Test 1 of Type 316 Stainless Steel – Lithium Thermal-Convection Loop, 1000 hr.

TABLE 28. OPERATING CONDITIONS FOR LITHIUM–TYPE 316 STAINLESS STEEL THERMAL-CONVECTION LOOPS

Loop No.	Time (hr)	Hot-Zone Temperature	Cold-Zone Temperature	ΔT (°C)
1	1000	810°C (1490°F)	660°C (1220°F)	150
2	1000	800°C (1472°F)	735°C (1355°F)	65
3	1000	705°C (1301°F)	590°C (1094°F)	115

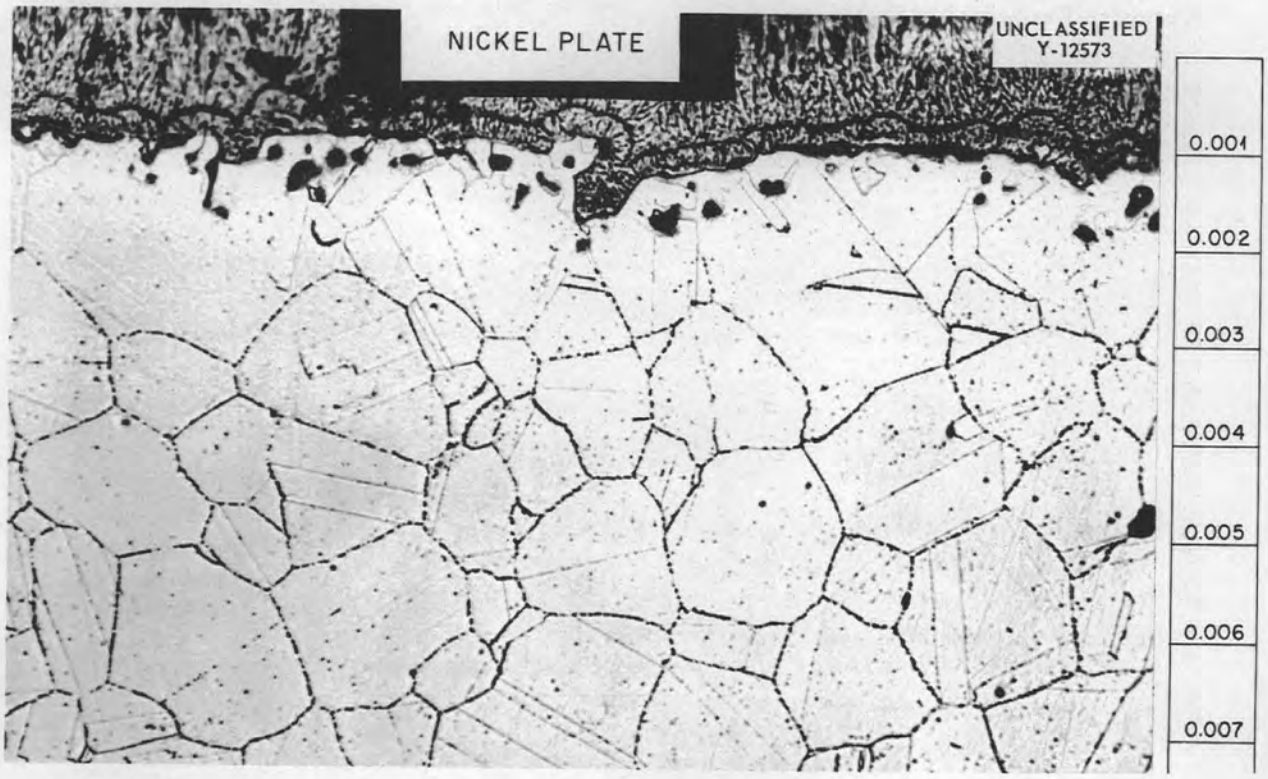

Fig. 94. Hot-Zone Surface of Type 316 Stainless Steel Loop Following a 1000-hr Exposure to Lithium at 810°C (1490°F) in Thermal-Convection Loop. This specimen was nickel-plated following test in order to prevent rounding-over of the specimen edge during metallographic polishing. Etchant: glyceria regia. 1000X.

TABLE 29. ANALYSIS OF LITHIUM IN LITHIUM–TYPE 316 STAINLESS STEEL THERMAL-CONVECTION LOOP TESTS

Source of Lithium	Chemical Analysis of Lithium (ppm)			Weight of Crystals Recovered from Lithium (g)
	Fe	Ni	Cr	
As-cast before test	40	10	<10	
From loop 1	160	150	<10	0.010
From loop 2	120	40	<10	0.001

The tar impregnated fired graphite is fabricated by tar impregnating and firing the graphite 16 times during its preparation The purpose of the repeated tar impregnations and firings is to produce a high density and a tough skin which could probably help reduce penetration of various liquid media This type of graphite has been described previously [2]

Corrosion Resistance of Graphite to Sodium and to Fluoride 44

An open Graphite crucible containing sodium and a sealed Graphite crucible containing fluoride 44 were static tested at 816°C for 100 hr in a vacuum atmosphere

[2] E E Hoffman W H Cook J E Pope and L R Trotter *ANP Quar Prog Rep June 10 1954* ORNL 1729 p 70

The sodium completely penetrated the 0 38 in thick wall and caused the crucible to crack and crumble This result agrees with that from an earlier test [2]

The wall thickness of the crucible that contained the fluoride 44 was not changed The only macroscopically visible sign of attack was that the inner surface had a higher gloss (Fig 100) than it had before the test Metallographic examination of sections of the crucible indicated irregular penetration from 0 to 5 mils A powder x ray examination indicated that a sample scraped from the penetrated zone was predominantly graphite and secondarily fluoride 44 Under the same conditions fluoride 30 in a tar impregnated fired crucible penetrated in a similar manner to a depth of from 0 to 2 mils

The carbon content of the two fluoride fuels did not change significantly in the tests (Table 31)

TABLE 30 CARBURIZATION OF INCONEL BY EXPOSURE TO SODIUM CONTAINING CARBON ADDITIONS AT 816°C (1500°F) FOR 100 hr

Inconel Exposure Conditions	Weight Change of Inconel Specimen During Test (%)	Carbon Inconel Test Specimen Three Analyses (%)
Unexposed (specimen before test)		0 054
		0 056
		0 058
		Av 0 056
Exposed to sodium plus 1% graphite	1 09	0 841
		0 871
		0 932
		Av 0 882
Exposed to odium plus 5% graphite	1 34	1 06
		1 06
		1 15
		Av 1 09
Exposed to sodium plus 10% graphite	1 63	1 14
		1 24
		1 35
		Av 1 24

On all tested specimens part of the weight change was due to the formation of a Cr_2O_3 film on the surface of the specimens

Carburization of an Austenitic Stainless Steel

In order to determine the relative carburization by tar-impregnated fired graphite and by C-18 graphite (reactor grade), cylinders of the same size of each type of graphite were static-tested in type 304 stainless steel tubes containing equal quantities of sodium at 816°C under a vacuum atmosphere. Tests of 100 and 500 hr were made on each type of graphite. The type 304 stainless steel was chosen because it carburizes more readily than other austenitic stainless steels. The results of these tests below the level of the molten sodium are shown in Fig. 101. In the 100-hr test the tar-impregnated fired graphite carburized the type 304 stainless steel to a slightly greater extent than did the C-18 graphite, but in the 500-hr test the tar-impregnated fired graphite clearly carburized the type 304 stainless steel to a greater extent than did the C-18 graphite. In the 500-hr tests for both types of graphite, the type 304 stainless steel in contact with the sodium had small

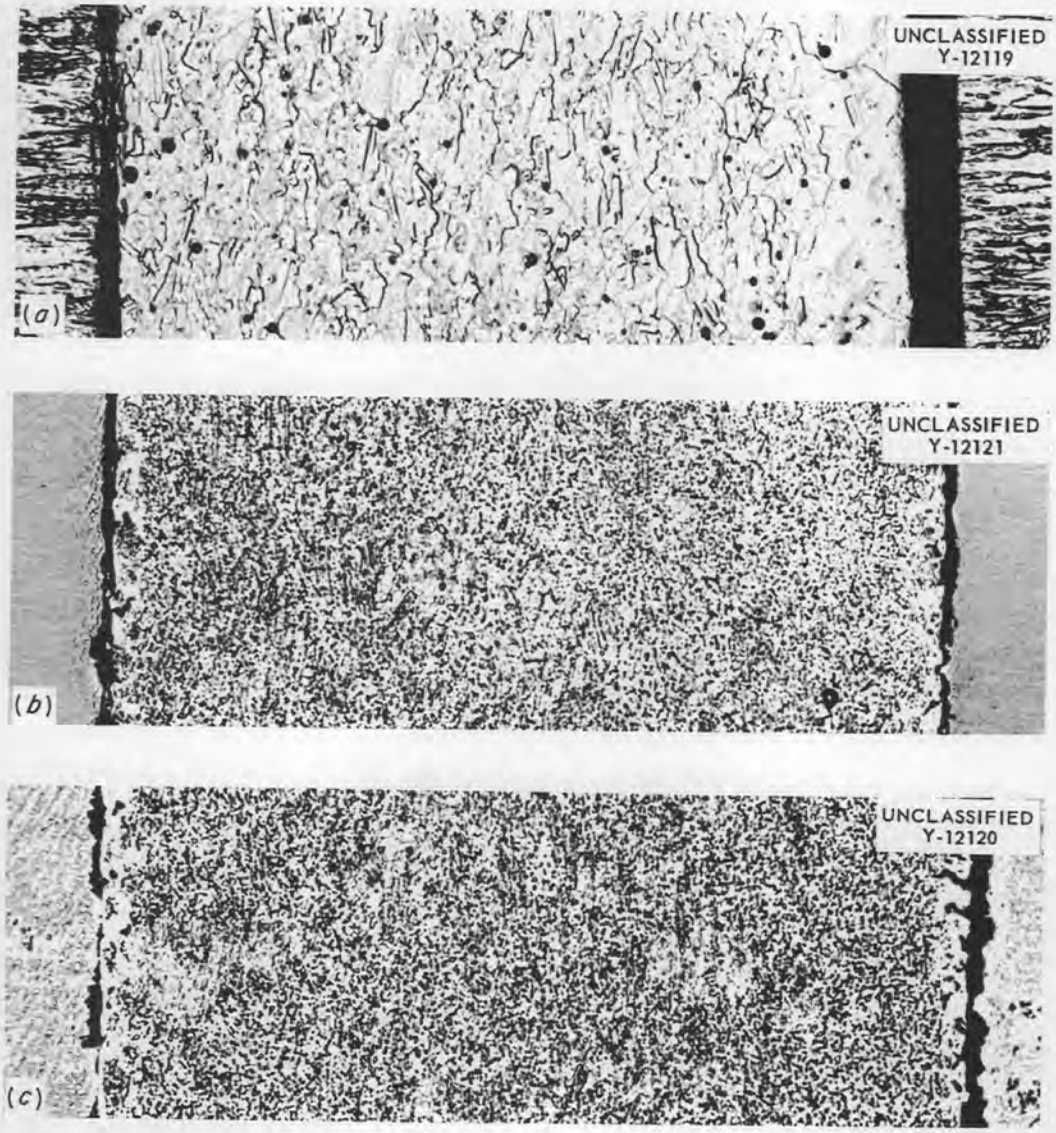

Fig. 95. Carburization of Inconel by Sodium Plus Graphite. All specimens were nickel-plated prior to metallographic examination. (*a*) Inconel specimen before test, 0.056% C. (*b*) Inconel specimen tested for 100 hr at 816°C (1500°F) in sodium plus 1% graphite, 0.882% C. (*c*) Inconel specimen tested for 100 hr at 816°C (1500°F) in sodium plus 10% graphite, 1.24% C. Etchant: glyceria regia. 250X.

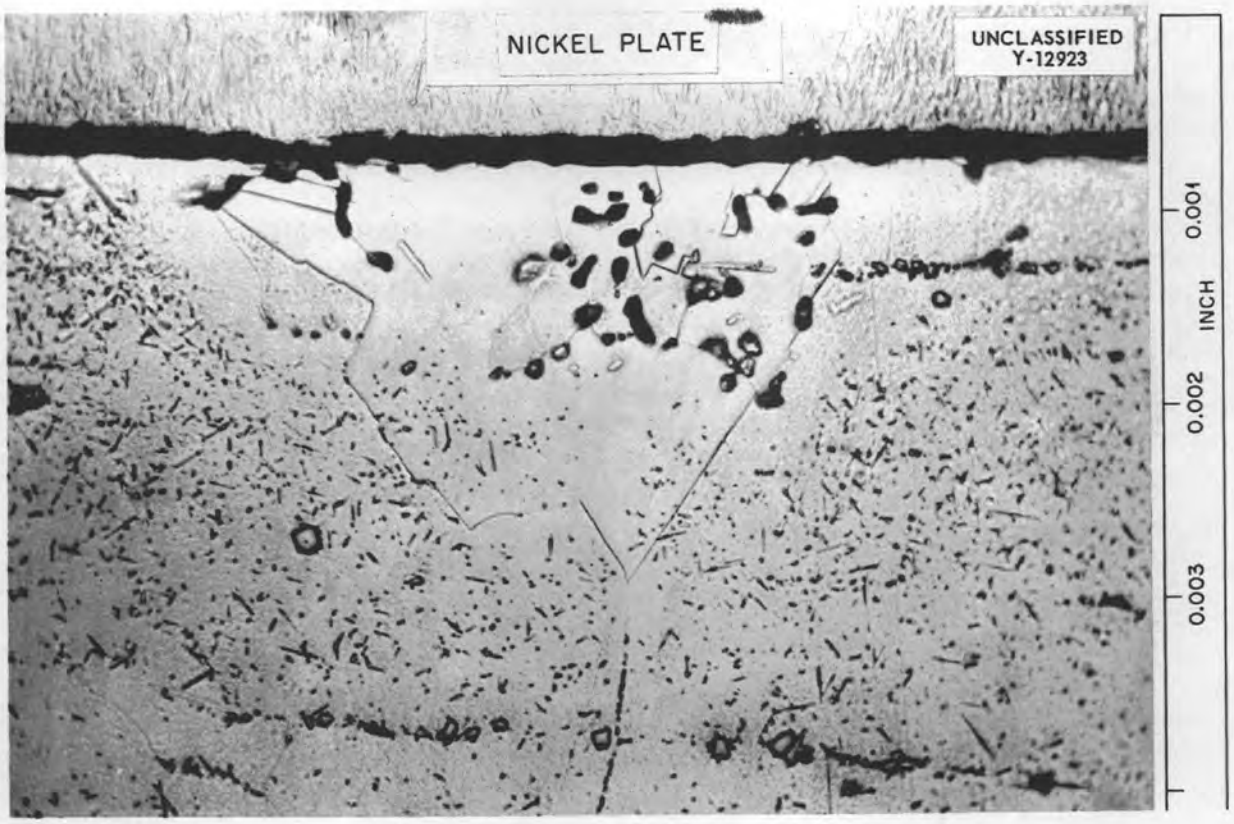

Fig. 96. Inconel Following Exposure to Static Rubidium for 100 hr at 898°C (1650°F). Note decarburization in attacked area. Specimen was nickel-plated following test. Etchant: glyceria regia. 1000X.

subsurface voids; this effect was most pronounced in the test with the tar-impregnated fired graphite (see Fig. 101).

The depth of carburization of the type 304 stainless steel above the level of the molten sodium covering the graphite cylinders was 1 mil in all the tests except the 500-hr test with a tar-impregnated fired graphite cylinder, which caused carburization to a depth of 2 mils.

Corrosion of Al_2O_3, $MgAl_2O_4$, MgO, ZrO_2, and SiC in Molten Media

Three ceramic oxides, Al_2O_3, $MgAl_2O_4$, and ZrO_2 (CaO stabilized), and one carbide, SiC, have been static-tested for corrosion screening in a vacuum atmosphere in each of four media – sodium, $NaF\text{-}ZrF_4\text{-}UF_4$ (53.5-40-6.5 mole %), lithium, and lead – at 816°C for 100 hr. A fourth ceramic oxide was tested under the same conditions in sodium and $NaF\text{-}ZrF_4\text{-}UF_4$ (53.5-40-6.5 mole %). The Al_2O_3 and $MgAl_2O_4$ test pieces were cut from single, synthesized crystals; the MgO test pieces were cleaved from a single, synthesized crystal. The nominal dimensions of the test pieces and the results of the tests are given in Table 32.

Attempts were made to determine, by powder x-ray examination, what happened to some of the least-corrosion-resistant specimens in each media. The data are summarized in Table 33.

In these tests SiC was generally the most resistant to corrosion, and Al_2O_3 was second most resistant. These single-run screening tests are only qualitative, and the results should be used with caution. This is typical of many corrosion tests on ceramics or cermets. It is planned that larger specimens will be tested; thus more accurate data can be obtained and additional examinations, such as metallographic and chemical analyses, can be made.

Corrosion of Cermets by Fluoride 30

Various titanium carbide cermet specimens have been screened by a dynamic-corrosion test in

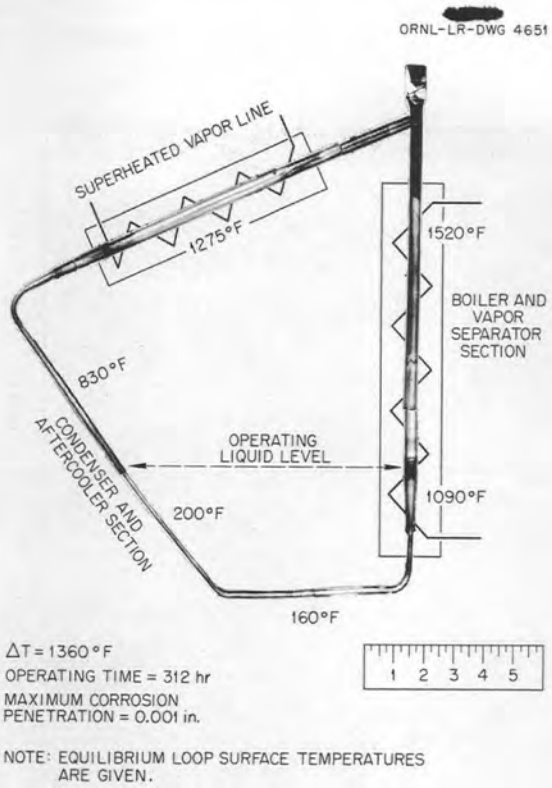

Fig. 97. Boiling Rubidium-Inconel Loop.

fluoride 30. These specimens were restricted in the hot zone (1500°F) of Inconel seesaw tubes and tested in fluoride 30 for 100 hr under vacuum atmospheres. The specimens were submitted by Kennametal Inc. (Kentanium specimens) and Sintercast Corp. of America. The results of these tests are given in Table 34. All these specimens had fair-to-good corrosion resistance in fluoride 30. Generally, the corrosion resistance of the cobalt-base-bonded specimens was equal to or slightly superior to that of the nickel-base-bonded specimens. In all cases the attack appeared to be along the surfaces of the titanium carbide particles, separating them from the binder. The corrosion attack along the surfaces of the titanium carbide particles might have been attack on a fabrication reaction product between the titanium carbide and binder. The Sintercast samples were too small to allow retention of a piece of each of the as-received specimens for metallographic examinations, which would have made possible more accurate depth-of-attack determinations on the test specimens. More Sintercast specimens have been received and are being tested to secure more accurate evaluation of their corrosion resistance in fluoride fuels. As-received specimens have been saved and will serve as a basis of comparison in these tests.

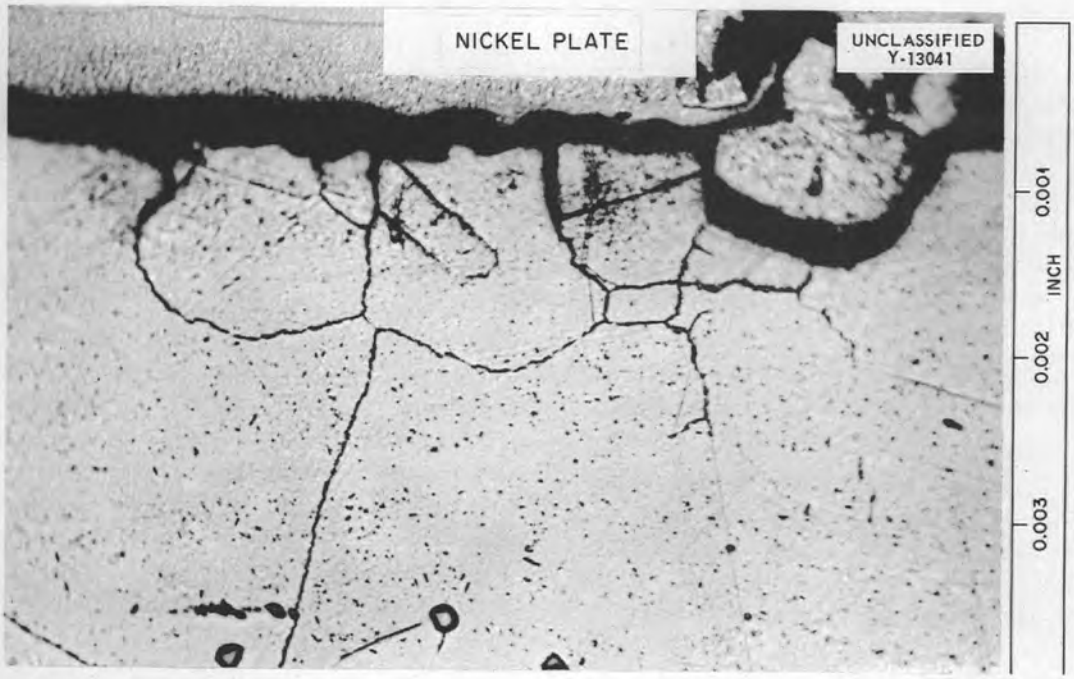

Fig. 98. Inconel Exposed to Rubidium Vapor for 312 hr at 1520°F. Note intergranular attack. Specimen was nickel-plated following test in order to preserve edge. Etchant: aqua regia. 1000X. Reduced 11%.

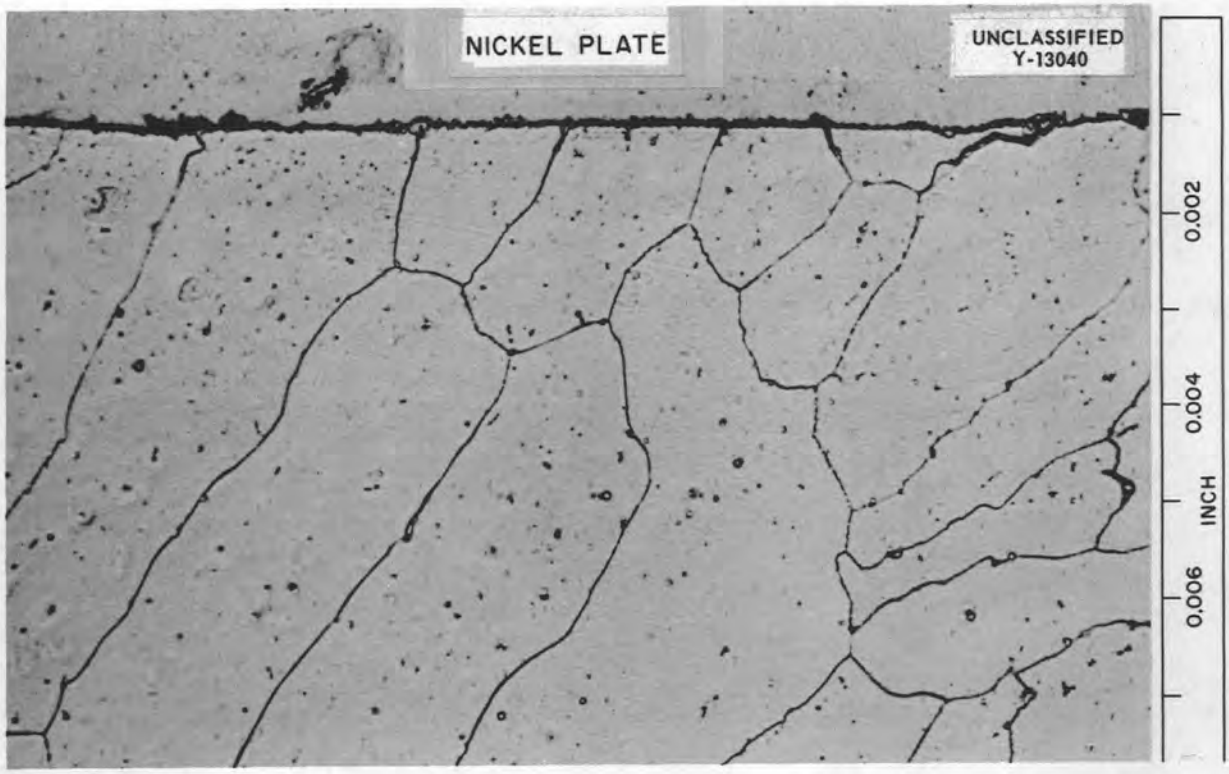

Fig. 99. Inconel Weld Below Bath Level Exposed to Rubidium Vapor for 312 hr at 1090°F. Specimen was nickel-plated following test in order to preserve edge. Etchant: aqua regia. 500X.

Beryllium-Sodium-Inconel Compatibility Tests

Nine dynamic tests (see Table 35) have been completed on beryllium-sodium-Inconel systems. The purpose of these tests is to determine whether sodium may be used to cool the beryllium moderator in the CFRE without cladding the beryllium with Inconel. Three types of tests have been performed to date. In the whirligig test a circular loop of Inconel tubing with a beryllium insert was partially filled with sodium which circulated at a velocity of 10 fps. Four of these tests were operated without a temperature differential and one with a 140°F differential. These whirligig tests were for about 300 hr. Two thermal-convection loops of Inconel with beryllium inserts were tested for 1000 hr with sodium circulating at a relatively low velocity (approximately 5 to 10 fpm). In addition, seesaw tests were performed in which beryllium specimens were retained in the hot zones of oscillating Inconel tubes partially filled with sodium which circulated at a velocity of 3 fpm.

Macroscopic examination revealed visible attack on the Inconel in only two cases, these being deposits. However, a black layer was formed in the annular space between the beryllium insert and the enclosing Inconel sleeve in the whirligig and thermal-convection loop tests. This layer was very adherent and made removal of the insert difficult; consequently, the weight-change data were not considered to be reliable. A picture of this layer from whirligig loop No. 39 (1300°F) is shown in Fig. 102. Later tests indicate that the porosity of the surface layer is due to attack by the plating solution. The maximum depth of attack on the inside surface of the Inconel, as determined microscopically, did not exceed ½ mil. Chemical analysis of the sodium bath revealed less than 0.04% beryllium in the sodium.

In all tests beryllium was detected on the Inconel tube-wall surface (see Figs. 103 and 104). This distribution was determined by a microdrilling technique perfected by the Spectrographic Laboratory of the Analytical Chemistry Division. X-ray analysis of the Inconel surface indicates that the beryllium is present as the metal. The beryllium concentration variation appears to be due both

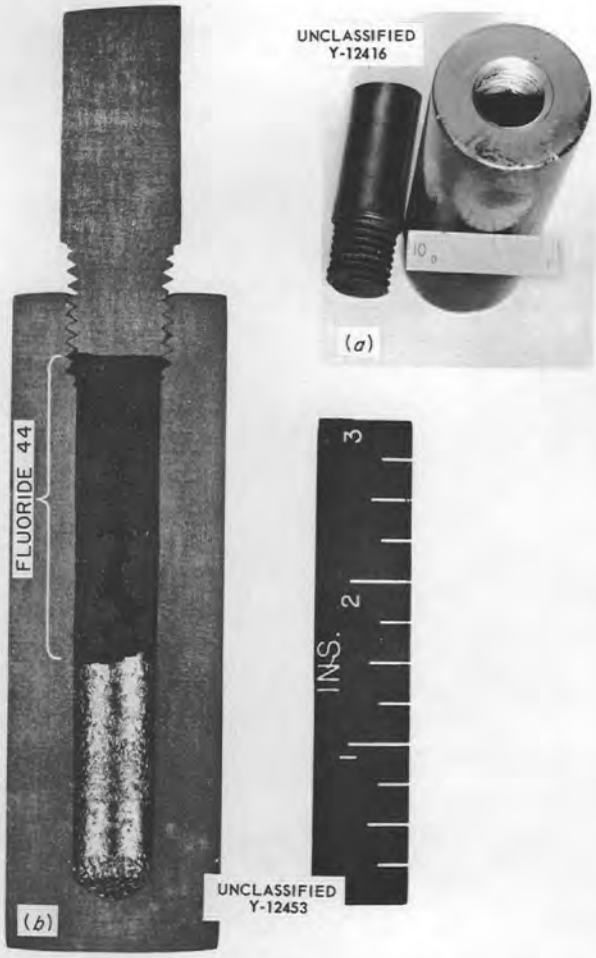

Fig. 100. Corrosion of Graph-i-tite Crucible by Fluoride 44. At the end of the test the crucible was inverted; this allowed the fluoride 44 to flow to the top of the crucible. (*a*) As received. (*b*) Contained fluoride 44 at 816°C for 100 hr.

TABLE 31. CARBON CONTENT OF FLUORIDE FUELS 30 AND 44 BEFORE AND AFTER BEING STATIC-TESTED IN GRAPH-I-TITE AT 816°C FOR 100 hr

Fluoride Fuel	Carbon (%)	
	Before Test	After Test
30	1.04	1.88
44	1.65	1.39*

*Average of the fluoride remaining in and the fluoride spilled from the crucible at the conclusion of the test.

to the temperature gradient and to the flow pattern of the sodium.

In the thermal-convection loops a deposit was formed between the contacting ends of the beryllium insert and Inconel tube. These deposits and those found in the whirligig loop were subjected to x-ray analysis, and beryllium, Inconel, and lines very similar to those of sodium bicarbonate were detected.

The beryllium specimens from the seesaw tests (see Fig. 105) were covered with a black flaky deposit which has been identified by x-ray analysis as beryllium oxide and beryllium. Again, lines similar to those of sodium bicarbonate were observed.

Microscopic examination of beryllium showed little attack on the inside surface, but attack up to 5 mils was observed on the outside surface, which was in contact with the sodium in the 0.005-in. annular space (see Fig. 106). The voids seen in Fig. 106*b* may be due to compound formation in the grain boundaries during the test and subsequent removal during metallographic preparation. The results of these tests indicate that a system of this type may be operated successfully at 1200°F and below.

Tests so far have indicated that beryllium is essentially unattacked where sodium flows at a relatively fast rate. The attack on the beryllium was heaviest in areas where the sodium was relatively stagnant – for example, in the annular space in the tests mentioned above – and was due to dissimilar-metal transfer.

WELDING AND BRAZING

P. Patriarca
G. M. Slaughter
J. M. Cisar
K. W. Reber
R. E. Clausing

High-Temperature Brazing-Alloy Development Program

Oxidation Resistance of High-Temperature Brazing Alloys. The extent and rate of high-temperature oxidation of brazing alloys at different times during service are important factors to be considered in determining the proper alloy to use in the fabrication of aircraft radiators. Inconel T-joints, brazed with several high-temperature brazing alloys, were subjected to an oxidizing atmosphere for 200, 500, and 1300 hr at 1500°F, and 200 and 550 hr at 1700°F. The results of

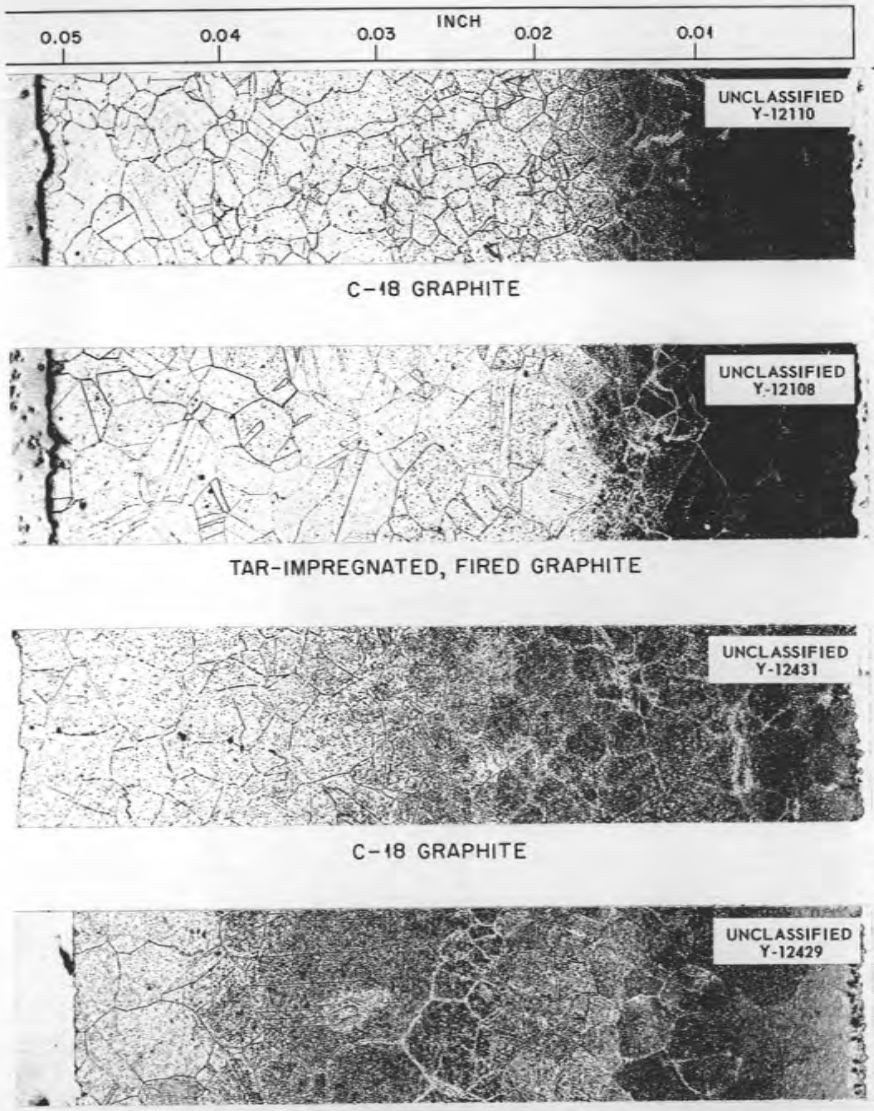

DEPTH OF CARBURIZATION, mils

	CONCENTRATED	TRACEABLE
100 hr	16	32
	18	32
500 hr	33	49+ (THROUGH THE TUBE WALL)
	40	49+ (THROUGH THE TUBE WALL)

Fig. 101. Relative Carburization by a Special Tar-Impregnated, Fired Graphite vs C-18 Graphite (Reactor Grade) on Type 304 Stainless Steel Below the Liquid Level of Molten Sodium at 816°C in a Vacuum Atmosphere. Etchant: glyceria regia on all specimens. 100X. Reduced 16.5%.

TABLE 32 SUMMARY OF THICKNESS AND WEIGHT CHANGES AND MACROSCOPIC EXAMINATION NOTES ON CERAMIC DISKS[a] (NOMINAL DIMENSIONS 0 75 × 0 021 i THICK) STATIC TESTED AT 816 C FOR 100 h IN VARIOUS MEDIA

B th	Ch g (%)										R m k
	Al_2O_3 S pph[b]		S C		$MgAl_2O_4$ Sp l[b]		Z O_2 (C O St b l ed)		MgO^c		
	Th k	W ght	Th k	W ght	Th k	W ght	Th k	W ght	Th kn	W ght	
S d m	−0 5	−0 9									T t h g d p m f m l l t p ent t t t wh t m t p t t t m ll k dg
			−0 9								U lt d by t t pt f b ght l pp mall p t f d k dg b k ff
					0 0						S mpl h pp d l ghtly dg ft t t th g lly l l t p t mpl h d lm t mpl t ly b p t t d by bl k l
							+8 6				Edg h pp d th l ght b ff l lt d t bl bl k l
									−0 5	−0 1	U lt d pp pt th t mpl h g d f m l l t l ght bl g y l
Fl d 44	−31										B k ft t t d w th fl d 44 b w d t f b tw fl o- d 44 d th pph
			−1 8								R d p f p m ppe d t b tt k d
											M th h lf f p m w ed ft t t th w d w th fl d 44 d pp ar d t be lm t ampl t ly lt d

TABLE 32 (o t ed)

B th	Ch ge (%)								Rem k
	Al_2O_3 Sapph[b]		S C		$MgAl_2O_4$ Sp el[b]		$Z O_2$ (C O Stab l ed)		MgO^c		
	Th ckne	W ght	Th ckne	W ght	Th kne	We ght	Th k	W ght	Th ck	We ght	
							d	*d*	*d*	*d*	
L th m	*d*	*d*									S me m ll pa t cle of S C em d fte te t
					d	*d*					Afte t t pe men w n m y m ll p e e l ght b ff olo h ged to a harco l bl k
									e		T t ot m de o spe men
L ad	0 0	+0 3									No v ble tt k g y h olo d small pot n spe m n ppa e tly th l d f lm
			+2 9								No ble tta k ft te t p c men b oke n lo d g
					0 0						No ble att ck aft te t hang d f m olo l to g y olor b oke la d g
							0 0	+0 5			No v bl tta k fte te t h g d f om l ght b ff to g y olor
											Te t ot m d o pe men

[a]The MgO p ce e pt o th y re om n lly 0 02 × 0 36 × 0 36
[b]C t f om gl yst l
[c]Cl d f om gl c y t l
[d]No v s ble tr f pe m ft te t
T t ot m de a pe m

TABLE 33 POWDER X RAY IDENTIFICATION OF THE PHASES OF SOME OF THE MOST CORRODED SPECIMENS

Spec men	Media	Powder X Ray Exam nat on	
		As Received	Tested
$MgAl_2O_4$	Sod um	Face centered cub c $a = 7\ 970$	Face centered cubic $a = 7\ 981$
$MgAl_2O_4$	NaF ZrF_4 UF_4 (53 5 40 6 5 mole %)	Face centered cubic $a = 7\ 970$	NaF ZrF_4 UF_4 (53 5-40 6 5 mole %) pattern
ZrO_2 (CaO stabilized)	Sodium	Primarily face centered cubic ZrO_2 secondarily monoclinic ZrO_2	Same as as received specimen
ZrO_2 (CaO stabili ed)	Lithium	Primarily face ce tered cubic ZrO_2 econd r ly mono l n c ZrO_2	Un dentif ed face-centered cubic $a = 4\ 674$

TABLE 34 RESULTS OF SEESAW TESTS OF TITANIUM CARBIDE CERMETS EXPOSED TO FLUORIDE 30 AT 1500°F FOR 100 hr

Material	Nom nal Composition	Depth of Attack (mils)	Metallographic Notes
Kentanium			
K 138 A	80% TiC TaC NbC–20% Co	0 5–1	Attack appeared to be on binder
K 153 B	60% TiC TaC NbC–40% Co	3	Attack to a un fo m depth attack was along the TiC particle surfaces separating the TiC particles from each other and from the binder
K 161 B	T C + N Mo	0	Te ted surface sl ghtly mo e ir egular than as received surface
Sintercast			
No 1	TiC + Co base binder	0 5–2	Many voids throughout specimen which were probably formed d r ng fabrication
No 4	TiC + Co base binder	1	Some of the TiC particles had a second phase within the part cles
No 5	TiC + Ni base binder	0	The binder appeared to be firmly attached to the TiC particles throughout the specimen
No 8	TiC + Ni base binder	2	Small section on corner of specimen not uniform appeared to be binder without TiC particles did not appear to be attacked
No 10	TiC + Ni base binder	5	Attacked along T C particle surfaces just enough to separate them from the binder

Percentages for the nominal composit on are not known

In all the following composit ons the titanium carbide component is approx mately 45 to 55 wt %

such tests during the past six months are compiled, along with previous results in Table 36

Corrosion Resistance of High Temperature Brazing Alloys The resistance to corrosion of high temperature brazing alloys in pressurized water has been investigated to obtain information which is useful in the fabrication of certain solid fuel element assemblies The results of the 1000 hr tests in distilled water at 250°C and 1200 psi are presented in Table 37

Heat Exchanger Development

Brazing Alloy–Base Metal Combinations for High Conductivity Fin Radiators At the conclusion of the oxidation tests described previously four alloys were selected for oxidation tests with various high conductivity fin materials in order to determine an optimum combination for fabrication of a sodium-to-air radiator Low melting Nicrobraz, Coast Metals 52, Electroless nickel and Ni P Cr

TABLE 35 RESULTS OF BERYLLIUM SODIUM INCONEL COMPATIBILITY TESTS

Test and No	Time (hr)	Temperature (°F)	Concentration of Beryllium on Surface of Inconel Tube ($\mu g/cm^2$)	Remarks
Whirligig				
No 37	300	1100 (isothermal)	5 3–7 9	Two dark deposits on Inconel which analyzed high in Be macroscopically Be showed finely pitted appearance
No 36	300	1200 (isothermal)	0 05	No visible deposits on Inconel Be appeared to be smooth but discolored
No 39	300	1300 (isothermal)	0 07	No visible deposits on Inconel Be showed dark discontinuous deposit covering surface
No 38	300	1400 (isothermal)	39 6–127 0	No visible deposits on Inconel Be surface pitted and partially covered with small deposits
No 40	270	Hot zone 1200 Cold zone 1060	See Fig 102	Loose adherent gray deposit found in cold zone analyzed high in sodium Be smooth but discolored
Thermal convection				
No 5	1000	Hot zone 1150 Cold zone 990	See Fig 103	Inconel appeared to be smooth and showed no visible deposits Be smooth but d scolored
No 6	1000	Hot zone 1300 Cold zone 1130	See Fig 103	Inconel appeared to be smooth and showed no visible deposits Be smooth and light gray in color
Seesaw				
No 192	300	Hot zone 1400 Cold zone 710	Hot zone 14 0 Middle 9 9 Cold zone 20 6	See Fig 105 Be specimen covered with black flaky deposit surface of Inconel tube discolored
No 193	300	Hot zone 1100 Cold zone 740	Hot zone 0 07 Middle 0 02 Cold zone 0 01	Similar to Fig 105

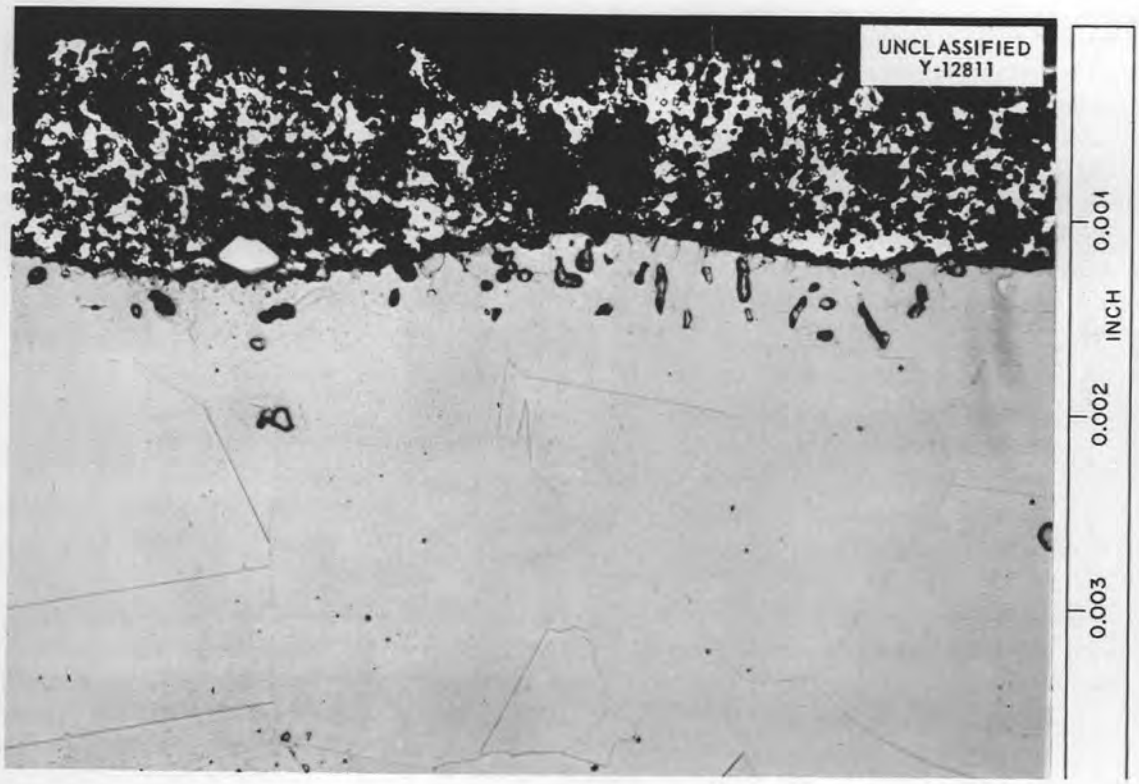

Fig. 102. Inside Surface of Inconel Sleeve Enclosing Beryllium Insert in Whirligig Test. Exposed to sodium for 300 hr at 1300°F. Etchant: glyceria regia. 1000X.

alloy were used to braze Inconel, type 310 stainless steel, and type 430 stainless steel, which were clad to high-conductivity copper fins. Compositions of these alloys and the brazing temperatures used are shown in Table 38. The evaluation of these alloys was based upon metallographic examination of tube-to-fin specimens after brazing in dry hydrogen and after exposure to static air at 1500°F for periods up to 600 hr.

Figure 107 is a microsection of a tube-to-fin joint of Inconel-clad copper fin material (0.002-in. Inconel, 0.006-in. copper, 0.002-in. Inconel) brazed to $\frac{3}{16}$-in.-OD, 0.025-in.-wall Inconel tubing with Electroless nickel (88% Ni–12% P) and then exposed to static air at 1500°F for 600 hr. Tube-wall solution was negligible, although a severe solution of the fin lip occurred during the brazing cycle. The hole formation in the copper layer, caused by diffusion into the fillet, and the excellent oxidation resistance of the resulting bronze joint are noteworthy. Examination of Inconel-clad copper specimens brazed with the other alloys revealed similar results; that is, minimum solution of tube walls and excellent oxidation resistance of the brazed joints.

The effects of diffusion, however, were in evidence after the test. Color changes in the copper core, along with the formation of voids, indicated that the use of Inconel-clad copper in a radiator would not be advisable; it was expected that both the void formation and the change in core chemistry from copper to copper-nickel alloy would seriously reduce the heat-transfer efficiency of the fin.

Types 310 and 430 stainless steels, each clad to copper, have been found to be relatively immune to these diffusion effects, and a number of brazed joints were evaluated to determine the optimum alloy for brazing these materials to Inconel tubing.

Figure 108 is a photomicrograph of a section of a tube-to-fin joint of type 310 stainless-steel-clad copper brazed to Inconel tubing with 88% Ni–12% P. Fin dilution and intergranular penetration into the tube wall occurred during brazing. This penetration, undetected in the case of Inconel-clad copper, appears to be due to the formation of a

TABLE 36 OXIDATION OF DRY HYDROGEN BRAZED INCONEL T JOINTS (AVERAGE FILLET THROAT 0 015)

Alloy	Comp t (wt %)	B g T mp t (F)	E t t f Att k				
			At A T mp t f 1500 F			At A T mp t re f 1700°F	
			Aft 200 h	Aft 500 h	Aft 1300 h	Aft 200 h	Aft 550 h
C mme l							
N rob	70 N –14 C –6 F –5 B–4 S –1 C	2150	Sl ght	Sl ght	Sl ght	Sl ght	Sl ght
L w-m lt g N b	80 N –5 C –6 F –5 S –3 B–1 C	1920	Sl ght	Sl gl t	Sl ght	Sl ght	Sl ght
C t M t l NP	50 N –12 S –28 F –4 Mo–4 5 P–1 Mn–0 5 C	2050	V y l ght				
C t M t l 50	92 N –4 S –3 B–1 F	2010	V y l ght				
C t M t l 51	92 N –4 5 S –3 B–0 5 F	2010	V y l ght				
Coa t M tal 52	89 N –5 S –4 B–2 F	1840	V ry l ght	Sl ght	Sl ght	Sl ght	Sl ght
C t M tal 53	80 N –4 S –8 C –3 F –5 B	1920	V ry l ght				
M d N kel C Alloy	64 Ag–33 Pd–3 M	2150	S t l d t	S t l d t	Seve t m l d t	Complet	
C pp	100 C	2050	C mpl t	C mpl t			
E p m t l							
N k l b							
G l El tr 62	69 N –20 C –11 S	2150	V y l ght				
G ral El t 81	66 N –19 C –10 S –4 F –1 M	2150	V y l ght	Sl ght	l t l d t	S r	S re
N G	75 N –25 G	2150	Sl ght	Sl ght	Sl ght	Mod t	S re
N C G	65 N –25 G –10 C	2140	V y l ght	Sl ght	l t l x d t	M der t	S
El tr l k l	88 N –12 P	1740	V y l ght	Sl ght	Sl ght		
N C P	80 N –10 C –10 P	1830	V y l ght	Sl ght	Sl ght		
N S	68 N –32 S	2150	Sl ght	Mode t	S t m l dat	Seve	C mpl te
N -M	40 N –60 M	1920	C mpl t	C mpl t			
N -Mn-C	35 N –55 M –10 C	2010	S				
N C -S	73 5 N –16 5 C –10 S	2150	V y l ght				
N -S	88 N –12 S	2150	V y l ght				
N M -G	50 N –25 M –25 Ge	2120	Sl ght				
P m t l b							
A N	82 A –18 N	1830	V y l ght	Sl ght	Sl ght	Mod te	M d te
A C	80 A –20 C	1740	M d t	C mpl t			
Pd Al	92 Pd–8 Al	2020	V y l ght	V y l ght	V ry l ght	V ry l ght	Sl ght
Pd-N	60 Pd–40 N	2280	V y l ght				
Pd N S	60 Pd–37 N –3 S	2150	Sl ght				
A Co	90 A –10 C	1830	V y l ght				
Pd-G	90 Pd–10 G	1740	V y l ght				

V ry l ght l th 0 001 p t t
Sl ght 0 001 t 0 002 p t t
M d t 0 002 t 0 005 p t t
S g t th 0 005 p t t
C mpl t f ll t mpl t ly d t y d
V d form t d t t l d t tb ll y f ll t–l l t f

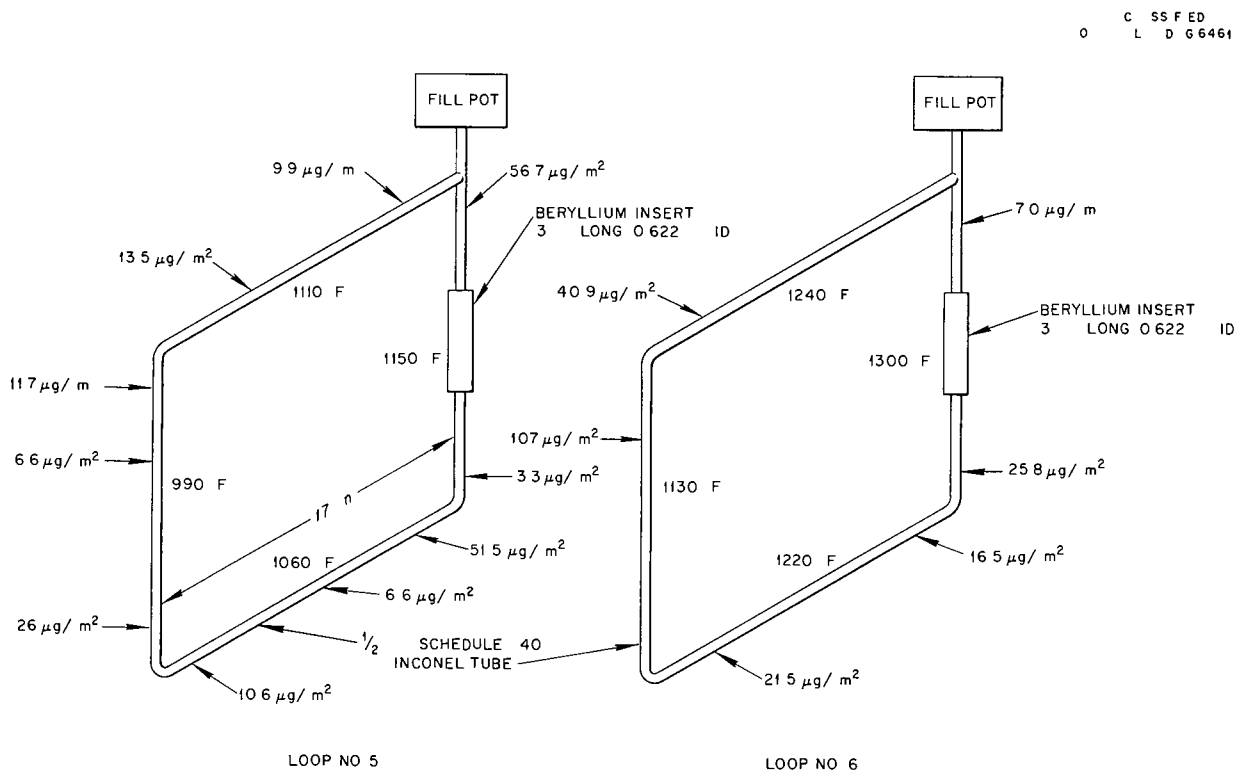

Fig 103 Distribution of Beryllium (micrograms per square centimeter) Around Thermal Convection Loops After 1000 hr of Sodium Circulation

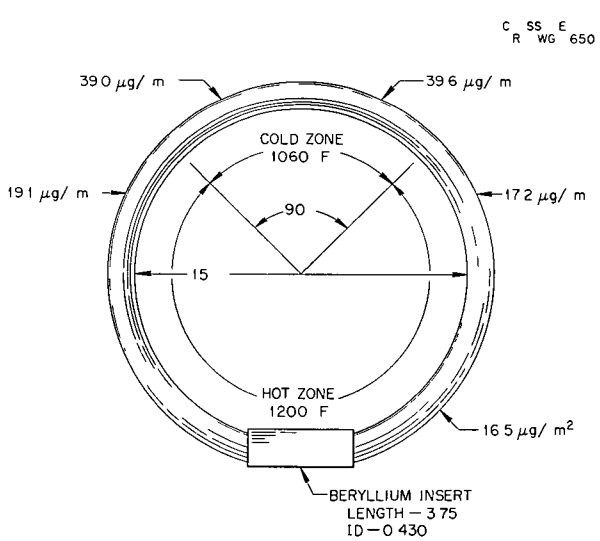

Fig 104 Distribution of Beryllium (micrograms per square centimeter) Around Inconel Whirligig Loop No 40 After 270 hr of Sodium Circulation

TABLE 37 CORROSION OF DRY HYDROGEN BRAZED JOINTS AFTER 1000 hr IN DISTILLED WATER AT 250°C AND 1200 psi

B a ing Alloy	Degree of Attack
Nicrobraz	Moderate
Low melt ng Nicrobra	Very light
Coast Metals 52	Severe
General Electric 81	Very slight
75 Ni–25 Ge	Moderate
88 Ni–12 P	Very slight
80 Ni–10 Cr–10 P	Moderate
68 Ni–32 Sn	Very slight
40 Ni–60 Mn	Complete attack
82 Au–18 Ni	Slight
100 Cu	Slight
40 Ni–60 Pd	Moderate
72 Ag–28 Cu	Complete attack

UNCLASSIFIED
Y-12901

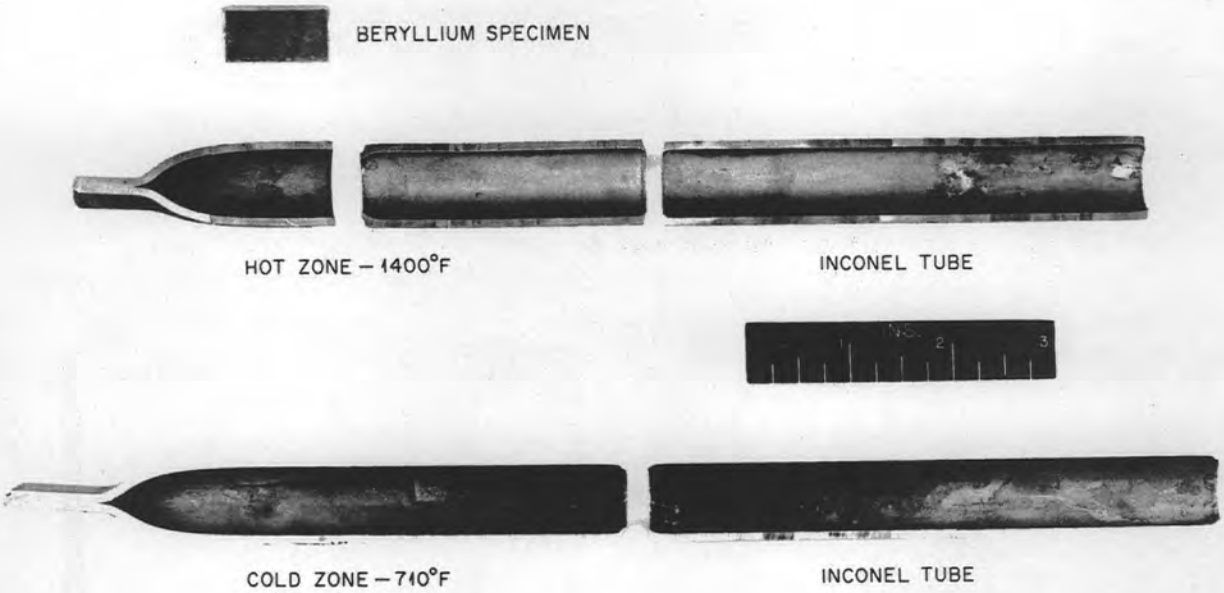

Fig. 105. Seesaw Test No. 192, Sodium-Beryllium-Inconel, 300 hr.

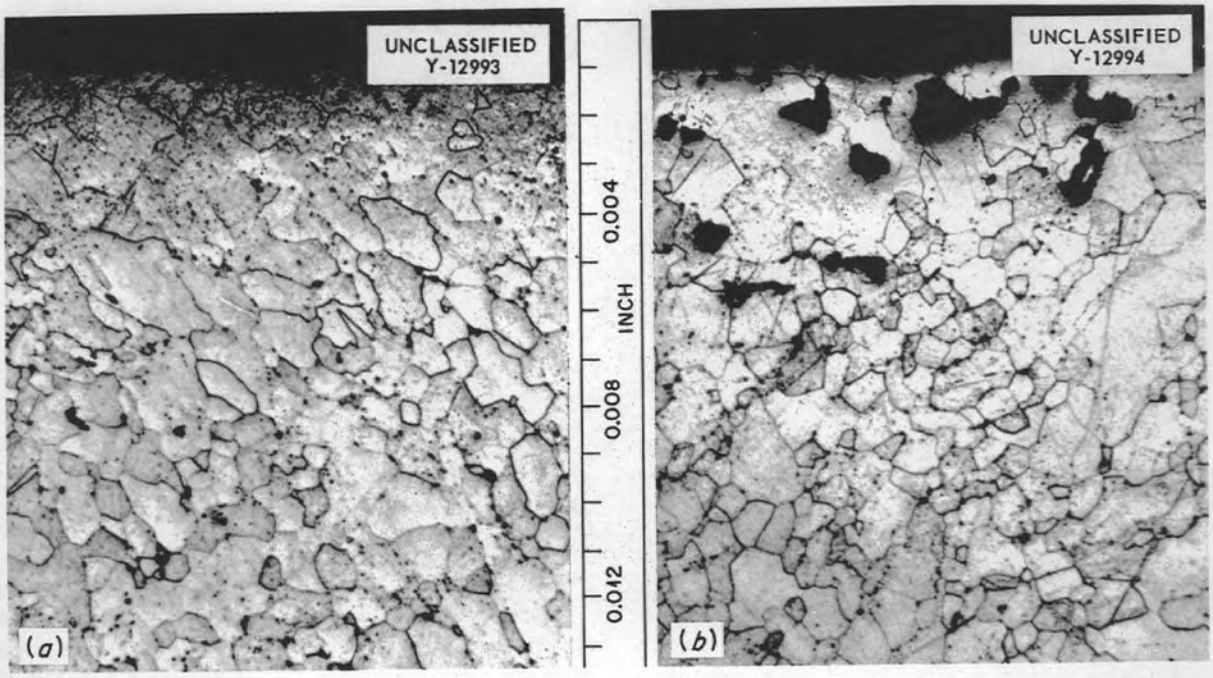

Fig. 106. Whirligig Test, 300 hr, 1300°F. (*a*) Surface of beryllium specimen exposed to flowing sodium. (*b*) Surface of beryllium specimen exposed to relatively stagnant sodium in the annular space between the specimen and the Inconel sleeve. Etchant: oxalic acid. 250X.

TABLE 38. BRAZING ALLOYS FOR HIGH-CONDUCTIVITY FINS

Alloy	Composition (wt %)	Brazing Temperature (°F)
Low-melting Nicrobraz	80 Ni–6 Fe–5 Cr–5 Si–3 B–1 C	1920
Coast Metals 52	89 Ni–5 Si–4 B–2 Fe	1840
Electroless nickel	88 Ni–12 P	1800
Ni-P-Cr	80 Ni–10 P–10 Cr	1800

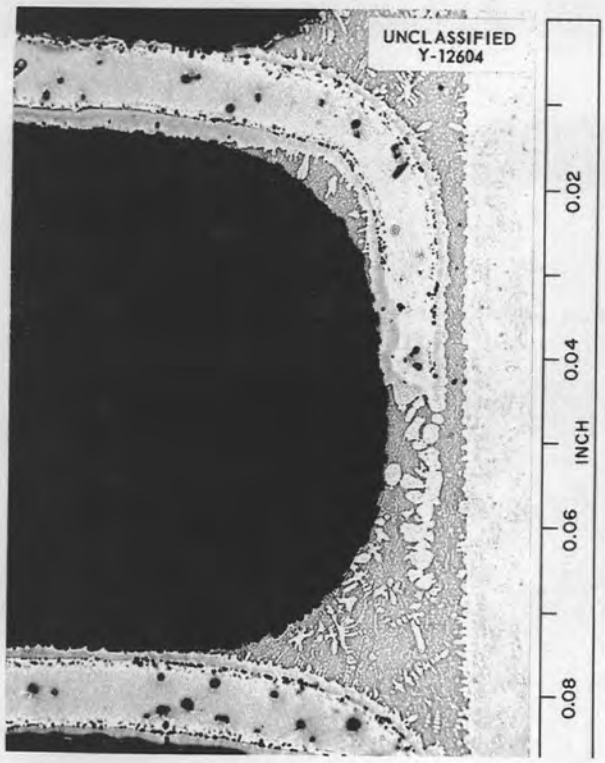

Fig. 107. Inconel-Clad Copper Fin Brazed to Inconel Tube with 88% Ni–12% P Alloy and Exposed to Static Air at 1500°F for 600 hr. Fins in horizontal plane at left; tube wall shown in vertical plane at right.

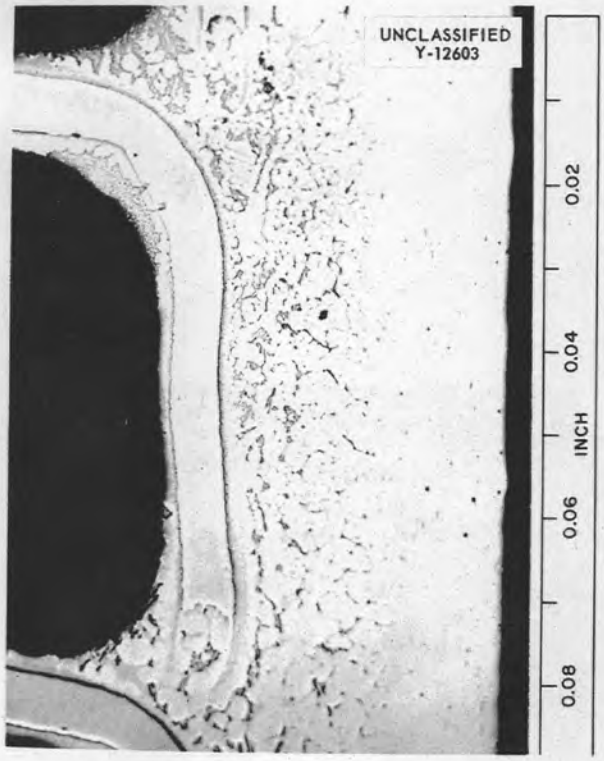

Fig. 108. Type 310 Stainless-Steel-Clad Copper Fins Brazed to Inconel Tubing with 88% Ni–12% P Alloy, as Brazed. 50X. Reduced 12.5%.

complex eutectic resulting from the presence of an iron-base, rather than a nickel-base, cladding material. This was further evidenced by the behavior of the 88% Ni–12% P alloy with type 430 stainless-steel-clad copper. Figure 109 is a photomicrograph of such a joint in the as-brazed condition. It may be noted that the intergranular penetration has occurred completely through the tube wall. Although the effect of this penetration on the physical properties of the tubing has not been determined yet, it seems advisable to use other brazing alloys such as Coast Metals 52, which is an Ni-Si-B alloy.

Figures 110 and 111 are photomicrographs of type 310 stainless-steel-clad copper and type 430 stainless-steel-clad copper, respectively, brazed to Inconel tubing with Coast Metals 52 and exposed for 400 hr to static air at 1500°F. It may

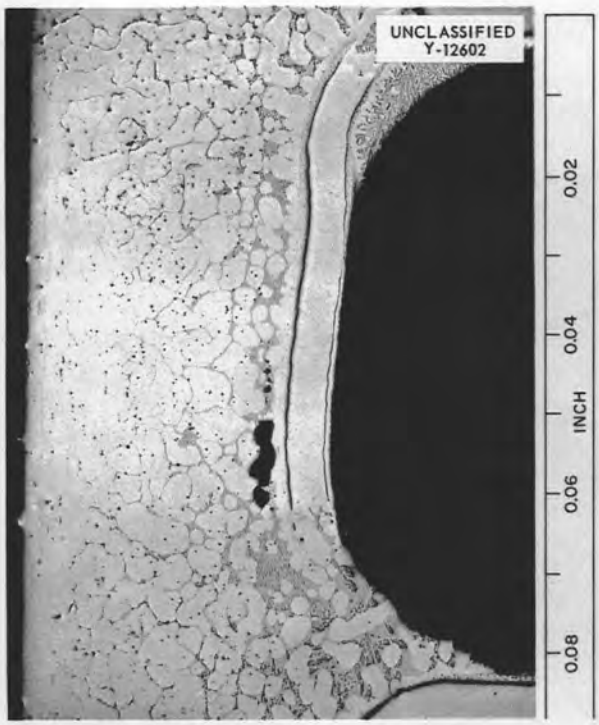

Fig. 109. Type 430 Stainless-Steel-Clad Copper Fins Brazed to Inconel Tubing with 88% Ni–12% P Alloy, as Brazed. 50X. Reduced 16%.

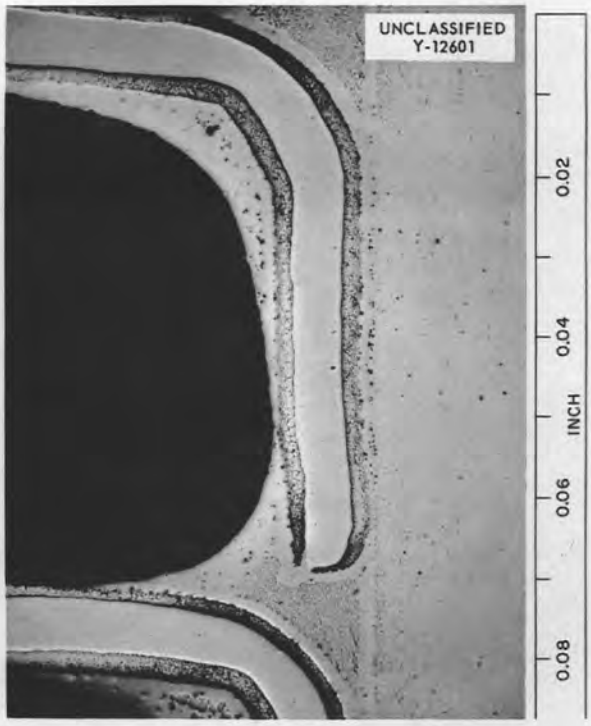

Fig. 110. Type 310 Stainless-Steel-Clad Copper Brazed with Coast Metals No. 52 Alloy and Exposed to Static Air at 1500°F for 400 hr, as Polished. 50X. Reduced 15%.

be observed that a negligible amount of dilution and a minor amount of boron diffusion into the Inconel have occurred.

Although low-melting Nicrobraz has been used successfully to braze all these clad materials to Inconel, its flow point (1050°C) is dangerously close to the melting point of copper (1083°C). Since the oxidation resistance and the boron effect of the Coast Metals 52 alloy are comparable with those properties of low-melting Nicrobraz, the Coast Metals 52 alloy was selected for the fabrication of the first high-conductivity radiator.

The problem of edge protection of the clad copper fins can be most easily resolved by adding aluminum to the copper, thereby improving its resistance to oxidation. The edges of fins can be dip-coated with aluminum, sprayed with aluminum metal, or painted with aluminum powder in a slurry of Nicrobraz cement. Specimens prepared accordingly and heated at 800°C for approximately ½ hr to accomplish diffusion exhibit excellent resistance to oxidation when subsequently exposed for 500 hr to static air at 1500°F. It appears that bronzing, which continues during oxidation testing, occurs to a depth of about $\frac{3}{32}$ to ⅛ in. in 500 hr. Batch treatment of numerous fins will be the subject of future work, the results of which will determine the feasibility of preparing large numbers of fins for radiator fabrication.

Inconel-Clad Copper High-Conductivity Fin Radiator. A radiator assembly was fabricated by furnace-brazing Inconel-clad copper high-conductivity fins to a tube assembly with Coast Metals 52 brazing alloy. Each radiator contained 3 in. (16 fins per inch) of fins, 12 in. long by 3¼ in. wide. The 90 Inconel tubes (0.185-in. OD, 0.025-in. wall thickness) were welded to a $\frac{1}{16}$-in. header plate, and the fins were fitted on these tubes. (Welding was accomplished by the semiautomatic device described in the section on "Tube-to-Header Welding.") Coast Metals alloy 52, containing nickel, silicon, boron, and iron, was placed on the tube-to-fin joints (approximately 4300). The other Inconel header was then welded to the tubes, and all tube-to-header welds were backed-up with the brazing alloy. This assembly was then furnace-brazed in

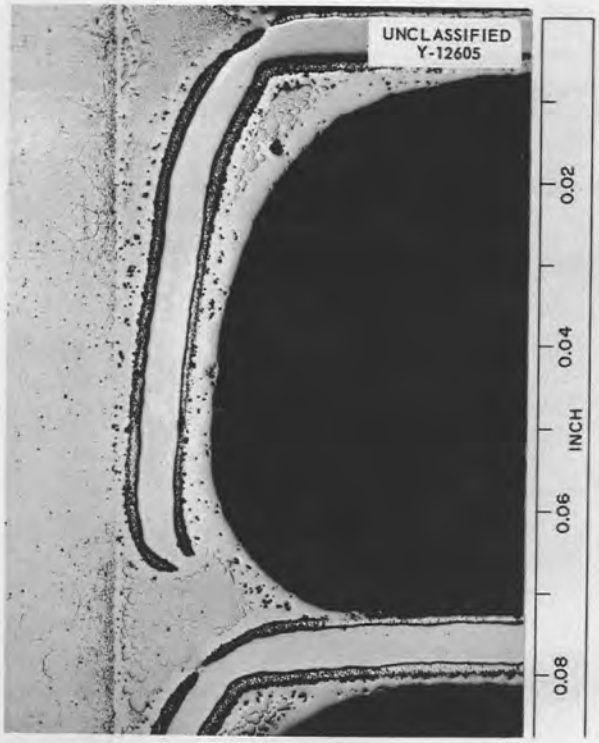

Fig. 111. Type 430 Stainless-Steel-Clad Copper Brazed with Coast Metals No. 52 Alloy and Exposed to Static Air at 1500°F for 400 hr.

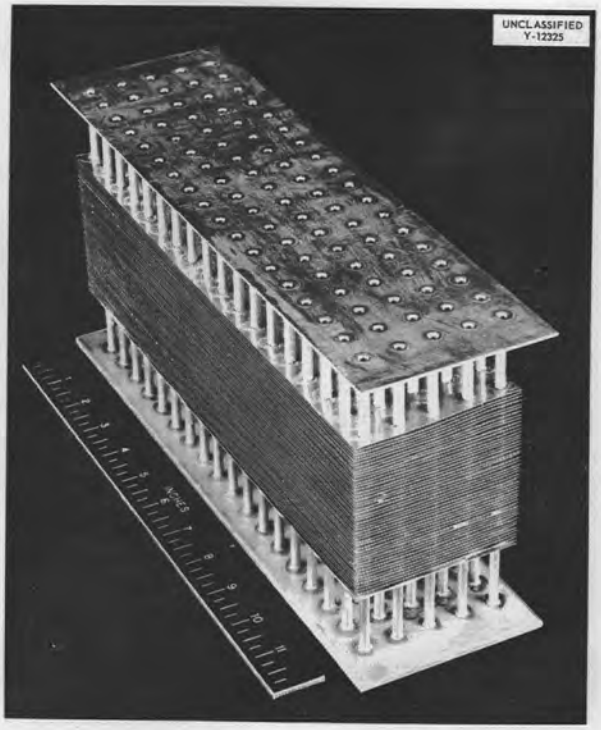

Fig. 112. Inconel-Clad Copper High-Conductivity Fin Radiator.

a hydrogen atmosphere. The completed radiator is shown in Fig. 112.

The brazing was accomplished by canning the radiator and inserting it in the Globar pit furnace recently installed in the Welding Laboratory. The thermal cycle employed preheating at 825°C to permit an equalization of temperatures over the assembly. This prevents the selective flowing of brazing alloy to the fins (which normally attain temperature quickest), which would leave the tube-to-fin joints unbrazed. This preheat temperature was below the sintering temperature; thus the boron diffusion from the brazing alloy was minimized. Thermocouples placed on various parts of the assembly and connected to a multipoint recorder showed that the temperature was controlled at 1025 ± 2°C. This careful control of the temperature kept fin distortion to a minimum.

Type 430 Stainless-Steel-Clad Copper High-Conductivity Fin Radiator. A sodium-to-air radiator containing 6 in. of type 430 stainless-steel-clad copper high-conductivity fins was fabricated by using a combination Heliarc-welding and brazing procedure. The tube-to-fin section was assembled and brazed with Coast Metals 52 (Ni-Si-B-Fe) alloy at 1020°C. The split headers were then assembled and Heliarc-welded by using the semiautomatic equipment available in the Welding Laboratory. A photograph of the radiator and welding torch after the welding of the 108 tube-to-header joints is shown in Fig. 113.

The remaining header sections were then manually Heliarc-welded with complete penetration. Although a pressure test indicated that six tube-to-header joints were not leaktight, it was decided that the back-brazing operation would satisfactorily seal these leaks and remove the effects of the notches as sources of stress concentrations. The completed unit, as shown in Fig. 114, was helium leaktight after the rebrazing operation and will now be used in conjunction with the 100-kw gas-fired liquid-metal heater system.

Tube-to-Header Welding. A semiautomatic process for the Heliarc welding of tube-to-header joints has been developed and used to fabricate the heat exchanger shown in Fig. 112. In this process, a commercially available Heliarc torch is rotated

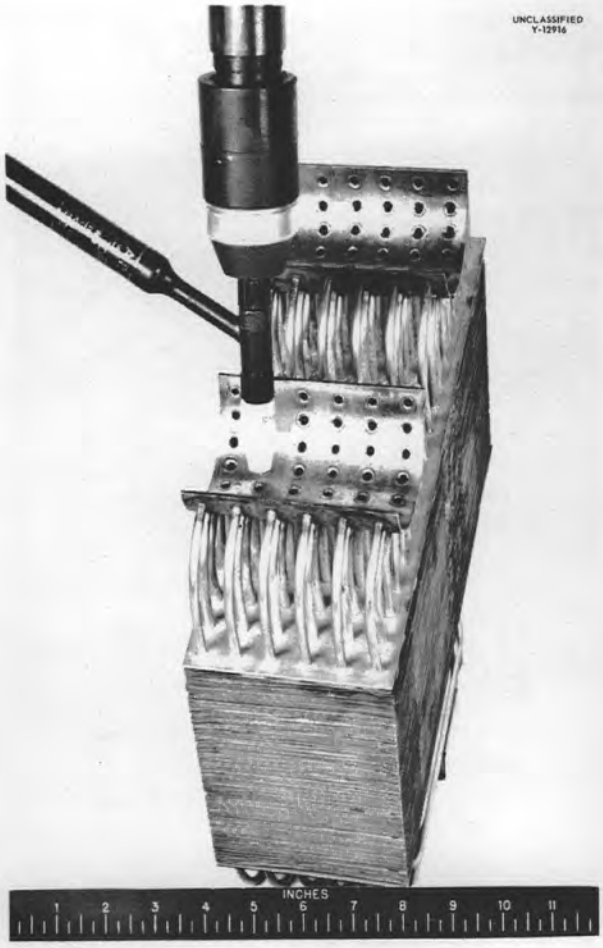

Fig. 113. Type 430 Stainless-Steel-Clad Copper High-Conductivity Fin Radiator and Welding Torch After Welding Tube-to-Header Joints.

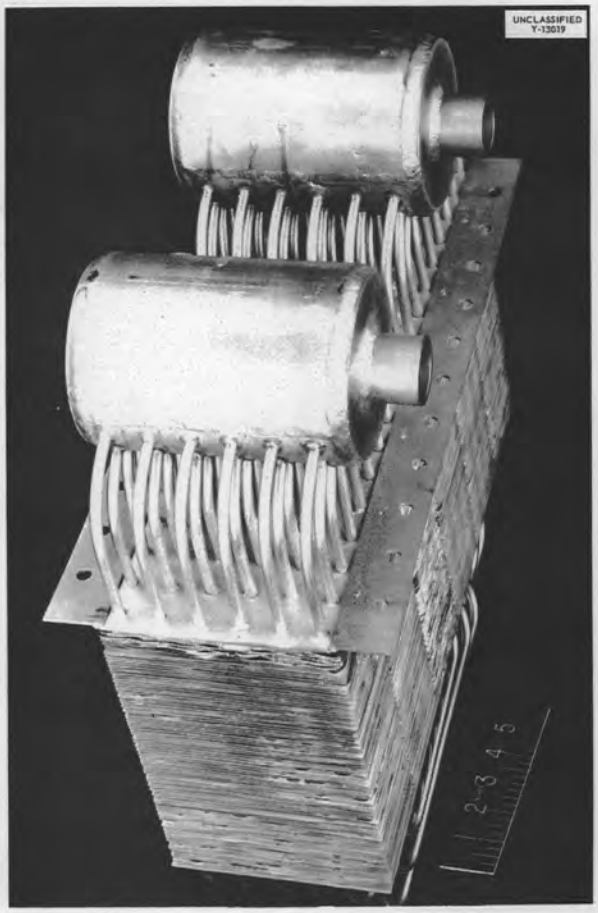

Fig. 114. Completed Type 430 Stainless-Steel-Clad Copper-Fin High-Conductivity Sodium-to-Air Radiator.

around the tube periphery by a variable-speed motor-driven offset-cam mechanism which can be adjusted to any desired diameter of swing. A photograph of this equipment is shown in Fig. 115.

Preliminary experiments, consisting of welding typical tube-to-header samples, were made to investigate the effects of arc current and welding speed upon weld size, hole constriction, and weld penetration. It was shown in these tests that welds comparable to those produced manually by a skilled operator[3] could be made semiautomatically. For example, satisfactory welds, having a penetration of at least one tube-wall thickness, could be made at a weld time of 7 sec over a welding-current range from 40 to 50 amp. The hole constriction resulting from welds made over this current range did not exceed 5%.

[3]P. Patriarca, G. M. Slaughter, and J. M. Cisar, *ANP Quar. Prog. Rep. Dec. 10, 1953*, ORNL-1649, p 86, Fig. 7.3.

Examination of Intermediate Heat Exchanger

The fluoride-to-sodium intermediate heat exchanger, which failed after 1680 hr of cycling between temperatures of 1080 and 1500°F, was submitted to the Metallography Section of the Metallurgy Division for metallographic examination and an evaluation of the probable mechanism of failure.

Tube-to-header joints of this heat exchanger were Heliarc-welded manually and were helium leaktight before assembly into the test rig. The unit was then put in service and operated until it failed. Visual examination indicated the presence of 19 fissures in the tube-to-header welds of a set of paired headers. The locations of the fissures

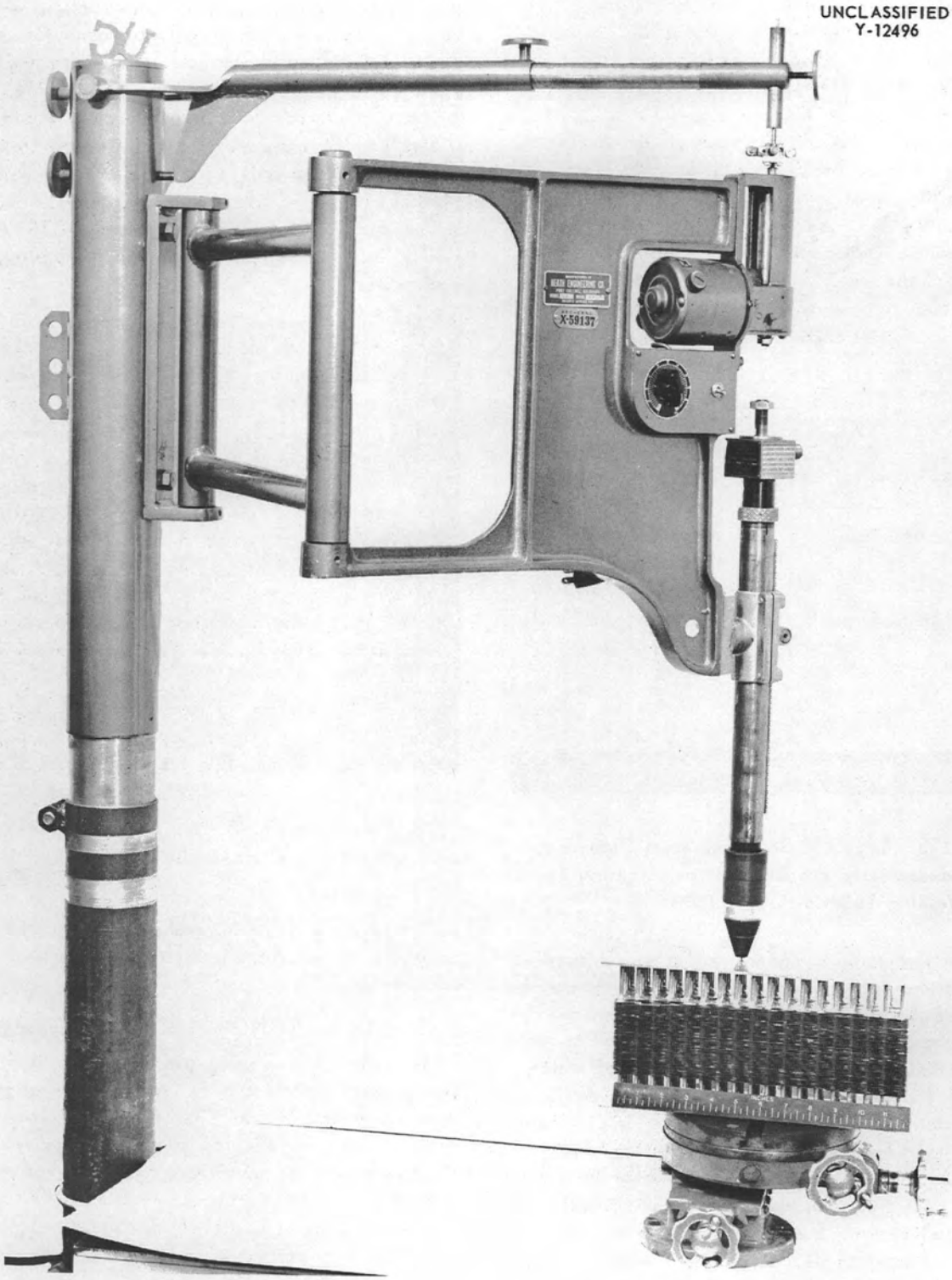

Fig. 115. Semiautomatic Heliarc-Welding Machine in Position for Tube-to-Header Welding on Radiator.

are shown in Fig 116 a schematic sketch of the top and bottom sections of the hot side A photo macrograph of the area marked in the schematic sketch is shown in Fig 117 Longitudinal views of tube to header joints are shown in Fig 118 which presents photomicrographs of an as welded tube and of three tubes after the service test It is apparent that a small fissure could be present in the as welded tube at the root of the tube to header weld Due to the stress concentrations at the root of the weld a crack would tend to propa gate through the weld under the influence of ex pansion and contraction of the tubes while they are in service

The investigation, as conducted to date em phasizes the extreme desirability of using back brazing as a means of minimizing the notch effect and of reducing the possibility of leaks developing in the system Corrosion tests in static sodium and fluorides by the General Corrosion Group in dicate that a 67% Ni–13% Ge–11% Cr–6% Si–2% Fe–1% Mn alloy may be useful for this appli cation This alloy which flows well at 2050°F, was found to be virtually unattacked in the fluoride fuel and corroded to a maximum of 0 004 in in 100 hr at 1500°F in sodium (see the section Corrosion)

Fabrication

Nozzles for the Gas Fired Liquid Metal Heater One of the design features of the 100 kw gas fired liquid metal heater now under construction is the packed rod nozzle assembly to be used for inlet control of the air and gas flow Test data and the theoretical considerations indicated that ⅛ in dia stainless steel rods triangularly packed would be satisfactory for this use Because furnace brazing should join these rods in a rigid bundle with a minimum of plugged interstices, the ductile oxida tion resistant high temperature alloy 82% Au–18% Ni was chosen for use in the fabrication of the nozzles

Proper jigging was extremely important in the fabrication of these nozzles Each layer of rods was tack welded for rigidity and each layer was then tack welded to form the assembly Since the amount of brazing alloy required was difficult to estimate an excess of material was used to ensure good bonding at all capillary joints The excess material was then removed from the nozzle inter stices by placing a flat nozzle cross section against a metal sheet on which many fine lines had been scribed Upon rebrazing these fine scratches acted as capillaries and the excess material was removed A completed air nozzle blank is shown in Fig 119

Another requirement of the natural gas nozzle design was that a regular pattern of interstices should be selectively closed This was accomp lished by inserting wires into predetermined holes and brazing these to the rods

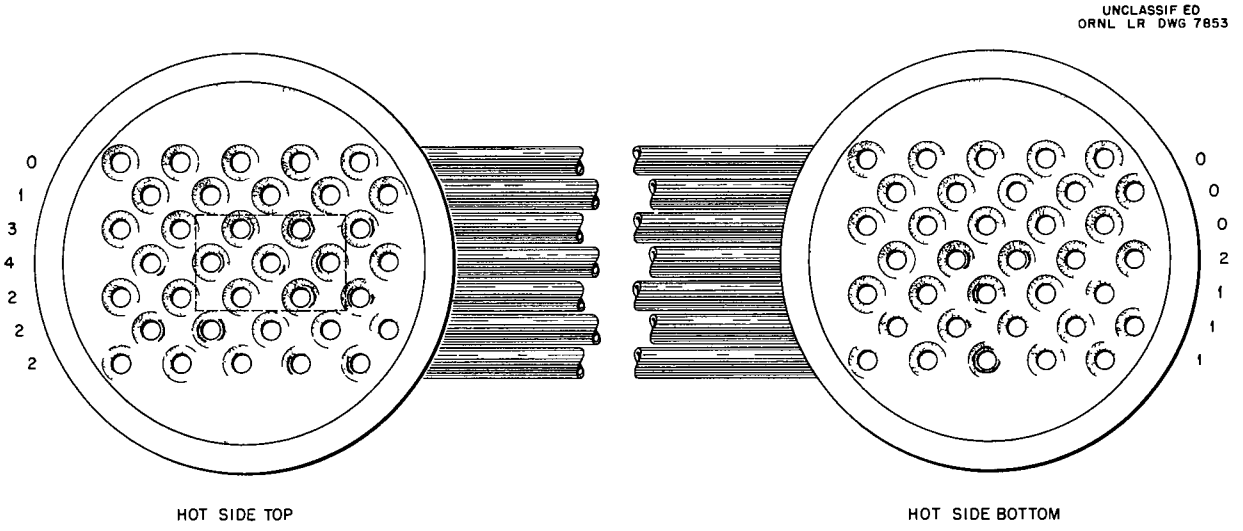

Fig 116 Schematic Sketch of Intermediate Heat Exchanger Showing Number and Locations of Fissures in Each Header

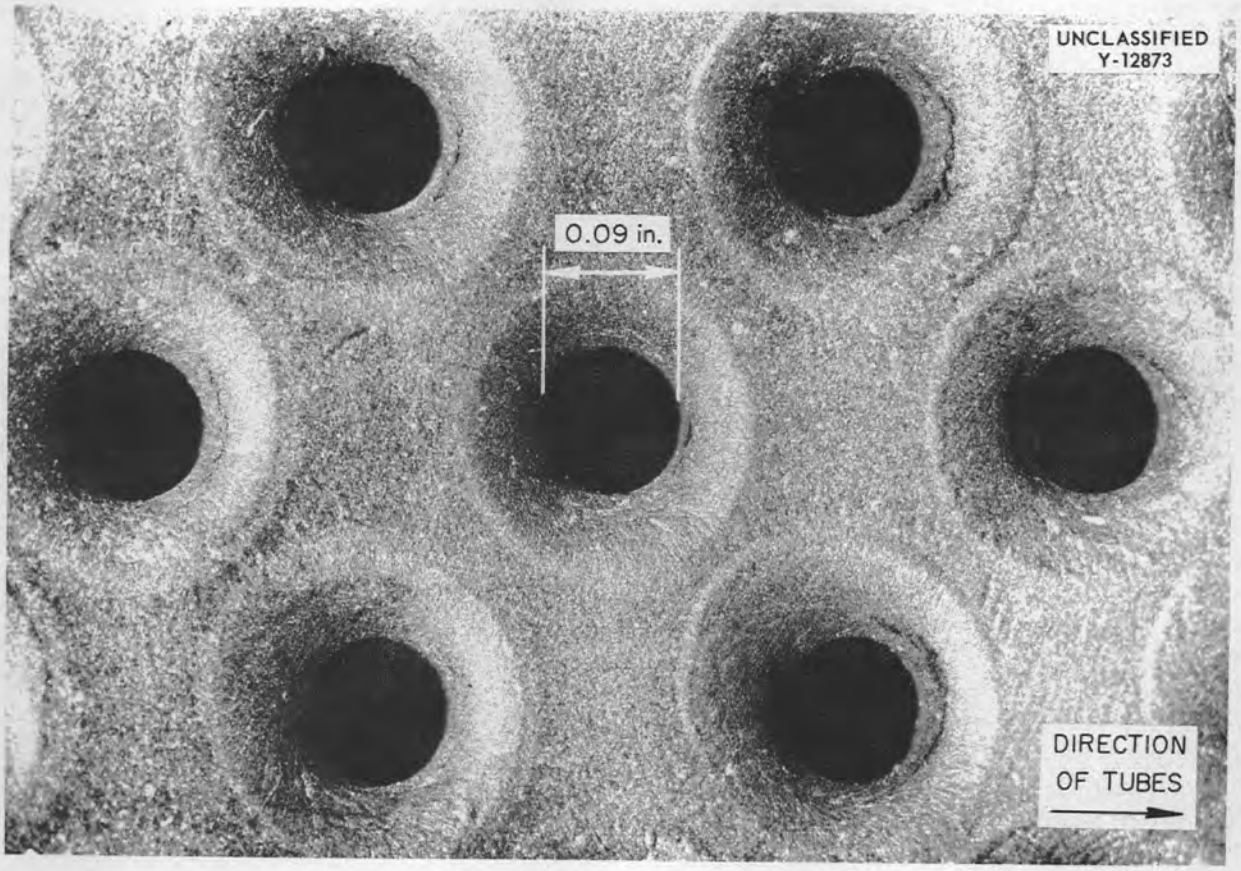

Fig. 117. Hot-Side Top Header as Shown in Dotted Lines of Fig. 116.

Approximately 20 nozzles have been completed, which satisfies the requirements for this liquid-metal heater unit.

Welded ARE Pump Impeller. Attempts by outside vendors to fabricate cast Inconel ARE pump impellers have been unsuccessful, the chief difficulties being the lack of fluidity of Inconel at pouring temperatures and the complexity of the blade design of the impeller. Hence a program was initiated at ORNL to fabricate such impellers by machining and welding. The program has resulted in the fabrication of impellers which have been exposed to, and passed, the necessary rigid tests prior to insertion in the ARE system.

The rough-machined parts of the impeller as received in the Welding Laboratory are shown in Fig. 120. These parts were subjected to a slow heat treatment for stress relief and to enable maintenance of precise dimensional tolerances. The thermal cycle involved heating at 125°C per hour to a temperature of 1000°C, maintaining this temperature for ½ hr, and cooling at 125°C per hour to room temperature.

The back flange was then tack-welded to a carbon steel strongback, to prevent warping during welding, and the vanes were Heliarc-welded in place. This operation is shown completed in Fig. 121. The assembly was then heat-treated in the same manner as before.

The vanes were then finish-machined; the front flange was Heliarc plug-welded in position, and the joint between the flange and the vanes was Heliarc-welded as far as accessible, as shown in Fig. 122. The assembly was then given another heat treatment as described above.

The welded impeller was then removed from the strongback and finish-machined; the completed assembly is shown in Fig. 123.

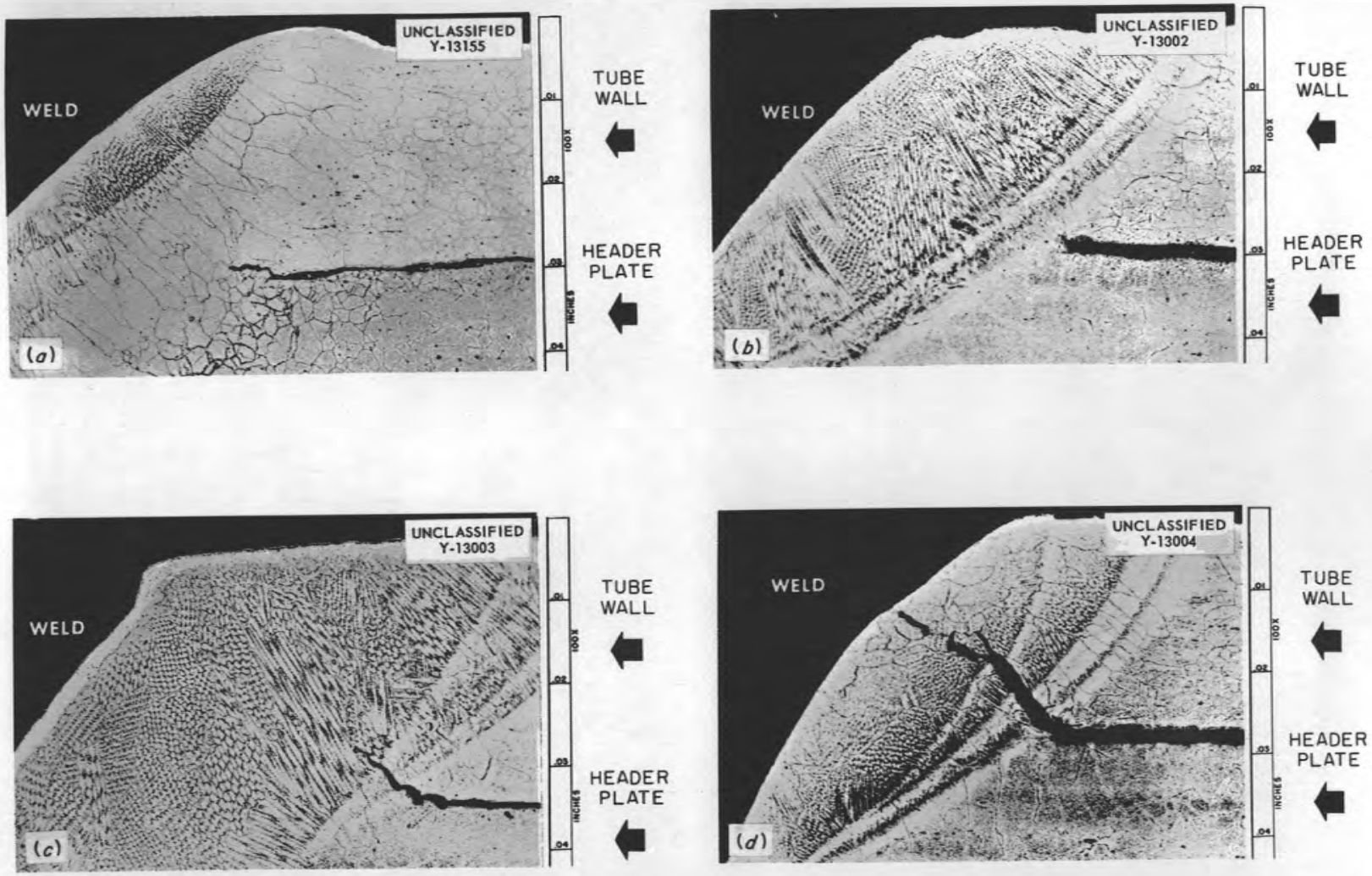

Fig. 118. Fissures in Heliarc Tube-to-Header Joints Exposed to Sodium and Fused Salts. (*a*) As welded. (*b*) Tube-to-header joint with no crack extending into the weld (after 2000 hr at 1350°F). (*c*) Tube-to-header joint with slight crack propagating into the weld (after 2000 hr at 1350°F). (*d*) Tube-to-header joint showing severe cracking (after 2000 hr at 1350°F); the fissures probably extend to the surface of the weld, with the resultant formation of a leak in the system.

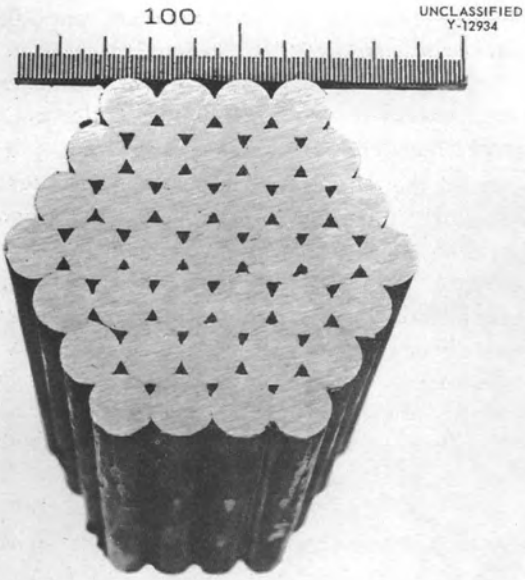

Fig. 119. Typical Brazed Air-Nozzle Blank. Note that bonding occurs only at the points of tangency of the stainless steel rods.

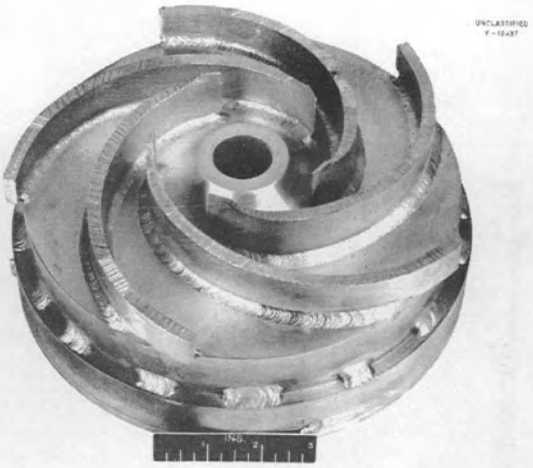

Fig. 121. Impeller Vanes Were Heliarc-Welded to Drive-Shaft Hub. Impeller is tack-welded to carbon-steel strongback.

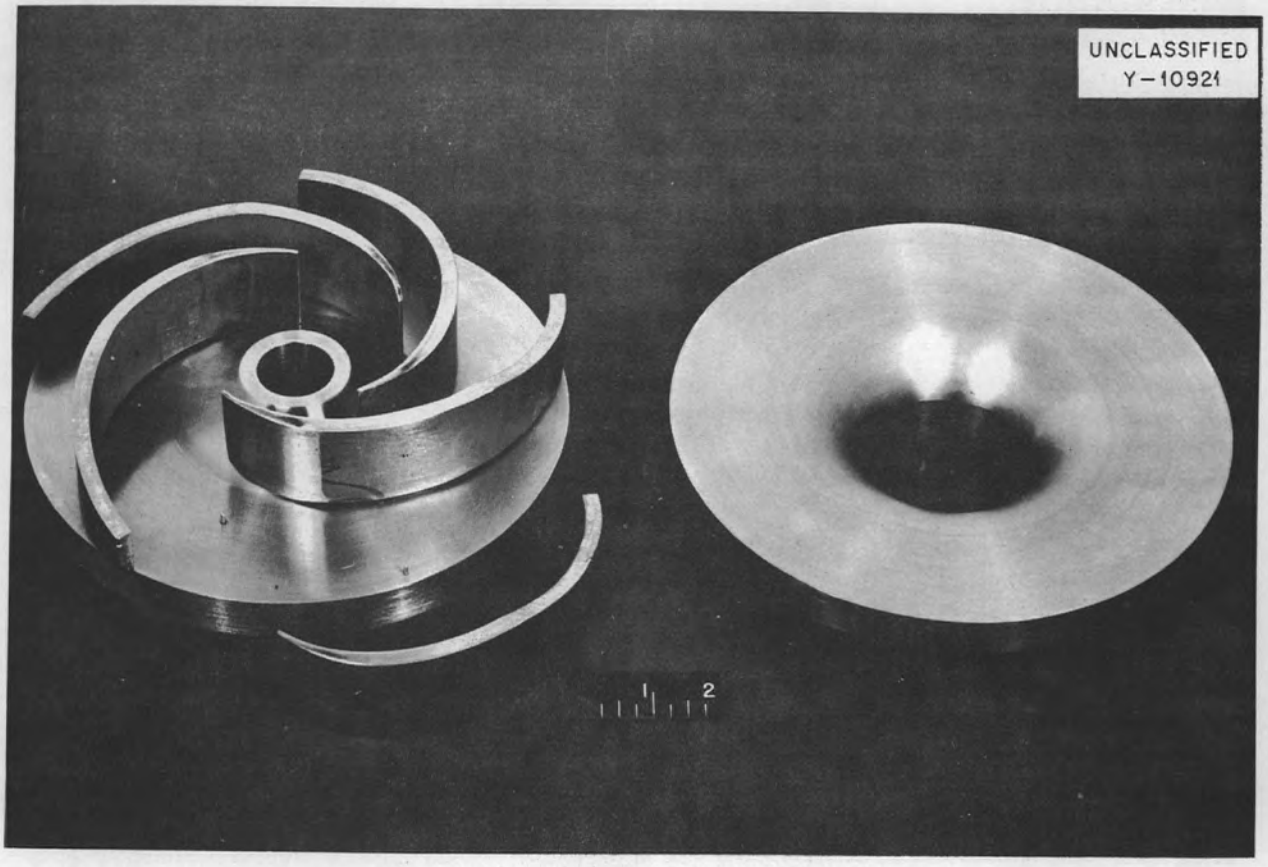

Fig. 120. Rough-Machined Parts of Inconel ARE Pump Impeller As Received.

Fig. 122. Impeller with Fluid-Entrance Hub Plug-Welded in Position.

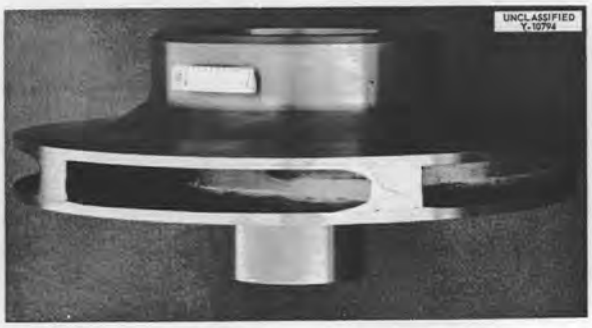

Fig. 123. Completed All-Welded ARE Pump Impeller.

MECHANICAL PROPERTIES

R. B. Oliver J. H. DeVan
D. A. Douglas J. W. Woods

During the past six months, considerable effort has been devoted to the study of stress-rupture properties of end-capped tubes and pipes, stressed with internal pressure. The purpose of this program is to duplicate many of the stress patterns inherent in circulating-fuel reactors, particularly in areas such as the heat exchanger and pressure shell. An initial series of tests was conducted on 0.5-in.-dia Inconel tubing having a wall thickness reduced to 0.010 in. along a 2-in. gage length. The tubing contained fused salt, and an argon atmosphere was maintained over the salt and surrounding the specimen. The rupture life exhibited in all these tests was much shorter than that observed in comparable tests on 0.060-in. sheet specimens stressed in tension.

Metallographic examination of the tubular specimens revealed that relatively little corrosive attack had occurred during the test. It was believed that the attack was slight as a result of the small volume of salt present as compared to the large surface area of the specimen. If, as is currently proposed, static corrosion of Inconel occurs through the reduction, by chromium, of metal fluorides such as iron and nickel, a large volume-to-surface-area ratio must be provided in order for corrosive attack to be pronounced.

Subsequent tube-burst tests were conducted with the specimen surrounded by the fused salt, thereby permitting a volume-to-surface-area ratio of 8 to 1. Figures 124*a* and *b* show the significant difference in corrosive attack that was noted under these two conditions. Tests under the more severe conditions show a decrease in rupture life of from 45 to 80%, as compared with the times to failure found in the first series of tests with salt contained internally.

A larger diameter, thicker walled pipe is currently being tested with fluorides outside and argon or sodium inside. As would be expected, since the attacked portion of the specimen represents a smaller fraction of the stressed cross section, rupture life for the heavier pipe appears to be considerably improved. The time to rupture vs stress for each series of tests is shown in Fig. 125.

The size effect or geometry of structural members, as related to mechanical strength at high temperatures, is also being investigated. If time to rupture is taken to be the strength criterion, rather than time to a specific strain, an observation of crack propagation indicates that thick plates or round bars would have longer lives than similar material in thinner gages for the same stress. Larger cross sections should be less affected than thinner gaged materials. Accordingly, three Inconel specimens were tested: a round bar with a 0.2-in. cross-sectional area, a square bar with a 0.2-in. cross-sectional area, and a round bar with a 0.048-in. cross-sectional area. The two largest bars, tested in argon at 3500 psi, ruptured in 5000 hr. The small bar, tested at the same stress, failed in 1400 hr – a lifetime comparable to that of sheet-type specimens having a nominal 0.03-in. area. Tests of the two largest bars in hydrogen indicated that

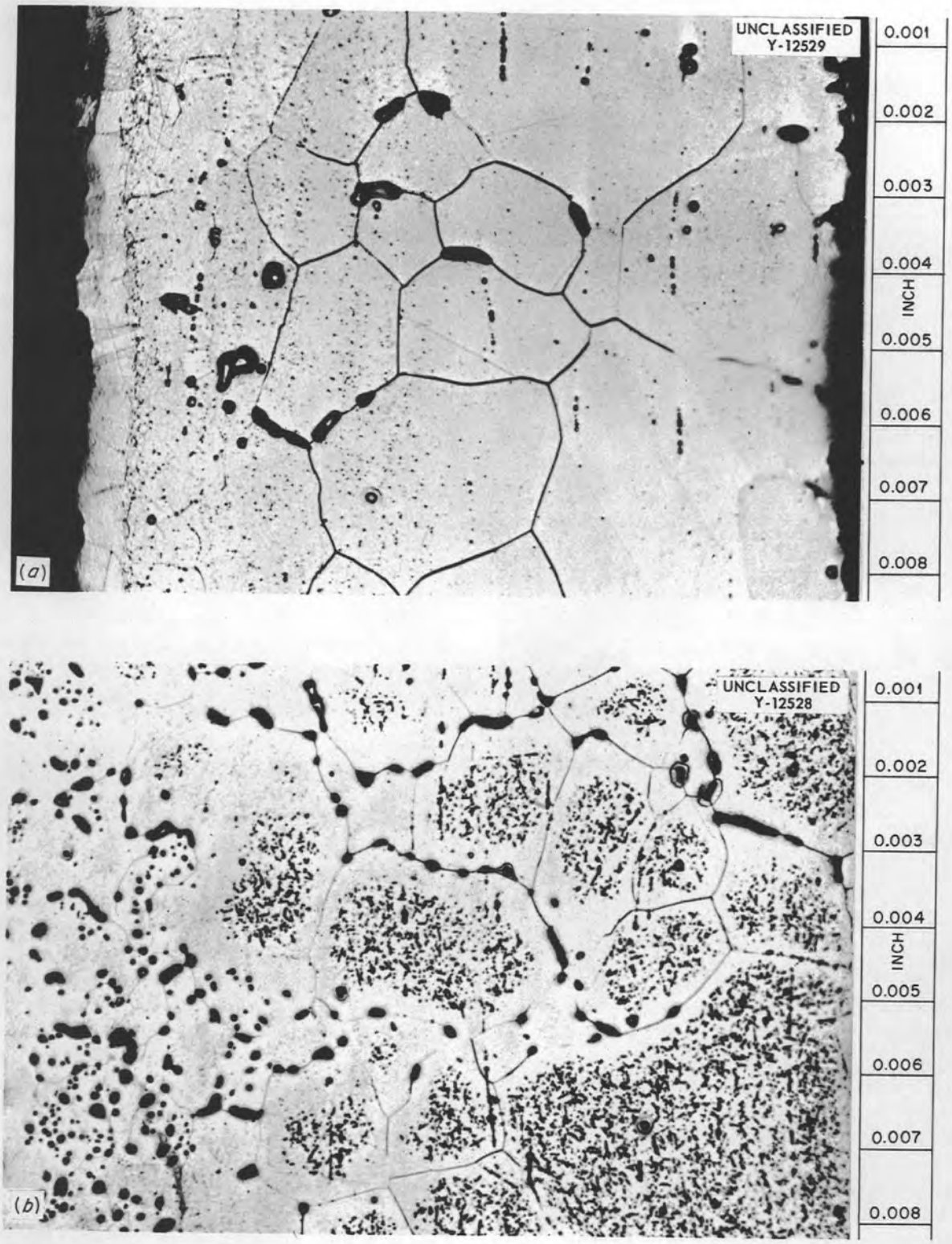

Fig. 124. Surface of Inconel Specimen Tested (*a*) with Fused Salts Surrounding the Tube and (*b*) in Contact with Fused Salts. Specimen (*b*) was tested with fused salts inside the tube and shows little evidence of attack as compared with specimen (*a*).

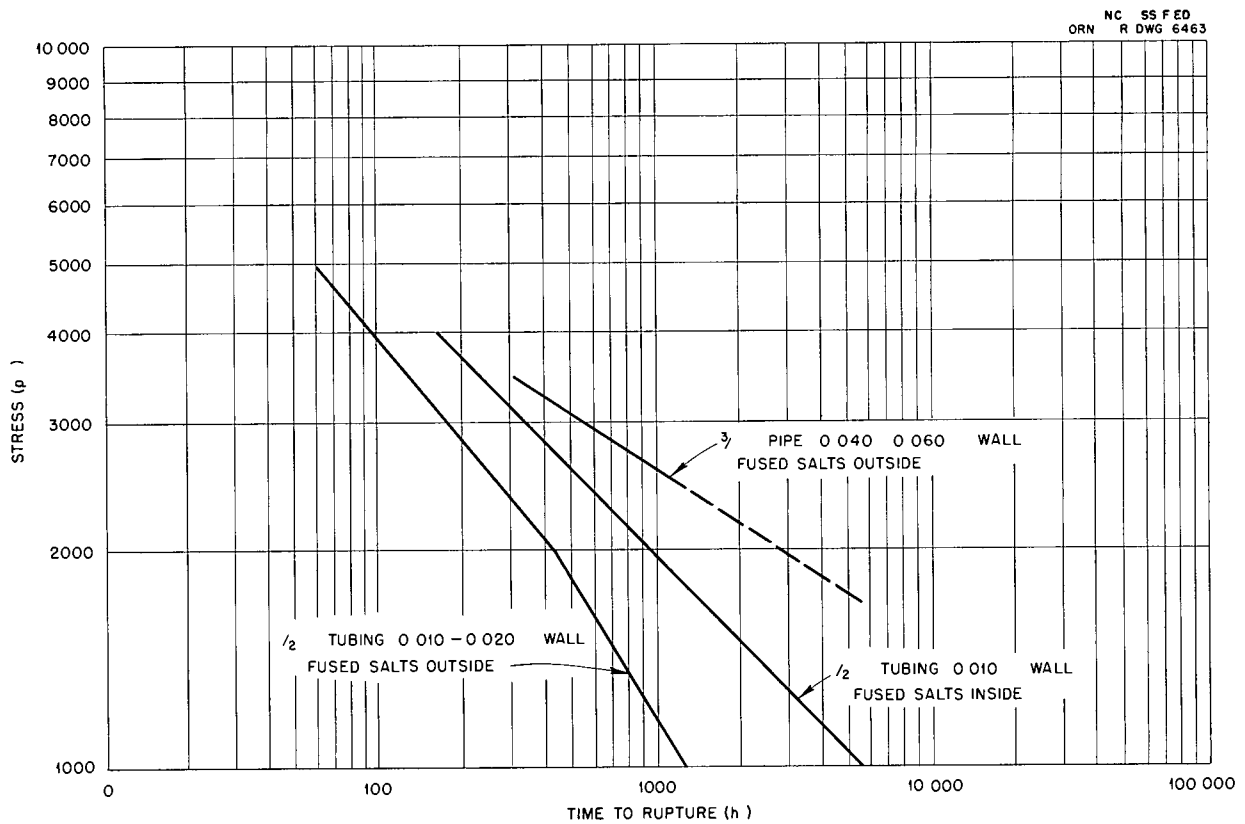

Fig 125 Stress Rupture Properties of Inconel from Tube Burst Tests at 1500°F

rupture life is decreased about 30% in this environment When the flat sheet type of specimen was tested in hydrogen it showed a 70% decrease in lifetime as compared with the value obtained when it was tested in argon Thus it would appear that in order to provide complete data to the design engineer a creep program should include not only the type of material the environment and the stress levels but also the particular geometry of the member in question

FABRICATION

J H Coobs H Inouye

ANP Radiator

The study of high thermal conductivity fin material and of its fabrication for heat exchangers was devoted to determining the strength of clad copper composites at 1500°F In addition some thermal conductivity data of a 6% Al–94% Cu alloy were obtained

Stress rupture and creep properties of type 310 stainless steel clad copper 0 008 in thick were determined at 1500°F at stresses between 500 and 2000 psi The material was obtained from the General Plate Div of Metals & Controls Corp and had an average clad thickness of 0 00187 in per side The maximum clad thickness was 0 0023 in per side

The results of the several tests show that some alteration of the copper occurs even though the specimen does not fracture This alteration was indicated by the brittleness of a normally ductile composite For long time exposures (1000 hr) stresses greater than 500 psi and less than 1000 psi are tolerable without any indication of brittleness in the core or oxidation due to cladding failure In all the tests in which the specimens ruptured oxidation of the copper at the point of fracture was complete and the copper which did not appear to be oxidized was brittle It was also noted that when the strain in 2½ in was 10% the copper remained ductile while strains of 20%

(regardless of exposure time) produced brittleness

The data obtained on this material are listed in Table 39

Thermal conductivity measurements of a 6% Al–94% Cu alloy were made on 0 100 in rod between 212 and 1562°F The thermal properties of an 8% Al–92% Cu alloy were also determined up to 392°F The values reported by the Solid State Division compare favorably with the data of Smith and Palmer [4] who made measurements up to 392°F The reported values more than exceeded the extrapolated values of the cited authors and the estimated value of six times that of stainless steel at 1500°F

The values of the thermal conductivity listed in Table 40 were not corrected for the volume expansion of the alloy with temperature and are considered to be accurate within ±5%

Although extensive diffusion occurs between the above alloys and copper additional increases in the thermal conductivity can be accomplished by cladding copper with these alloys The composition gradient existing in a diffused composite results in an increase in the conductivity of the clad material (due to the inward diffusion of aluminum) and a decrease in the conductivity of the copper core

[4] C S Smith and E W Palmer *Am Inst Mining Met Engrs Tech Publs* 2 No 6 Technical Paper 648 1–21 (1935)

Sigma Phase Alloys

Additional tubing was made for use in continuing the study of sigma phase alloy corrosion by liquid lead Two ingots of 48 2% Cr–51 8% Fe and two ingots of 45% Fe–40% Cr–15% Ni were vacuum cast into 1½ in -dia ingots 6 in long These alloys were hot-rolled in air atmosphere at 1250°C to rod ⅝ in in diameter After annealing at 1100°C for 2 hr and quenching the rod was easily machined into tubing

The transformation of the ferrite to sigma will be accomplished by aging at 1425°F Two of the

TABLE 40 THERMAL CONDUCTIVITY OF ALUMINUM BRONZES
[cal/cm² sec (°C/cm)]

Temperature (°F)	6 2% Al–93 8% Cu	8 4% Al–91 6% Cu
212	0 178	0 176
302	0 240	0 210
392	0 280	0 250
1156	0 55	
1562	0 77	

TABLE 39 STRESS RUPTURE PROPERTIES OF TYPE 310 STAINLESS STEEL CLAD COPPER AT 1500°F
(0 002 n Clad on Each S de of 0 004 n Coppe)

Stress (psi)	Rupture Time (hr)	Elongation in 2½ in (%)	Remark
2000	96	39	Copper embrittled
1800	336	50	Copper embrittled
1650	528	40	Copper embrittled
1500	887		Copper embrittled
1400	1220		In progress
1000	1000	27½	Test terminated in 1000 hr oxidized throughout
1000	500	20	Test terminated in 500 hr oxide stringers on surface
500	1000	10	No indicated failure
500	500	5	No indicated failure

tubes (Fe Cr) were cold swaged 12% to determine the effect on the distribution of sigma

Duplex Tubing

This phase of development work was directed toward the fabrication of duplex seamless tubing in order to arrive at alloy composites possessing unique properties such as good corrosion resistance on the inside of the tubing and good oxidation resistance on the outside

The first approach to this problem consisted in attempts to deep draw duplex blanks 4 in in diameter The blanks were made by hot pressing and also by hot rolling The following combinations were made by hot pressing under an argon atmosphere in Al_2O_3 coated graphite dies at 1500 psi

Combination	Temperature (°C)
0 025 in copper plus 0 025 in type 310 stainless steel	1000
0 025 in Inconel plus 0 025 in type 310 stainless steel	1200
0 025 in Inconel plus 0 025 in Hastelloy B	1200
0 025 in Hastelloy B plus 0 025 in type 310 stainless steel	1200

Copper was also clad on one side with type 310 stainless steel by hot rolling at 1000°C a three ply composite with copper in the center and cover plates of Inconel was used One of the cover plates was oxidized at 1100°C for 2 hr to prevent bonding during rolling

Included in these experiments were some tests involving the fabrication of single clad molybdenum with Inconel The purposes of these tests were to determine (1) the conditions necessary to obtain a metallurgical bond by hot rolling (2) the extent of directional properties due to the molybdenum and (3) the ability of such a combination to be deep drawn

The first rolling experiments were made on an evacuated capsule at 1225°C with reductions of 10% per pass The total reduction was 79% in thickness No bonding was obtained when nickel was used as an intermediate layer between the Inconel and the molybdenum

In a second series of experiments the rolling temperature was reduced to 1000°C with reductions of 40% per pass and a total reduction of 85% in thickness The lower rolling temperature reduces the tendency for intermetallic compounds to form at the interface Bonding was achieved with nickel again used as an intermediate layer and evidences of intermetallic compounds were apparent only at high magnifications The final thickness of the composite was 0 010 in of molybdenum on 0 040 in of Inconel

All the above combinations were successfully reduced from 4 in blanks to 2½ in cups by the Guerin forming process (male parts of die are hard rubber) at room temperature

Future experiments will be devoted to determining the maximum molybdenum to-Inconel ratio that does not exhibit the directional properties of wrought molybdenum and to the continuation of deep drawing experiments

Thermal Convection Loop Fabrication

Two molybdenum loops clad with stainless steel were assembled with threaded molybdenum joints and then subsequently protected from oxidation by welded cover plates Both loops failed early in a corrosion test as a result of leakage of the fluoride and fracture in the cover plates It is believed that overheating of the cover plate occurred because the loops were initially heated by electrical resistance Because no metallurgical bond existed between the molybdenum and the clad separation became more pronounced with increased temperature and finally all the current was being carried by the rather thin cover plates

Future molybdenum loops will be made from arc melted molybdenum so that they will be weldable and the heavy nickel electrodes will be welded directly to the molybdenum tube instead of to the cladding

Columbium clad with type 310 stainless steel has been Heliarc welded in air into a loop Tests on this loop are awaiting further machining of accessory parts

Eight thermal convection loops of Inconel type alloys were fabricated with ordinary precautions being taken No unusual welding behavior was noted The composition and the room temperature properties are listed in Table 41 The fabrication of these alloys was described in previous reports

TABLE 41 PROPERTIES OF HIGH PURITY INCONEL TYPE ALLOYS*

Heat No	Nominal Composition (wt %)	Tensile Strength (psi)	Yield Point (psi)	Elongations (%)
14	18 Cr–7 Fe–75 Ni	85 000	41 500	49
15	10 Cr–15 Fe–75 Ni	77 700	38 800	44
16	5 Cr–20 Fe–75 Ni	72 700	34 200	47
17	10 Cr–7 Fe–83 Ni	76 000	36 000	44
18	5 Cr–10 Fe–75 Ni–10 Mo			

Data reported by the Superior Tube Co

Nickel Molybdenum Base Alloys

This investigation was undertaken to develop alloys having greater high temperature strength and better resistance to fluoride corrosion than Inconel These characteristics are found in Hastelloy B however some poor fabrication qualities and properties have been encountered or noted and are listed below

1 In castings and fusion welds a whole range of compositions result because of severe coring during freezing Consequently the alloy has varied properties from one area to another that is the microstructures are not in equilibrium even after long aging treatments The transformation due to aging results in great increases in hardness with corresponding decreases in ductility

2 At temperatures between 1200 and 1800°F the wrought material exhibits its poorest ductility as a result of hot shortness This arises from trace impurities or in this case probably from the precipitation of equilibrium phases Thus the alloy is being considered for use in the temperature range of poorest ductility

3 At temperatures above 1400°F Hastelloy B is not recommended for use in air because it oxidizes excessively A potential source of trouble is molybdenum the oxide of which has been reported to cause catastrophic oxidation of surrounding structures especially the steels

The solutions to these problems are being approached in two major ways First attempts will be made to find suitable melting methods and heat treatments for Hastelloy B which will reduce the degree of age hardening in both the casting and wrought materials so that they will possess acceptable properties in the temperature range of interest Second alloys which are a modified type of Hastelloy will be studied with regard to their suitability as substitutes for Hastelloy B Both phases of investigation will involve a study of the extrusion of seamless tubing since the present Hastelloy B tubing is made by welding strip

Aging studies of the following materials are in progress at temperatures between 1200 and 1700°F commercial wrought Hastelloy B plate vacuum melted as cast Hastelloy B cast and wrought 20% Mo–80% Ni and wrought 24% Mo–76% Ni

Some of the properties of the 20% Mo–80% Ni alloy were determined during this period This alloy appears to be easier to fabricate than Hastelloy B from an extrusion standpoint sound tubing could be made from the 20% Mo–80% Ni alloy but none was obtained from Hastelloy B Additional properties are listed below

1 The recrystallization temperature of 60% cold worked sheet is approximately 1900°F for an annealing time of 30 min

2 At 1500°F the alloy oxidizes in air at a faster rate than does Hastelloy B Under a temperature cycle between room temperature and 1500°F the rates are similar The oxide scale spalls near room temperature

3 Sheet 0 065 in can be Heliarc welded without causing porosity Argon arc welding produces porosity

4 Factors indicative of its high temperature strength (1500°F) are

Creep 90 hr rupture life at 8000 psi
Elongation 3% in 600 hr at 5000 psi
Tensile strength 40 000 psi 10% elongation

Oxidation and oxidation protection studies are in progress to find suitable methods for protection of thermal convection loops and creep test apparatus These studies will be the groundwork for further studies in the protection of reactor components

The coatings being studied are those that can be applied by the methods now available in the Metallurgy Division and are as follows chromium plate chromium plus nickel plate nickel plus aluminum spray and aluminum spray In constant temperature tests chromium plate is beneficial Aluminum sprayed specimens are being tested Chromium plus nickel combinations have not been evaluated

In oxidation tests involving cycling between room temperature and 1500°F these coatings aid in lessening the spalling of Hastelloy B The chromium plate and the chromium plus nickel combination afford the best protection These test specimens have now been heated for 350 hr

Boron Carbide Shield for CFRE

Experimental fabrication of the $\frac{1}{8}$ to $\frac{3}{16}$ in thick shield pieces has shown little improvement in the final boron density The maximum density obtained by warm pressing the B_4C Cu compositions at 450°C was 1 25 g of boron per cubic centimeter The required density is 1 5 g/cc Further use of this technique has been discontinued in favor of molding with nonmetallic binders Suggestions concerning the fabrication of suitable composites have been received through correspondence with Norton Company and The Carborundum Company These pieces would be fabricated by cold molding followed by sintering in order to develop suitable physical properties Suggested bonding materials suitable from nuclear considerations and stable at the expected service temperature include sodium silicate silica silicon and boron nitrides boric oxide and carbon Arrangements are being made to secure samples of these materials for compatibility tests with Inconel under operating conditions

The B_4C density in the proposed shield pieces would be about 1 9 g/cc or equivalent to a boron density of 1 5 g/cc The pieces would be molded in the form of equilateral triangles or diamond shapes 2 to 3 in on a side so as to cover the sphere with an integral number of pieces Edges would be overlapped by beveling to prevent leakage of neutrons on a radial path Since several thousand pieces will be required to cover the two spheres arrangements are being made to have the pieces fabricated by either the Norton Company or The Carborundum Company from B^{10} supplied by the Laboratory Any boron base bonding material would of course be made of the same special boron

In addition to the problem of fabricating a satisfactory shield the effects of boron diffusion must be studied Since the shield will be in contact with Inconel extensive diffusion of boron may occur

Previous compatibility experiments indicated only about 5 mils diffusion of boron from B_4C into Inconel at 1500°F after 100 hr Two supplementary tests have been completed and are awaiting examination A third test is being set up to compare the compatibility of boron and boron carbide with Inconel

Tubular Fuel Elements

Twenty tubular elements are being prepared for further drawing experiments at Superior Tube Co These are being assembled and high fired UO_2 of 30- to 55 μ particle size and fine granular UO_2 prepared by steam treatment of uranium turnings are being used The metallic core matrices being used include prealloyed stainless steel powders of two types and elemental stainless steel as well as iron and nickel

Plans are also being made to try to hot swage the tubes in an attempt to reduce stringer formation in the cores by reducing the amount of cold working Hot swaging on a mandrel may prove successful if bonding to the mandrel can be prevented by an oxide scale or coating

DYNAMIC FLUORIDE CORROSION

G M Adamson

UF_3-Containing Fuels

Practically all the loops reported previously except some of those with additions have had circulated in them fluoride mixes with the uranium present as UF_4 During the period covered by this report several batches with the uranium as UF_3 were circulated both in batches with zirconium fluoride bases and in others with alkali metal bases

Zirconium Fluoride Base Mixtures. The first loop, 438, circulated under standard conditions a zirconium fluoride base mixture in which all the uranium was present as UF_3. The uranium concentration was low, being only 2.8 wt %. After 500 hr no observable subsurface voids or intergranular type of attack occurred in the loop. The hot-leg surface was partially covered by a thin unidentified layer. No change in the uranium analysis was noted.

A mixture with a higher, but still low, uranium concentration was circulated in the second loop, No. 443. The uranium concentration was 5.8 wt %, and, to obtain this high a concentration, a mixture of UF_3 and UF_4 had to be used. Estimates and analyses of the relative amounts of the two compounds have varied from 100% UF_3 to 100% UF_4. While a definite figure cannot be obtained, a reasonable value for the UF_3 seems to lie between one-half and three-fourths the total amount of uranium. This loop also showed no attack after 500 hr. A layer was present in both legs but was thicker in the hot leg.

Loop 503 circulated a mixture containing 2.1 wt % trivalent uranium and 2.4% total uranium. After 500 hr of operation the fluorides were drained while the loop was held at operating temperature. Metallographic examination, as shown in Fig. 126, did not reveal any hot-leg attack but did show a hot-leg layer. A diffusion zone between the layer and the base metal was also noted. Since a layer was found in this loop, it must have formed during the operating period, rather than during the cooling period as had been desired. C. Feldman of the Chemistry Division examined the layer, by use of a microspark spectrographic technique, and found it to be predominantly zirconium. The method is not sensitive to uranium; thus uranium could also have been present.

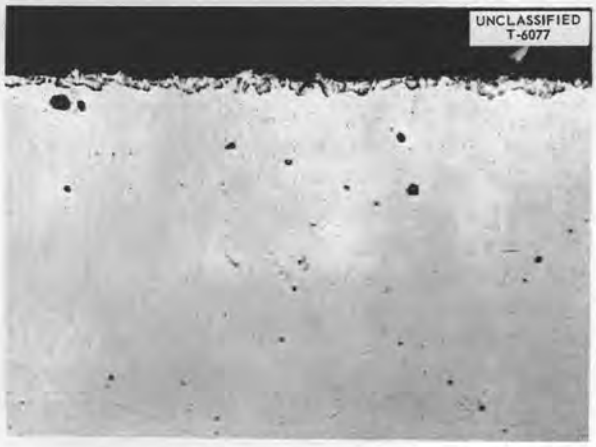

Fig. 126. Hot Leg of Inconel Thermal-Convection Loop After Circulation of a Zirconium Fluoride Base–Fluoride Mixture with UF_3 for 500 hr. 250X. Reduced 30%.

One fluoride mix containing UF_3 was circulated for 2000 hr in loop 457. Some voids were found to a depth of 4 mils during the metallographic examination, but they were not normal in appearance and are thought to have resulted from brittle crystals, formed by diffusion, which fell out during polishing. No normal hot-leg attack was found, but a definite layer, to 0.5 mil, was found on the hot-leg surface. Feldman also reported this layer to be predominantly zirconium. The UF_3-base coolants seem to reduce both the mass-transfer and impurity stages of the attack.

These facts tend to indicate that the layer is formed by the dissociation of the UF_3-producing uranium metal, at least some of which, in turn, reduces the zirconium fluoride to produce zirconium metal. The accuracy of the analytical determination for zirconium is not sufficient to confirm this reaction, since some zirconium, as ZrF_4, is lost by sublimation.

With zirconium fluoride base mixtures it is possible to add only about 2.5 wt % uranium as UF_3, which is not enough for most high-temperature reactors. To obtain a fuel with sufficient uranium, it would be necessary to use a mixture of UF_3 and UF_4. Data obtained from loops operated with such mixtures and from loops operated with standards containing all UF_4 are given in Table 42.

Loops 491 and 492 were filled from the same batch, and it does not seem possible that segregation can explain the differences in analyses. The analytical laboratory has encountered considerable difficulty in making such determinations, so they must be considered as being tentative. From these data it is obvious that a mixture of UF_3 and UF_4 will produce a reduced attack; but attack will not be eliminated. With mixtures containing UF_4 the average depth after 2000 hr is 15 mils for the 8% uranium batches and slightly deeper for those with more uranium; thus it is possible that a slight reduction in mass-transfer rate may also be found, but this cannot be determined from the few loops examined.

TABLE 42. DATA FROM LOOPS CONTAINING MIXTURES OF ZIRCONIUM FLUORIDE BASE WITH UF_3 AND UF_4

Loop No.	Total Uranium (wt %)	Uranium as UF_3 (wt %)	Time (hr)	Hot-Leg Appearance	Cold-Leg Appearance
473	8.7	1.2	500	Moderate intergranular subsurface voids to 4 mils	Occasional metal crystals
488	8.7	?	2000	Light-to-moderate subsurface voids to 7 mils	Thin metallic deposits
491	12.8	2.5	500	Moderate-to-heavy intergranular subsurface voids to 7 mils	Deposit to 0.3 mil
492	14.2	1.8	2000	Moderate-to-heavy intergranular subsurface voids to 15 mils	Deposit to 1 mil
469	8.5	0	500	Heavy general and intergranular subsurface voids to 8 mils	No deposit
462	13.9	0	500	Moderate-to-heavy intergranular subsurface voids to 10 mils	Metallic deposit to 0.3 mil

Alkali-Metal Base Mixtures. Work is being resumed on alkali-metal base fluorides containing UF_3, UF_4, and mixtures of the two, because UF_3 is assumed to have a greater solubility in these than in zirconium fluoride base mixtures. The Materials Chemistry Division has encountered considerable difficulty in making and in analyzing these mixtures.

Two Inconel loops were operated for 500 hr with NaF-LiF-KF (11.5-46.5-42.0 mole %) base mixture to which UF_3 and UF_4 were added. Because of the sampling and analytical difficulties, the relative amounts of UF_3 and UF_4 are not known, but it appears that about one-third the uranium was present as UF_3. Loop 508 contained 10.4 wt % total uranium and developed a light, widely scattered attack to 1 mil in depth; the surface was quite rough (Fig. 127). Loop 509 contained 7.4 wt % uranium and developed a void-type attack that varied from light to heavy, with a maximum penetration of 2 mils; this surface was also rough. In both loops a layer was found in the cold leg but not in the hot leg. The use of these mixtures looks promising, in that the depth of the subsurface voids was greatly reduced in comparison with the depths found with either the zirconium fluoride base mixtures or the alkali metal mixtures with only UF_4, and a hot-leg deposit does not seem to be present. More work is needed to determine whether the rough surfaces represent a different type of attack and whether the cold-leg deposits are NaK_2CrF_6, which interferes with heat transfer.

Temperature

Most of the work on the effect of temperature has been concerned with mass transfer. One series of loops was operated for 2000 hr in an effort to find how variations in maximum hot-leg temperatures affect the rate of mass transfer; the data from

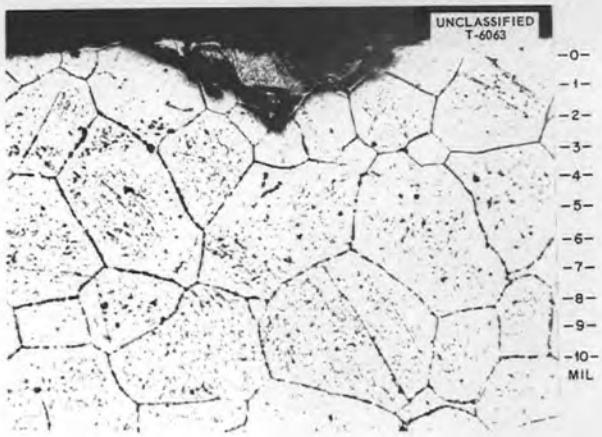

Fig. 127. Hot Leg of Inconel Thermal-Convection Loop After Circulation of Alkali-Metal Fluorides with UF_3 and UF_4 for 500 hr. 250X. Reduced 34%.

these loops are presented in Table 43 Again the data are meager and preliminary but the rate of mass transfer does seem to increase with increasing hot leg temperature This is shown both by the increase in depth of attack and by the increase in the cold leg layers

In previous loops [5] operated 500 hr at 1200°F (with different batches of fluorides) attacks to depths of 3 and 5 mils were found Another loop operated 500 hr at 1250°F developed a 3 mil attack Since the depths of attack indicated in Table 43 for the 2000 hr loops are greater than those reported previously for similar loops operated for 500 hr some attack still occurs after 500 hr While the rate of attack is less than that found[6] at 1500°F some mass transfer still occurs at the lower temperature

Time

A maximum penetration of 27 mils was found with loop 344 which had circulated NaF ZrF_4 UF_4 (50 46 4 mole %) for 5000 hr at 1500°F The fluorides in this loop were from the same batch as those used in a time series previously reported [7] The depth after 5000 hr fell surprisingly close to the straight line value for the second stage of attack [8] This confirms the depths found for the loops operated for shorter periods From the attack curve it is seen that the average increase in depth of attack is about 0 004 in for every 1000 hr of operation after the first 250 hr In the 5000 hr loop a layer about ¼ in thick of dendritic chromium metal crystals was found in the trap at the bottom of the cold leg

Another time series similar to that discussed above has been placed in operation The purposes of this series are to confirm the time curve and to provide samples from which a reaction rate may be determined by hole volume determinations The hole volume study has not been completed even on the short time loops The data for the initial portion of the series are presented in Table 44 These data do confirm the curve as discussed above including the change of slope at around 250 hr The depth reported for the 1000 hr loop is out of line both with the other data in this series and with data from similar previous loops

Additions to Fluorides

Zirconium Hydride As part of the work previously discussed concerning reduced mixtures various amounts of ZrH_2 were added to NaF ZrF_4 UF_4 (50 46 4 mole %) The hydride was added to small portions of fluorides taken from the same

[5] G M Adamsan *Met Semiann Prog Rep April 10 1954* ORNL 1727 p 42

[6] *Ib d* p 40

[7] G M Adamson *Met Sem ann Prog Rep Oct 10 1953* ORNL 1625 p 26

[8] *Ibid* p 30 Fig 13

TABLE 43 EFFECT OF TEMPERATURE ON MASS TRANSFER

Loop No	Temperature (°F)	Max mum Penet at on (mils)	Hot Leg Appearance	Cold Leg Appearance
391	1200	7	Very heavy general attack with small voids	No deposit
449	1250	6	Intergranular moderate to heavy	No deposit
392	1400	8	Heavy general attack to 4 mils with occasional deeper inter granular penetrations	Intermittent metallic deposit
393	1600	13	Intergranular moderate to heavy large voids	Thin but continuous metallic deposit

Terminated after 1313 hr after circulation had been stopped for the second time by a power failure

original batch Filters were used in the transfer lines from the small batches The data from these batches are given in Table 45 Layers were found in the cold legs of all loops to which the additions had been made These data show that to obtain enough reducing power in the fuels to eliminate corrosion some uranium will be lost both in the treatment pot and in the loop during operation Some attack was still found in loop 470 nevertheless a reduction in uranium concentration is apparent

Hydrogen Fluoride Gas Small amounts of hydrogen fluoride gas were added to a batch of NaF ZrF_4 UF_4 (50 46 4 mole %) Portions of this batch were then circulated for varying times in Inconel loops The data obtained are summarized in Table 46 The double depth of penetration found in loop 415 as compared with loop 421 confirms the adverse effect of small amounts of HF on the initial rate of attack Although a standard loop was not filled with these fluorides and allowed to circulate for 2000 hr on the basis of experience from previous loops a maximum penetration of 12 mils would be expected in such a loop The difference in penetration between these loops and the standards is about the same after 2000 hr as it was after 500 hr This is additional confirmation of the opinion that mass transfer is not sensitive to initial purity

Uranium Concentration

Two loops were operated with a high purity NaF ZrF_4 UF_4 (53 5 40 6 5 mole %) mixture This mixture compares with the one to be used in the ARE and is higher in uranium than the one normally used The hot leg attack in both loops was of the usual subsurface void type The intensity of the attack was heavy with a maximum penetration of

TABLE 44 LOOP CORROSION

Loop No	Operating Time (hr)	Maximum Penetration (mils)	Hot Leg Attack
431	10	2	Light with intermittent moderate areas
432	50	3	Moderate
433	100	4½	Light to moderate
434	250	8	Moderate to heavy primarily intergranular
435	500	8	Heavy primarily intergranular
436	1000	14	Heavy intergranular
445	1500	13	Heavy intergranular
437	2000	16	Heavy intergranular

TABLE 45 EFFECT OF ADDING ZIRCONIUM HYDRIDE TO FLUORIDES

Loop No	ZrH_2 Added (%)	Hot Leg Attack	Uranium (%)	
			Before	After
469		Heavy general and intergranular voids to 8 mils	8 5	8 8
459	0 2	Moderate to heavy to 6 mils	8 6	8 5
470	0 5	Light to moderate to 3 mils	7 5	7 1
460	0 9	Thin hot leg deposit no attack	5 4	5 1
471	2 0	Hot leg layer to 1 mil no attack	4 0	4 1

TABLE 46 EFFECT OF ADDING HYDROGEN FLUORIDE TO FLUORIDES

Loop No	HF Concentration (μmole/liter)	Original Impurity (ppm)		Circulation (hr)	Maximum Penetration (mils)	Hot Leg Attack
		Ni	Fe			
421 standard	1 2	10	110	500	5	Moderate to heavy
415	3 4			500	10	Intergranular moderate to heavy
416	6	10	345	1000	12	Heavy intergranular
417	6	10	195	2000	17	Intergranular moderate to heavy with large voids

10 mils This is slightly deeper than the 6 to 8 mils found with the lower uranium mixes Thin metallic appearing layers were found in the cold legs of both loops The results from these loops confirm the results found previously with similar but impure mixtures

Inconel Grain Size

To produce varying grain size Inconel pipe was annealed at two temperatures All the loops of this series were filled from the same batch of NaF ZrF_4 UF_4 (50 46 4 mole %) and operated for 500 hr Two loops annealed at 2100° F had 1 to 1½ grains per square inch at 100X whereas the as received loop and the one annealed at 1600° F contained about 6 grains per square inch Very little difference in hot leg attack was found in these loops Those with the larger grains may have had a slightly deeper attack (1 mil) but this cannot be determined from two loops The loops with the larger grain size usually showed a heavier general attack and the deep penetrations were concentrated into fewer boundaries

Various Containers

Hastelloy B The major effort on Hastelloy B loops has been that of learning how to operate a loop without inadvertently causing failure Loops both in the as welded and in the overaged condition were operated satisfactorily The operating mortality rate has been reduced from the original 100% to zero in the last group of four The increase in hardness during operation is not so great in the overaged loops but with proper care the as welded ones may be operated

A ½ in tubing loop of Hastelloy B was finally obtained which circulated NaF ZrF_4 UF_4 (50 46 4 mole %) for 500 hr at 1500° F After fabrication and welding this loop had been solution annealed for 1 hr at 2150° F and aged for 30 hr at 1950° F After circulation the inner surface of the hot leg was rough Light subsurface voids to 2 mils were found The tubing had been fabricated by seam welding and this weld bead showed much less attack than the parent metal The metallographic structure of the cold leg was similar to that of the hot leg except that fewer voids were present Results of chemical analysis confirm the low attack rate found metallographically since neither nickel nor molybdenum increased in the fluorides After the loop was operated the molybdenum content of the fluoride in all sections was reported as being less than 1 ppm This presents an optimistic picture from the mass transfer view point since it is difficult to picture mass transfer taking place with this low a concentration

In loop 154 which circulated NaF ZrF_4 UF_4 (50-46 4 mole %) for 1000 hr very little attack was found The attack occurred as occasional voids to a maximum depth of 1 mil with possibly some increase in surface roughness Most of the surface roughness was present in the as received tubing Figure 128 presents photomicrographs of both conditions

Special Inconel A special series of alloys with slight changes from the usual Inconel analysis were vacuum cast at X 10 and drawn into ½ in tubing with a 0 065 in wall by Superior Tube Co The first lot was made into loop 472 and has circulated NaF ZrF_4 UF_4 (50 46 4 mole %) for 500 hr A portion of the chromium normally found in Inconel had been replaced by molybdenum the resulting analysis is Cr 6 0% Fe 10 0% Ni

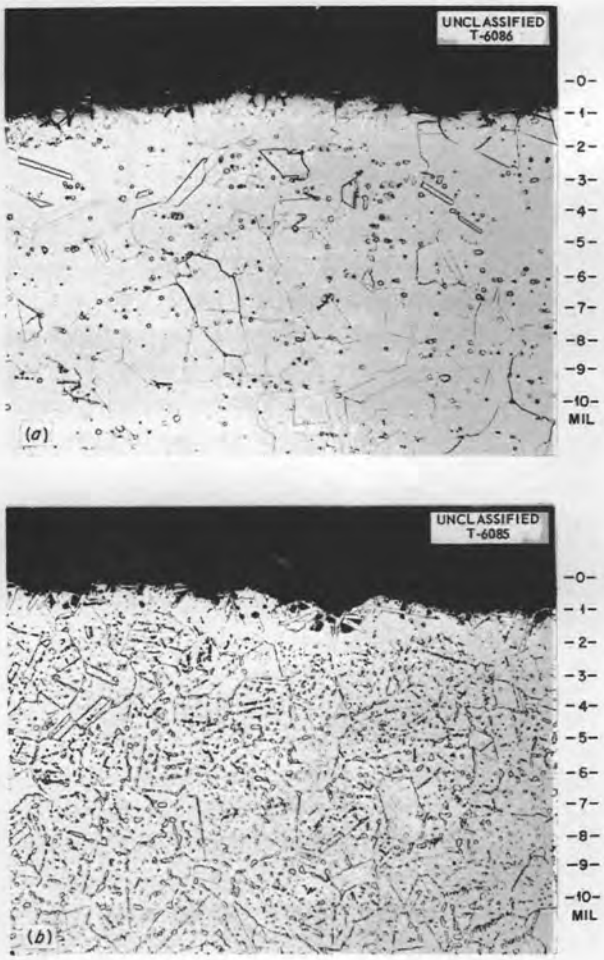

Fig. 128. Comparison of (*a*) As-Received Hastelloy B Tubing and (*b*) the Hot Leg of Loop 154 After Circulation of NaF-ZrF_4-UF_4 (50-46-4 mole %) for 1000 hr. 250X. Reduced 31%.

74.4%; Mo, 9.8%. After circulation, a light attack with a maximum penetration of 3½ mils was found, Fig. 129. Standard Inconel loops of ½-in. tubing developed moderate-to-heavy attack 4 to 5 mils deep.[9] Some reduction in depth has been realized but not so much as was expected; however, a considerable reduction in amount of attack may be noted. To magnify the effects of mass transfer, additional loops will be operated for longer times.

Stainless Steel. A second type 430 stainless steel loop was operated with NaF-ZrF_4-UF_4 (50-46-4 mole %). The hot leg developed a very

[9]G. M. Adamson, *Met. Semiann. Prog. Rep. April 10, 1954*, ORNL-1727, p 44–45.

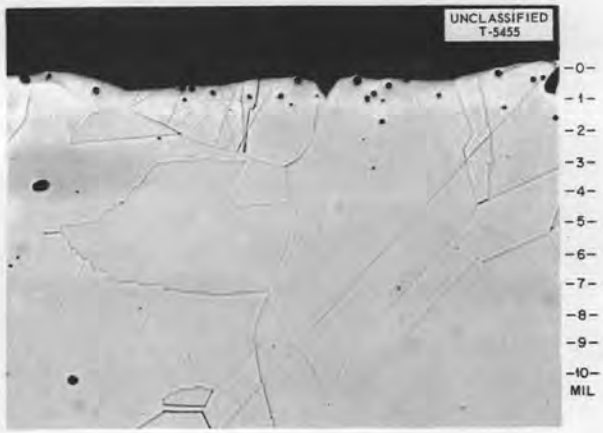

Fig. 129. Hot Leg of Special-Alloy Loop 472 (6.0 wt % Cr–10.0 wt % Fe–74.4 wt % Ni–9.8 wt % Mo) After Circulation of NaF-ZrF_4-UF_4 (50-46-4 mole %) for 500 hr at 1500°F. 250X. Reduced 34%.

light, widely scattered, subsurface-void attack to a maximum depth of 7 mils. A phase change to what appears to be martensite was noted in the vicinity of the voids. In an area up to 10 mils deep from the surface, the carbides have apparently gone back into solution and grain growth has occurred. The cold leg had particles of metal deposited on the surface, and metallic crystals were found in the adhering fluorides. While the attack was less than that found in Inconel loops, more metallic crystals were visible. The attack was also greater than that found in the first type 430 stainless steel loop.[9]

Sodium-Beryllium-Inconel System

A series of loops are being operated to determine the effect of dissimilar-metal mass transfer in the sodium-beryllium-Inconel system. These studies are being carried out in Inconel loops, with short beryllium cylindrical inserts in the hot legs; molten sodium is used as the liquid. Results are reported in Table 47 for loops that operated for 500 hr. Others are now in operation that will circulate for longer periods.

Photomicrographs of the outsides of the inserts are shown in Fig. 130. A black flaky material was found in the cold leg of all these loops and in the hot leg of loop 412. This layer has not yet been identified by spectrographic or diffraction studies. The deposit found on the Inconel

TABLE 47 CORROSION IN BERYLLIUM INCONEL LOOPS CONTAINING SODIUM

Loop No	Temperature (°F)	Beryllium	Hot Leg – Inconel
412	1500	Outside of insert showed holes to 14 mils inside slightly rough	Depos t opposite the insert
495	1300	Intergranular penetrations to 2 mils on outside no attack on inside	No attack or depos t
494	1100	No layer or attack	No attack or deposit
493	900	No layer or attack	No attack or deposit

opposite the insert in loop 412 is shown in Fig 131 this deposit has been identified as a nickel beryllium alloy

In another loop 420 the insert was in the lower cold leg No attack was found in the Inconel hot leg of this loop A thin metallic deposit was visible on the surface of the Inconel below the insert but not on that above it The insert showed some attack on both faces – surface roughness intergranular penetrations and voids to a maximum depth of 2 mils Again some even removal was possible No metallic crystals were found in this loop but a black scale of the same type as that discussed above was found in all sections

As a consequence of these low temperature results it is hoped that the beryllium may be used up to 1200°F without being clad This conclusion cannot however be made definitely until more data are available from both short and long time loops

PHYSICAL CHEMISTRY

G P Smith

Corrosion Testing

J V Cathcart M E Steidlitz
W H Bridges

Mass Transfer in Liquid Lead The investiga tion of corrosion and mass transfer in lead has been continued As in the previous work [10 12] tests were performed in small quartz thermal convection loops in which metal specimens were held in the hot and cold legs

During the period covered by this report em phasis was placed on an attempt to explain the greater resistance to mass transfer of certain al loys as compared with the resistance of their pure components Thus it was found that the time re quired in a loop for the mass transfer of a given quantity of 400 series stainless steel was much greater than that required when the test specimens were pure iron or pure chromium

Previously obtained data indicated that this effect might be associated with the ability of the alloying constituents to form intermetallic com pounds Alloys showing a relatively high resis tance to mass transfer in liquid lead included types 410 and 446 stainless steel (Fe Cr alloys) 2% Si–14% Cr–84% Fe 25% Mo–75% Ni and Hastelloy B (5% Fe–28% Mo–64% Ni) in every case at least one intermetallic compound is shown in the phase diagrams for the alloys On the other hand Inconel (7% Fe–14% Cr–78% Ni) Nichrome V (20% Cr–80% Ni) 30% Ni–70% Fe and types 304 and 347 stainless steel all showed relatively poor resistance to mass transfer either the components of these alloys do not form intermetallic compounds or else the compositions of the alloys are so far removed from the compositions of possible inter metallics that no compound formation is likely

To test this hypothesis further two other alloys were studied The first one had a composition of 16% Ni–37% Cr–47% Fe This particular alloy was chosen because its composition corresponded to a sigma rich region in the nickel iron chromium phase diagram for temperatures in the neighborhood of 800°C By means of suitable heat treatments

[10] G P Smith *Met Semiann Prog Rep April 10 1953* ORNL 1551 p 17

[11] J V Cathcart *Met Sem ann Prog p Oct 10 1953* ORNL 1625 p 36

[12] J V Cathcart *Met Semiann Prog Rep April 10 1954* ORNL 1727 p 47

the test specimens could be converted into sigma-plus-austenite phases or into austenite-plus-ferrite phases. Thus it was possible to prepare specimens rich in an intermetallic component (sigma phase) and also specimens having the same composition but having virtually no sigma phase present. Two loops containing the specimens rich in sigma phase were operated; the hot- and cold-leg temperatures in the first loop were 820 and 510°C, respectively, and the loop plugged after 456 hr. The second loop operated for 306 hr before plugging, with hot- and cold-leg temperatures of 805 and 550°C, respectively. In addition, two loops containing non-sigma-phase specimens (austenite-plus-ferrite) were also operated. The hot- and cold-leg temperatures in both loops were 801 and 510°C, respectively. The plugging time for the first loop was 287 hr and for the second loop 101 hr. As is evident, there was a pronounced lack of reproducibility in the plugging times for these four loops; however, both loops containing the sigma-rich specimens required longer to plug than the nonsigma loops. There are two factors which could account for the discrepancy in plugging times. First, there may have been a variation in the degree of transformation in the different specimens during the preliminary heat treatment. Second, the hot-leg temperatures for these loops correspond closely to the sigma-transformation temperature. Thus it is conceivable that appreciable quantities of sigma phase either were formed or were transformed into ferrite during the operation of the loops themselves.

A transverse section from the hot leg of Pb–16% Ni–37% Cr–47% Fe loop No. 1 (sigma-rich) is

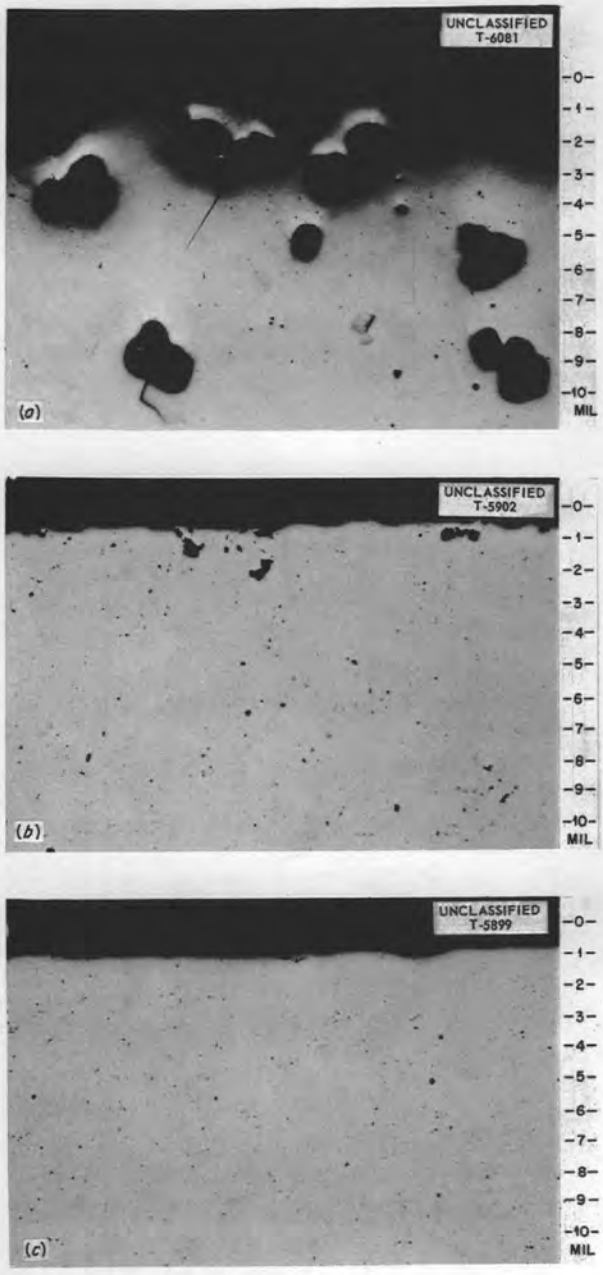

Fig. 130. Outer Surface of Cylindrical Beryllium Inserts in Hot Legs of Inconel Thermal-Convection Loops. Sodium was circulated at (*a*) 1500°F, (*b*) 1300°F, and (*c*) 1100°F. 250X. Reduced 32%.

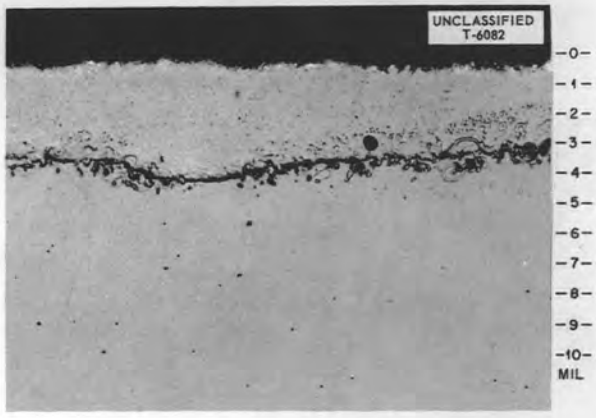

Fig. 131. Layer on Hot Leg of Inconel Thermal-Convection Loop Opposite a Beryllium Insert. Sodium has been circulated for 500 hr at 1500°F. 250X. Reduced 32%.

shown in Fig. 132. The sigma phase is present as the precipitated phase. The specimen suffered fairly severe and irregular penetration by the lead, but, as can be seen in the photograph, virtually all the sigma region was essentially unattacked, the channels of lead passing around and between the sigma particles. The transverse sections from the hot-leg specimens of the nonsigma loops were similar in appearance to that shown in Fig. 132, except that the development of the sigma phase was considerably less pronounced. The appearance of any sigma phase at all can probably be attributed to the fact, as mentioned above, that the hot-leg temperature in these loops corresponded to the sigma-transformation temperature.

The second alloy tested had a composition of 45% Cr–55% Co. This composition was chosen because it corresponded to a sigma-rich region in the Co-Cr phase diagram. The loop was operated for 768 hr before plugging occurred; hot- and cold-leg temperatures were 820 and 510°C, respectively. By contrast, loops containing pure cobalt and pure chromium and operated at approximately these same temperatures plugged after only 80 and 100 hr, respectively. Thus the 45% Cr–55% Co alloy furnished another example of a case in which the resistance of an alloy to mass transfer in liquid lead was much greater than that of the pure components alone. A transverse section from the hot-leg specimen from Pb–55% Co–45% Cr loop No. 1 is shown in Fig. 133.

As outlined above, all the data which have been obtained thus far indicate that the resistance to mass transfer in liquid lead of an alloy is likely to be appreciably greater than that of its pure components, provided that there is a tendency for intermetallic formation in the alloy and provided that, when the possibility of compound formation

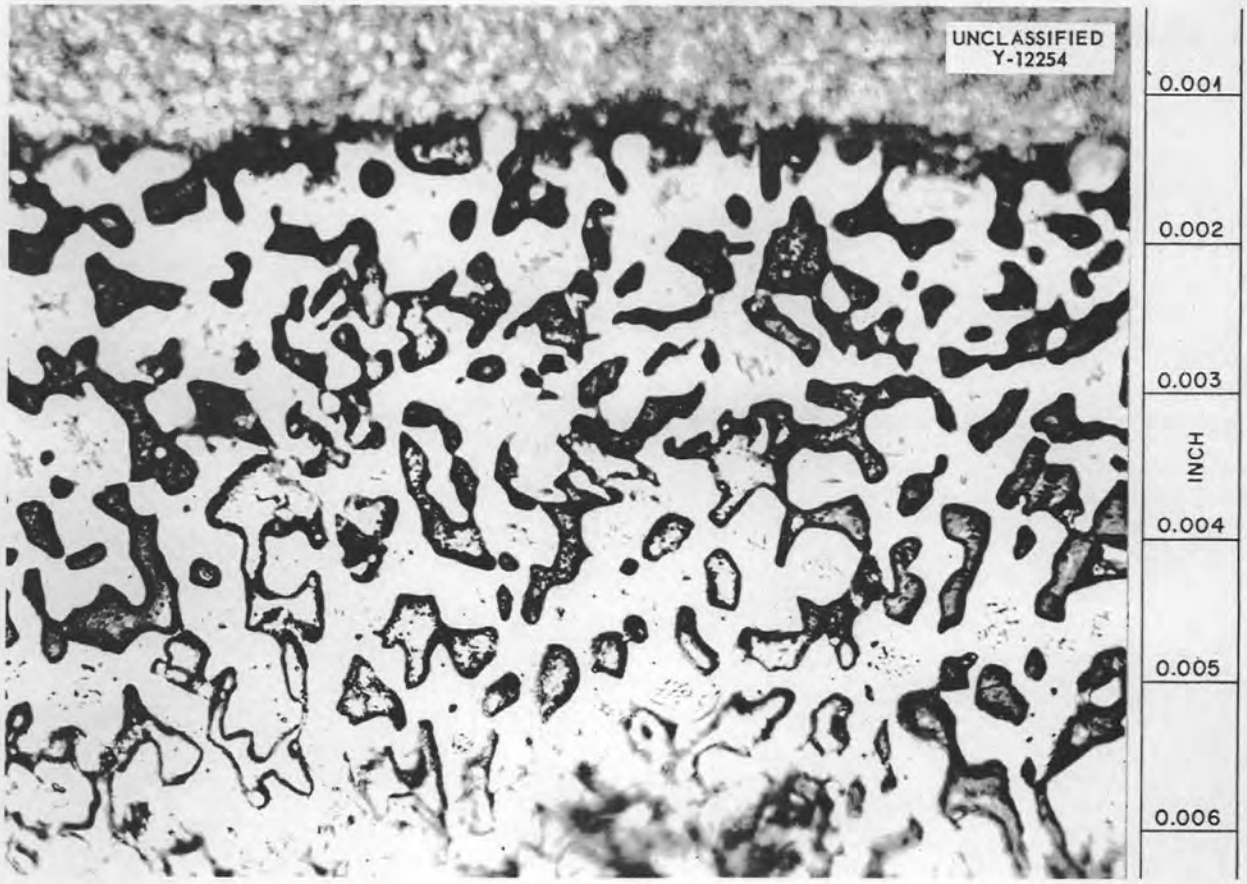

Fig. 132. Transverse Section of the Hot Leg of Lead–16% Ni–37% Cr–47% Fe Loop No. 1 (Sigma-Rich).

does exist, the composition of the alloy is reasonably close to the composition of the compound.

Future work will include further tests of a 50% Cr–50% Fe alloy. In addition, an iron-molybdenum alloy containing an intermetallic phase will also be studied.

Mass Transfer in Fused Hydroxides. As described previously,[13] a testing device has been operated which is suitable for determining the effect of blanketing atmospheres on mass transfer in fused alkali-metal hydroxides. Since last February, an apparatus consisting of five of these test units has been under construction.

[13] W. H. Bridges, *Met. Semiann. Prog. Rep. April 10, 1954*, ORNL-1727, p 52.

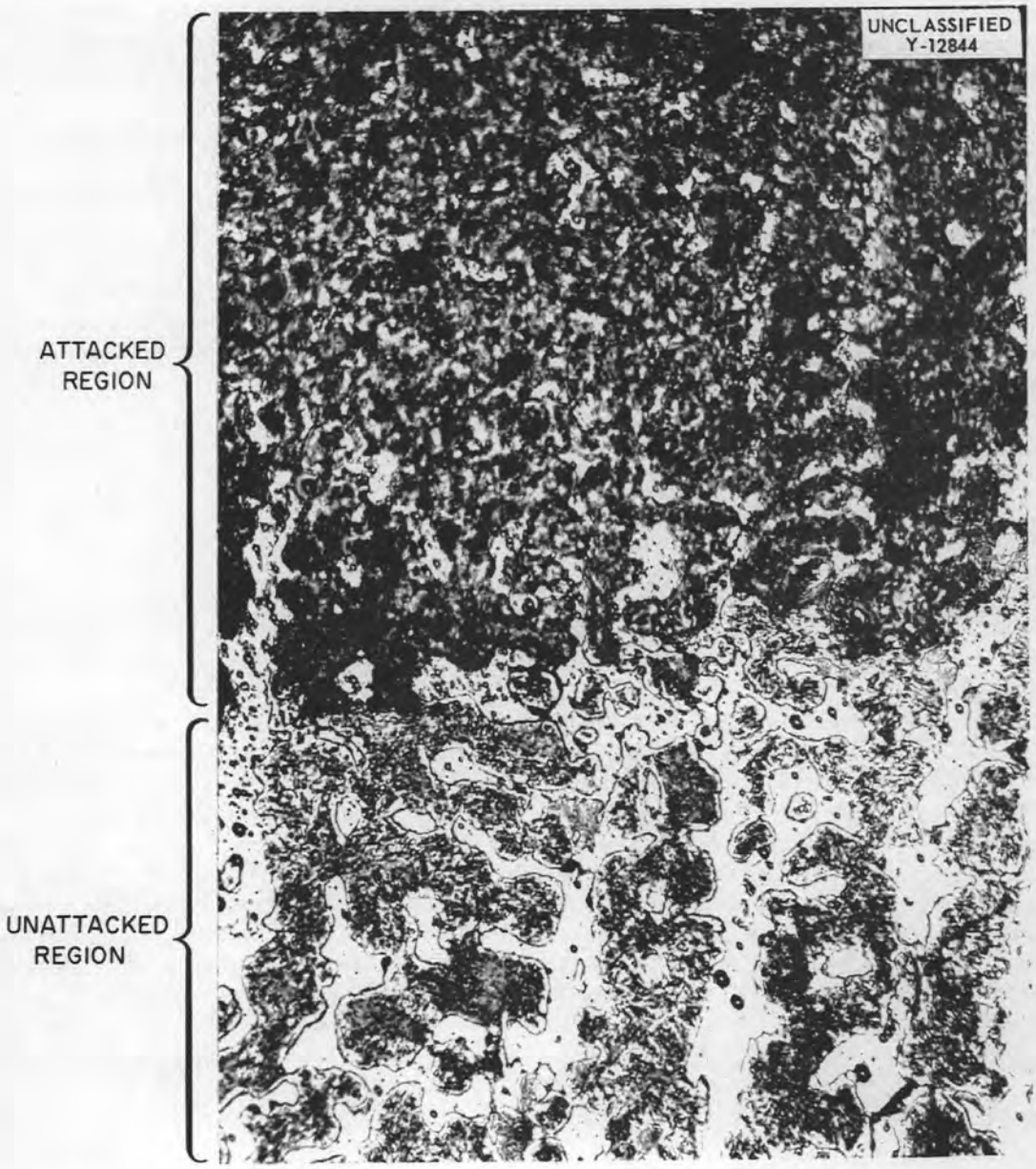

Fig. 133. Transverse Section of the Hot Leg of Lead–55% Co–45% Cr Loop No. 1.

Film Formation on Metals Oxidation of Sodium

J V Cathcart R F Sessions[14]

As has already been reported rate measurements of the oxidation of sodium near room temperature showed that the reaction does not obey a linear rate law This fact was surprising in that it has been predicted that sodium on account of the relatively high density of its oxide should oxidize by a mechanism which is not influenced by the presence of an oxide film That is on theoretical grounds sodium is presumed to form a nonprotective oxide film

The theory from which these predictions are derived the old crack theory of Pilling and Bedworth [15] is the only general theory yet proposed which attempts to establish criteria for protective film formation It is based on the idea that the degree of protectiveness of a film is dependent upon the tendency for crack formation in the film Sodium is a metal which fulfills completely the conditions required for nonprotective film formation Hence the failure of the theory in the case of sodium indicates that the entire current theoretical approach to the problem of protective film formation is incorrect

This fact is of particular significance for two reasons (1) film formation plays a decisive role in many technologically important processes for example many corrosion phenomena in metal systems are governed by the degree to which the metal surfaces are covered by a protective film (2) apparently there exists a fundamental misconception as to the nature of the oxidation mechanism for the alkali metals if not for metals in general Thus the results which have already been obtained from a study of the oxidation of sodium show clearly that the only theoretical basis for understanding the nature of protective film formation is unsatisfactory and outmoded Both from a fundamental and an applied point of view a thorough reinvestigation of the whole problem is in order

The oxidation of sodium was chosen as a vehicle for the study of the criteria of protective film formation for several reasons

1 A study of oxidation rather than some other comparable process represents a logical choice because so much groundwork has been laid by previous investigators

2 Little progress has been made toward understanding the criteria for protective film formation through studies of metals which theoretically should and experimentally do form protective films It was hoped that an investigation of the oxidation of metals which theoretically do not form protective films would prove more fruitful

3 Sodium is a metal which theoretically definitely should not form a protective oxide film In addition it is relatively easy to purify and can be handled in glass apparatus at moderately low temperatures

4 The oxidation of sodium and the other alkali metals is also of interest per se The highly ionic character of sodium oxide should greatly facilitate the theoretical interpretation of the oxidation data and the fact that the heavier alkali metals tend to form stable peroxides and superoxides makes a study of their oxidation characteristics especially significant

Experimental Results The investigation of the oxidation rates of sodium has been continued As in previous experiments rate measurements were made by following the pressure changes in a sealed reaction chamber with a sensitive differential manometer Although several details have been altered the principal features of the experimental apparatus are the same as those described in an earlier report [16]

Rate measurements have been made at 25 48 and 65°C Data for typical experiments at 25 and 48°C are shown in Fig 134 Measurements at 65°C have not yet been completed and will not be discussed here

At neither 25 nor 48°C was a linear oxidation rate found A high initial rate followed by a gradual decrease was characteristic of the oxidation It will be noted that a linear relationship between film thickness and time was not obtained even in a log log plot such as is shown in Fig 134 Thus the oxidation does not obey any of the usual rate equations of the form

$$x^n = kt$$

where x is the thickness of the oxide film formed

[14] ORINS Summer Participant

[15] N B Pilling and R E Bedworth *J Inst Metals* 29 577 (1923) see also U R Evans *Metallic Corrosion Passivity and Protection* Longmans Green and Co 1948 p 102

[16] J V Cathcart *Met Semiann. Prog Rep Oct 10 1953* ORNL 1625 p 33

in time t and n and k are constants A further check of the data has also shown that the logarithmic oxidation law is not obeyed

Although a detailed mathematical analysis of the data has not yet been completed the following conclusions may be drawn

1 The oxidation of sodium does not follow a linear rate law in the temperature range 25 to 48°C

2 The lack of linearity in the log log plots of the data indicates that either the mechanism of oxidation is completely different from the mechanisms which have been proposed for other metals or else two or more of the conventional mechanisms are simultaneously or consecutively operative Thus in the very early stages of oxidation the rate might be linear then as the oxide films grow thicker there might be a transition into a parabolic cubic or even a logarithmic rate

Since the oxidation rate is sensitive to the structure of a metal it is important that information be obtained as to the structures of the oxidation specimens In the case of copper for example a tenfold difference in oxidation rate has been shown to exist between the (311) and (100) crystallographic planes at 150°C For this reason an attempt has been made to determine whether the sodium films used in the oxidation experiments possessed a random orientation or whether a high degree of preferred orientation existed in them The problem was complicated by the necessity for protecting the films from air during x ray measurements This difficulty was surmounted by coating the x ray specimens with degassed Vaseline before the specimens were removed from the vacuum chamber in which the films were formed The Vaseline coating proved to be sufficiently impervious to air and water vapor to allow the sample

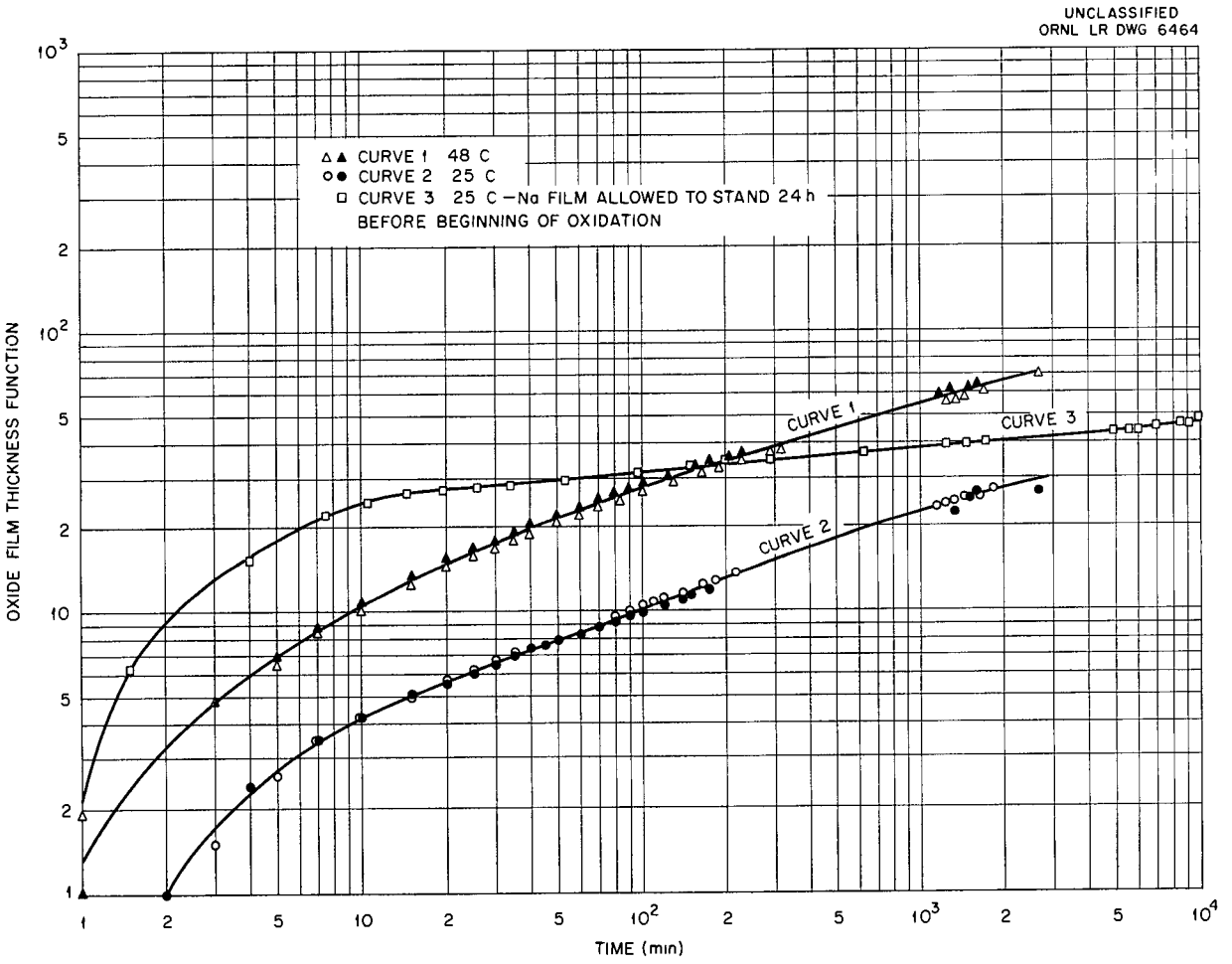

Fig 134 Oxidation Curves for Sodium

to be handled in air for several hours without any noticeable changes occurring in the sodium These experiments are still in the preliminary stage but the few results obtained indicated that the films possessed at least a small degree of (110) preferred orientation

The presence of small amounts – even trace quantities – of foreign material in the reaction vessel can also have a profound influence on oxidation rates For example the oxidation rate of copper was found to increase from two to ten times in the presence of very small quantities of vapor from stopcock grease Sodium appears to possess a similar sensitivity to such contamination Thus it was almost impossible to obtain reproducible rate measurements with sodium until all stopcocks were removed from the vicinity of the reaction chamber Similarly great care had to be exercised in the preparation of the sodium films in order to remove all occluded and adsorbed gases from the sodium

Aside from a general irreproducibility of the oxidation rates when the above precautions were not taken another manifestation of the influence of contamination has been noted The sodium films were prepared by vacuum distillation followed by deposition on the walls of the reaction chamber The usual experimental procedure was to begin the oxidation within about 30 min after the end of the distillation When however the sodium film was allowed to stand in a vacuum of 10^{-6} mm Hg for approximately 24 hr before oxygen was admitted to the system a marked deviation from the usual oxidation curve was observed The results of a typical experiment of this sort are shown by curve 3 in Fig 134 It will be seen that the initial oxidation rate was much more rapid in this experiment than it was in the usual experiments and that the subsequent decrease in rate was also greater Since no change in the structure of the sodium films with time was noted in these experiments it is believed that this behavior can probably be attributed to a slow accumulation of foreign material on the sodium film One very important part of this research will be not only to determine how to prevent this effect but also to understand how these foreign atoms change the oxidation mechanism of sodium

Future work on this project will include a continuation of the oxidation rate measurement at several temperatures Efforts will be made to make a more precise determination of the structures of the sodium films and to obtain information as to the structure and composition of the oxide films themselves It is also planned to study the surface topography of the oxide films by using electron microscopy techniques

Flammability of Alkali-Metal Solutions[17]

G P Smith M E Steidlitz

Previous work[18] on the flammability of jets of liquid sodium alloys has been extended to include the sodium cadmium system a more detailed study of the sodium bismuth system attempts to study the sodium mercury system at higher temperatures and studies of four alkali metal–alkali metal halide systems

Sodium Bismuth System Figure 135 shows the relative reactivity of sodium bismuth solutions at 700°C with dry air as a function of the mole fraction of sodium N_{Na} The relative reactivity scale is arbitrary Pure sodium was assigned a reactivity of four units Unreactive solutions were assigned a reactivity of zero At 700°C measurements were not made for mole fractions of sodium between 0 6 and 1 0 because a solid compound of composition Na_3Bi precipitates from solution at a mole fraction of sodium somewhat greater than 0 6

[17] Temperature values previously reported for these studies are herein revised according to a more accurate calibration of the apparatus

[18] M E Steidlitz and G P Smith *Met Semiann. Prog Rep April 10 1954* ORNL 1727 p 53

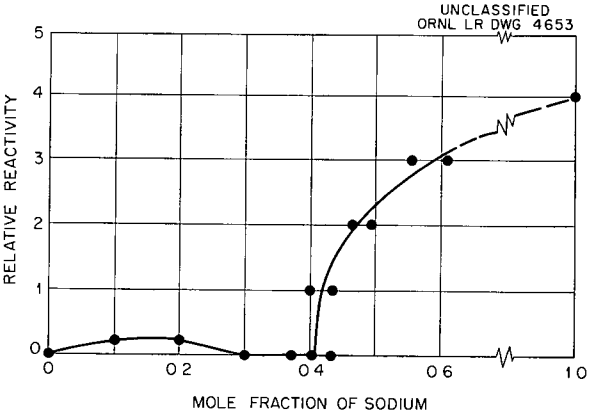

Fig 135 Relative Reactivity of Sodium Bismuth Solutions at 700°C with Dry Air

Figure 136 is a temperature composition diagram for liquid sodium bismuth solutions on which is plotted a curve that approximately separates the region of reaction from the region of negligible reaction The circles and triangles on this diagram represent the temperature composition values at which tests were conducted Most of the circles represent two to four tests each The open circles represent tests in which reaction occurred while the black circles represent those which showed no reaction The black triangles represent conditions under which part of the tests showed no reaction while the rest of the tests showed a slight reaction The two open triangles represent tests which showed an exceedingly slight amount of reaction The broken portion of the curve is poorly defined inasmuch as it may actually pass beneath the open triangles rather than above them as shown It will be noted that jets of pure bismuth showed appreciable reactivity at 800°C but not at 750°C

When air was saturated with water vapor the line of zero reactivity was shifted toward lower sodium concentrations by a small but appreciable amount for both sodium bismuth and sodium mercury solutions This effect is shown for sodium bismuth solutions at 700°C by Fig 137 In this figure test data for moist air are plotted together with a curve representing the results for dry air It will be seen that although data for moist air scatter badly there is unquestionably a small shift toward lower sodium concentrations

Changing the pressure of air from 1 down to $\frac{1}{4}$ atm did not produce an appreciable change in the reactivity of sodium bismuth solutions

Other Binary Alloys Cadmium sodium solutions at 700°C burned violently in dry air at 1 atm pressure with N_{Na} = 0 10 Both the cadmium and the sodium burned

Attempts were made to extend the data on sodium mercury solutions to temperatures higher than those previously reported These attempts were not successful because of the formation of dense fogs of liquid mercury

Alkali Metal–Alkali Metal Halide Solutions Flammability studies have been made of four of the six alkali metal–alkali metal halide systems for which phase-diagram data are available The results described in Table 48 represent one test of each system at the temperature indicated The temperatures chosen lie in the single phase region and are generally about 50°C above the two liquid phase region All tests were made on halide-rich solutions

Fused Hydroxide Chemistry

C R Boston G F Petersen
M E Steidlitz E S Amis
G P Smith

Studies of corrosion chemistry of fused hydroxides by this group have brought out two empirical facts which have been the basis of a good portion of the recent government sponsored research on

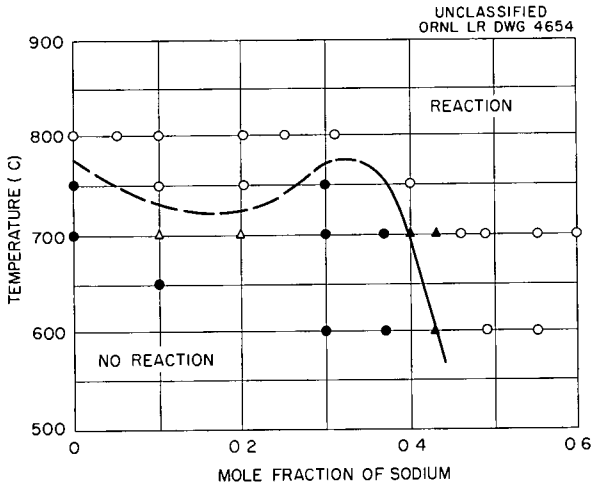

Fig 136 Temperature Composition Diagram Showing Reactivity of Sodium Bismuth Solutions

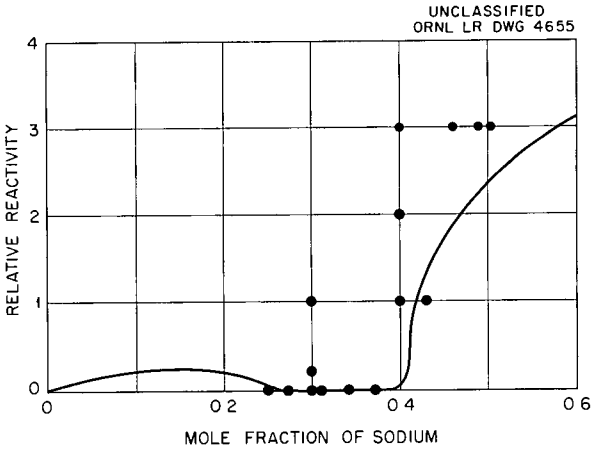

Fig 137 Relative Reactivity of Sodium Bismuth Solutions at 700°C with Moist Air The curve represents data for dry air

TABLE 48 FLAMMABILITY OF ALKALI METAL–ALKALI METAL HALIDE SYSTEMS

System	Metal Content (mole %)	Test Temperature (°C)	Reaction
Na NaF	2	1050	Mild
	5	1050	Violent
	10	1050	Violent
Na NaCl	2	850	Little
	5	900	Violent
	30	1050	Violent
Na NaI	2	700	Mild
	5	800	Mild
	10	900	Violent
	20	1000	Violent
K KF	2	900	Mild
	5	900	Violent
	10	900	Violent

hydroxides First the nature of the blanketing atmosphere exerts a controlling influence on corrosion and mass transfer Oxygen gas accelerates mass transfer and corrosion compared with neutral atmospheres while hydrogen markedly slows down these processes Second the nongaseous products of hydroxide corrosion are usually oxy salts rather than oxides

Recently another phenomenon has been encountered which may also be fundamental to the hydroxide corrosion problem This phenomenon has to do with the kinetics of the reaction of metallic sodium with sodium hydroxide The observations which have been made together with their possible significance will be discussed below

The major portion of the research to be described is devoted to various aspects of the first two fundamental empirical facts In addition secondary efforts are being devoted to an examination of the kinetics of the sodium metal–sodium hydroxide reaction in order to determine whether or not this subject deserves further study and to the solid state transformation in sodium nickelate(III) This latter work is a good fundamental problem in solid state chemistry but is not being emphasized because it probably will contribute little or nothing to an understanding of corrosion

Finally studies which were made on container materials and work on the design and construction of a special dry box were key experimental undertakings important to all the rest of the hydroxide chemistry research

Inert-Container-Material Research In the majority of chemical investigations the existence of an adequately inert container material is taken for granted In studies of fused alkali hydroxides however the selection of a suitable container material has been the most important unsolved problem in experimental technique During the past half year the writers studied this problem and have found what seems to be a satisfactory answer namely vessels machined from massive single crystals of synthetic periclase (high purity magnesium oxide)

In this study metallic containers and most commercial ceramics were discarded from consideration A few metals such as nickel and silver are reasonably inert toward fused caustic but only under such special conditions as to preclude their general use On the other hand most commercial ceramics contain binders such as silica which react almost violently with fused caustic as shown by studies which were made by this group three years ago

Special crucibles made of pure sintered materials were investigated These included beryllium oxide ceric oxide magnesium oxide Morganite (high purity recrystallized aluminum oxide) and aluminum titanate Tests were conducted with fused caustic at 600 to 700°C None of the materials was entirely satisfactory Beryllium oxide ceric oxide and magnesium oxide crucibles quickly absorbed large quantities of the fused hydroxide which in some cases leaked through and frequently caused the crucible to lose its mechanical strength With aluminum titanate a large quantity of gray reaction product was formed after 11 hr The results with Morganite agreed with those from previous tests made by the authors and by others namely the hydroxide picked up 1 to 3 wt % aluminum but the crucible was not observably changed A few oxide ceramics were studied in closed systems In these cases an analysis of the gas phase showed the formation of considerable water

These results were interpreted as having been caused by two phenomena The first was the reaction of the caustic with the crucible to form a sodium oxysalt and water For example

$$2NaOH + Al_2O_3 \rightarrow 2NaAlO_2 + H_2O$$

The second was the well known capillary activity

of sodium hydroxide which results from its high surface tension combined with its ability to wet all substances which have been tested This capillary activity causes sodium hydroxide to creep extraordinary distances up the walls of a vessel and to enter into minute pores

The lesser reactivity of the Morganite crucibles was probably due to three factors First these crucibles were so completely sintered that no pores are present Second several studies lead to the belief that the solubility of sodium aluminate in fused caustic is approximately such as to give the observed aluminum pickup Third sodium aluminate films on aluminum oxide do not scale off and hence greatly hinder such diffusion as would be required for solid state reaction

Since magnesium oxide is one of the few potential materials of construction which does not form a sodium oxysalt the failure of the crucibles was attributed to porosity alone The inherent corrosion resistance of this material was tested by placing a small single crystal of periclase in fused sodium hydroxide contained in Morganite There was almost no pickup of magnesium by the melt although it was recognized that sodium aluminate may have had some influence On the basis of the success of this test attempts were made to fabricate nonporous crucibles by sintering magnesium oxide However these attempts were unsuccessful

Success was finally achieved by fabricating vessels directly from massive single crystals of pure synthetic periclase Pure magnesium oxide powder was arc melted and slowly cooled by the Norton Company to produce a solid mass containing a number of large crystals This mass was sent to the writers and large single crystal fragments were then separated from the mass by cleavage Tnese crystals show excellent cubic cleavage and can be machined with surprising ease considering their brittleness Furthermore despite the unfortunate experiences of others the writers have had no trouble from thermal stress cracking on uniform heating at a rapid rate or from visible recrystallization of surfaces which were cold worked either by machining or by grinding and polishing

The most severe of the tests made to ascertain the resistance to thermal stress cracking is illustrated in Fig 138 A thermocouple well 3 5 mm in diameter and 10 mm long was drilled in one end of a periclase crystal 27 mm long and 8 by 10 mm

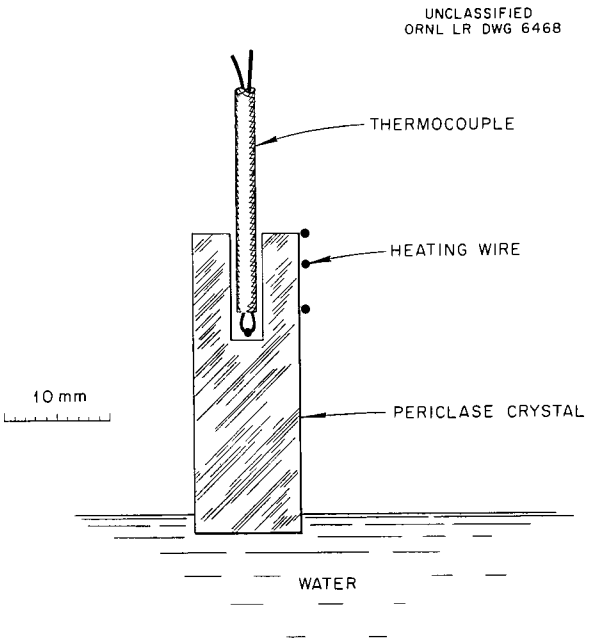

Fig 138 Test for Thermal Stress Cracking in a Periclase Single Crystal

in cross section The end of the crystal containing the thermocouple well was heated by an externally wound coil of resistance wire The opposite end was cooled by immersion for a depth of 1 mm into water The temperature measured in the thermocouple well was 300°C At the opposite end of the crystal the water boiled In the first test small cracks formed at the cooled end but did not grow Before the second test the lower edges and corners of the crystal were ground off No cracks formed in this test

The corrosion resistance of periclase containers has been most satisfactory When they contained fused sodium hydroxide for 24 to 36 hr at 600 to 700°C the magnesium pickup by the melt was less than 0 05 wt % Cleaved surfaces exposed to fused sodium hydroxide for 100 hr at temperatures up to 900°C showed no visible signs of etching However a ground and polished surface developed a whitish blush after 1 hr at 750°C

In the section on Spectrophotometry of Fused Hydroxides below the fabrication of containers by quite different techniques is described

Dry Box Considerable time has been spent in the design and construction of a dry box which incorporates many features peculiar to the specific

needs of this group These features include two pass chambers of unusual dimensions high-amperage electrical connections and provisions for operating a microscope inside the box and for attaching a large vacuum furnace as an integral part of the box In general design the box is of the Le Valle type It can be evacuated to 1 μ by means of a mechanical pump and has a leak rate when evacuated of 25 μ/hr The helium atmosphere is purified by passing through 25 ft of $\frac{3}{4}$ in copper tubing filled with absorbent charcoal and cooled with liquid nitrogen Carbon dioxide and water are the impurities of primary concern During operation the box is continuously flushed All the external plumbing including vacuum pump and gas purification system is compact enough to fit beneath the box

Note on the Kinetics of the Sodium Hydroxide–Sodium Reaction It has generally been supposed that reactions in fused hydroxides reach thermodynamic equilibrium very rapidly unless mechanically hindered as by the presence of a scale at an interface Some simple experiments have been done which show that the reaction

$$Na + NaOH \rightarrow Na_2O + \tfrac{1}{2}H_2$$

approaches equilibrium in solution with significant slowness

When pieces of sodium were dropped into fused sodium hydroxide at about 400°C the metal slowly went into solution and imparted an intense blue green color to the hydroxide At a distance of $\frac{1}{2}$ to 1 cm from the dissolving sodium gas bubbles were evolved in a narrow zone and beyond the gas bubbles the hydroxide was light gray There was no evidence of gas evolution anywhere in the system except along the narrow zone where the blue-green color faded into gray

From these observations two tentative conclusions can be drawn that are independent of the reaction mechanism First there is a time delay before the reaction goes to completion This delay is whatever time is required for the species which gives the blue green color to diffuse from the dissolving sodium out to the zone of gas bubbles Second the existence of a narrow zone of bubbles suggests that the gas evolution step in the reaction is autocatalytic A secondary deduction here is that the reaction zone should move toward the sodium at the rate of diffusion of hydrogen in fused sodium hydroxide

The writers have been able to devise a number of alternative mechanisms to explain these experiments but the most attractive of these is the simple chain reaction given by the following equations

$$Na + \tfrac{1}{2}H_2 \rightarrow NaH$$

$$NaH + NaOH \rightarrow Na_2O + \tfrac{1}{2}H_2 + \tfrac{1}{2}H_2 \quad \text{escapes}$$

It is assumed that sodium does not react directly with sodium hydroxide but that it dissolves readily as it does in its halides On the other hand it is assumed that sodium hydride reacts readily with sodium hydroxide as shown above Some source of hydrogen acts as a chain starter In order for this reaction to continue and to remain nonexplosive it is necessary that the ratio of escaping hydrogen to reacting hydrogen stay close to unity at all times It may be shown that such a balance is possible under the experimental conditions described

The significance of this reaction lies in the insight which it may give into the kinetics of mass transfer and into the chemistry of sodium–sodium hydride as a hydrogen carrier in a fused hydroxide moderator The latter application is especially direct in that the steps of the above chain reaction are precisely the processes which would be expected to occur in engineering scale operations

It is impossible to devote any great amount of time to studies of the sodium hydroxide–sodium reaction However some progress should be made in the next few months

Computations of Free Energies of Formation Numerical data for the standard free energies of formation of the alkali metal hydroxides and related compounds are an essential guide in studies of hydroxide chemistry These free energy data have been computed as a function of temperature for the hydroxide peroxide and superoxide of sodium and are presented in Fig 139 together with the data for the oxide and water which are used in subsequent computations in this report

Values of the standard free energies of formation at 25°C are available[19] for sodium oxide sodium peroxide and sodium superoxide The

[19] L Brewer *Chem Revs* 52 6 (1953)

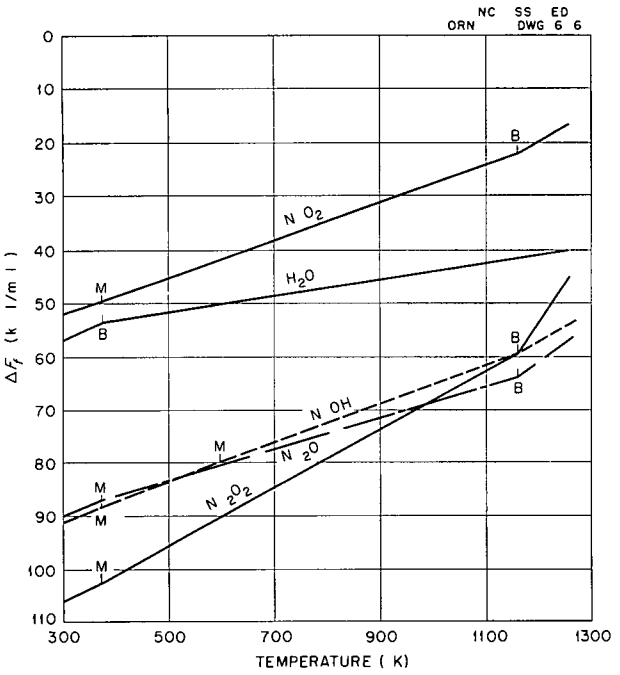

Fig 139 Standard Free Energies of Formation of the Hydroxide and Oxides of Sodium

value for sodium hydroxide may readily be computed from the values for the standard heat of formation of sodium hydroxide[20] and the entropies of sodium hydroxide [21] hydrogen oxygen and sodium in their standard reference states It is thus computed that ΔF°_{298}(NaOH) = −91 0 kcal/mole At higher temperatures values of the standard free energy of formation have been given in the literature for only sodium oxide [22] Values have been estimated however for sodium peroxide sodium superoxide and sodium hydroxide in the following way The curves for standard free energy of formation vs temperature for the class of compounds under consideration are known to a fairly good degree of approximation to consist of segmented straight lines with abrupt changes in slope at the transition points of the compound and of its component elements One point on each of these curves is fixed from the values for the standard free energy of formation at 25°C mentioned above The slope at this point is determined from values of the standard entropy of formation by use of the relation

$$\left(\frac{\partial \Delta F_f^{\circ}}{\partial T}\right)_P = -\Delta S_f^{\circ}$$

These entropy data are obtained from the standard state entropy values The change in slope at each transition point is determined from the transition entropy which of course is readily computed from the heat of transition

Recent data[23] on the heat capacity of liquid sodium hydroxide will permit a more precise evaluation of the slope of the free energy curve from the melting point up to 1000°C

The heat of fusion of sodium peroxide (T_M = 980°K) was not available but it should introduce only a small change in slope which may be considered negligible for the computations which follow

Computations of Decomposition Pressures In considering any solvent as a reactior medium it is important to determine whether the solvent tends to decompose to an appreciable extent particularly if any of the products of the decomposition take part in the reaction The classic example is of course water Here the covalent water molecules decompose slightly into ions The resulting equilibrium frequently exerts a controlling influence on the course of aqueous reactions The following is an outline of the results to date of a theoretical search for the significant decomposition equilibria in fused alkali metal hydroxides It should be emphasized that the work presented here is in no sense definitive or complete

The most important result of the treatment given here is the evidence for the possible occurrence of appreciable quantities of peroxide accompanied by gaseous hydrogen as the result of decomposition equilibria In a later report it will be shown how this peroxide may play a decisive role in mass transfer and corrosion

Consider a fused alkali metal hydroxide in an inert environment such that the volume of any gas

[20] Unles otherwise specified literature values used herein are taken from *Selected Values of Chemical Thermodynamic Properties* by F D Rossini National Bureau of Standards Washington D C 1952

[21] J C R Kelly and P E Snyder *J Am Chem Soc* 73 4114 (1951)

[22] F D Richardson and J H E Jeffes *J Iron Steel Inst (London)* 160 261 (1948)

[23] W D Powers and G C Blalock *Enthalpies and Specific Heats of Alkali and Alkaline Earth Hydroxides at High Temperatures* ORNL 1653 (Jan 7 1954)

phase is small when compared with that of the liquid phase The fused hydroxide may be regarded thermodynamically as being in equilibrium with every chemical species composed of nothing more than oxygen hydrogen and the alkali metal In practice many of these chemical species can be ignored for either of two reasons First the equilibrium concentration of the species in question may be insignificant Second the rate of formation of the species in question may be so slow that it does not approach equilibrium in any given time period Since the following discussion is thermodynamic only the first reason will be treated

There are three particularly useful theoretical measures of the significance of a decomposition reaction They are (1) the equilibrium constant (2) the standard free energy change and (3) the concentration of the products of decomposition The third is the most directly related to experiment and hence at the present stage the most useful The only concentration in a fused hydroxide which we can measure at temperature by present methods is the partial pressure of a gaseous product Hence considerable emphasis will be placed on possible decomposition reactions which produce gaseous products and on an expression of their equilibrium concentrations in terms of the decomposition pressure

The decomposition pressure of a pure substance with regard to a gaseous product will be defined as that partial pressure of the gaseous product which when in equilibrium with the condensed phase is required to maintain the over all composition of the condensed phase equal to the composition of the pure substance The pressure so defined is unique for a given temperature If there are several gaseous products there is a decomposition pressure for each such product

Standard states will be selected as those conventionally chosen in defining the standard free energy of formation Although this is not the usual choice of standard states in the case of solutes it is definitely the most convenient choice for the computations which follow

Four possible decomposition reactions will be considered each of which gives a gaseous product at the temperatures at which the hydroxides are liquid These are

$$(1) \qquad 2MOH \overset{K_1}{=} M_2O + H_2O \qquad \Delta F_1^\circ$$

$$(2) \qquad 2MOH \overset{K_2}{=} M_2O_2 + H_2 \qquad \Delta F_2^\circ$$

$$(3) \qquad 2MOH \overset{K_3}{=} MO_2 + M + H_2 \qquad \Delta F_3^\circ$$

$$(4) \qquad 2MOH \overset{K_4}{=} MO_2 + MH + \tfrac{1}{2}H_2 \qquad \Delta F_4^\circ$$

where all substances are partitioned among all phases present and where K_i and ΔF_i° are the equilibrium constants and standard free energies of reaction respectively

The sparsity of reliable information on the alkali metal–oxygen compounds raises serious questions about the application of all the above equilibria to all the alkali metals This subject is treated by Brewer[19] and will not be repeated here However it is the essential point of this treatment to determine whether unsaturated oxygen ions such as the peroxide and superoxide ions may occur as decomposition products in addition to the saturated oxide ion The existence of some sort of unsaturated oxygen ion is certain for all the alkali metals and it is known that the stability of the unsaturated species increases in going from lithium to cesium Therefore the basic competition referred to below between hydrogen and the monoxide for water should be a characteristic of all hydroxide decomposition equilibria and should lead to a water hydrogen equilibrium in the gas phase of the type discussed The data for sodium compounds are reasonably reliable Hence sodium hydroxide will be treated separately

By definition of the equilibrium constant

$$K_1 = \frac{a_{M_2O}\, a_{H_2O}}{a_{MOH}^2} = \frac{\gamma_{M_2O}\, N_{M_2O}\, \gamma_{H_2O}\, N_{H_2O}}{\gamma_{MOH}^2\, N_{MOH}^2}$$

where a_X is the activity of substance X in the hydroxide phase and N_X and γ_X are the corresponding mole fraction and activity coefficient respectively Let the mole fractions be those which are in equilibrium with the decomposition pressure Then $N_{M_2O} = N_{H_2O}$ and it is possible to write

$$K_1 = \Gamma_1 \frac{a_{H_2O}^2}{a_{MOH}^2} \qquad \Gamma_1 = \frac{\gamma_{M_2O}}{\gamma_{H_2O}}$$

Likewise for Eqs 2 through 4

$$K_2 = \Gamma_2 \frac{a_{H_2}^2}{a_{MOH}^2} \qquad \Gamma_2 = \frac{\gamma_{M_2O_2}}{\gamma_{H_2}}$$

$$K_3 = \Gamma_3 \frac{a_{H_2}^3}{a_{MOH}^2} \qquad \Gamma_3 = \frac{\gamma_{MO_2}\gamma_M}{\gamma_{H_2}^2}$$

$$K_4 = \Gamma_4 \frac{a_{H_2}^{5/2}}{a_{MOH}^2} \qquad \Gamma_4 = 4\frac{\gamma_{MO_2}\gamma_{MH}}{\gamma_{H_2}^2}$$

The above equations are exact However a more useful form can be obtained by assuming that the extent of decomposition is very small As will be shown later this assumption involves a negligible error for all four reactions From this assumption two conclusions can be drawn (1) the activity of the hydroxide as used in the above equations may be taken to be unity because of the choice of standard states (2) the partial pressures of water and hydrogen in the gas phase may be taken to be equal to the fugacities in the gas phase and hence equal to the fugacities in the liquid phase Finally note that the fugacity of the gases in the standard reference state is unity Substituting these conclusions into the above equations solving for the partial pressures and applying the reaction isotherm give

$$(5a) \quad p_{H_2O} = \left(\frac{K_1}{\Gamma_1}\right)^{1/2} = \frac{1}{\Gamma^{1/2}} \exp\left(-\frac{\Delta F_1^\circ}{2RT}\right)$$

$$(5b) \quad (p_{H_2})_2 = \left(\frac{K_2}{\Gamma_2}\right)^{1/2} = \frac{1}{\Gamma_2^{1/2}} \exp\left(-\frac{\Delta F_2^\circ}{2RT}\right)$$

$$(5c) \quad (p_{H_2})_3 = \left(\frac{K_3}{\Gamma_3}\right)^{1/3} = \frac{1}{\Gamma_3^{1/3}} \exp\left(-\frac{\Delta F_3^\circ}{3RT}\right)$$

$$(5d) \quad (p_{H_2})_4 = \left(\frac{K_4}{\Gamma_4}\right)^{2/5} = \frac{1}{\Gamma_4^{2/5}} \exp\left(-\frac{2\Delta F_4^\circ}{5RT}\right)$$

where $(p_{H_2})_z$ is to be read as the partial pressure of hydrogen z provided that no other hydrogen producing reaction is operative save the zth

From the original choice of mole fractions note that the above partial pressures are the decomposition pressures There are three values of the decomposition pressure with respect to hydrogen Except over unique temperature ranges one of these three decomposition pressures will be much larger than the other two and hence by the law of mass action will stabilize the others Thus only one of the three pressures will be the decomposition pressure of MOH with regard to hydrogen

Because of the lack of thermodynamic data on all the alkali metal hydroxides except sodium ratios of decomposition pressures must be used in most applications Thus assume that reactions 1 and 2 are simultaneously at equilibrium and that they determine the gaseous water and hydrogen pressures respectively By dividing Eq 5*b* into 5*a* the decomposition pressure ratio is

$$(6a) \left(\frac{p_{H_2O}}{p_{H_2}}\right)_{12} = \left(\frac{K_{12}}{\Gamma_{12}}\right)^{1/2} = \frac{1}{\Gamma_{12}^{1/2}} \exp\left(-\frac{\Delta F_{12}^\circ}{2RT}\right)$$

where

$$\Delta F_{12}^\circ = \Delta F_1^\circ - \Delta F_2^\circ$$

$$K_{12} = \frac{K_1}{K_2}$$

$$\Gamma_{12} = \frac{\Gamma_1}{\Gamma_2} = \frac{\gamma_{M_2O}\gamma_{H_2}}{\gamma_{M_2O_2}\gamma_{H_2O}}$$

It will be noted that ΔF_{12}° unlike ΔF_1° and ΔF_2° does not contain the free energy of formation of the hydroxide

The concentrations of the oxide in reaction 1 and of the peroxide in reaction 2 are not independent

but are related through the equilibrium

$$(7) \qquad M_2O + \tfrac{1}{2}O_2 \overset{K_7}{=} M_2O_2 \qquad \Delta F_7^\circ$$

Furthermore the concentrations of oxygen in this equilibrium and of hydrogen in reaction 2 are related through the equilibrium

$$(8) \qquad H_2 + \tfrac{1}{2}O_2 \overset{K_8}{=} H_2O \qquad \Delta F_8^\circ$$

The existence of these equilibria is compatible with Eq 6*a* as may be seen from the fact that $\Delta F^\circ_{1\,2} = \Delta F^\circ_8 - \Delta F^\circ_7$ $K_{1\,2} = K_8/K_7$ Hence Eq 6*a* could have been derived by using equilibria 7 and 8 because the two sets of equilibria 1 and 2 and equilibria 7 and 8 are both equivalent to the one equilibrium

$$(9) \qquad M_2O_2 + H_2 \overset{K_{1\,2}}{=} M_2O + H_2O \qquad \Delta F^\circ_{1\,2}$$

From Eq 9 it will be noted that the pressure ratio $(p_{H_2O}/p_{H_2})_{1\,2}$ is determined by the competition between the oxide and hydrogen for oxygen with the one trying to form the peroxide and the other trying to form water

In like manner an expression analogous to Eq 6*a* can be derived under the assumption that equilibria 1 and 3 determine the water and hydrogen pressures respectively This expression is

$$(6b) \qquad \left(\frac{p_{H_2O}}{p_{H_2}}\right)_{1\,3} = \frac{K_{1\,3}}{\Gamma_{1\,3}} = \frac{1}{\Gamma_{1\,3}} \exp\left(-\frac{\Delta F^\circ_{1\,3}}{6RT}\right)$$

where

$$\Delta F^\circ_{1\,3} = 3\Delta F^\circ_1 - 2\Delta F^\circ_3$$

$$K_{1\,3} = \frac{K_1^{1/2}}{K_3^{1/3}}$$

$$\Gamma_{1\,3} = \frac{\Gamma_1^{1/2}}{\Gamma_3^{1/3}}$$

By using the free energy data computed above for sodium hydroxide the representative values shown in Table 49 were obtained The pressure–activity coefficient products in this table give the pressures which would be obtained if the solutions were ideal Figure 140 shows the relative importance of equilibria 1 and 2 in terms of the logarithm of the pressure ratio as a function of the reciprocal of the absolute temperature Figure 141 gives the free energy differences $\Delta F^\circ_{1\,2}$ and $\Delta F^\circ_{1\,3}$ as functions of the absolute temperature

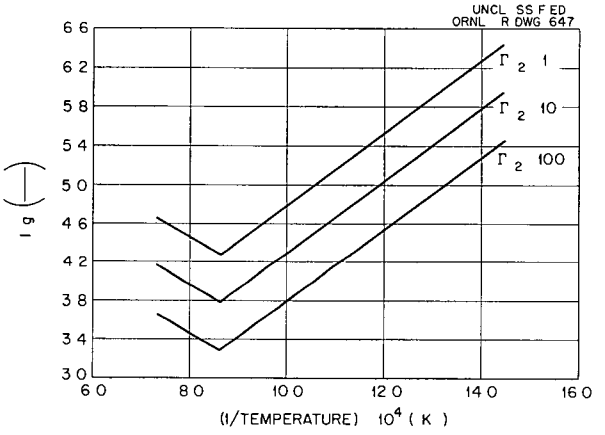

Fig 140 Decomposition Pressure Functions for Sodium Hydroxide

TABLE 49 DATA ON THE DECOMPOSITION OF SODIUM HYDROXIDE

Temperature (°C)	ΔF_1° (kcal)	ΔF_2° (kcal)	K_1	K_2	K_3	$p_{H_2O}\sqrt{\Gamma_1}$ (mm Hg)	$p_{H_2}\sqrt{\Gamma_2}$ (mm Hg)
25	35 3	76 0	10^{-26}	10^{-56}	10^{-95}		
600	21 4	64 4	$4\ 7 \times 10^{-6}$	10^{-18}	10^{-27}	1 7	$7\ 4 \times 10^{-6}$
900	13 5	59 9	3×10^{-3}	8×10^{-12}	10^{-18}	42 0	$2\ 1 \times 10^{-3}$

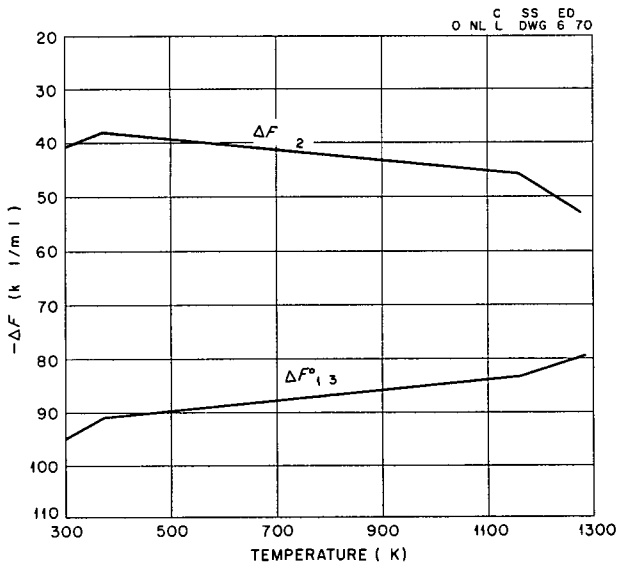

Fig 141 Free-Energy Differences as Functions of Temperature

Examination of these data shows the following

1 Apart from unexpectedly large deviations from ideality equilibrium 1 will predominate at all temperatures

2 Assuming ideality hydrogen evolution from fused sodium hydroxide in an inert container will be small at all temperatures but it should be measurable at 900°C Likewise the peroxide concentration at all temperatures may be small but it should be appreciable at 900°C

3 Deviations from ideality of a moderate amount could make hydrogen and peroxide formation either insignificant or greatly important at high temperatures

There are no satisfactory heat of formation data for any of the alkali metal hydroxides other than sodium hydroxide Therefore only the relative importance of the decomposition equilibria can be studied Some of the entropy values for the higher oxides have been estimated and are reported in the literature However the heats of formation for rubidium and cesium oxides are quite uncertain and it is presently believed that the accuracy of the $\Delta F^\circ_{1\,2}$ and $\Delta F^\circ_{1\,3}$ values given in Table 50 would not be improved by using these entropy estimates Therefore calculations will be limited to the use of enthalpy values but it will be shown that this restriction is not so serious as it might at first seem to be

TABLE 50 APPROXIMATE $\Delta F^\circ_{1\,2}$ AND $\Delta F^\circ_{1\,3}$ AT 25°C

M	$\Delta F^\circ_{1\,2}$ (kcal)	$\Delta F^\circ_{1\,3}$ (kcal)
Li	−47	
Na	−36	−94
K	−25	−76
Rb	−34	−73
Cs	−35	−70

Comparing equilibria 1 and 2 shows that

$$\Delta F^\circ_{1\,2} = \Delta F^\circ_{M_2O} + \Delta F^\circ_{H_2O} - \Delta F^\circ_{M_2O_2}$$

$$= \Delta H^\circ_{M_2O} + \Delta F^\circ_{H_2O} - \Delta H^\circ_{M_2O_2} + T(\Delta S^\circ_{M_2O} - \Delta S^\circ_{M_2O_2})$$

All the data required in the above equation are available except those for the entropy term Since this term represents a difference in entropy for two similar substances it may be supposed that its omission will not be serious A similar situation obtains for $\Delta F^\circ_{1\,3}$ Hence the following approximations will be used

$$\Delta F^\circ_{1\,2} \cong \Delta H^\circ_{M_2O} + \Delta F^\circ_{H_2O} - \Delta H^\circ_{M_2O_2}$$

$$\Delta F^\circ_{1\,3} \cong \Delta H^\circ_{M_2O} + \Delta F^\circ_{H_2O} - \Delta H^\circ_{MO_2}$$

The degree of approximation can be checked by using the data for sodium compounds In this case $\Delta F^\circ_{1\,2}$ is −35 5 kcal when the approximation is used as compared with the correct value of −40 7 kcal Likewise $\Delta F^\circ_{1\,3}$ is −94 2 kcal compared with the correct value of −94 9 kcal

In Table 50 are listed the approximate values of $\Delta F^\circ_{1\,2}$ and $\Delta F^\circ_{1\,3}$ for all the alkali metal hydroxides at 25°C

Table 50 shows that hydrogen and the peroxide should be produced most readily in potassium hydroxide and least readily in lithium hydroxide Nevertheless equilibrium 1 is predominant and equilibrium 3 and hence equilibrium 4 are insignificant

A knowledge of decomposition equilibria of a solvent acting as a reaction medium is basic to an

understanding of the influence of the solvent on the reaction The computations which are presented above indicate the extent to which it is possible to obtain information concerning decomposition equilibria in fused alkali metal hydroxides within the limitations of existing thermodynamic and general inorganic chemical data Primarily these limitations are the absence of any activity coefficient data uncertainty as to the types of unsaturated oxygen compounds for the heavier alkali metals and the sparsity of reliable thermodynamic data for all the alkali metal compounds concerned except those of sodium In spite of these limitations it has been possible to estimate for the first time the decomposition pressures for sodium hydroxide and to show that a basic decomposition equilibrium for all the alkali metals involves the competition between the oxide ion and hydrogen for oxygen with the one trying to form an unsaturated oxygen species and the other trying to form water The importance of this latter result lies in the fact that unsaturated oxygen ions if present in appreciable quantity may exert a controlling influence on the reactions producing corrosion and mass transfer in the fused hydroxides

The numerical results indicate that in the absence of excess oxygen sodium hydroxide should become corrosive to metals by virture of peroxide formation somewhat above 600°C This result is in agreement with experimental observation

Experimental Studies of the Dissociation of Hydroxides Thermodynamic considerations outlined in the preceding section indicate that the alkali metal hydroxides not only should dissociate in the expected way to liberate water but also should liberate a lesser but measurable amount of hydrogen at elevated temperatures There have been no successful studies of the thermal dissociation of sodium hydroxide or of the heavier alkali metal hydroxides although there has been interest in this subject for over 50 years The difficulty has been the lack of an inert container material Zelezney[24] at the NACA Laboratories in Cleveland made a notable attempt to determine indirectly the temperature at which sodium hydroxide begins to undergo measurable decomposition He tried to avoid the container problem by focusing the light from a large carbon arc on sodium hydroxide contained in a water cooled copper chamber His idea was to use solid sodium hydroxide as a container for the liquid (An arc lamp was used rather than sunlight because the latter was unavailable during the months when these tests were being made) His results were interesting but could not be explained

The writers believe that having found periclase to be a suitable container material they are in a position to attack this difficult problem Several experiments have been conducted in which sodium hydroxide was heated at temperatures from 500 to 900°C in a periclase crucible in a static system with small gas space and also with continuous Toepler pumping Gas samples were taken and analyzed mass spectrometrically In each experiment significant quantities of hydrogen were found in addition to much greater quantities of water Experimental difficulties were encountered however which preclude placing any quantitative significance on the numerical values obtained Hydroxide escaped from the crucible by two mechanisms namely vaporization and creep This hydroxide reacted with the hot envelope of the system which was made of silica The writers believe that the reaction with silica is of the following type

$$n\mathrm{NaOH} + \mathrm{SiO_2} \rightarrow (\mathrm{Na_2O})_n\,\mathrm{SiO_2} + \frac{n}{2}\mathrm{H_2O}$$

where n is probably 2 (ref 25) so that the observed hydrogen came directly from the hydroxide and not from the reaction with the envelope Attempts were made to avoid this difficulty by using a long thin walled crucible of sintered magnesium oxide between the periclase and the silica The results were not satisfactory because of the porosity of the sintered material

From the studies thus far it is concluded that hydrogen is a significant product of the thermal dissociation of liquid sodium hydroxide

Attempts are now being made to fabricate all the heated parts of the system from a periclase single crystal

Spectrophotometry of Fused Hydroxides It has been pointed out[26] that fused hydroxides undergo

[24] W Zelezney private communication

[25] J D Ans and J Loffler *Ber* **63B** 1446 (1930)

[26] C R Boston and M E Steidlitz *Met Semiann Prog Rep April 10 1954* ORNL 1727 p 57

reversible color changes with changes in temperature and blanketing atmosphere and that fused hydroxide solutions of various substances such as sodium peroxide and silver oxysalts produce distinctive colors under conditions at which the hydroxide would be colorless in their absence These qualitative results suggest that high temperature absorption spectrophotometry would be a unique and powerful tool to aid in the study of fused hydroxide chemistry for the following reasons

First it has been shown that the blanketing atmosphere over a fused hydroxide melt exerts a controlling influence on corrosion and mass transfer reactions Two gases are known to affect these reactions oxygen and hydrogen and each of them interacts with fused hydroxides in a reversible way to produce distinctive colors These colored species which undoubtedly play a role in mass transfer and corrosion can be studied *in situ* by means of high temperature spectrophotometry

Second the reaction of sodium with sodium hydroxide is accompanied by color changes This phenomenon and its importance are discussed above High temperature spectrophotometry would be of great assistance in studying this reaction

Third the oxysalts of silver give intense distinctive colors in fused hydroxide solution It is not unlikely that the oxysalts of other metals do likewise Therefore spectrophotometry could be used to study directly the kinetics of corrosion and mass transfer reactions at temperature without disturbing the system and without imposing extreme conditions to get a measurable amount of reaction

Fourth it is not unlikely that absorption spectra may become useful in determining the molecular structure of species present in fused hydroxide solution Experience with aqueous solutions however warns that this application will be limited

Current research is devoted to the construction of a high temperature spectrophotometer from available odds and ends of equipment The purpose of building this preliminary apparatus is to allow the solution of numerous optical problems with the least expense For this work a small Coleman Universal spectrophotometer model 14 is being used as a monochromator The photocell was removed and a 20 mm hole was drilled through the instrument case to permit passage of the light beam The dimensions of this light beam are defined by suitable lenses and slits so that it passes through only the windows of the absorption cell and is then spread out over the area of the photocell The various components are mounted on an optical bench to facilitate adjustment The measuring circuit for the photocell is not completely satisfactory and will have to be modified Optical alignment is accomplished by using in the absorption cell a sugar solution of the same refractive index as fused sodium hydroxide

For some time the primary drawback to quantitative absorption studies has been the lack of a transparent and inert material from which an absorption vessel could be fabricated The work on periclase described above indicates that in all probability this problem has been solved

Two types of absorption cells have been constructed The first type is simple to make but has an awkward geometry from an optical point of view The second type is much more difficult to construct but has an almost ideal geometry The two cell types are illustrated in Fig 142

The first type shown on the left in the photograph was made as follows A cylinder was machined from a single crystal of periclase and drilled axially for about three quarters of its depth to form a cup Two flat surfaces were ground and polished on opposite sides of the cylinder to form windows The inside was polished cylindrically This cell has the disadvantage that its windows are cylindrical plano concave lenses of short focal length Hence the incident light beam must be strongly convergent so that the transmitted beam will not diverge significantly beyond the angle intercepted by the photocell Furthermore this geometry leads to pronounced reflections from the cell interfaces so that an appreciable fraction of the emergent beam passes through the cell wall but not through the hydroxide

The second type was made by taking advantage of the cubic cleavage of periclase A crystal blank with parallel faces was cleaved from a single crystal Intersecting cavities were core drilled in the blank The cuspidated sides of the resultant cavity were cleaved away to form flat surfaces parallel to one another and parallel to two of the outside surfaces These parallel surfaces form flat windows on opposite sides of the cell as may be seen in the photograph The cell in the center of the photograph was made with two large holes which gave narrow windows The cell on the right was made with five smaller holes which gave

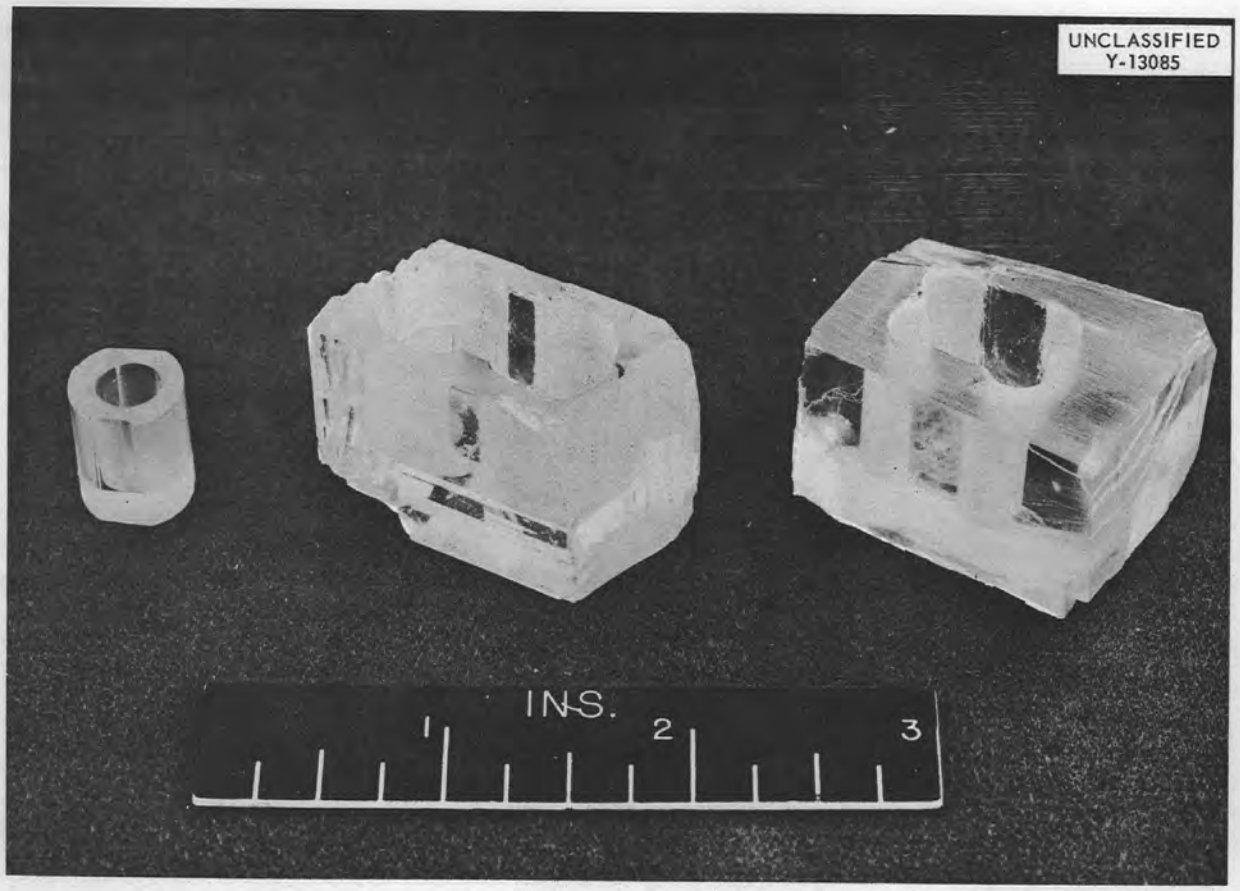

Fig. 142. Spectrophotometric Absorption Cells Made from Synthetic Periclase Single Crystals for Use with Fused Sodium Hydroxide at High Temperatures.

wider windows. The irregular corners of this cell are portions of the original surfaces of the crystal fragment before cleavage. Had the initial crystal been generously large, a cell with the outer surfaces forming a rectangular parallelepiped could have been made.

The techniques for making these cells have not yet been perfected to the desired degree.

Synthesis of Compounds in the Na_2O-NiO System. Several substances have been isolated as products of the reaction between nickel metal and sodium hydroxide. These substances all appear to be oxysalts of the system Na_2O-NiO. Attempts are being made to isolate and identify these compounds,[27] to determine some of their chemical properties, and to determine their crystal structures. Previous to this work, the only compound in this series which had been prepared was sodium orthonickelate(II), Na_2NiO_2, and nothing was known about it except its empirical formula.

The research procedure which is being followed consists in two parallel and equally essential endeavors. Mixtures of various proportions of sodium monoxide and nickelous oxide are sintered together. Following sintering, the x-ray powder patterns and chemical formulas will be determined. This information will provide the empirical formulas of the possible oxysalts, as well as some information concerning solid-state solubility and the x-ray powder patterns. Apparatus which have been completed for this sintering procedure include: three vacuum furnaces which have been tested cold and are capable of maintaining a pressure of 2×10^{-6} mm without special precautions, an apparatus for manufacturing sodium monoxide and nickelous oxide of higher purity than can be obtained commercially, and a ball mill for service in the dry

[27] H. L. Yakel, Jr., and G. P. Smith, *Met. Semiann. Prog. Rep. April 10, 1954*, ORNL-1727, p 54.

box. This ball mill, shown in Fig. 143, will be used for mixing the powders before sintering. The operation of this mill appears to be satisfactory inasmuch as it will reduce sodium chloride to 250-mesh powder in 24 hr.

The powder sintering procedure will produce a crystal size much too small for single-crystal x-ray work, and the sintered mixture will not be pure enough for chemical studies. Hence, attempts are being made to recrystallize compounds from fused sodium hydroxide solution. The oxysalt is prepared in the fused hydroxide at about 900°C, as previously described, and slowly cooled to give a large crystal size. The section of reaction tube containing the solidified hydroxide is then placed in the filtration apparatus shown in Fig. 144. The joints and stopcock on this apparatus are designed so that it will fit in one of the pass chambers of the dry box and can thus be loaded and unloaded under an inert atmosphere. After loading, the filtration apparatus is evacuated and heated to a temperature above the melting point of the hydroxide. The hydroxide flows out of the reaction tube and passes through the sintered nickel filter, leaving the compound behind.

Crystal Lattice Parameters for $NaNiO_2$. A recalculation of the x and z lattice parameters of the low-temperature crystal form of sodium nickelate(III) has led to minor corrections. The undetermined lattice parameter z of the high-temperature crystal form has been estimated from theoretical considerations.

The low- and high-temperature crystal structures of $NaNiO_2$ have been determined by this group.[28] These two modifications will be referred to as α-$NaNiO_2$ and β-$NaNiO_2$, respectively. The values of x^{α} and z^{α}, which were reported, were graphically determined from a Fourier plot. Recent theoretical

[28] L. D. Dyer, B. S. Borie, Jr., and G. P. Smith, *J. Am. Chem. Soc.* **76**, 1499 (1954).

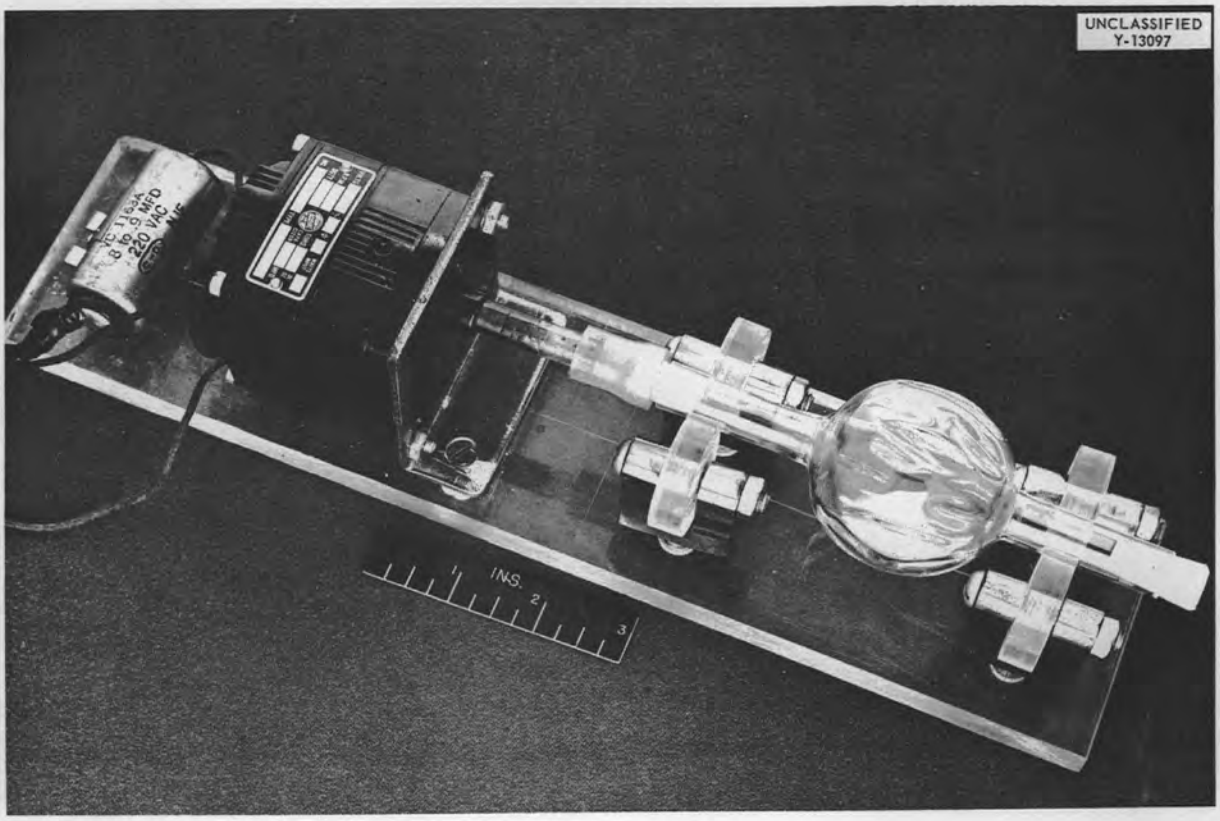

Fig. 143. Ball Mill for Mixing Reactive Powders in a Dry Box.

considerations of the mechanism of the crystal structure transformation raised questions concerning the accuracy of these values Therefore they were redetermined by the weighted least squares method by using the same intensity data from which the Fourier plot was drawn The results of these computations are as follows

$$x^{\alpha}\text{(previous)} = 0\ 278$$
$$\text{Correction} = 0\ 0024 \pm 0\ 0022$$
$$x^{\alpha}\text{(corrected)} = 0\ 2804 \pm 0\ 0022$$
$$z^{\alpha}\text{(previous)} = 0\ 795$$
$$\text{Correction} = 0\ 0045 \pm 0\ 0023$$
$$z^{\alpha}\text{(corrected)} = 0\ 7995 \pm 0\ 0023$$

The positions of the oxygen atoms in β $NaNiO_2$ could not be obtained from x ray data because powder samples used in the high temperature studies showed preferred orientation Studies of the transformation mechanism require a knowledge of the positions of the oxygens Hence a theoretical computation of probable positions has been made

Considerations of symmetry place the oxygens on the body diagonal of the rhombohedral unit cell Hence the single parameter z^{β} is sufficient to fix the oxygen coordinates Assume that the lattice is ionic and that Ni(III) ions are sufficiently small to allow anion anion contact when placed in the octahedral holes of a close packed oxygen ion lattice Then a greatest value of z^{β} is fixed by the nearest approach of oxygen and sodium ions and a least value by anion anion contact Then from the geometry of the lattice

$$z^{\beta}_{m} = \frac{1}{6} + \frac{1}{c}\sqrt{(r_O + r_N)^2 + \frac{a^2}{3}}$$

$$z^{\beta}_{mi} = \frac{1}{3} - \frac{1}{2c}\sqrt{(2r_O)^2 - \frac{a^2}{3}}$$

where a and c are the dimensions of the unit cell in terms of hexagonal coordinates and r_O and r_N are the ionic radii of oxygen and sodium respectively By using the ionic radii of Pauling [29] the values $z^{\beta}_{max} = 0\ 269$ and $z^{\beta}_{min} = 0\ 266$ are obtained with an average of 0 268

Note on the Transformation of $NaNiO_2$ A study of $NaNiO_2$ indicates that this substance may undergo a displacive transformation of the martensitic

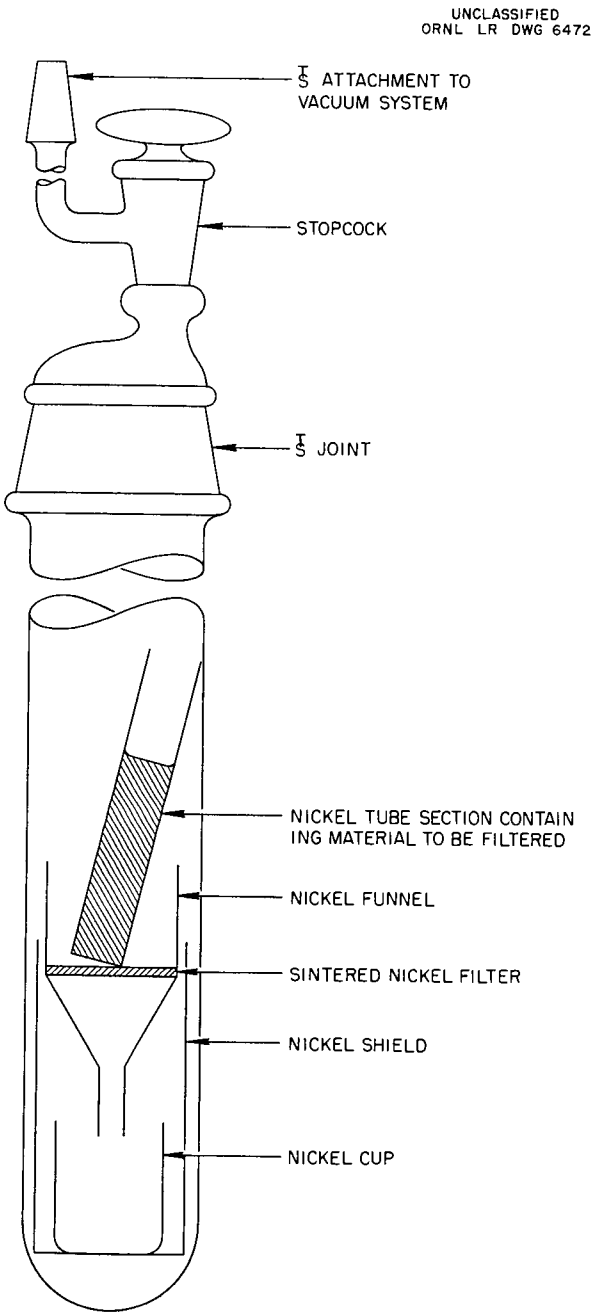

Fig 144 Fused Hydroxide Filtration Apparatus

[29] L C Pauling *The Nature of the Chemical Bond*, Cornell University Press Ithaca N Y 1945 p 350–356

type in passing from the high-temperature beta structure to the low-temperature alpha structure. This transformation is of interest for two reasons: First, it is a rhombohedral-to-monoclinic transformation, whereas all other known examples are more symmetric, since the high-temperature form is always cubic. Second, martensitic transformations are unknown for nonmetallic substances. The studies of sodium nickelate(III) are in a preliminary stage. Therefore, only an indication will be made here of the work which has been done during the past six months.

The microstructure of $NaNiO_2$ is of the type known to mineralogists as polysynthetic twinning; in metallurgy it is associated both with martensitic transformations in nonferrous alloys and with deformation twins. Many inorganic compounds have this microstructure, and Barrett[30] has pointed out the similarity between one of these, barium titanate, and the martensitic microstructure.

Experimental proof has been obtained which shows that the bands in the microstructure of $NaNiO_2$ were formed by a macroscopic displacive process.

Sodium nickelate(III) was prepared and then was precipitated from solution in fused sodium hydroxide at 800°C. Figure 145 is a photomicrograph at 910× magnification of one of the particles thus obtained. Several important characteristics are shown. This specimen was undoubtedly a single crystal of β-$NaNiO_2$ with the *c*-axis perpendicular to the plane of the photograph when the crystal was grown. (The deviation of the angles from the expected habit form and the curvature of the edges are both explained by the transformation on cooling.) When the crystal was cooled, it transformed at 220°C to α-$NaNiO_2$, with the development of the banded structure. This structure is brought out only by the use of polarized light, which is rotated in opposite directions upon reflection from adjacent lamellae. This banded structure represents lamellar crystals of α-$NaNiO_2$ so arranged that adjacent crystals have different orientations and alternate crystals have the same orientation. The set of bands shown on this specimen represents one of several orientation relationships which have been found between the parent phase and the transformed phase.

[30] C. S. Barrett, *Structure of Metals, Crystallographic Methods, Principles and Data*, 2d ed., McGraw-Hill, New York, 1952, p 575.

Figure 146 shows a portion of a banded specimen at 1220× magnification. The surface gives the illusion of having ridges, but actually it is flat. The fine black parallel lines have been identified as being the edges of growth steps. The abrupt bending of these lines at the edges of bands could have been caused only by that process which created the bands themselves. These bends constitute proof of the displacive nature of the process but do not distinguish between deformation twinning and a martensitic transformation.

A list of studies which are now in progress is given below. In these studies special precautions have to be exercised to prevent exposure of the crystals to air, inasmuch as they react with carbon dioxide and water vapor. Since many of the alkali-metal oxysalts are likewise unstable in air, all the special apparatus and techniques which have

Fig. 145. Specimen That Had Been a Single Crystal of β-$NaNiO_2$ When It Was Grown from Solution in Fused Sodium Hydroxide. Banded structure and deformation of the edges are believed to have been caused by a displacive transformation to α-$NaNiO_2$. 910X.

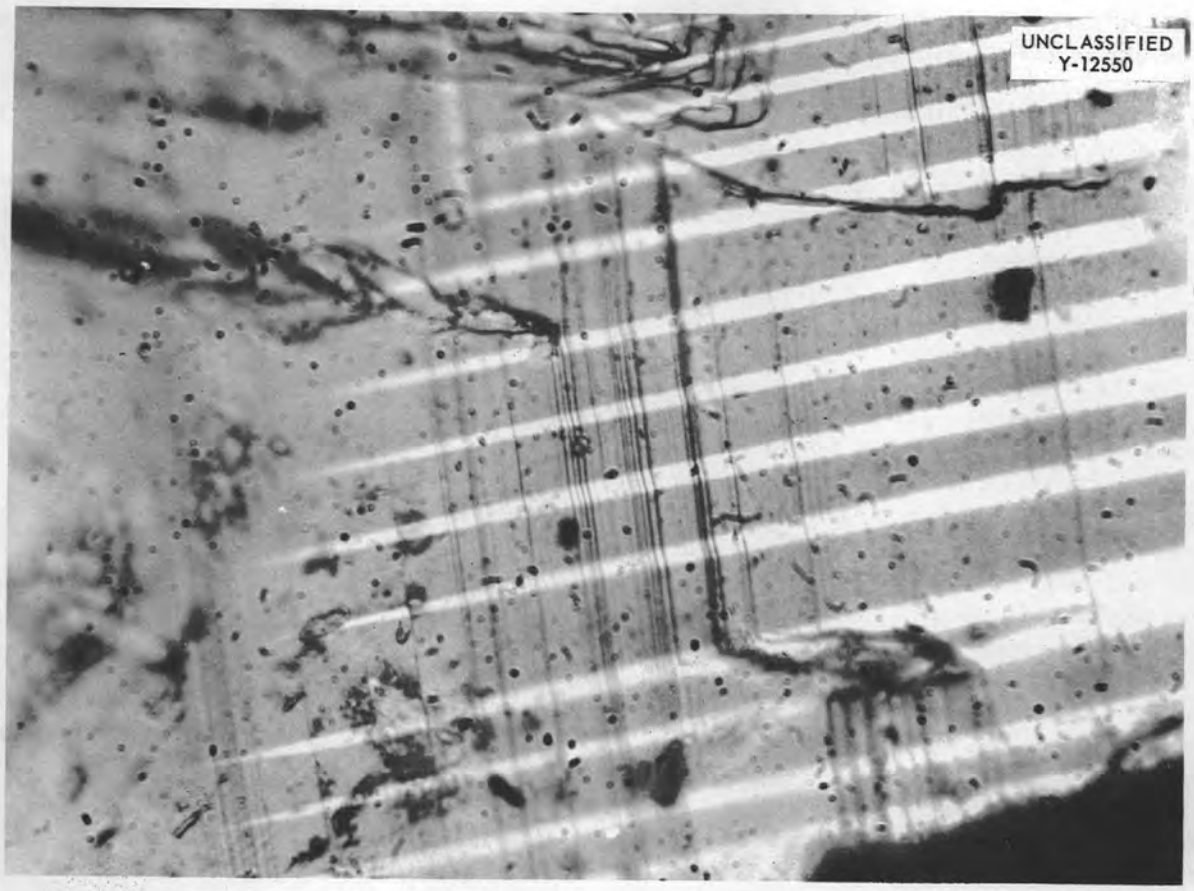

Fig. 146. Banded Microstructure of $NaNiO_2$, Showing Macroscopic Distortion of Growth Steps. 1220X.

been developed will be applicable to studies of various properties of other oxysalts.

1. A microscope hot stage is being built which will allow crystals, extracted from the hydroxide, to be observed without exposure to air. This controlled-atmosphere hot stage will be used to determine whether or not the banded structure is developed at the moment of transformation. This is possible because with the aid of reflected polarized light the alpha phase can be identified as soon as it forms. This measurement will provide vital data in a determination of whether the banded structure is formed by a displacive transformation or by deformation twinning.

2. A high-temperature x-ray spectrometer is being designed in order to determine the lattice constants as a function of temperature in the neighborhood of the transformation point. These data will be needed for a detailed theoretical analysis of the transformation.

3. Attempts are being made to determine the orientation relationships among sets of bands and to determine the orientation relationships between the parent and transformed phases. This task is laborious but necessary. Already, a very large number of microscopic measurements of the angles between sets of bands have been made. The theory of the action of absorbing anisotropic media on plane polarized light is being applied in what appears will be a successful attempt to determine the orientation of the crystal axes in individual bands by the use of reflected polarized light. Special optical equipment has been procured for this latter work.

4. The macroscopic distortions accompanying the displacive process are being determined from

measurements of the bending of growth lines such as are shown in Fig 146 and the bending of crystal edges

5 Theoretical analyses are being made which have shown that a martensitic transformation is reasonable in terms of the crystal structures and which should enable a determination of the atomic motions which produce the transformation to be made as soon as the experimental parameters have been determined

FABRICATION METALLURGY

J E Cunningham

EXPERIMENTAL FABRICATION OF ALUMINUM FUEL ELEMENT

Fabrication studies were conducted on the preparation of composite fuel plates with the thickness of aluminum cladding reduced to 10 and 5 mils The purpose of the studies is to improve reactor performance of the resulting fuel component by further lowering the aluminum to water volume ratio

Examination of the test plates revealed that thin clad fuel plates can be successfully prepared by the present technique with only one defect The defect appeared as small pockmarks or pits randomly located on the surface of the plates immediately after the flux-annealing operation In some instances these surface pits extended to a depth of approximately 3 mils or one half the depth of the cladding at this point in the fabrication schedule for the preparation of fuel plates with 5 mils of aluminum cladding

Although these surface imperfections are essentially ironed out during the following cold rolling step additional work was performed in an effort to determine the exact cause of the objectionable surface pits and to eliminate them In the flux annealing operation where the defect occurs a slurry of commercial aluminum brazing flux (Eutector 190) and methyl alcohol is employed to facilitate removal of hydrogen to prevent blister formation

Type 2S aluminum plates immersed in a large volume of molten Eutector 190 flux heated to both the flux annealing and brazing temperature were completely corroded away in a relatively short time Chemical analysis indicated that the resulting globule that formed in the bottom of the crucible was actually a Zn Al alloy containing 5 to 30 wt % Zn The source of the zinc was undoubtedly the brazing flux which contains 8 to 14 wt % $ZnCl_2$

Similar tests showed that the amount of alloying or pitting could be greatly reduced by lowering the $ZnCl_2$ content of the brazing flux The substitution of $SnCl_2$ for the zinc compound arrested the alloying action completely Brazed T joints prepared with the modified low zinc and stannous chloride–bearing fluxes showed a corrosion resistance superior to that of samples prepared with regular Eutector 190 flux when tested for 24 hr in boiling water Initial attempts to braze full sized dummy fuel elements with these modified fluxes however were not successful and indicate a need for further investigation The low zinc content brazing flux is presently being employed in the flux annealing operation during manufacture of enriched fuel components

MANUFACTURE OF REACTOR COMPONENTS

J H Erwin

Replacement Fuel and Control Rod Units for MTR

A total of 105 fuel units and two control rods were fabricated and forwarded for operation of the MTR and startup of the Reactivity Measuring Facility (RMF) during the period from March 1 through September 1 1954 The fuel units were the 19 plate type prepared with braze clad side plate material and each contained 200 g of U^{235} Fuel units containing plates of heat Nos D 292 through D 301 were flux annealed with 1 5% zinc–bearing flux

One of the control rods forwarded was of standard design while the other was modified with a single piece aluminum extrusion substituted for the four piece lower bearing stainless steel section

New Loading of BSF Fuel Elements

A new set of enriched fuel elements was prepared for service at higher power in the Bulk Shielding Facility The loading consisted of 25 standard full fuel sections for housing control rods and two dummy fuel components

Borax Model II Fuel Units

A total of 68 enriched fuel elements and 22 unassembled fuel plates were supplied to Argonne National Laboratory for Borax Model II experiments The standard unit consisted of a 10 plate element and each unit was loaded with 93 3 g of U^{235} fuel

Special Fuel Assembly for LITR

A special assembly consisting of nine enriched fuel–bearing plates spaced to provide a central

cavity for irradiation experiments in the LITR was supplied to the Solid State Division

Test Elements for Omega West Reactor

Six dummy fuel units were fabricated and forwarded to the Los Alamos Scientific Laboratory for preoperational checking before startup of the Omega West Reactor The units have identical end box adapters on each end to permit inversion of the unit after part time service

Control Rods for Pennsylvania State College

A set of three safety control rods and one regulating rod was furnished for service in the proposed research reactor at Pennsylvania State College

Film Boiling Experiment

A modified control rod and four enriched fuel test sections with varying fuel contents of U^{235} are in process of fabrication for MTR film boiling experiments by Phillips Petroleum Co

Alclad U Al Alloy Test Plates for BNL

An order for 120 MTR type fuel plates was completed for testing and component assembly studies at Brookhaven National Laboratory The order consisted of 30 depleted uranium plates each of (1) 5 wt % U–Al alloy core with 20 mils aluminum cladding (2) 5 wt % core alloy with 15 mils cladding and (3) 14 wt % core alloy with 20 mils cladding and 14 wt % core alloy with 15 mils cladding

Neutron Production Slugs for Hanford and Savannah River

Cast enriched U Al alloy billets supplied by Y 12 were extruded and drawn into rod stock needed in the production of approximately 2000 slugs for Savannah River and 5000 slugs for Hanford

Enriched Fuel Plates for GE ANP

Thirty two composite fuel plates of aluminum clad U Al alloy were prepared and forwarded to General Electric Company ANP Division Cincinnati Ohio for experimental purposes

PREPARATION OF U Al ALLOY PRODUCTS FOR CHEMICAL PROCESSING STUDIES

Normal Uranium MTR Fuel Components for Phillips Petroleum Co

Ten normal uranium fuel elements of the design currently employed in operation of the MTR were prepared and shipped to the Idaho Chemical Plant for chemical processing studies

Depleted U Al Alloy Slugs for DuPont

Approximately 4000 extruded and 1000 cast depleted U Al alloy slugs of various specifications were prepared and delivered to Savannah River

Miniature U Al Alloy Slugs

The Chemical Technology Division was furnished approximately 30 000 extruded and 2000 cast subsized slugs of 5 wt % U–Al alloy for continuous dissolving studies

Cast and Extruded J Slugs for Phillips Petroleum Co

Approximately 1000 cast and 2000 extruded J slugs of 7–5 wt % normal and depleted U–Al alloy were prepared and shipped to the Idaho Chemical Processing Plant

Cast and Extruded J and SRO Slugs

Approximately 4000 extruded and 3000 cast slugs of both 5 and 7–5 wt % normal U–Al alloy were produced for processing studies by the Chemical Technology Division

MISCELLANEOUS FABRICATION WORK

Iodine Thorium Wire and Foil for North American Aviation Inc

Experimental samples of iodine thorium wire and foil were prepared for North American Aviation Inc The foil samples measured 1 by 48 in by 3 5 10 and 20 mils in thickness while 100 ft of wire in each of the 3 10 and 20 mil dia size was supplied

Highly Depleted Uranium Slugs for LITR Irradiation

Several highly depleted (0 035% U^{235}) uranium slugs were fabricated for canning and irradiation in the LITR The slugs were prepared by extrusion of a 4 in dia cast billet to 1 5 in dia rod which was machined into 1 8-cm dia by 4 cm long slugs

Enriched U Al Alloy Slabs for Savannah River

Two highly enriched U Al alloy slabs were fabricated to assist DuPont in developing tubular fuel elements The alloy composition of the slabs was 15 and 19 9 wt % U^{235} aluminum alloy but both slabs measured 8 9 × 36 × 0 080 in in thickness

Zirconium Alloy Specific Heat Specimens

Specimens of zirconium containing 1 and 4 at % silver and 10 20 and 30 at % aluminum were prepared from solution treated arc cast melts and forwarded to Carnegie Institute of Technology for specific heat measurements An 8 at % silver alloy was also prepared but on metallographic examination an unidentified phase was revealed at the grain boundaries which probably was the result of incomplete quenching The specimen will be solution treated again with a faster quench in an effort to eliminate the objectionable phase

Enriched Uranium Disk for Lid Tank Facility

A new enriched metallic uranium source plate is being fabricated for the Lid Tank Facility of the ORNL Graphite Reactor The plate contains approximately 2 kg of U^{235} and measured 28 in in diameter by approximately 0 040 in in thickness